Astrophysics and Space Science Library 424

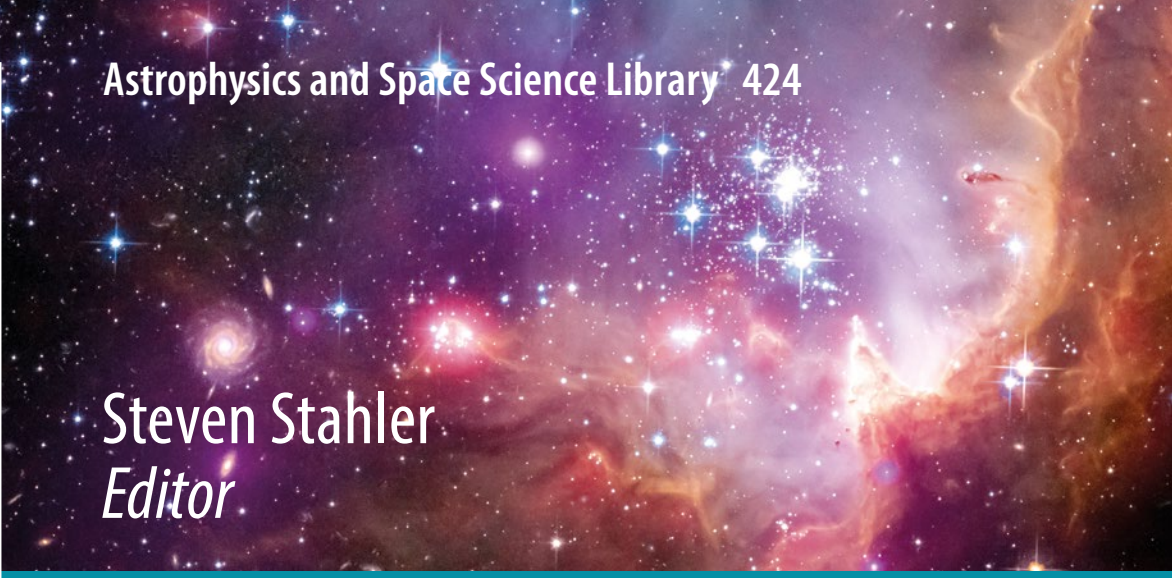

Steven Stahler
Editor

The Birth of Star Clusters

ASSL

Springer

The Birth of Star Clusters

Astrophysics and Space Science Library

More information about this series at http://www.springer.com/series/5664

Steven Stahler
Editor

The Birth of Star Clusters

Springer

Editor
Steven Stahler
Department of Astronomy
University of California
Berkeley
California, USA

ISSN 0067-0057 ISSN 2214-7985 (electronic)
Astrophysics and Space Science Library
ISBN 978-3-319-22800-6 ISBN 978-3-319-22801-3 (eBook)
DOI 10.1007/978-3-319-22801-3

Library of Congress Control Number: 2017956041

Cover illustration: Composite picture of the young open star cluster NGC 602. Taken Under the “Wing” of the Small Magellanic Cloud. Credit: X-ray: NASA/CXC/Univ.Potsdam/L.Oskinova et al; Optical: NASA/STScI; Infrared: NASA/JPL-Caltech

Printed on acid-free paper

This Springer imprint is published by Springer Nature
The registered company is Springer International Publishing AG
The registered company address is: Gewerbestrasse 11, 6330 Cham, Switzerland

Preface

It has long been accepted that most stars originate in groups, rather than in isolation. How the groups themselves arise is a major, unsolved puzzle. At first sight, it might seem odd that such a problem should exist at all. Granted, we certainly do not understand every detail of how individual stars form. Our ignorance is especially severe in the case of massive stars that quickly disperse any parent gas. For the more common, lower-mass stars like the Sun, however, a general picture has been in place for some time, and continues to be filled in. Why, then, is there a separate problem of cluster formation? If we jump ahead a few decades and imagine that low-mass stellar birth is even more secure, will such a problem remain?

The answer is that it would, for at least two basic reasons. First, there is the obvious fact that stellar groups form out of much larger molecular clouds than the dense cores spawning single, solar-type objects. Understanding the structure and dynamics of dense cores is facilitated by the fact that these entities are relatively quiescent, supported largely by ordinary thermal pressure. In contrast, all clouds massive enough to form clusters are characterized by internal turbulence, for which quantitative modeling remains primitive at best.

A second reason the conundrum will persist is that stellar groups span an enormous range of properties. There are moving groups consisting of a few dozen members. At the opposite end of the spectrum are the monstrous and ancient globular clusters, some of which still contain a million stars. Just as no one theoretical model of single-star formation is likely to explain both M dwarfs and O stars, it is equally implausible that one mechanism underlies such diverse stellar aggregates. We must, at present, consider different aspects of the problem and do our best to understand them. In this volume, we offer a selection of current research, from both observers and theorists, on key topics in this active field of study.

We begin with an account of the very youngest clusters, those still embedded in relatively large and turbulent molecular clouds. Joana Ascenso first tells us how these groups are identified in practice. Given the variety of optically revealed clusters, it is not surprising that their optically revealed counterparts exhibit a range of morphologies, which Ascenso also describes. As yet, we have no means to assign even rough ages to these groups. Nor can we yet identify the specific forerunners of,

say, OB associations. We may hope that further observations will begin to fill these gaps.

Turning to the theoretical problem of cluster formation, Patrick Hennebelle relates the current status of numerical simulations. The basic program here is to employ a computational box of gas in which gravity overwhelms any internal pressure. In current simulations, the gas is both magnetized and stirred in a way to mimic true, astrophysical turbulence. Under the action of self-gravity, the gas collapses into a myriad of high-density regions. These presumably would go on to become stars, although no one simulation can cover that final transition. As Hennebelle describes, the necessary and realistic introduction of an embedded magnetic field has led to the paradoxical result that disks around stars cannot form. Feedback from the stars themselves, especially in the form of ionizing radiation, presents similar technical and astrophysical problems.

In many astrophysical problems, we gain insight by exploring how a process plays out under a broad range of conditions. Within our Galaxy, no environment is more extreme than the Galactic center. As Jessica Lu relates in her chapter, this region contains the densest molecular gas. Thus, it might not seem surprising that the star formation rate per unit volume is also the highest. On the other hand, the extraordinarily rich Young Nebular Cluster, one of the three that Lu describes, actually surrounds the central, massive black hole, a fact that renders its formation especially puzzling. The other two clusters, dubbed the Arches and Quintuplet, have similar ages as the central system, a few million years, but distinct morphologies. Lu details the rapid progress being made in discerning the substructure and stellar mass distribution in these groups. As she emphasizes, the very large amount of dusty gas surrounding them poses a special challenge to observers.

Angela Adamo and Nate Bastien widen the perspective to consider the statistics of cluster birth and death on galactic scales. They first summarize the distribution of cluster masses. While a simple power law, with a universal exponent, is adequate in many galaxies, there is always a departure from this relation at the upper end. Interestingly, this cutoff varies with the galactic environment. So, too, does the fraction of clusters that are gravitationally bound, which is higher in galaxies with greater star formation rates. Moreover, the age distribution of clusters depends on the specific mass in question. All these trends will eventually help us see how the largest clouds form clusters. They will also lend insight into the purely stellar dynamical problem of cluster dispersion.

Returning to our own Galaxy, Eric Feigelson provides an update on a concerted effort, using a variety of observational tools, to study the structure and history of the youngest OB associations, those still partially embedded in molecular gas. Feigelson and colleagues combined X-ray and infrared observations with published catalogs of O and B stars. In addition, they estimated ages for thousands of objects using a bolometric luminosity and a stellar mass derived empirically from X-ray luminosities. Their single most significant result is the wide diversity of surface densities and detailed morphologies in several dozen associations. There is good evidence for cluster expansion over time. Moreover, stars near the center of any

cluster are systematically younger than those on the outskirts, indicating that star formation is an ongoing, inside-out process.

The OB associations studied by Feigelson will eventually undergo dispersion, a process we have long observed, through proper motion studies, in their optically revealed descendents. There exist, however, equally young and massive groups, presently devoid of gas, that appear to be gravitationally bound. Sambaran Banerjee and Pavel Kroupa provide a theoretical perspective on the origin of such systems, which include the Galactic Center clusters studied by Lu, as well as others found in the Milky Way disk. Thus far, direct numerical simulations cannot track both the stellar and gas dynamics of such populous groups. As an alternative, simulators follow the stars using a standard, N-body code, but crudely account for the gas through a background gravitational potential. To mimic sudden expulsion of the gas, researchers force the potential to vanish. Banarjee and Kroupa show that such calculations do reproduce the basic properties of several well-studied systems. Further, they argue that the contrasting picture of merging substructures is too slow and produces clusters that are far too dense.

These contributions take us some distance toward a better understanding of cluster origins, but they also highlight the outstanding questions yet to be answered. I would list, near the very top, the issue of why some clusters emerge from their clouds as gravitationally bound systems, while others are unbound and disperse. The smallest aggregates, containing up to several hundred members, are unbound, or become so after their parent cloud dissipates. Groups of a thousand stars or more develop into classic OB associations, also unbound. But between the lowest-mass groups and OB associations lies the regime of open clusters, all bound and remarkably long-lived. Furthermore, as Banerjee and Kroupa describe, groups more massive than OB associations can also be bound. By now, the pattern is clear and also completely unexplained.

The traditional idea is that a bound cluster arises when a relatively large fraction of the parent cloud's mass turns into stars. By now, it is widely recognized that this explanation, while it may have a grain of truth, is inadequate. First, the theoretically required mass fraction is far above most observational estimates. A second objection is that such a simple model is unlikely to suffice in the two very disparate regimes where we find bound clusters. Indeed, observers have searched in vain for clouds that could be precursors to the most populous bound clusters. At this end of the mass spectrum, we may need to explore the possible merger of pre-existing aggregates. Explaining the birth of open clusters will rest on another issue raised at the start of this Introduction—the structure and dynamics of large molecular clouds. Clearly, observers and theorists will be busy for a long time to come.

Berkeley, CA, USA Steven Stahler
May 2017

Contents

Chapter 1
Embedded Clusters

Joana Ascenso

Abstract The past decade has seen an increase of star formation studies made at the molecular cloud scale, motivated mostly by the deployment of a wealth of sensitive infrared telescopes and instruments. Embedded clusters, long recognised as the basic units of coherent star formation in molecular clouds, are now seen to inhabit preferentially cluster complexes tens of parsecs across. This chapter gives an overview of some important properties of the embedded clusters in these complexes and of the complexes themselves, along with the implications of viewing star formation as a molecular-cloud scale process rather than an isolated process at the scale of clusters.

1.1 Introduction

The study of embedded clusters dates back to the first infrared detectors for astronomical use. Still enshrouded in the dusty environment of their natal molecular cloud, embedded clusters are invisible to optical telescopes but reveal themselves as rich and fascinating objects at longer wavelengths. They contain the youngest stars formed and are therefore invaluable probes of the star formation process. Their stars share the initial conditions of their parent clump of gas, inheriting some of its characteristics, later probed by humans in an attempt to understand the sequence of events dominated by the interplay between gravity, turbulence, and magnetic fields that ultimately forms them.

Both observations and theoretical simulations of star formation have grown in number and in detail since the seminal review of Lada and Lada (2003) on embedded clusters. Observationally, the largest leaps forward were the widespread shift from the study of individual embedded clusters to the larger context of their molecular clouds, and the large sky surveys to build an increasingly complete census of the

J. Ascenso (✉)
CENTRA, Instituto Superior Tecnico, Universidade de Lisboa, Av. Rovisco Pais 1, 1049-001 Lisbon, Portugal

Departamento de Engenharia Física da Faculdade de Engenharia, Universidade do Porto, Rua Dr. Roberto Frias, s/n, P-4200-465 Porto, Portugal
e-mail: jascenso@fe.up.pt

S. Stahler (ed.), *The Birth of Star Clusters*, Astrophysics and Space Science Library 424, DOI 10.1007/978-3-319-22801-3_1

star formation in the Galaxy. Also important, the detailed study of extreme star formation events, even by Milky Way's standards, has expanded the parameter space for studies of star formation to the limit of extragalactic studies. These advances were made possible at such a large scale by the deployment of near- and mid-infrared telescopes and instruments, both in ground-based and in space observatories. The Two Micron All Sky Survey (2MASS, Skrutskie et al. 2006), that covers the entire sky, and later the *Spitzer Space Telescope* were invaluable at revealing the detailed intricacies of entire star forming regions as well as to allow a multitude of large scale surveys. *Spitzer* legacy programs such as the Cores to Disks (c2d, Evans et al. 2003), the Galactic Legacy Infrared Mid-Plane Survey Extraordinaire (GLIMPSE, Churchwell et al. 2009; Benjamin et al. 2003), and the MIPSGAL (Carey et al. 2009) programs, as well as dedicated surveys of individual regions, have greatly advanced our understanding of star forming regions, producing numerous catalogues, most of which yet to be fully explored. Ground-based observatories have also contributed significantly with near-infrared telescopes used for surveys (e.g. 2MASS, UKIRT, ESO VISTA), and with near-infrared adaptive optics assisted instruments for deep and high-resolution studies of individual regions (e.g. GEMINI, VLT). In the far-infrared, the *Herschel Space Observatory* (André and Saraceno 2005) is currently providing invaluable insight into the youngest stages of star formation, bridging the gap between the study of pre- and proto-stellar molecular clouds with sub-millimetre and radio telescopes, and the study of embedded clusters at NIR wavelengths. On the opposite end of the spectrum, sensitive X-ray observations of star forming regions, made possible greatly through the *Chandra X-ray Observatory*, have strongly contributed to the effort of assessing the stellar populations of star forming regions.

This chapter provides an overview of the observable properties of embedded clusters in the important context of their molecular clouds, brought to light by this massive technological development. The analysis is limited to Galactic regions—those that can be studied in greater detail—and does not include the interesting star formation taking place at and around the Galactic Centre; the reader is referred to the review by Longmore et al. (2014) for the latter. Section 1.2 of this chapter elaborates on the difficulty of adopting one single definition of "cluster" for all studies of star formation, reviewing the most common definitions in the literature, and what they entail. Section 1.3 reviews the observed structure and morphology of embedded clusters and star forming regions, highlighting the trends that have emerged from the increasing sample of studied clouds, and what they reveal in terms of the underlying processes at play. Section 1.4 describes the constraints on the timescales for star formation, crucial in any theory of star formation, derived from the observations of the ages and age distributions in embedded clusters and cluster complexes.

Other very interesting topics could be addressed in detail in the context of embedded clusters and are only mentioned briefly in this chapter. The stellar mass distributions in clusters and on the molecular cloud scale can reveal important properties of the star formation process; the universality of the initial mass function, and whether or not embedded clusters are mass segregated have been the subject of many interesting studies in the past decade; the consequences of the clustered

environment to individual forming stars at different stages of their evolution, and in particular their formation along with massive stars is also an active topic of research, and one that can help understand the probability of a given star developing planets with certain characteristics. The analysis of the efficiency and of the rate of star formation, both at the embedded cluster and at the molecular cloud scales, is also starting to be possible at great detail for a statistically significant sample of known regions in the Galaxy. The topics included in this chapter are a naturally biased selection of what the author considers the most robust observational advances in the last decade and most susceptible of providing solid constraints to existing theories.

1.2 What Is an Embedded Cluster?

An embedded cluster is a group of young stars that is still embedded in its natal molecular cloud (Fig. 1.1). Although seemingly simple, this definition is all but trivial. The definitions we adopt reflect and, at the same time, somehow limit our understanding of star formation. Let's start with the definition of "embedded" and then move on to the definition of "cluster".

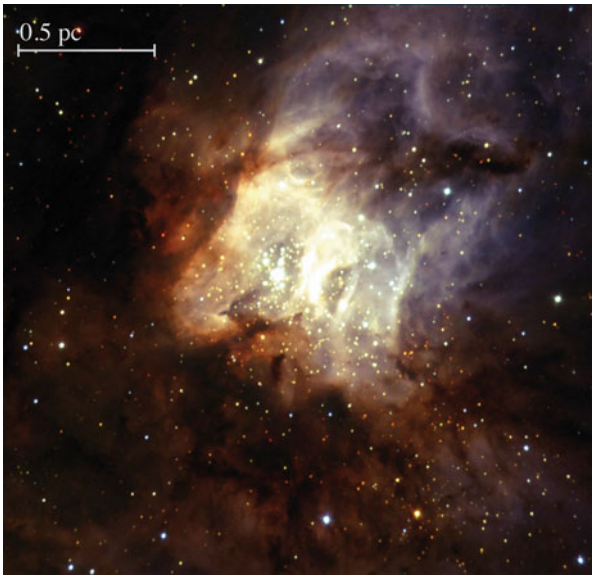

Fig. 1.1 RCW 38 is a young embedded cluster, imaged here in the near-infrared bands J, H and K_S with ESO/NTT/SOFI (Ascenso, Alves et al.)

1.2.1 Defining "Embedded"

An embedded star (or cluster) is one that is still enshrouded in its natal molecular cloud. It is typically not (fully) observable at optical wavelengths due to the heavy obscuration caused by the dust grains in the cloud, but it can be seen in the near-infrared, where young stars emit significantly (e.g. Adams et al. 1987; Robitaille et al. 2006), and the dust is more transparent (Savage and Mathis 1979; Cardelli et al. 1989; Rieke and Lebofsky 1985; Draine 2011). Near-infrared telescopes and instruments are therefore the choice of excellence to detect and characterise embedded objects, and indeed both ground-based and space telescopes equipped with infrared detectors and filters have boosted our demographics and our understanding of embedded clusters exponentially in the past three decades.

It should be noted, perhaps trivially, that not all heavily obscured objects are embedded: there are objects that are just seen behind molecular clouds, and are therefore not within them (e.g. Alves et al. 2001). Objects that are in fact embedded notoriously display signatures of youth. Since stars tend to disperse their natal gas and dust via accretion and feedback over time an embedded star or cluster is one that is necessarily young, and this leads to some unspoken confusion regarding the "embedded" nature of clusters.

The canonical timescale for a cluster to clear enough material to become optically visible is around 5 Myr (Leisawitz et al. 1989), although more recently Morales et al. (2013) analysed the association of several young clusters with molecular material, and proposed an upper limit of the embedded phase of 3 Myr, while Portegies Zwart et al. (2010) quote a duration of 1–2 Myr for the embedded phase of a cluster. But a cluster's embedded phase should be a sensitive function of the mass of the stars being formed. For example, massive stars develop HII regions that are much more efficient in dispersing the cloud material than the outflows from low-mass stars (Matzner 2002), so clusters with massive stars should be the fastest to clear their surroundings and to emerge from their molecular clouds. Therefore, although the condition of being embedded is enough to attest to an object's youth, it is, by itself, a poor criterion for a sample of clusters of uniform age.

On some accounts, the definition of "embedded" is narrowed to refer to a state when the potential of the cluster is dominated by the mass of the molecular cloud (Gutermuth et al. 2009), according to which many known young clusters can no longer be considered embedded. Trumpler 14, Westerlund 2, and NGC3603, for example, are all believed to be well under 5 Myr old, but even though they are still partially obscured by cloud material, they have already cleared most of their intracluster gas. So these clusters are embedded only in the sense that they are still associated with the molecular cloud, since their gravitational potential is no longer dominated by the gas.

For the purpose of this chapter we will focus on clusters that are younger than 5 Myr and still associated with their molecular clouds, regardless of their potential being dominated by the gas.

1.2.2 *Defining "Cluster"*

The definition of "cluster" is more controversial, and it is non-trivial for many reasons. The need to define "cluster" arises in several different contexts, each focused on different aspects. In the context of large-scale observational surveys, for example, a set of uniform criteria is paramount to detect (new) clusters against the field of the Galaxy in an automated yet robust way. When analysing the birth conditions and the evolution of clusters over time, the most useful criterion is probably their dynamical state. Depending on the question one is trying to address, the physical aspects that are considered relevant—and that should therefore be used to define clusters as entities—may vary. Additionally, the details that numerical simulations of star forming molecular clouds are increasingly capable of producing raise the pressure to find observable signatures of some key property of young stellar populations that can be tied to a dominant physical process. It is therefore not surprising to see several definitions of "cluster" in the literature, nor that they evolve alongside with the progress in our numerical capabilities.

Previous to any definition of cluster, one practical difficulty arises already in finding the stars that actually make up a population, since knowing whether a given star is physically associated with its neighbours or if it is only co-located in projection is challenging, especially for more evolved populations like open clusters. Stars younger than a few million years offer the advantage that they share properties that are distinguishable from older stars, providing important clues to their membership (e.g. Lada 1987; Shu and Adams 1987; Adams et al. 1987; Gutermuth et al. 2009; Meyer et al. 1997; Feigelson and Montmerle 1999; Feigelson 2010). Observational studies of clusters therefore often start by identifying the young stellar objects (YSOs), usually by analysing their near-infrared colours and/or X-ray properties, and then proceed to finding over-densities that qualify as clusters by some measure. The cloud material associated with embedded clusters in particular effectively blocks a fraction of background stars, partially filtering out stars unrelated to the cluster and increasing the local stellar density contrast.

Low density groups are sometimes distinguished from clusters and classified as O(B) associations if they contain O (and B) stars (e.g. Blaauw 1964), T associations, if they only contain low-mass stars (Herbig 1962), or R associations, intermediate between the two and associated with bright, reflection nebulæ (van den Bergh 1966). These classes overlap in many cases and have largely fallen into disuse over time. When no criteria other than an overdensity of stars is used, the terminologies "stellar aggregate", "stellar grouping" or similar are also found. The concept of "Correlated Star Formation Event" was introduced by Kroupa et al. (2013) as an alternative to the concept of "cluster"; it refers to all the stars that were formed in one given star formation event over a spatial scale of about one parsec, regardless of their spatial distribution in a star forming region at present. These stars would be coeval to within the duration of the star forming event. Although the identification of such events observationally is limited by our ability to determine individual stellar ages, this is an interesting concept that is perhaps more meaningful in understanding the progression of star formation in a cloud than the overdensity concept of cluster.

1.2.2.1 Morphological Criteria

Empirically, a cluster is an overdensity of physically co-located stars. This definition is often used loosely to refer to all instances of stellar groups. In this sense, detecting clusters can be as straightforward as finding surface density peaks by eye on large-scale images, with or without some additional criterion to minimise contamination from spurious stellar density fluctuations. In the case of young clusters, these criteria are usually a minimum number of members, or the association with some tracer of youth, like outflows, ionised gas, or molecular gas and dust, for example (Faustini et al. 2009; Dutra and Bica 2000; Bica et al. 2003a,b; Borissova et al. 2011, 2014; Majaess 2013; Froebrich et al. 2007).

Quantitatively, several authors have defined several empirical criteria, most often calibrated to detect previously known clusters in blind surveys. Ivanov et al. (2002), for example, require a stellar surface density contrast of at least 3-σ above the galactic background, and at least 50 members to claim the detection of a cluster. Similarly, Kumar et al. (2006) require a stellar surface density contrast greater than 2-σ above the local background, but a minimum number of only eight members. Carpenter (2000) requires that the total number of stars within a closed 2-σ surface density contour exceeds a 5-σ enhancement with respect to the expected stellar background. Porras et al. (2003) differentiate between "clusters" and "groups" based on whether a given region contains more or less than 30 stars, respectively. Alternatively, in a variation of the density-threshold algorithm, Gutermuth (2005), following Casertano and Hut (1985), use the distance to the Nth nearest neighbour as a proxy for local density, eliminating the need to bin the data spatially to produce density maps where to look for enhancements.

Gutermuth et al. (2009) devised a more sophisticated method to isolate what they called "cluster cores" from co-spatial, extended young stellar populations also associated with the cloud; they analyse the separation between neighbouring stars using the minimum spanning tree (MST) algorithm, and define the edge of a cluster core where the MST branch lengths become larger than some critical distance. Bastian et al. (2007) employ the minimum spanning tree in a slightly different way, truncating the separation between stars to a maximum allowed distance to define clusters. Mercer et al. (2005) detect clusters using an algorithm that calculates the probability of a given overdensity being an actual cluster and not a chance projection effect considering the statistical distribution of the background field, still based on geometrical and density enhancement arguments but also on luminosity and colour criteria.

Schmeja (2011) compares the performance of a few different algorithms in finding star clusters, and gives additional references to works where the algorithms were applied. This author finds, as expected, that strongly peaked clusters are easily detected by all algorithms, whereas low contrast clusters can fall below the radar, which reflects the ambiguity in the very definitions.

1.2.2.2 Dynamical Criteria

The previous definitions of clusters as overdensities of stars, although powerful, lack physical grounds. A common physical criterion to define "cluster" observationally is the inferred relative stability of the stellar groups. Lada and Lada (2003) classify a group of young stars as a "cluster" on the basis of its survivability against tidal disruption up to the age of typical open clusters (100 Myr). According to this definition, a group of stars is considered a cluster if it contains more than 35 members, and if its density is higher than $1.0\,M_{\odot}pc^{-3}$; an *embedded* cluster is one that is also "fully or partially embedded in interstellar gas and dust".

In theoretical work and in numerical simulations of star formation, "cluster" is usually synonymous with *bound* group of stars. This definition is useful because it simultaneously contains important information about the molecular cloud from which the cluster formed and about its long-term survivability, and because it leaves out any spurious overdensity of unrelated sources. It is also a *possible* definition in those contexts, since theory has all the information about a given system under investigation, which is almost never the case in the context of observations. Portegies Zwart et al. (2010) (see also Gieles and Portegies Zwart 2011) distinguish between clusters (bound systems) and associations (unbound systems) on the basis of their age with respect to the system's dynamical time.[1] A system whose age is, at present, a few times its dynamical time has survived disruption by dynamical effects for long enough to be considered a "cluster" according to this definition. These systems are likely to survive as bound entities for a significant fraction of a Hubble time (Portegies Zwart et al. 2010).

A dynamical analysis enables many interesting studies, including a comparison between the molecular clouds and their stellar products: systems (or subsystems) that are bound when they are very young are likely to have formed monolithically from a bound, gravity dominated cloud, whereas their unbound counterparts are more likely to have formed from unbound, turbulence supported clouds. But the dynamical state of a cluster is often difficult to assess, and one subject to many uncertainties. In Portegies Zwart et al. (2010), for example, the definition of "cluster" depends strongly on the knowledge of the cluster's age, of its mass, and of its virial radius. The determination of a cluster's age from photometric surveys depends mostly on the knowledge of the distance to the cluster, which can be uncertain by a large amount for clusters that are too far away for current measures of parallax; for example, the distance to the cluster Westerlund 2 ranges from 2.8 to 8 kpc, even in the recent literature (Ascenso et al. 2007a; Carraro et al. 2013; Zeidler et al. 2015; Rauw et al. 2011). ESA's mission Gaia (Gaia Collaboration et al. 2016) will be an invaluable resource for clusters that are already partially revealed in the optical. The determination of a cluster's age (and age spread) is

[1] The dynamical time is the time a typical star would take to cross the system ($t_{dyn} = R_{cl}/\sigma_V$). This is not to be confused with the system's relaxation time—the timescale on which the system reaches equipartition of energy via two-body encounters—which is much larger.

also importantly sensitive to uncertainties in other properties like unresolved stellar multiplicity, differential extinction between cluster members and stellar variability, including episodic accretion, and to the accuracy of the stellar evolutionary tracks themselves (Hartmann 2001; Jeffries 2010; Preibisch 2012). Estimates of cluster masses, on their turn, can be severely affected by incompleteness, poor membership assessment or variable detectability over the surveyed area due to, for example, extended, uneven bright nebula or patchy extinction. Estimates of mass are also only as reliable as the measurements of distance and age of the cluster, which, as outlined above, are significantly uncertain. And depending on the wavelength, they are more or less sensitive to the shape of the local extinction law, and also to the specific pre-main-sequence evolutionary tracks chosen to convert luminosity into mass. Finally, a cluster's virial radius is taken as a factor of the half-light radius and assumes a given stellar density profile. In rigour, only a spectroscopic analysis of a significant fraction of cluster members at moderate spectral resolution can determine their velocity distribution and allow for a proper characterisation of a cluster's dynamical state, but this is discouragingly expensive in observation time. As a consequence, our knowledge of the dynamical state of the many known clusters is still limited to an educated guess, and in particular it is still too unreliable to be a strong observational constraint to theories of star formation.

The very significance of the definitions of "cluster" based on dynamical arguments inferred by observations has been called into question by studies that suggest that there is no fundamental difference between the stellar density distributions of "clusters" and "non-clusters" by any one definition. Bressert et al. (2010), for example, do not find any bimodal signature in the stellar density distribution of several star forming regions that suggests a preferred or a threshold density for "clusters", although their sample includes only a few clusters, of relatively low-mass, and their diagnostics may be considered ambiguous (Pfalzner et al. 2012; Gieles et al. 2012).

In light of the previous arguments, it is clear that we are currently not in position to make a statistically accurate comparison of bound and unbound clusters, or of clusters and associations. At best, we can attempt to rank known clusters in order of density, mass, luminosity, or age, and try to find meaningful correlations that can be used to constrain the physical conditions for star formation under different environments.

In the context of this chapter, a "cluster" will be taken as its most simple literary meaning: a collection of physically associated stars.

1.3 Morphology and Structure

Embedded clusters come in a variety of forms. This can be inferred instantly by comparing the images of a few star forming regions. It was the striking morphological difference between different young clusters that led to their traditional classification as "centrally condensed" or "hierarchical" (Lada and Lada 2003): the first refers to clusters where the surface density has one strong peak and then

smoothly declines radially, and the latter to density distributions with multiple peaks and a high level of substructure.

The importance of defining a cluster's morphology extends beyond the need for uniform characterisation criteria. Rather, different morphologies are produced by different conditions of the progenitor cloud, they reflect different dominant physical phenomena, and they can be predictive of the cluster's survival as bound entities on large timescales or of their demise into field stars.

1.3.1 Observational Challenges

Similar to detecting clusters, analysing their morphology has important observational challenges. Incompleteness is the obvious enemy of morphological studies: often only a relatively small fraction of a cluster's members can be detected. The distance and the limited sensitivity of instruments act against the detection of faint stars; the limited resolution of the instruments acts against resolving individual stars in a cluster, an effect that is additionally amplified in very dense and/or distant clusters; the presence of bright stars hampers the detection of less luminous neighbours out to significant projected distances; and the interstellar extinction and the bright nebula typical of star forming regions, which are almost always variable in embedded clusters, change the detection limits and the completeness spatially, producing artificial structure in the observed distribution of cluster members. Also important is the contamination from field stars, as mentioned before in Sect. 1.2.2; unless cluster members are efficiently distinguished from field stars, the analysis of their spatial distribution can be significantly biased, especially in the case of low surface density clusters.

Infrared observations can minimise some of these effects. Extinction at longer wavelengths is significantly lower than in the optical (Rieke and Lebofsky 1985), providing deeper and more uniform completeness levels. Also, the dynamic range of stellar brightness is lower in the infrared than in the optical, i.e. the luminosity contrast between the massive and low-mass stars will be smaller, making the latter easier to detect.

1.3.2 Cluster Morphologies

The human brain can readily distinguish between a centrally condensed distribution and one that is more substructured, but an objective measure of structure that can be applied uniformly to a large sample, and one that can be quantitatively compared with results from simulations and between different regions is required to build a statistical framework for the properties of star forming regions.

Clusters visually recognised as centrally condensed are generally relatively isolated clusters, with most members located in a relatively small projected area

in the sky. It is possible to define a "centre" for the cluster as the location of the maximum stellar surface density, for example, and the surface density itself then decays away from that centre as a smooth function in a way somewhat resembling globular clusters. Analytically, the surface density decay of a centrally condensed cluster is typically well described by a simple power-law, power-law with a flat core (Elson et al. 1987) or King profile (King 1962, 1966). The latter is parametrised by the density at the cluster's core, by its core radius, and by a tidal radius, and formally describes the density distribution expected of a single-mass dynamically relaxed population that is tidally truncated by an external (galactic) potential. While this is not an accurate description of embedded clusters, the King profile is used as a convenient function with few parameters, allowing for a uniform description of the morphology of centrally condensed clusters (e.g. Hillenbrand and Hartmann 1998; Ascenso et al. 2007a,b; Gutermuth et al. 2008; Sung and Bessell 2004; Wang et al. 2008; Harfst et al. 2010; Kuhn et al. 2010). The Elson et al. (1987) profile is often preferred in numerical simulations of clusters, although it is also used to fit observed density profiles of young clusters (Brandner et al. 2008; Gutermuth et al. 2008; Gouliermis et al. 2004; Sana et al. 2010).

Conversely, the stellar surface density of substructured clusters does not follow a smoothly decaying radial function, instead showing multiple peaks over some projected area. Several metrics have been proposed to describe their fractal-like structure, including the two-point correlation function (Gomez et al. 1993), to describe the probability distribution of any given star having a companion at increasing distances, the distribution of mean surface density of companions of cluster members (Larson 1995, see also Bate et al. (1998)), the normalised correlation length, $\bar{s}$ (Cartwright and Whitworth 2004), defined as the mean separation between cluster members normalised to the radius of the cluster, and the normalised mean edge length, $\bar{m}$, of the minimum spanning tree defined by the cluster members. Cartwright and Whitworth (2004) review these methods in some detail (see also Schmeja and Klessen 2006), and propose what they call the Q-parameter as the most robust parameter to characterise the morphology of a cluster. The Q-parameter is defined as the ratio between $\bar{m}$ and $\bar{s}$, and is able to quantify the degree of subclustering, as well as to distinguish between a centrally condensed morphology and a hierarchical morphology: a Q parameter larger or smaller than 0.8 implies a large-scale radial density gradient or the presence of subclustering, respectively. This parameter has since become a widespread tool to analyse the structure of embedded clusters.

It is worth noting that, in rigour, a substructured distribution of stars, although commonly dubbed "hierarchical", is not necessarily fractal. The loose classification of "hierarchical" in the context of clusters usually refers simply to clusters with more than one peak in stellar density, but Bate et al. (1998) caution that the surface stellar density distribution in a few known star forming regions previously classified as fractal was also consistent with the stars being distributed in random sub-clusters, a non-fractal distribution. This distinction is important when interpreting observations of cloud structure and stellar density distributions in young clusters in light of the dominant physical processes, and also when the number of stars is small enough that statistical fluctuations can lead to the illusion of substructure (Fig. 1.2).

Fig. 1.2 The large-scale view of NGC 6334 imaged by ESO/VISTA in the near-infrared bands J, H and K_S (galactic North is up, galactic East is to the left, credit ESO/J. Emerson/VISTA). NGC 6334 contains several embedded clusters along its actively star forming ridge

1.3.3 The Molecular Cloud Scale

The prolific effort to find new clusters in the Galaxy has already yielded a sizeable database of embedded cluster candidates. Some surveys target individual clusters and are typically deep enough to produce a comprehensive census of the stellar population down to the low-mass end of the YSO mass spectrum; due to observational time constraints and spatial resolution limitations, these surveys are mostly limited to nearby, low-mass clouds, that harbour relatively low-mass clusters as well. Other works encompassed observations of entire molecular clouds, revealing interesting patterns of young stellar populations (Fig. 1.2). A few examples of deep surveys covering the molecular cloud scale are the early works of Lada et al. (1991), Lada (1992) and Strom et al. (1993), for example, and the more recent dedicated surveys of, e.g. Allen et al. (2007), Carpenter (2000), Evans et al. (2009), Román-Zúñiga et al. (2008), Gutermuth et al. (2009), Gutermuth et al. (2011) and Kuhn et al. (2014). On the massive end, only two surveys covered the molecular cloud scale to a level comparable to more nearby star forming regions: Preibisch et al. (2014) and Reipurth and Schneider (2008, see also Wright et al. (2014)) review the stellar population and the clusters of the Carina and of the Cygnus X complexes, respectively, each containing well over 10^4 $M_\odot$ in young stars.

Blind, large scale or even full sky surveys provide more complete censuses of embedded clusters at the galactic scale, necessarily covering a wider range in cluster mass and different environments. Even though so far most of the cluster candidates identified in these surveys are not yet sufficiently characterised—for most cases even

the number of stars belonging to each cluster is not yet properly assessed—several tendencies have already began to emerge, mostly supporting on a larger scale the understanding derived from surveys of local star forming regions.

1.3.3.1 Cluster Complexes

Surveys of individual molecular clouds have long suggested that star forming regions are significantly substructured. Rather than containing one single cluster with all or most YSOs, many nearby regions contain several clusters organised in a more or less hierarchical way (Fig. 1.3). A few well-known examples covering the low-mass end are Serpens and Perseus, Lupus, and Chameleon (I and II); Orion, the Rosette Complex, Vela, the W3/W4/W5 complex, and RCW 106 are examples in the intermediate-mass range; and among the most massive we know the Carina complex, Cygnus X, NGC 6334, W51, W49A, that contain clusters that are more massive individually than entire lower-mass cluster complexes (see several authors in Reipurth (2008a,b), and Evans et al. (2009), Román-Zúñiga et al. (2008), Nguyen et al. (2015) for descriptions of these regions).

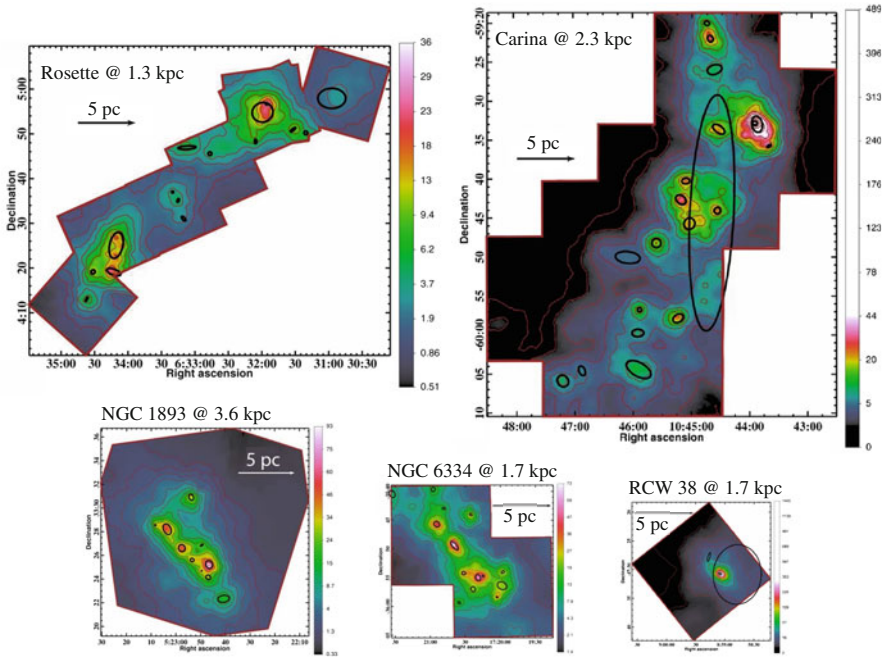

Fig. 1.3 Observed YSO surface density distributions for a few star forming regions registered to the same physical scale (adapted from Kuhn et al. 2014). These distributions illustrate well the cluster complex morphology in almost all regions that were observed in this work at the few-parsec scale. The colour bars are in units of stars pc^{-2}

The same tendency is found in the most recent embedded cluster catalogues that span wider ranges in heliocentric distance, and presumably in mass; in the sample of Bica et al. (2003a) 25% of embedded clusters have other clusters in their immediate (projected) surroundings; Morales et al. (2013) find that more than 50% of the clusters in their sample are in cluster complexes; Kuhn et al. (2014) find substructured distributions of YSOs in all of their targeted clouds. In their sample of very young embedded clusters, Kumar et al. (2006) also find a strong tendency for complexes to show substructure with 80% of the clouds exhibiting multi-peaked surface density distributions, already at very young ages; these authors applied the same morphological classification to the relatively older embedded clusters of Lada and Lada (2003) and found a similar fraction. Although these numbers are not yet entirely reliable given the incompleteness of these surveys, they suggest that the most common outcome of star formation from molecular clouds is then cluster complexes,[2] as opposed to single clusters.

The size of these cluster complexes in the Galaxy varies from a few to a few tens of parsecs along their largest dimension. The spread in their clusters' size is smaller, around 1 pc (e.g. Kuhn et al. 2014; Banerjee and Kroupa 2017), mostly depending on the definition of cluster size and on differing observational limitations. To some degree, the distinction between a centrally concentrated and a hierarchical stellar distribution can be regarded as a matter of scale, as already hinted by Lada and Lada (2003): at the tens of parsec scale (cluster complex scale) substructure is ubiquitous, whereas at the 1-pc scale (cluster scale) whatever observed substructure is usually undistinguishable from statistical number fluctuations in a centrally peaked, more or less elongated, distribution.

Overall, the distribution of young stars in cluster complexes is reminiscent of the distribution of dense gas in molecular clouds (e.g. Lada et al. 1996; Testi et al. 2000; Gutermuth et al. 2009), both with respect to their hierarchical structure and to their geometry. Like molecular clouds (e.g. Rathborne et al. 2006; Peretto and Fuller 2009; Churchwell et al. 2009, see also Fig. 1.4), cluster complexes have elongated morphologies with large aspect ratios. This resemblance is expected if cluster complexes are younger than the dynamical timescale for the clouds, otherwise they would have had time to dissolve and take on more spherical geometries. At the cluster scale, because it is smaller, there may have already been significant dynamical mixing during the early embedded phase or even earlier, in the gas phase (Elmegreen 2006). Still, although the presence of substructure in a stellar density distribution implies that the system is not yet dynamically relaxed, some authors caution against taking the similarity of cloud morphology and the distribution of YSOs at face value, showing numerical simulations that produce hierarchical distributions of YSOs that bear little resemblance to the original distribution of dense gas (Parker and Dale 2015). Also, even though substructure is typically

[2] I will refer to "cluster complex" as the global clustered YSO population within one cloud, and to "cluster" as the individual clusters within the complex.

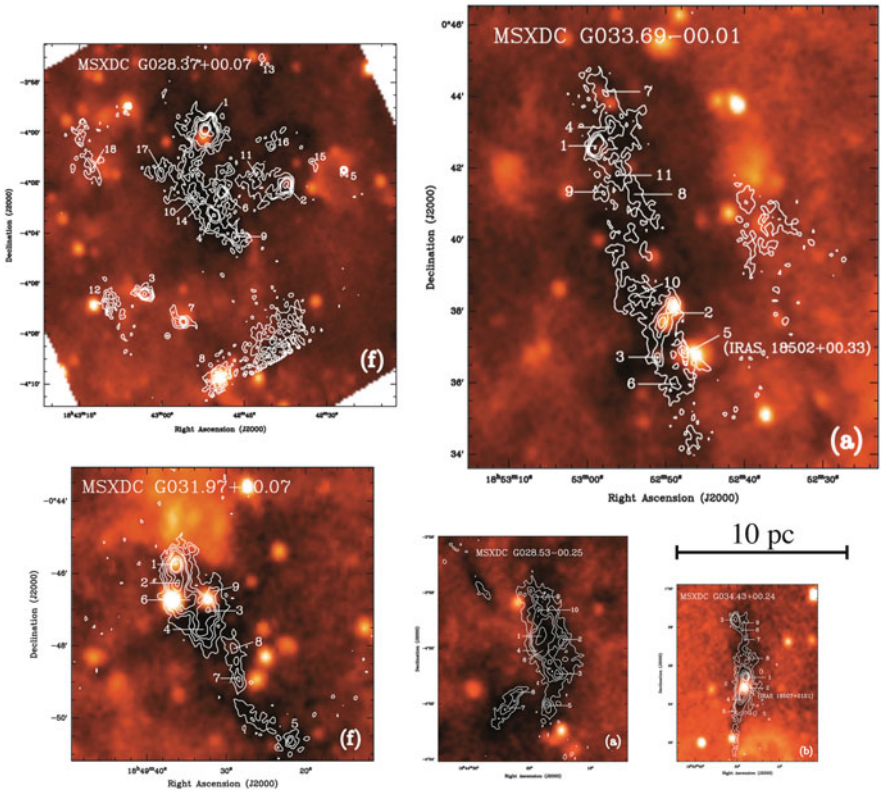

Fig. 1.4 Infrared dark clouds, presumably the precursors to clusters, often show elongated morphologies with large aspect ratios and multi-peaked density distributions over scales of ∼10 pc, similar to cluster complexes. Figure adapted from Rathborne et al. (2006)

interpreted as evidence of turbulence as an important agent in driving the process of star formation, Krumholz (2014) argue that a hierarchical distribution of YSOs does not necessarily stem from turbulence-dominated initial conditions.

1.3.3.2 Isolated Clusters

Although the majority of star forming regions that have been studied in detail exhibits a significant degree of substructure over scales of the order of tens of parsecs (cluster complexes), there are a few interesting exceptions—single clusters that appear to be the sole significant product of their natal molecular cloud. In the Galaxy, excluding the peculiar vicinities of the Galactic Centre, a few embedded clusters stand out as relatively isolated, as far as current data suggests: Westerlund

2, NGC 3603, NGC 6611 and RCW 38 are a few of those,[3] and it is likely that more examples will emerge as the new candidate catalogues start to be explored at higher detail with state-of-the-art instrumentation. These clusters exhibit centrally concentrated morphologies with faint hints of substructure at most, and sizes less than, or of the order of 1 pc, similar to individual clusters in the cluster complexes mentioned in the previous section. However, their progenitor clouds do not seem to harbour other clusters at present.

Low mass clusters are not considered in this context; since their density contrast with respect to their surroundings is typically small, any low-level extended population of young stars in the cloud will provide comparable numbers of stars that they cannot be considered isolated anymore. This introduces a bias that needs to be kept in mind: the fact that the four isolated clusters considered here are significantly more massive than the average individual cluster in cluster complexes does not necessarily mean that isolated clusters tend to be massive, nor that massive clusters tend to be isolated (Carina is an excellent counter-example of the latter). We will come back to these isolated clusters later.

1.3.3.3 Unclustered Young Stars

As implied above, not all young stars reside in the cores of embedded clusters. Rather, a variable fraction of these stars is found distributed throughout the embedding molecular cloud in relative isolation (Fig. 1.5). Large scale infrared surveys, and later the *Spitzer Space Telescope* were instrumental in showing that these distributed populations are ubiquitous in star forming regions, most notably in cluster complexes. X-ray and infrared combined YSO maps, less vulnerable to contamination from unrelated sources albeit also less complete in particular mass ranges, confirm the presence of widespread populations of young stars outside the main clusters in star forming regions.

A reliable estimate of the actual fraction of isolated stars is contingent on the definition of cluster and on several observational parameters. To zeroth order, accounting for a significant fraction of the YSOs in a given region requires a sensitive sample with uniform completeness limits, which is often challenging (see Sect. 1.3.1). Also, since these objects are scattered over large areas, observations should cover a large enough field of view outside the main clusters, ideally covering the full extent of the molecular cloud at comparable depth, which is observationally expensive. It is equally important to accurately estimate the number of stars that are *in* clusters, since underestimating this number will enhance the weight of the extended population; this often requires high resolution observations to adequately

[3] A few other known clusters could be mentioned, such as W40, GM 24 or NGC 6618, for example, but the YSO populations of these clusters are not yet sufficiently well characterised to establish them as isolated in their clouds, or they are too close to other star forming regions that they may be part of a larger complex.

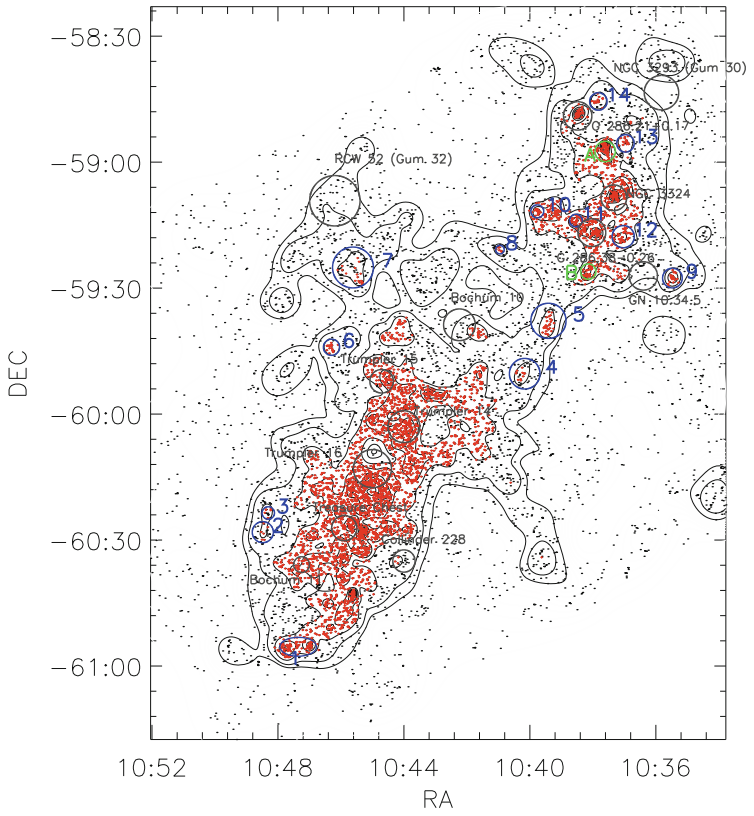

Fig. 1.5 YSOs are often found permeating entire star forming regions. This plot of the position (*left*) and surface density (*right*) of YSOs in the Carina Nebula from Zeidler et al. (2016) shows a widespread population of unclustered YSOs throughout the complex

resolve the crowded cores of dense clusters and account for the most of their stellar population as possible. And finally, a reliable decontamination from field stars and distant galaxies is paramount, since unrelated objects will artificially inflate the fraction of distributed YSOs fairly easily. Once the young star population is properly accounted for, the definitions of cluster and of the boundaries of clusters obviously play an critical role in the calculation of the fraction of stars that are outside clusters.

With this in mind, most estimates point to a relatively low fraction of stars found outside clusters: in Orion A and B estimates are of a maximum of 25% distributed YSOs (Allen et al. 2007; Carpenter 2000), around the same fraction as for Ophiucus (11–32%, Allen et al. 2007) and Perseus (20%, Carpenter 2000; Jørgensen et al. 2008; Evans et al. 2009); in Lupus and in the Rosette complex, the fraction of YSOs found outside clusters is estimated around 15% (Merín et al. 2008; Román-Zúñiga et al. 2008, respectively); Monoceros R2 has a higher fraction of distributed YSOs, about 44% (Carpenter 2000). On the more massive end, in the W3/W4/W5 complex

more than 50% of the stars are found in the five most massive clusters; since the complex contains nineteen clusters in total, this suggests that only a small fraction of YSOs is distributed (Carpenter 2000); in the Carina complex an estimated 35% of YSOs is found outside the main cluster cores (Feigelson et al. 2011), although the number of cluster members could be underestimated in this particular case since these observations cannot fully resolve the highly crowded cores of the most massive clusters, significantly underestimating the number of stars in these clusters. Surveys including multiple star forming regions estimate an overall fraction of "isolated" objects between 10 and 20%, with upper limits of 40% (Porras et al. 2003; Koenig and Leisawitz 2014; Gutermuth et al. 2009; Evans et al. 2009).

The spatial distribution of these isolated stars in the cloud can be useful in constraining their origin. They are often found to be spread throughout the molecular clouds in a more or less uniform way, or, in more quiescent clouds, still tracing the dense gas. These stars can have formed at their current locations in relative isolation, they can have been ejected from the nearby clusters, or they can be the populations of slightly older clusters formed in the same cloud that have already began to disperse away. A typically small fraction of these stars is found in the nearby outskirts of clusters, toward structures that were created by their feedback, for example at the edges of bubbles or in pillars carved by the strong winds of the most massive stars. Theoretically, stellar feedback is capable of collecting and compressing existing molecular gas and create the conditions for star formation in regions that would otherwise probably not form stars, and this is likely the origin of some of the stars in the distributed populations, but results from numerical simulations suggest that this may account for only a small fraction. All these scenarios produce stars with different ages compared to the stars in clusters.

1.4 Age Spreads

As we have seen above, embedded clusters and star forming regions in general are complex systems. It is not surprising that their histories are also not simple. A molecular cloud does not form only one generation of stars; rather, it is common to find populations separated in age by a few million years associated with the same molecular cloud, clearly suggesting that star formation does not occur in a single burst and then stops. Understanding these age spreads, which reflect the star formation history of the cloud, is fundamental to understand the very process of star formation.

A review of the methods used to determine ages is beyond the scope of this book, and the reader is referred to recent reviews (Preibisch 2012; Soderblom 2010, and references therein) for a discussion. It is nevertheless important to mention that the determination of ages is subject to many uncertainties, and that it is common for different methods to return significantly different values. This is caused both by observational limitations and by uncertainties in the pre-main-sequence evolutionary models used to convert luminosities and colours into ages

and masses (e.g. Getman et al. 2014; Jeffries 2010; Baraffe et al. 2012; Preibisch 2012; Naylor 2009; Hartmann 2001; Burningham et al. 2005; Hillenbrand et al. 2008). Using synthetic clusters, Preibisch (2012), for example, showed that a coeval population of 3 Myr stars with the stellar variability, excess emission from circumstellar material, and binarity fraction expected for young stars, and subject to the differential interstellar extinction typically found toward embedded clusters can present near-infrared colours consistent with an age spread of more than 1 Myr.

For this reason the absolute ages inferred observationally for star forming regions are still rather unreliable. Relative ages can be more robust, as these are often inferred indirectly through the analysis of the presence of circumstellar material. Circumstellar envelopes and discs dissipate over time, such that the fraction of stars in a cluster with circumstellar discs, for example, can provide a good handle on the relative age of a cluster (Haisch et al. 2001; Briceño et al. 2007): clusters with a large fraction of stars still with strong disc emission are presumably younger than clusters where the majority of stars is already discless. The characterisation of the emission from the circumstellar material via spectral energy distribution (SED) fitting (Robitaille et al. 2006) provides a finer age classification, since the dispersal of discs follows a predictable logic. These have the inconvenient that the timescale for the dissipation of discs is mass-dependent, and that the fraction and characteristics of discs may vary for the same age as a function of environment; for example, the circumstellar material of stars that have close massive neighbours may be affected by their strong feedback (e.g. Preibisch et al. 2011; Johnstone et al. 1998). But in general SEDs allow the distinction between younger and older pre-main-sequence stars, which, along with colour information and reasonably complete censuses of the young stellar populations, is useful in constraining the progression of star formation in a cloud.

Understanding age spreads in star forming regions is important at several different scales, which again argues for surveys of entire molecular clouds as important complements to narrower surveys of individual clusters. On the scale of individual clusters, it is interesting to assess the timescale over which their stars form, whether individual clusters are formed rapidly, in a timescale comparable to their dynamical time, or slowly and in quasi-equilibrium (e.g. Elmegreen 2000; Tan et al. 2006); it is interesting to assess whether they are formed monolithically already as large clusters from a massive clump of gas, or are assembled from several subclusters. These different scenarios require different conditions from the progenitor cloud, and they operate under the influence of different dominant physical processes, so they provide invaluable constraints towards a predictive theory of cloud evolution and star formation. At the scale of cluster complexes—essentially the molecular cloud scale—it is interesting to understand whether a cloud forms stars as a whole, or rather if different regions collapse to form stars at different times; if the prompter for star formation is internal or external to the cloud; if star formation develops spontaneously from quiescent gas or if it is induced by some event. Often neglected, the unclustered population distributed in the cloud is intimately connected with the star formation on the clustered scales, and its age distribution also contains important information.

The characterisation of age spreads and of star formation histories at any scale is most meaningful in young regions for two reasons. First, the relation of age with the fraction of stars with circumstellar material becomes less sensitive for older populations, as stars dissipate their discs. While the class 0/I phase is very short, around 0.5 million years (Evans et al. 2009), class II and III stages last longer, around a few million years. Second, given enough time, dynamical processes will erase most of the imprint of the properties of the progenitor molecular cloud on the stellar distributions, decreasing the sensitivity of the analysis of ages and age spreads in the context of their spatial distributions to the star formation history of the cloud.

The term "age spread" will be used here to refer to the age distribution of stars in a given context. We will review age spreads within individual clusters, age spreads in molecular clouds and age spreads of the distributed/unclustered population of molecular clouds. Some authors prefer the term "age difference" when referring to the different ages of several clusters in the same molecular cloud, reserving the term "age spread" to populations that have formed together, in the same local event of star formation (Preibisch 2012).

1.4.1 Age Spreads in Cluster Complexes

There is still not sufficient evidence to say whether different parts of the same molecular cloud "know" about each other's status of star formation. Depending on which phenomenon triggers star formation in a cloud, it is possible that it occurs independently in regions that are sufficiently far apart, that events of star formation are sequentially triggered internally, or that the same trigger initiates star formation in the cloud as a whole in a more or less synchronised way. The differences are significant from the point of view of the mechanisms at play, which means that studies of star formation benefit greatly from analysing molecular clouds globally rather than only individual regions within them. Cluster complexes in particular offer a unique opportunity to study the progression of star formation in a cloud, since each cluster can be viewed as a local event of star formation within the common global history of the cloud.

Clusters of the same cluster complex often show different ages, separated by as much as a few million years, as is illustrated in Fig. 1.6 for the Carina Nebula. This is seen across the mass spectrum of star forming regions. In the low-mass end, Palla and Stahler (2000), for example, found age spreads larger than 3 Myr in several nearby star forming regions (Taurus-Auriga, Lupus, Chamaeleon, Upper Scorpius, and NGC 2264). Massive complexes, such as Orion, Carina, or Cygnus, for example, show similar age spreads. Interestingly, the maximum age gap between clusters of the same complex if ordered chronologically is not too wide. There are a few known examples of clouds that have "very old" (a few tens of million years) and very young clusters with nothing in between (Chamaeleon may be one such example), but most clouds show smaller inter-cluster age gaps of the order of 1 Myr

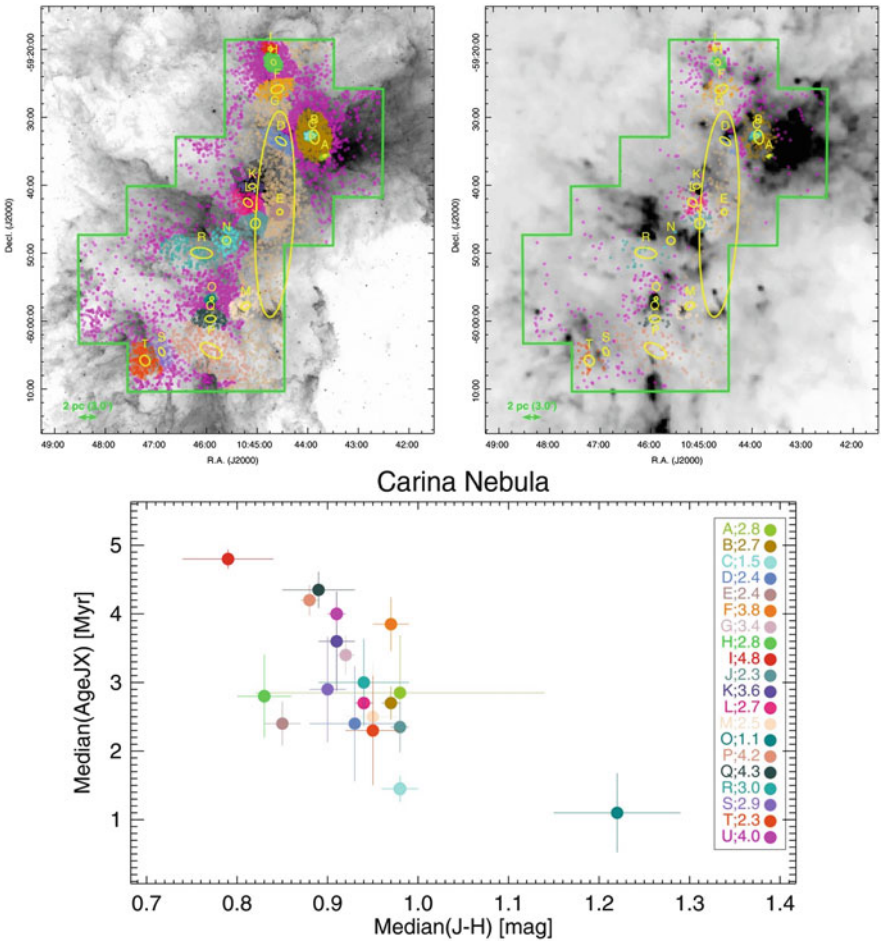

Fig. 1.6 Most cluster complexes harbour clusters with different ages but the global age spread is not too wide, nor is the age gap between any two clusters ordered chronologically. As in the Carina Nebula shown in this figure (from Getman et al. 2014), the spatial distribution of ages is often inconsistent with internal triggering being the dominant mechanism for the propagation of star formation within the cloud

or less. In other words, molecular clouds do not typically take long breaks between forming clusters once they start, but they do not seem to collapse as a whole either.

It is tempting to interpret the temporal proximity between different clusters in the same cloud as evidence for sequential star formation, with the first star formation event(s) triggering the formation of the following, especially in clusters containing massive stars, those that produce the most feedback. Although feedback can have a destructive potential at small distances from the source star (e.g. Ngoumou et al. 2015), it can also collect and compress less dense gas farther in the molecular

cloud, or just precipitate the collapse of pre-existing neighbouring clumps that would otherwise take longer to, or never even, form stars and clusters (Elmegreen and Lada 1977; Bertoldi 1989; Whitworth et al. 1994; Dale et al. 2007). The exact importance of these mechanisms as triggers for star formation depends on the density distribution of the cloud prior to the influence of feedback, and on the mass and location of the star(s) that produce the feedback. The latter is particularly relevant because only stars capable of producing an HII regions are able to trigger the collapse of neighbouring clumps. In theory, the perturbation from the first generation of stars is able to propagate and produce new stars (and clusters) at the necessary speed across a typical cloud to reproduce the observed age spreads at the observed distances between clusters[4] (e.g. Elmegreen and Lada 1977), but in this scenario the spatial distribution of ages at the scale of the cloud should show a coherent progression. In the sample of star forming regions of Getman et al. (2014)—the largest to date with stellar ages determined uniformly within molecular clouds—only about one-third of the complexes show reasonably coherent age gradients between clusters, suggesting that internal triggering may not be the dominant controller of the progression of cluster formation in molecular clouds.

Alternatively, an external event such as the passage of a spiral density wave, nearby supernova events, or cloud–cloud collisions (e.g. Elmegreen 1998; Cedrés et al. 2013; Dobbs and Pringle 2009; Dobbs et al. 2015; Dale 2015; Fierlinger et al. 2016) could produce age distributions in clusters that are not necessarily ordered, depending on the geometry and alignment of the cloud relative to the triggering event. This would explain the lack of a coherent age gradient mentioned above, and that some cluster complexes show no significant age spread between clusters at all. For example, Ybarra et al. (2013) suggest that star formation started everywhere in the Rosette Complex around the same time, suggesting that star formation was somehow synchronised globally, presumably by an external event. Also NGC 6334, the Cat's Paw Nebula, hosts a couple of slightly older clusters, already partially revealed in the optical, and then a molecular ridge spanning 10 pc of active star formation occurring in discrete pockets at present (Persi and Tapia 2008), challenging any reasonable internally triggered star formation interpretation. The external trigger scenario is attractive to explain such a large scale coordination of star formation, although it is equally difficult to prove. At some level it is not much different to discuss the formation of stars at the molecular cloud scale and the formation of the density structure in molecular clouds themselves, since it is not likely that molecular clouds and dense clumps within them form spontaneously from the interstellar medium. Considering that stars form everywhere there is dense enough gas (Lada et al. 2010), the problem of the progression of star formation within a cloud is reduced to the problem of the formation of molecular clouds.

[4]For a 10 pc long cloud with a global age spread of 5 million years, star formation would have to propagate at an average speed of at least 2 pc Myr^{-1}, or 2 km s^{-1}. This is about 10 times the typical sound speed in molecular clouds assuming a temperature of 10 K ($c_S = (kT/m_{H_2})^{1/2} \sim 0.2$ km s^{-1}). For example, Getman et al. (2014) suggest a propagation speed of star formation around 5 km s^{-1} in some of their clouds.

At the molecular cloud scale, massive isolated clusters (see Sect. 1.3.3.2) are particularly interesting from their age distribution perspective. These are apparently the sole products of their molecular clouds: what is their history? Can they just be the first generation of star formation in clouds that will later form other clusters and host cluster complexes? Since the known clusters of this type are already around 1–2 Myr old and their clouds do not show evidence for substantial ongoing star formation, this scenario would produce complexes with considerable age spreads, depending on the timescale for star formation in different parts of the cloud. This would not be unseen; the age spread in Chamaeleon between regions I and III is likely larger than 10 Myr, and there does not seem to be any cluster with an age intermediate between these two regions. But this appears to be a rather atypical case. Carina, for example, has an estimated age spread for clusters of ∼8 million years, between Trumpler 15 and the Treasure Chest cluster (Preibisch et al. 2011; Smith et al. 2005) but small age gaps between consecutively formed clusters. Westerlund 2, classified above as one such isolated clusters, has a very young, very embedded cluster forming just outside its borders, with hints of massive star formation even, suggesting that clustered star formation is still ongoing in its progenitor cloud. This is, however, the only site of active cluster formation known in the cloud, which suggests that this cloud is not likely to form a complex with many clusters, at least not with a small age spread. Other clouds that contain clusters as massive as Westerlund 2 (e.g. Carina, Cygnus, W49A) all contain several similarly massive clusters, reinforcing the idea that Westerlund 2 (and also NGC 3606 by similar arguments) is indeed different from cluster complexes. RCW 38, the youngest of the three isolated clusters considered here, also shows some evidence for ongoing clustered star formation in its vicinities (Winston et al. 2011); given its younger age (0.5 Myr) this cluster is more likely to evolve into a (small) cluster complex than Westerlund 2 or NGC 3603.

The observation of cluster complexes is thus unveiling a non-obvious scenario for the progression of star formation in molecular clouds. It is clear that molecular clouds do not collapse globally but rather in clumps that form clusters, and that there is no unique trend for the age distribution of the clusters they produce. Also important, molecular clouds seem to exhaust their star formation potential fairly rapidly, on timescales of the order of a few Myr, the maximum age spreads found in cluster complexes and the time in which they typically disperse.

1.4.2 Age Spreads in Individual Clusters

Individual clusters refer here to clusters that have formed in a single event, regardless of having formed alongside other clusters in the same cloud. The Orion Nebula Cluster is an example of an individual cluster in a molecular cloud (Orion A) that hosts other clusters.

Most detailed studies suggest that the age spread in individual embedded clusters is very small, typically within the age determination uncertainties, if it exists at

all (e.g. Preibisch et al. 2002; Moitinho et al. 2001; Jeffries et al. 2011; Banerjee and Kroupa 2014, 2015; Getman et al. 2014). The main observational difficulty when analysing individual clusters—more important even than the uncertainties from the age determination method—is contamination from stars that do not belong to the cluster under study. Since clusters often reside in cluster complexes, the contamination by stars from the complex may be significant, and since the contaminant stars will also be young, distinguishing them from a given cluster population can be difficult. As such, published claims of significant age spreads within young clusters are often challenged by subsequent larger scale surveys that reveal populations of older YSOs spread out in the cloud, distributed more or less uniformly far beyond the cluster's borders, suggesting that they are not part of that cluster but are rather different populations within the complex (see Sect. 1.4.3). If these stars are taken as cluster members they will misleadingly present as evidence for age spreads within the cluster.

The Orion Nebula Cluster is an example where considerable age spreads have often been reported (Palla and Stahler 1999; Huff and Stahler 2007; Da Rio et al. 2010). The recent study of Getman et al. (2014) suggests a shallow radial gradient of increasing age that is interpreted by the authors as the cluster having formed outside-in. However, these results are equally compatible with the cluster having a small age spread and being immerse in a distributed population of older stars that do not belong to the cluster: the cluster stars would bias the age toward younger values in the centre, and the older, extended population would start to weigh in toward the peripheries as it outnumbered the cluster members. An older population, unrelated to the ONC but extending well into its foreground, has indeed been found by Alves and Bouy (2012), which could account for the older stars that make up the observed pseudo age spread. On the more massive end, Ascenso et al. (2007b) found hints of a core-halo morphology in their small field survey of the cluster Trumper 14, where the "halo" stars seemed older and appeared unclustered; later, a significant population of older stars permeating the entire Carina Complex was uncovered by a large-scale survey (Preibisch et al. 2011).

Indeed, studies of the population of YSOs in different stages of evolution at the molecular cloud scale, made possible largely through *Spitzer* observations, reveal this as a pattern: although young sources are clustered in general (see Sect. 1.3), class 0/I YSOs—those with the most circumstellar material and the youngest—consistently appear more tightly clustered than their class II and class III counterparts. Figure 1.7 illustrates this typical distribution for the Orion clouds. Since the class 0/I stage is very short-lived, the position of these stars is very likely the position at which they formed, supporting the view that stars form in dense configurations within clouds (e.g. Lada and Lada 2003). The wider distribution of class II and class III sources likely reflects the characteristics of the unclustered population of stars in molecular clouds (see Sect. 1.4.3).

Massive clusters are particularly interesting in terms of their age spreads. They contain extraordinary numbers of stars, which means they were formed from an extraordinarily massive gas clump or assembled by mergers of smaller clusters. Observationally, some of the most massive embedded clusters known in the Galaxy

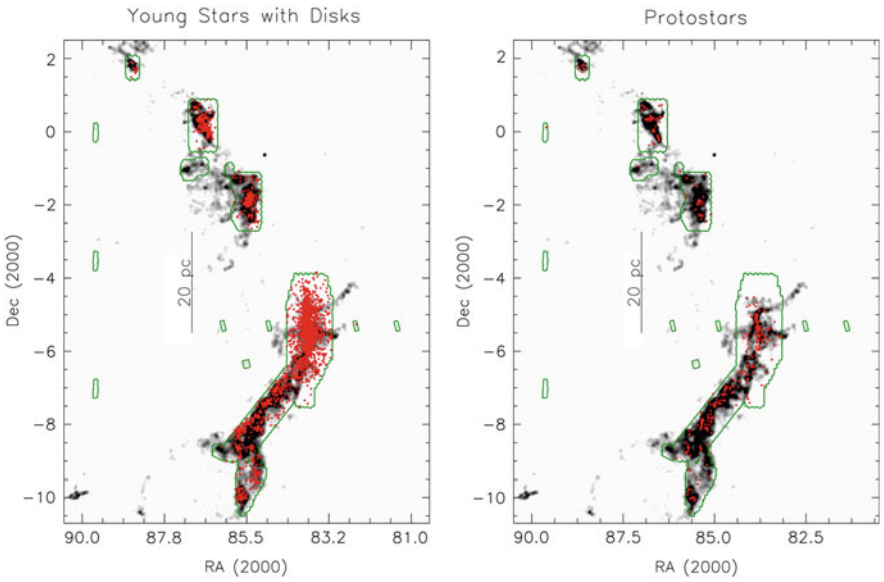

Fig. 1.7 Younger, class 0/I sources are typically found more tightly clustered than the older, class II sources. This is illustrated in this figure from Megeath et al. (2012) of the Orion molecular clouds showing the distribution of protostars (*right*) and the distribution of older stars with discs (*left*)

outside the Galactic Centre do not show evidence for significant age spreads (Kudryavtseva et al. 2012; Stolte et al. 2004; Ascenso et al. 2007a,b). Banerjee and Kroupa (2014, 2015) find that the observed properties of NGC 3603 in particular are compatible with a starburst scenario and incompatible with it having been formed through the coalescence of smaller clusters. The suggested near-instantaneous, monolithic formation of such massive clusters raises important questions regarding the support of molecular clouds against gravitational collapse over long enough timescales to assemble the necessary amount of dense gas (see Sect. 1.6).

In light of existing evidence, individual clusters do not seem to have significant intrinsic age spreads. Events that form individual clusters seem to operate on very small timescales, of the order of, or smaller than, the local dynamical times (less than 1 Myr for typical clusters).

1.4.3 Age Spreads of the Unclustered Stars

The distributed stars found both in and around cluster complexes and isolated clusters (see Sect. 1.3.3.3) show a wide range in ages. Several of these populations[5]

[5]In this context, I use the term "population" loosely to refer to the collection of stars that are not clustered, without any implication regarding common properties or origin.

were found and studied in multiple works using observations and methods sensitive to different ages, from less than 1 to 20 Myr. Adding to the results of the individual studies, this diversity shows that the age spreads of these distributed populations is rather large; and rather extreme as well: the oldest, and often the youngest, stars in a star forming region are found in the distributed population.

The youngest distributed stars are often found toward the edges of the clouds, projected against shells, bright-rimmed clouds or pillars, that are illuminated and carved by the action of a cluster of slightly older stars. This spatial correlation, sometimes backed by other indicators, has been widely interpreted as evidence for star formation triggered by existing stars or clusters. Dale et al. (2015) compiled a list of the many studies that have claimed observational evidence for triggered star formation, most from positional arguments.

A small fraction of very young stars and protostars is sometimes found along dense filaments of gas and dust in more quiescent regions of the clouds, although not far from the location of the older stars and clusters. These are not randomly distributed in the clouds, but apart from their ordered location along the filaments, they are not significantly clustered at the individual cluster ($\sim$1 pc) scale, unlike the majority of stars of the same age.

Most of the distributed population of stars in a cloud is made up of intermediate age pre-main-sequence stars (class II). Although they usually also follow the overall clustering pattern of the star forming region, they are typically less clustered than class 0/I objects. It is not uncommon to find class II stars pervading the clouds at the cluster complex scale (a few to a few tens of parsecs), both in embedded and in less embedded regions. At this point it is useful to note that class II (and III) sources can represent a wide range of stellar ages, since more massive stars dissipate their circumstellar material more rapidly, therefore acquiring the SED signatures characteristic of class II YSOs at younger ages (Williams and Cieza 2011). It is therefore expected that (younger) class II sources be found clustering with coeval class I sources, and that older class II sources be found spread out in the cloud, as observed.

Wide distributions of old pre-main-sequence stars, as old as 20 Myr, have also been reported in star forming regions dominated by younger stars and clusters. In the Galaxy, Orion A, the Carina Complex, NGC 3603 and NGC 6611 in the Eagle Nebula all have reports of "old" populations in their clouds. Interestingly, in Orion A and in Carina, these populations can tentatively be attributed to an identifiable cluster, namely NGC 1980 and Trumpler 15, respectively, both containing massive stars. Conversely, the "old" populations of NGC 6611 and of NGC 3603 have not been associated with any existing cluster, although a giant molecular shell is observed in the Eagle Nebula that can be the remnant of a supernova event (Moriguchi et al. 2002), suggesting a possible association with the old pre-main-sequence population.

1.5 Stellar Mass Distributions

This chapter would not be complete without a dedicated word about stellar mass distributions in clusters. It is widely accepted that the observed stellar mass distribution of a young cluster is a good approximation of its initial mass function (IMF), and that this IMF seems to be fairly universal across the spectrum of cluster properties (e.g. Lada and Lada 2003; Bastian et al. 2010; Kroupa et al. 2013). On the theoretical side, we have presently reached a stage where all accepted theories of star formation are capable of producing the observed IMF of clusters, undermining its predictive or constraining power. But recent and upcoming observing facilities may change that by changing the focus of IMF studies slightly.

For example, it is not yet clear when exactly the IMF becomes fully assembled, or whether massive or low mass stars preferentially form first, or what impact, if any, the first formed stars have on the formation of the subsequent population. In the future it will become increasingly easy to study extremely young clusters, including of the more distant massive clusters in the Galaxy, with adequate resolution and sensitivity. Is the IMF of these clusters any different from that of older clusters that have presumably already finished most of their star formation activity, suggesting that different mass stars form at different stages?

Also, it is only apparently clear that the IMF is indeed universal in all environments. The same IMF is found in most star forming regions, but some "regions", especially the less massive, include stars from large physical volumes, sometimes from entire clouds, whereas others refer only to individual clusters at the 1-pc scale. It is not clear how these similar IMFs over such different scales can be made consistent. As more and more cluster complexes are studied it will become increasingly possible to assess the mass distribution of the entire stellar population formed by one cloud with respect to the IMF of the individual clusters, and to the IMF of the distributed population. We must then understand what is the meaning of an IMF at the molecular cloud scale. If different star formation events (clusters) in the same cloud (cluster complex) are independent from each other, then so should their IMFs, otherwise star formation must be set at the global scale of the cloud rather than locally, reducing the distance between studies of stars in clusters and cluster complexes and studies of molecular clouds and assembly of dense gas, towards a consistent picture of star formation.

1.6 Embedded Clusters and Star Formation

Clusters and cluster complexes reveal intricate and often puzzling star formation histories in molecular clouds. Observational results suggest that star formation is a rapid and likely discontinuous process at the molecular cloud scale. Rather than forming one cluster, each cloud typically forms multiple clusters over timescales of a few million years. Individual clusters themselves appear to be mostly coeval, but

around and between them significant populations of stars with wide age spreads are often found. What can these spatial and age distributions tell us about the origin and the progression of star formation in clouds?

Different possibilities considered by theory and reproduced by several flavours of numerical simulations predict different properties for star forming regions that are becoming increasingly possible to compare with observations. To this end one important step has been taken in the last decade: more and more star forming regions are being studied at the molecular cloud scale. The structure and age distributions of young stars in molecular clouds are particularly relevant in constraining the timescales for star formation, both locally and globally, indirectly favouring one or other aspect of the theoretical possibilities.

Individual embedded clusters span a wide range in mass and density, but there is very little convincing evidence that they have large age spreads (see Sect. 1.4.2). Individual embedded clusters younger than $\sim$1 Myr are common, which suggests that clusters are formed fairly rapidly, on timescales comparable to their dynamical times. Their smoothly peaked morphologies at the $\sim$1 pc scale already at these very young ages suggest that they were formed from a molecular cloud clump that was itself already dense with a peaked density distribution, or that any initial substructure must have been erased very efficiently. The latter would argue for a slower process of star formation that would allow time for dynamics to act on pre-existing structure, but large scale observations of pre- or proto-stellar clumps in massive, infrared dark clouds, presumably the precursors to embedded clusters, often show individual clumps about the size of embedded clusters already with fairly symmetric density distributions (Shirley et al. 2003; Ragan et al. 2012; Traficante et al. 2015). A large fraction of these clumps shows signs of star formation, supporting further the view that the starless phase of a dense molecular clump is very short. Taken at face value, this and the small age spreads in individual embedded clusters require that, for each cluster, a significant amount of dense gas be gathered prior to the onset of star formation, and that it does not fragment significantly in the process. This may require a support against gravitational collapse until conditions are met that precipitate the quasi-instantaneous formation of a whole cluster of stars, especially for the most massive; or, alternatively, this could be achieved if the dense gas itself was gathered by a rapid phenomenon, such as collisions between molecular clouds, collisions of filaments within molecular clouds or through the action of external agents, such as supernovae.

Cloud–cloud collisions have been recently invoked to explain the rapid formation of massive clusters such as NGC 3603 and Westerlund 2. Based on radio kinematic data, Furukawa et al. (2009) and Fukui et al. (2014) find that each of these clusters lies at the interface between two massive molecular clouds that seem to be moving towards each other with relative velocities of $\sim$20 km/s. Hydrodynamical simulations confirm that cloud–cloud collisions can form bound and massive clumps and cores (Habe and Ohta 1992; Anathpindika 2010; Inoue and Fukui 2013; Wu et al. 2015), but studies of the characteristics of the produced stellar population are still necessary to show that this mechanism is capable of forming entire (massive) clusters. The same type of kinematical signature is found in clouds harbouring lower

mass and more substructured star forming regions, such as M20 (Torii et al. 2011) and RCW120 (Torii et al. 2015), suggesting that this mechanism, if indeed capable of forming clusters, can reproduce a range of observed properties. This scenario is particularly appealing in the cases of isolated massive young clusters, where the gathering of the required amounts of dense gas is particularly challenging.

Competing theories, complete with numerical simulations, posit that clusters may be assembled hierarchically, with stars forming along filaments and then falling to the deepest part of the potential well, forming a cluster (Bonnell et al. 2003; McMillan et al. 2007; Bate 2009; Maschberger et al. 2010). Filaments are a distinct characteristic in all molecular clouds, and young stars within them are also ubiquitous in star forming regions, especially in low-mass environments, lending support to this scenario. These simulations do not require a mechanism to assemble massive clumps of gas prior to star formation, and they also form clusters very rapidly, although the actual duration of the star formation event depends sensitively on the initial conditions. As a by-product, very extended haloes of stars must form from stars that are ejected from the cluster core through dynamical interactions as the subclusters merge together. This could provide a natural origin for the extended population of young stars that is very often found in star forming regions (Sects. 1.3.3.3 and 1.4.3), and an overall consistent picture for the formation of all stars in star forming regions. However, the age of the extended population should be consistent with the (narrow) age range of the final clusters, whereas the majority of the distributed stars is often older than the clustered population. Unless, since ages are often inferred through the presence of circumstellar material, the ejection process strips or truncates the discs from these stars, making them appear older to such age diagnostics. For lack of computational power, it is also not yet clear that numerical simulations that form clusters via hierarchical assembly can produce clusters as massive as the most massive observed, or that they can reproduce the larger scale cluster-complex morphology prevalent in clouds with the observed age spreads under realistic initial conditions.

References

Adams, F.C., Lada, C.J., Shu, F.H.: Spectral evolution of young stellar objects. Astrophys. J. **312**, 788–806 (1987). doi:10.1086/164924

Allen, L., Megeath, S.T., Gutermuth, R., Myers, P.C., Wolk, S., Adams, F.C., Muzerolle, J., Young, E., Pipher, J.L.: The structure and evolution of young stellar clusters. In: Protostars and Planets V, pp. 361–376 (2007). astro-ph/0603096

Alves, J., Bouy, H.: Orion revisited. I. The massive cluster in front of the Orion nebula cluster. Astron. Astrophys. **547**, A97 (2012). doi:10.1051/0004-6361/201220119. 1209.3787

Alves, J.F., Lada, C.J., Lada, E.A.: Internal structure of a cold dark molecular cloud inferred from the extinction of background starlight. Nature **409**, 159–161 (2001)

Anathpindika, S.V.: Collision between dissimilar clouds: stability of the bow-shock, and the formation of pre-stellar cores. Mon. Not. R. Astron. Soc. **405**, 1431–1443 (2010). doi:10.1111/j.1365-2966.2010.16541.x

André, P., Saraceno, P.: Probing the earliest phases of star formation: an Herschel photometric survey of nearby molecular clouds. In: Wilson, A. (ed.) ESA Special Publication, vol. 577, pp. 179–184

Ascenso, J., Alves, J., Beletsky, Y., Lago, M.T.V.T.: Near-IR imaging of Galactic massive clusters: Westerlund 2. Astron. Astrophys. **466**, 137–149 (2007a). doi:10.1051/0004-6361:20066433

Ascenso, J., Alves, J., Vicente, S., Lago, M.T.V.T.: NTT and VLT diffraction limited imaging of Trumpler 14: revealing a massive core-halo cluster. Astron. Astrophys. **476**, 199–215 (2007b). doi:10.1051/0004-6361:20077210

Banerjee, S., Kroupa, P.: A perfect starburst cluster made in one go: the NGC 3603 young cluster. Astrophys. J. **787**, 158 (2014). doi:10.1088/0004-637X/787/2/158. 1403.4601

Banerjee, S., Kroupa, P.: The formation of NGC 3603 young starburst cluster: 'prompt' hierarchical assembly or monolithic starburst? Mon. Not. R. Astron. Soc. **447**, 728–746 (2015). doi:10.1093/mnras/stu2445, 1412.1473

Banerjee, S., Kroupa, P.: How can young massive clusters reach their present-day sizes? Astron. Astrophys. **597**, A28 (2017). doi:10.1051/0004-6361/201526928. 1510.04293

Baraffe, I., Vorobyov, E., Chabrier, G.: Observed luminosity spread in young clusters and FU Ori stars: a unified picture. Astrophys. J. **756**, 118 (2012). doi:10.1088/0004-637X/756/2/118, 1206.2374

Bastian, N., Ercolano, B., Gieles, M., Rosolowsky, E., Scheepmaker, R.A., Gutermuth, R., Efremov, Y.: Hierarchical star formation in M33: fundamental properties of the star-forming regions. Mon. Not. R. Astron. Soc. **379**, 1302–1312 (2007). doi:10.1111/j.1365-2966.2007.12064.x, 0706.0495

Bastian, N., Covey, K.R., Meyer, M.R.: A universal Stellar initial mass function? A critical look at variations. Annu. Rev. Astron. Astrophys. **48**, 339–389 (2010). doi:10.1146/annurev-astro-082708-101642, 1001.2965

Bate, M.R.: The dependence of star formation on initial conditions and molecular cloud structure. Mon. Not. R. Astron. Soc. **397**, 232–248 (2009). doi:10.1111/j.1365-2966.2009.14970.x, 0905.3562

Bate, M.R., Clarke, C.J., McCaughrean, M.J.: Interpreting the mean surface density of companions in star-forming regions. Mon. Not. R. Astron. Soc. **297**, 1163–1181 (1998). doi:10.1046/j.1365-8711.1998.01565.x, astro-ph/9804154

Benjamin, R.A., Churchwell, E., Babler, B.L., Bania, T.M., Clemens, D.P., Cohen, M., Dickey, J.M., Indebetouw, R., Jackson, J.M., Kobulnicky, H.A., Lazarian, A., Marston, A.P., Mathis, J.S., Meade, M.R., Seager, S., Stolovy, S.R., Watson, C., Whitney, B.A., Wolff, M.J., Wolfire, M.G.: GLIMPSE. I. An SIRTF legacy project to map the inner galaxy. Publ. Astron. Soc. Pac. **115**, 953–964 (2003). doi:10.1086/376696. astro-ph/0306274

Bertoldi, F.: The photoevaporation of interstellar clouds. I - Radiation-driven implosion. Astrophys. J. **346**, 735–755 (1989). doi:10.1086/168055

Bica, E., Dutra, C.M., Barbuy, B.: A Catalogue of infrared star clusters and Stellar groups. Astron. Astrophys. **397**, 177–180 (2003a). doi:10.1051/0004-6361:20021479, astro-ph/0210302

Bica, E., Dutra, C.M., Soares, J., Barbuy, B.: New infrared star clusters in the Northern and Equatorial Milky Way with 2MASS. Astron. Astrophys. **404**, 223–232 (2003b). doi:10.1051/0004-6361:20030486, astro-ph/0304379

Blaauw, A.: The O associations in the solar neighborhood. Annu. Rev. Astron. Astrophys. **2**, 213 (1964). doi:10.1146/annurev.aa.02.090164.001241

Bonnell, I.A., Bate, M.R., Vine, S.G.: The hierarchical formation of a stellar cluster. Mon. Not. R. Astron. Soc. **343**, 413–418 (2003). doi:10.1046/j.1365-8711.2003.06687.x, arXiv:astro-ph/0305082

Borissova, J., Bonatto, C., Kurtev, R., Clarke, J.R.A., Peñaloza, F., Sale, S.E., Minniti, D., Alonso-García, J., Artigau, E., Barbá, R., Bica, E., Baume, G.L., Catelan, M., Chenè, A.N., Dias, B., Folkes, S.L., Froebrich, D., Geisler, D., de Grijs, R., Hanson, M.M., Hempel, M., Ivanov, V.D., Kumar, M.S.N., Lucas, P., Mauro, F., Moni Bidin, C., Rejkuba, M., Saito, R.K., Tamura, M., Toledo, I.: New Galactic star clusters discovered in the VVV survey. Astron. Astrophys. **532**, A131 (2011). doi:10.1051/0004-6361/201116662. 1106.3045

Borissova, J., Chené, A.N., Ramírez Alegría, S., Sharma, S., Clarke, J.R.A., Kurtev, R., Negueruela, I., Marco, A., Amigo, P., Minniti, D., Bica, E., Bonatto, C., Catelan, M., Fierro, C., Geisler, D., Gromadzki, M., Hempel, M., Hanson, M.M., Ivanov, V.D., Lucas, P., Majaess, D., Moni Bidin, C., Popescu, B., Saito, R.K.: New galactic star clusters discovered in the VVV survey. Candidates projected on the inner disk and bulge. Astron. Astrophys. **569**, A24 (2014). doi:10.1051/0004-6361/201322483, 1406.7051

Brandner, W., Clark, J.S., Stolte, A., Waters, R., Negueruela, I., Goodwin, S.P.: Intermediate to low-mass stellar content of Westerlund 1. Astron. Astrophys. **478**, 137–149 (2008). doi:10.1051/0004-6361:20077579, 0711.1624

Bressert, E., Bastian, N., Gutermuth, R., Megeath, S.T., Allen, L., Evans, N.J. II, Rebull, L.M., Hatchell, J., Johnstone, D., Bourke, T.L., Cieza, L.A., Harvey, P.M., Merin, B., Ray, T.P., Tothill, N.F.H.: The spatial distribution of star formation in the solar neighbourhood: do all stars form in dense clusters? Mon. Not. R. Astron. Soc. **409**, L54–L58 (2010). doi:10.1111/j.1745-3933.2010.00946.x, 1009.1150

Briceño, C., Hartmann, L., Hernández, J., Calvet, N., Vivas, A.K., Furesz, G., Szentgyorgyi, A.: 25 Orionis: a kinematically distinct 10 Myr old group in Orion OB1a. Astrophys. J. **661**, 1119–1128 (2007). doi:10.1086/513087. astro-ph/0701710

Burningham, B., Naylor, T., Littlefair, S.P., Jeffries, R.D.: Can variability account for apparent age spreads in OB association colour-magnitude diagrams? Mon. Not. R. Astron. Soc. **363**, 1389–1397 (2005). doi:10.1111/j.1365-2966.2005.09535.x, astro-ph/0508487

Cardelli, J.A., Clayton, G.C., Mathis, J.S.: The relationship between infrared, optical, and ultraviolet extinction. Astrophys. J. **345**, 245–256 (1989). doi:10.1086/167900

Carey, S.J., Noriega-Crespo, A., Mizuno, D.R., Shenoy, S., Paladini, R., Kraemer, K.E., Price, S.D., Flagey, N., Ryan, E., Ingalls, J.G., Kuchar, T.A., Pinheiro Gonçalves, D., Indebetouw, R., Billot, N., Marleau, F.R., Padgett, D.L., Rebull, L.M., Bressert, E., Ali, B., Molinari, S., Martin, P.G., Berriman, G.B., Boulanger, F., Latter, W.B., Miville-Deschenes, M.A., Shipman, R., Testi, L.: MIPSGAL: a survey of the inner galactic plane at 24 and 70 μm. Publ. Astron. Soc. Pac. **121**, 76–97 (2009). doi:10.1086/596581

Carpenter, J.M.: 2MASS observations of the Perseus, Orion A, Orion B, and Monoceros R2 molecular clouds. Astron. J. **120**, 3139–3161 (2000). doi:10.1086/316845. astro-ph/0009118

Carraro, G., Turner, D., Majaess, D., Baume, G.: The distance to the young open cluster Westerlund 2. Astron. Astrophys. **555**, A50 (2013). doi:10.1051/0004-6361/201321421, 1305.4309

Cartwright, A., Whitworth, A.P.: The statistical analysis of star clusters. Mon. Not. R. Astron. Soc. **348**, 589–598 (2004). doi:10.1111/j.1365-2966.2004.07360.x. astro-ph/0403474

Casertano, S., Hut, P.: Core radius and density measurements in N-body experiments connections with theoretical and observational definitions. Astrophys. J. **298**, 80–94 (1985). doi:10.1086/163589

Cedrés, B., Cepa, J., Bongiovanni, Á., Castañeda, H., Sánchez-Portal, M., Tomita, A.: Density waves and star formation in grand-design spirals. Astron. Astrophys. **560**, A59 (2013). doi:10.1051/0004-6361/201321588. 1310.4325

Churchwell, E., Babler, B.L., Meade, M.R., Whitney, B.A., Benjamin, R., Indebetouw, R., Cyganowski, C., Robitaille, T.P., Povich, M., Watson, C., Bracker, S.: The Spitzer/GLIMPSE surveys: a new view of the Milky way. Publ. Astron. Soc. Pac. **121**, 213–230 (2009). doi:10.1086/597811

Da Rio, N., Robberto, M., Soderblom, D.R., Panagia, N., Hillenbrand, L.A., Palla, F., Stassun, K.G.: A multi-color optical survey of the Orion Nebula cluster. II. The H-R diagram. Astrophys. J. **722**, 1092–1114 (2010). doi:10.1088/0004-637X/722/2/1092, 1008.1265

Dale, J.E.: The modelling of feedback in star formation simulations. New Astron. Rev. **68**, 1–33 (2015). doi:10.1016/j.newar.2015.06.001, 1508.06054

Dale, J.E., Bonnell, I.A., Whitworth, A.P.: Ionization-induced star formation - I. The collect-and-collapse model. Mon. Not. R. Astron. Soc. **375**, 1291–1298 (2007). doi:10.1111/j.1365-2966.2006.11368.x, astro-ph/0612128

Dale, J.E., Haworth, T.J., Bressert, E.: The dangers of being trigger-happy. Mon. Not. R. Astron. Soc. **450**, 1199–1211 (2015). doi:10.1093/mnras/stv396. 1502.05865

Dobbs, C.L., Pringle, J.E.: A simple model for the relationship between star formation and surface density. Mon. Not. R. Astron. Soc. **396**, 1579–1588 (2009). doi: 10.1111/j.1365-2966.2009.14815.x, 0903.4098

Dobbs, C.L., Pringle, J.E., Duarte-Cabral, A.: The frequency and nature of 'cloud–cloud collisions' in galaxies. Mon. Not. R. Astron. Soc. **446**, 3608–3620 (2015). doi:10.1093/mnras/stu2319, 1411.0840

Draine, B.T.: Physics of the interstellar and intergalactic medium (2011)

Dutra, C.M., Bica, E.: New star clusters projected close to the Galactic Centre. Astron. Astrophys. **359**, L9–L12 (2000), astro-ph/0006409

Elmegreen, B.G.: Observations and theory of dynamical triggers for star formation. In: Woodward, C.E., Shull, J.M., Thronson, H.A. Jr (eds.) Origins, Astronomical Society of the Pacific Conference Series, vol. 148, p. 150 (1998). astro-ph/9712352

Elmegreen, B.G.: Star formation in a crossing time. Astrophys. J. **530**, 277–281 (2000). doi:10.1086/308361, astro-ph/9911172

Elmegreen, B.G.: Formation and Evolution of Young Massive Clusters (2006). ArXiv Astrophysics e-prints astro-ph/0610679

Elmegreen, B.G., Lada, C.J.: Sequential formation of subgroups in OB associations. Astrophys. J. **214**, 725–741 (1977). doi:10.1086/155302

Elson, R.A.W., Fall, S.M., Freeman, K.C.: The structure of young star clusters in the Large Magellanic Cloud. Astrophys. J. **323**, 54–78 (1987). doi:10.1086/165807

Evans, N.J. II, Allen, L.E., Blake, G.A., Boogert, A.C.A., Bourke, T., Harvey, P.M., Kessler, J.E., Koerner, D.W., Lee, C.W., Mundy, L.G., Myers, P.C., Padgett, D.L., Pontoppidan, K., Sargent, A.I., Stapelfeldt, K.R., van Dishoeck, E.F., Young, C.H., Young, K.E.: From molecular cores to planet-forming disks: an SIRTF legacy program. Publ. Astron. Soc. Pac. **115**, 965–980 (2003). doi:10.1086/376697. astro-ph/0305127

Evans, N.J. II, Dunham, M.M., Jørgensen, J.K., Enoch, M.L., Merín, B., van Dishoeck, E.F., Alcalá, J.M., Myers, P.C., Stapelfeldt, K.R., Huard, T.L., Allen, L.E., Harvey, P.M., van Kempen, T., Blake, G.A., Koerner, D.W., Mundy, L.G., Padgett, D.L., Sargent, A.I.: The spitzer c2d legacy results: star-formation rates and efficiencies; evolution and lifetimes. Astrophys. J. Suppl. Ser. **181**, 321-350 (2009). doi:10.1088/0067-0049/181/2/321, 0811.1059

Faustini, F., Molinari, S., Testi, L., Brand, J.: Properties of Stellar clusters around high-mass young stars. Astron. Astrophys. **503**, 801–816 (2009). doi:10.1051/0004-6361/20079145, 0904.3342

Feigelson, E.D.: X-ray insights into star and planet formation. Proc. Natl. Acad. Sci. **107**, 7153–7157 (2010). doi:10.1073/pnas.0913952107

Feigelson, E.D., Montmerle, T.: High-energy processes in young stellar objects. Annu. Rev. Astron. Astrophys. **37**, 363–408 (1999). doi:10.1146/annurev.astro.37.1.363

Feigelson, E.D., Getman, K.V., Townsley, L.K., Broos, P.S., Povich, M.S., Garmire, G.P., King, R.R., Montmerle, T., Preibisch, T., Smith, N., Stassun, K.G., Wang, J., Wolk, S., Zinnecker, H.: X-ray star clusters in the Carina complex. Astrophys. J. Suppl. Ser. **194**, 9 (2011). doi:10.1088/0067-0049/194/1/9, 1103.0802

Fierlinger, K.M., Burkert, A., Ntormousi, E., Fierlinger, P., Schartmann, M., Ballone, A., Krause, M.G.H., Diehl, R.: Stellar feedback efficiencies: supernovae versus stellar winds. Mon. Not. R. Astron. Soc. **456**, 710–730 (2016). doi:10.1093/mnras/stv2699, 1511.05151

Froebrich, D., Scholz, A., Raftery, C.L.: A systematic survey for infrared star clusters with |b| lt 20 deg using 2MASS. Mon. Not. R. Astron. Soc. **374**, 399–408 (2007). doi:10.1111/j.1365-2966.2006.11148.x, astro-ph/0610146

Fukui, Y., Ohama, A., Hanaoka, N., Furukawa, N., Torii, K., Dawson, J.R., Mizuno, N., Hasegawa, K., Fukuda, T., Soga, S., Moribe, N., Kuroda, Y., Hayakawa, T., Kawamura, A., Kuwahara, T., Yamamoto, H., Okuda, T., Onishi, T., Maezawa, H., Mizuno, A.: Molecular clouds toward the super star cluster NGC 3603 possible evidence for a cloud–cloud collision in triggering the cluster formation. Astrophys. J. **780**, 36 (2014). doi:10.1088/0004-637X/780/1/36. 1306.2090

Furukawa, N., Dawson, J.R., Ohama, A., Kawamura, A., Mizuno, N., Onishi, T., Fukui, Y.: Molecular clouds toward RCW49 and Westerlund 2: evidence for cluster formation triggered by cloud–cloud collision. Astrophys. J. Lett. **696**, L115–L119 (2009). doi:10.1088/0004-637X/696/2/L115, 0904.0286

Gaia Collaboration, Prusti, T., de Bruijne, J.H.J., Brown, A.G.A., Vallenari, A., Babusiaux, C., Bailer-Jones, C.A.L., Bastian, U., Biermann, M., Evans, D.W., et al.: The Gaia mission. Astron. Astrophys. **595**, A1 (2016). doi:10.1051/0004-6361/201629272, 1609.04153

Getman, K.V., Feigelson, E.D., Kuhn, M.A., Broos, P.S., Townsley, L.K., Naylor, T., Povich, M.S., Luhman, K.L., Garmire, G.P.: Age gradients in the stellar populations of massive star forming regions based on a new stellar chronometer. Astrophys. J. **787**, 108 (2014). doi:10.1088/0004-637X/787/2/108. 1403.2741

Gieles, M., Portegies Zwart, S.F.: The distinction between star clusters and associations. Mon. Not. R. Astron. Soc. **410**, L6–L7 (2011). doi:10.1111/j.1745-3933.2010.00967.x. 1010.1720

Gieles, M., Moeckel, N., Clarke, C.J.: Do all stars in the solar neighbourhood form in clusters? A cautionary note on the use of the distribution of surface densities. Mon. Not. R. Astron. Soc. **426**, L11–L15 (2012). doi:10.1111/j.1745-3933.2012.01312.x, 1207.2059

Gomez, M., Hartmann, L., Kenyon, S.J., Hewett, R.: On the spatial distribution of pre-main-sequence stars in Taurus. Astron. J. **105**, 1927–1937 (1993). doi:10.1086/116567

Gouliermis, D., Keller, S.C., Kontizas, M., Kontizas, E., Bellas-Velidis, I.: Mass segregation in young Magellanic Cloud star clusters: four clusters observed with HST. Astron. Astrophys. **416**, 137–155 (2004). doi:10.1051/0004-6361:20031702, arXiv:astro-ph/0311477

Gutermuth, R.A.: The initial configuration of young stellar clusters. PhD thesis, University of Rochester, New York (2005)

Gutermuth, R.A., Myers, P.C., Megeath, S.T., Allen, L.E., Pipher, J.L., Muzerolle, J., Porras, A., Winston, E., Fazio, G.: Spitzer observations of NGC 1333: a study of structure and evolution in a nearby embedded cluster. Astrophys. J. **674**, 336–356 (2008). doi:10.1086/524722, 0710.1860

Gutermuth, R.A., Megeath, S.T., Myers, P.C., Allen, L.E., Pipher, J.L., Fazio, G.G.: A spitzer survey of young stellar clusters within one kiloparsec of the sun: cluster core extraction and basic structural analysis. Astrophys. J. Suppl. Ser. **184**, 18–83 (2009). doi:10.1088/0067-0049/184/1/18, 0906.0201

Gutermuth, R.A., Pipher, J.L., Megeath, S.T., Myers, P.C., Allen, L.E., Allen, T.S.: A correlation between surface densities of young stellar objects and gas in eight nearby molecular clouds. Astrophys. J. **739**, 84 (2011). doi:10.1088/0004-637X/739/2/84, 1107.0966

Habe, A., Ohta, K.: Gravitational instability induced by a cloud–cloud collision - the case of head-on collisions between clouds with different sizes and densities. Publ. Astron. Soc. Jpn. **44**, 203–226 (1992)

Haisch, K.E. Jr., Lada, E.A., Lada, C.J.: Disk frequencies and lifetimes in young clusters. Astrophys. J. Lett. **553**, L153–L156 (2001). doi:10.1086/320685. astro-ph/0104347

Harfst, S., Portegies Zwart, S., Stolte, A.: Reconstructing the Arches cluster - I. Constraining the initial conditions. Mon. Not. R. Astron. Soc. **409**, 628–638 (2010). doi:10.1111/j.1365-2966.2010.17326.x, 0911.3058

Hartmann, L.: On age spreads in star-forming regions. Astron. J. **121**, 1030–1039 (2001). doi:10.1086/318770

Herbig, G.H.: The properties and problems of T Tauri stars and related objects. Adv. Astron. Astrophys. **1**, 47–103 (1962)

Hillenbrand, L.A., Hartmann, L.W.: A preliminary study of the Orion Nebula Cluster structure and dynamics. Astrophys. J. **492**, 540–553 (1998). doi:10.1086/305076

Hillenbrand, L.A., Bauermeister, A., White, R.J.: An assessment of hr diagram constraints on ages and age spreads in star-forming regions and young clusters. In: van Belle, G. (ed.) 14th Cambridge Workshop on Cool Stars, Stellar Systems, and the Sun, Astronomical Society of the Pacific Conference Series, vol. 384, p. 200 (2008), astro-ph/0703642

Huff, E.M., Stahler, S.W.: Cluster formation in contracting molecular clouds. Astrophys. J. **666**, 281–289 (2007). doi:10.1086/520574, 0708.1004

Inoue, T., Fukui, Y.: Formation of massive molecular cloud cores by cloud–cloud collision. Astrophys. J. Lett. **774**, L31 (2013). doi:10.1088/2041-8205/774/2/L31. 1305.4655

Ivanov, V.D., Borissova, J., Pessev, P., Ivanov, G.R., Kurtev, R.: Discovery of new Milky Way star clusters candidates in the 2MASS point source catalog. Astron. Astrophys. **394**, L1–L4 (2002). doi:10.1051/0004-6361:20021208. astro-ph/0208376

Jeffries, R.: Ages and age spreads in young clusters. In: JENAM 2010, Joint European and National Astronomy Meeting, p. 177 (2010)

Jeffries, R.D., Littlefair, S.P., Naylor, T., Mayne, N.J.: No wide spread of stellar ages in the Orion Nebula Cluster. Mon. Not. R. Astron. Soc. **418**, 1948–1958 (2011). doi:10.1111/j.1365-2966.2011.19613.x, 1108.2052

Johnstone, D., Hollenbach, D., Bally, J.: Photoevaporation of disks and clumps by nearby massive stars: application to disk destruction in the Orion Nebula. Astrophys. J. **499**, 758–776 (1998). doi:10.1086/305658

Jørgensen, J.K., Johnstone, D., Kirk, H., Myers, P.C., Allen, L.E., Shirley, Y.L.: Current star formation in the ophiuchus and perseus molecular clouds: constraints and comparisons from unbiased submillimeter and mid-infrared surveys. II. Astrophys. J. **683**, 822–843 (2008). doi:10.1086/589956. 0805.0599

King, I.: The structure of star clusters. I. an empirical density law. Astron. J. **67**, 471–485 (1962)

King, I.R.: The structure of star clusters. III. Some simple dynamical models. Astron. J. **71**, 64 (1966). doi:10.1086/109857

Koenig, X.P., Leisawitz, D.T.: A classification scheme for young stellar objects using the wide-field infrared survey explorer AllWISE catalog: revealing low-density star formation in the outer galaxy. Astrophys. J. **791**, 131 (2014). doi:10.1088/0004-637X/791/2/131, 1407.2262

Kroupa, P., Weidner, C., Pflamm-Altenburg, J., Thies, I., Dabringhausen, J., Marks, M., Maschberger, T.: The stellar and sub-stellar initial mass function of simple and composite populations, p 115 (2013). doi:10.1007/978-94-007-5612-0_4

Krumholz, M.R.: The big problems in star formation: The star formation rate, stellar clustering, and the initial mass function. Phys. Rep. 539:49–134 (2014). doi:10.1016/j.physrep.2014.02.001, 1402.0867

Kudryavtseva, N., Brandner, W., Gennaro, M., Rochau, B., Stolte, A., Andersen, M., Da Rio, N., Henning, T., Tognelli, E., Hogg, D., Clark, S., Waters, R.: Instantaneous starburst of the massive clusters Westerlund 1 and NGC 3603 YC. Astrophys. J. Lett. **750**, L44 (2012). doi:10.1088/2041-8205/750/2/L44. 1204.5481

Kuhn, M.A., Getman, K.V., Feigelson, E.D., Reipurth, B., Rodney, S.A., Garmire, G.P.: A Chandra observation of the obscured star-forming complex W40. Astrophys. J. **725**, 2485–2506 (2010). doi:10.1088/0004-637X/725/2/2485, 1010.5434

Kuhn, M.A., Feigelson, E.D., Getman, K.V., Baddeley, A.J., Broos, P.S., Sills, A., Bate, M.R., Povich, M.S., Luhman, K.L., Busk, H.A., Naylor, T., King, R.R.: The spatial structure of young stellar clusters. I. Subclusters. Astrophys. J. **787**, 107 (2014). doi:10.1088/0004-637X/787/2/107, 1403.4252

Kumar, M.S.N., Keto, E., Clerkin, E.: The youngest stellar clusters. Clusters associated with massive protostellar candidates. Astron. Astrophys. **449**, 1033–1041 (2006). doi:10.1051/0004-6361:20053104, astro-ph/0512266

Lada, C.J.: Star formation - From OB associations to protostars. In: Peimbert, M., Jugaku, J. (eds.) Star Forming Regions, IAU Symposium, vol. 115, pp. 1–17 (1987)

Lada, C.J., Lada, E.A.: Embedded clusters in molecular clouds. Annu. Rev. Astron. Astrophys. **41**, 57–115 (2003). doi:10.1146/annurev.astro.41.011802.094844. astro-ph/0301540

Lada, C.J., Alves, J., Lada, E.A.: Near-infrared imaging of embedded clusters: NGC 1333. Astron. J. **111**, 1964 (1996). doi:10.1086/117933

Lada, C.J., Lombardi, M., Alves, J.F.: On the star formation rates in molecular clouds. Astrophys. J. **724**, 687–693 (2010). doi:10.1088/0004-637X/724/1/687. 1009.2985

Lada, E.A.: Global star formation in the L1630 molecular cloud. Astrophys. J. Lett. **393**, L25–L28 (1992). doi:10.1086/186442

Lada, E.A., Bally, J., Stark, A.A.: An unbiased survey for dense cores in the LYNDS 1630 molecular cloud. Astrophys. J. **368**, 432–444 (1991). doi:10.1086/169708

Larson, R.B.: Star formation in groups. Mon. Not. R. Astron. Soc. **272**, 213–220 (1995). doi:10.1093/mnras/272.1.213

Leisawitz, D., Bash, F.N., Thaddeus, P.: A CO survey of regions around 34 open clusters. Astrophys. J. Suppl. Ser. **70**, 731–812 (1989). doi:10.1086/191357

Longmore, S.N., Kruijssen, J.M.D., Bastian, N., Bally, J., Rathborne, J., Testi, L., Stolte, A., Dale, J., Bressert, E., Alves, J.: The formation and early evolution of young massive clusters. In: Protostars and Planets VI, pp. 291–314 (2014). doi:10.2458/azu_uapress_9780816531240-ch013, 1401.4175

Majaess, D.: Discovering protostars and their host clusters via WISE. Astrophys. Space Sci. **344**, 175–186 (2013). doi:10.1007/s10509-012-1308-y, 1211.4032

Maschberger, T., Clarke, C.J., Bonnell, I.A., Kroupa, P.: Properties of hierarchically forming star clusters. Mon. Not. R. Astron. Soc. **404**, 1061–1080 (2010). doi: 10.1111/j.1365-2966.2010.16346.x, 1002.4401

Matzner, C.D.: On the role of massive stars in the support and destruction of giant molecular clouds. Astrophys. J. **566**, 302–314 (2002). doi:10.1086/338030, astro-ph/0110278

McMillan, S.L.W., Vesperini, E., Portegies Zwart, S.F.: A dynamical origin for early mass segregation in young star clusters. Astrophys. J. Lett. **655**, L45–L49 (2007). doi:10.1086/511763, arXiv:astro-ph/0609515

Megeath, S.T., Gutermuth, R., Muzerolle, J., Kryukova, E., Flaherty, K., Hora, J.L., Allen, L.E., Hartmann, L., Myers, P.C., Pipher, J.L., Stauffer, J., Young, E.T., Fazio, G.G.: The spitzer space telescope survey of the Orion A and B molecular clouds. I. A census of dusty young stellar objects and a study of their mid-infrared variability. Astron. J. **144**, 192 (2012). doi:10.1088/0004-6256/144/6/192, 1209.3826

Mercer, E.P., Clemens, D.P., Meade, M.R., Babler, B.L., Indebetouw, R., Whitney, B.A., Watson, C., Wolfire, M.G., Wolff, M.J., Bania, T.M., Benjamin, R.A., Cohen, M., Dickey, J.M., Jackson, J.M., Kobulnicky, H.A., Mathis, J.S., Stauffer, J.R., Stolovy, S.R., Uzpen, B., Churchwell, E.B.: New star clusters discovered in the GLIMPSE survey. Astrophys. J. **635**, 560–569 (2005). doi:10.1086/497260

Merín, B., Jørgensen, J., Spezzi, L., Alcalá, J.M., Evans, N.J. II, Harvey, P.M., Prusti, T., Chapman, N., Huard, T., van Dishoeck, E.F., Comerón, F.: The spitzer c2d survey of large, nearby, interstellar clouds. XI. Lupus observed with IRAC and MIPS. Astrophys. J. Suppl. Ser. **177**, 551–583 (2008). doi:10.1086/588042, 0803.1504

Meyer, M.R., Calvet, N., Hillenbrand, L.A.: Intrinsic near-infrared excesses of T Tauri stars: understanding the classical T Tauri star locus. Astron. J. **114**, 288–300 (1997). doi:10.1086/118474

Moitinho, A., Alves, J., Huélamo, N., Lada, C.J.: NGC 2362: a template for early stellar evolution. Astrophys. J. Lett. **563**, L73–L76 (2001). doi:10.1086/338503, astro-ph/0111106

Morales, E.F.E., Wyrowski, F., Schuller, F., Menten, K.M.: Stellar clusters in the inner Galaxy and their correlation with cold dust emission. Astron. Astrophys. **560**, A76 (2013). doi:10.1051/0004-6361/201321626, 1310.2612

Moriguchi, Y., Onishi, T., Mizuno, A., Fukui, Y.: Discovery of a molecular supershell towards two HII regions M16 and M17: possible evidence for triggered formation of stars and GMCs. In: Ikeuchi, S., Hearnshaw, J., Hanawa, T. (eds.) 8th Asian-Pacific Regional Meeting, Vol. II, pp. 173–174 (2002)

Naylor, T.: Are pre-main-sequence stars older than we thought? Mon. Not. R. Astron. Soc. **399**, 432–442 (2009). doi:10.1111/j.1365-2966.2009.15295.x, 0907.2307

Ngoumou, J., Hubber, D., Dale, J.E., Burkert, A.: First investigation of the combined impact of ionizing radiation and momentum winds from a massive star on a self-gravitating core. Astrophys. J. **798**, 32 (2015). doi:10.1088/0004-637X/798/1/32, 1410.5279

Nguyen, H., Nguyen Lu'o'ng, Q., Martin, P.G., Barnes, P.J., Muller, E., Lowe, V., Lo, N., Cunningham, M., Motte, F., Indermühle, B., O'Dougherty, S.N., Hernandez, A.K., Fuller, G.A.: The three-mm ultimate Mopra Milky Way survey. II. Cloud and star formation near the filamentary ministarburst RCW 106. Astrophys. J. **812**, 7 (2015). doi:10.1088/0004-637X/812/1/7, 1504.02246

Palla, F., Stahler, S.W.: Star formation in the Orion Nebula Cluster. Astrophys. J. **525**, 772–783 (1999). doi:10.1086/307928

Palla, F., Stahler, S.W.: Accelerating star formation in clusters and associations. Astrophys. J. **540**, 255–270 (2000). doi:10.1086/309312

Parker, R.J., Dale, J.E.: On the spatial distributions of stars and gas in numerical simulations of molecular clouds. Mon. Not. R. Astron. Soc. **451**, 3664–3670 (2015). doi:10.1093/mnras/stv1223, 1506.00646

Peretto, N., Fuller, G.A.: The initial conditions of stellar protocluster formation. I. A catalogue of Spitzer dark clouds. Astron. Astrophys. **505**, 405–415 (2009). doi:10.1051/0004-6361/200912127, 0906.3493

Persi, P., Tapia, M.: Star Formation in NGC 6334, p. 456 (2008)

Pfalzner, S., Kaczmarek, T., Olczak, C.: Modes of clustered star formation. Astron. Astrophys. **545**, A122 (2012). doi:10.1051/0004-6361/201219881. 1208.0479

Porras, A., Christopher, M., Allen, L., Di Francesco, J., Megeath, S.T., Myers, P.C.: A catalog of young stellar groups and clusters within 1 kiloparsec of the sun. Astron. J. **126**, 1916–1924 (2003). doi:10.1086/377623. astro-ph/0307510

Portegies Zwart, S.F., McMillan, S.L.W., Gieles, M.: Young massive star clusters. Annu. Rev. Astron. Astrophys. **48**, 431–493 (2010). doi:10.1146/annurev-astro-081309-130834. 1002.1961

Preibisch, T.: The reliability of age measurements for young stellar objects from Hertzsprung-Russell or color-magnitude diagrams. Res. Astron. Astrophys. **12**, 1–25 (2012). doi:10.1088/1674-4527/12/1/001

Preibisch, T., Brown, A.G.A., Bridges, T., Guenther, E., Zinnecker, H.: Exploring the full stellar population of the upper Scorpius OB association. Astron. J. **124**, 404–416 (2002). doi:10.1086/341174

Preibisch, T., Hodgkin, S., Irwin, M., Lewis, J.R., King, R.R., McCaughrean, M.J., Zinnecker, H., Townsley, L., Broos, P.: Near-infrared properties of the X-ray-emitting young stellar objects in the Carina Nebula. Astrophys. J. Suppl. Ser. **194**, 10 (2011). doi:10.1088/0067-0049/194/1/10, 1103.2052

Preibisch, T., Zeidler, P., Ratzka, T., Roccatagliata, V., Petr-Gotzens, M.G.: The VISTA Carina Nebula survey . I. Introduction and source catalog. Astron. Astrophys. **572**, A116 (2014). doi:10.1051/0004-6361/201424045

Ragan, S., Henning, T., Krause, O., Pitann, J., Beuther, H., Linz, H., Tackenberg, J., Balog, Z., Hennemann, M., Launhardt, R., Lippok, N., Nielbock, M., Schmiedeke, A., Schuller, F., Steinacker, J., Stutz, A., Vasyunina, T.: The earliest phases of star formation (EPoS): a Herschel key program. The precursors to high-mass stars and clusters. Astron. Astrophys. **547**, A49 (2012). doi:10.1051/0004-6361/201219232, 1207.6518

Rathborne, J.M., Jackson, J.M., Simon, R.: Infrared dark clouds: precursors to star clusters. Astrophys. J. **641**, 389–405 (2006). doi:10.1086/500423. astro-ph/0602246

Rauw, G., Sana, H., Nazé, Y.: A spectroscopic investigation of early-type stars in the young open cluster Westerlund 2. Astron. Astrophys. **535**, A40 (2011). doi:10.1051/0004-6361/201117000, 1109.1086

Reipurth, B.: Handbook of Star Forming Regions, Volume I: The Northern Sky. Astronomical Society of the Pacific Monograph Publications, San Francisco (2008a)

Reipurth, B.: Handbook of Star Forming Regions, Volume II: The Southern Sky. Astronomical Society of the Pacific Monograph Publications, San Francisco (2008b)

Reipurth, B., Schneider, N.: Star Formation and Young Clusters in Cygnus, p. 36. Astronomical Society of the Pacific Monograph Publications, San Francisco (2008)

Rieke, G.H., Lebofsky, M.J.: The interstellar extinction law from 1 to 13 microns. Astrophys. J. **288**, 618–621 (1985). doi:10.1086/162827

Robitaille, T.P., Whitney, B.A., Indebetouw, R., Wood, K., Denzmore, P.: Interpreting spectral energy distributions from young stellar objects. I. A grid of 200,000 YSO model SEDs. Astrophys. J. Suppl. Ser. **167**, 256–285 (2006). doi:10.1086/508424. astro-ph/0608234

Román-Zúñiga, C.G., Elston, R., Ferreira, B., Lada, E.A.: A FLAMINGOS deep near-infrared imaging survey of the rosette complex. I. Identification and distribution of the embedded population. Astrophys. J. **672**, 861–887 (2008). doi:10.1086/523785, 0709.3004

Sana, H., Momany, Y., Gieles, M., Carraro, G., Beletsky, Y., Ivanov, V.D., de Silva, G., James, G.: A MAD view of Trumpler 14. Astron. Astrophys. **515**, A26 (2010). doi:10.1051/0004-6361/200913688, 1003.2208

Savage, B.D., Mathis, J.S.: Observed properties of interstellar dust. Annu. Rev. Astron. Astrophys. **17**, 73–111 (1979). doi:10.1146/annurev.aa.17.090179.000445

Schmeja, S.: Identifying star clusters in a field: a comparison of different algorithms. Astron. Nachr. **332**, 172 (2011). doi:10.1002/asna.201011484, 1011.5533

Schmeja, S., Klessen, R.S.: Evolving structures of star-forming clusters. Astron. Astrophys. **449**, 151–159 (2006). doi:10.1051/0004-6361:20054464. astro-ph/0511448

Shirley, Y.L., Evans, N.J. II, Young, K.E., Knez, C., Jaffe, D.T.: A CS J = 5–>4 mapping survey toward high-mass star-forming cores associated with water masers. Astrophys. J. Suppl. Ser. **149**, 375–403 (2003). doi:10.1086/379147. arXiv:astro-ph/0308310

Shu, F.H., Adams, F.C.: Star formation and the circumstellar matter of young stellar objects. In: Appenzeller, I., Jordan, C. (eds.) Circumstellar Matter, IAU Symposium, vol. 122, pp. 7–22 (1987)

Skrutskie, M.F., Cutri, R.M., Stiening, R., Weinberg, M.D., Schneider, S., Carpenter, J.M., Beichman, C., Capps, R., Chester, T., Elias, J., Huchra, J., Liebert, J., Lonsdale, C., Monet, D.G., Price, S., Seitzer, P., Jarrett, T., Kirkpatrick, J.D., Gizis, J.E., Howard, E., Evans, T., Fowler, J., Fullmer, L., Hurt, R., Light, R., Kopan, E.L., Marsh, K.A., McCallon, H.L., Tam, R., Van Dyk, S., Wheelock, S.: The two Micron All Sky Survey (2MASS). Astron. J. **131**, 1163–1183 (2006). doi:10.1086/498708

Smith, N., Stassun, K.G., Bally, J.: Opening the treasure chest: a newborn star cluster emerges from its dust pillar in Carina. Astron. J. **129**, 888–899 (2005). doi:10.1086/427249, astro-ph/0411178

Soderblom, D.R.: The ages of stars. Annu. Rev. Astron. Astrophys. **48**, 581–629 (2010). doi:10.1146/annurev-astro-081309-130806, 1003.6074

Stolte, A., Brandner, W., Brandl, B., Zinnecker, H., Grebel, E.K.: The secrets of the nearest starburst cluster. I. Very large telescope/ISAAC photometry of NGC 3603. Astron. J. **128**, 765–786 (2004). doi:10.1086/422705

Strom, K.M., Strom, S.E., Merrill, K.M.: Infrared luminosity functions for the young stellar population associated with the L1641 molecular cloud. Astrophys. J. **412**, 233–253 (1993). doi:10.1086/172915

Sung, H., Bessell, M.S.: The initial mass function and Stellar content of NGC 3603. Astron. J. **127**, 1014–1028 (2004). doi:10.1086/381297

Tan, J.C., Krumholz, M.R., McKee, C.F.: Equilibrium star cluster formation. Astrophys. J. Lett. **641**, L121–L124 (2006). doi:10.1086/504150. astro-ph/0603278

Testi, L., Sargent, A.I., Olmi, L., Onello, J.S.: Star formation in clusters: early subclustering in the serpens core. Astrophys. J. Lett. **540**, L53–L56 (2000). doi:10.1086/312858, astro-ph/0005522

Torii, K., Enokiya, R., Sano, H., Yoshiike, S., Hanaoka, N., Ohama, A., Furukawa, N., Dawson, J.R., Moribe, N., Oishi, K., Nakashima, Y., Okuda, T., Yamamoto, H., Kawamura, A., Mizuno, N., Maezawa, H., Onishi, T., Mizuno, A., Fukui, Y.: Molecular clouds in the Trifid Nebula M20: possible evidence for a cloud–cloud collision in triggering the formation of the first generation stars. Astrophys. J. **738**, 46 (2011). doi:10.1088/0004-637X/738/1/46. 1106.3603

Torii, K., Hasegawa, K., Hattori, Y., Sano, H., Ohama, A., Yamamoto, H., Tachihara, K., Soga, S., Shimizu, S., Okuda, T., Mizuno, N., Onishi, T., Mizuno, A., Fukui, Y.: Cloud–cloud collision as a trigger of the high-mass star formation: a molecular line study in RCW120. Astrophys. J. **806**, 7 (2015). doi:10.1088/0004-637X/806/1/7, 1503.00070

Traficante, A., Fuller, G.A., Peretto, N., Pineda, J.E., Molinari, S.: The initial conditions of stellar protocluster formation - II. A catalogue of starless and protostellar clumps embedded in IRDCs in the Galactic longitude range 15 deg $\leq l \leq$ 55 deg. Mon. Not. R. Astron. Soc. **451**, 3089–3106 (2015). doi:10.1093/mnras/stv1158, 1506.05472

van den Bergh, S.: A study of reflection nebulae. Astron. J. **71**, 990–998 (1966). doi:10.1086/109995

Wang, J., Townsley, L.K., Feigelson, E.D., Broos, P.S., Getman, K.V., Román-Zúñiga, C.G., Lada, E.: A Chandra study of the rosette star-forming complex. I. The Stellar population and structure of the young open cluster NGC 2244. Astrophys. J. **675**, 464–490 (2008). doi:10.1086/526406. 0711.2024

Whitworth, A.P., Bhattal, A.S., Chapman, S.J., Disney, M.J., Turner, J.A.: Fragmentation of shocked interstellar gas layers. Astron. Astrophys. **290**, 421–427 (1994)

Williams, J.P., Cieza, L.A.: Protoplanetary disks and their evolution. Annu. Rev. Astron. Astrophys. **49**, 67–117 (2011). doi:10.1146/annurev-astro-081710-102548. 1103.0556

Winston, E., Wolk, S.J., Bourke, T.L., Megeath, S.T., Gutermuth, R., Spitzbart, B.: The structure of the star-forming cluster RCW 38. Astrophys. J. **743**, 166 (2011). doi:10.1088/0004-637X/743/2/166, 1110.2660

Wright, N.J., Drake, J.J., Guarcello, M.G., Aldcroft, T.L., Kashyap, V.L., Damiani, F., DePasquale, J., Fruscione, A.: The Chandra Cygnus OB2 Legacy Survey: Design and X-ray Point Source Catalog (2014). arXiv e-prints 1408.6579

Wu, B., Van Loo, S., Tan, J.C., Bruderer, S.: GMC collisions as triggers of star formation. I. Parameter space exploration with 2D simulations. Astrophys. J. **811**, 56 (2015). doi:10.1088/0004-637X/811/1/56, 1503.01873

Ybarra, J.E., Lada, E.A., Román-Zúñiga, C.G., Balog, Z., Wang, J., Feigelson, E.D.: The progression of star formation in the rosette molecular cloud. Astrophys. J. **769**, 140 (2013). doi:10.1088/0004-637X/769/2/140. 1303.1226

Zeidler, P., Sabbi, E., Nota, A., Grebel, E.K., Tosi, M., Bonanos, A.Z., Pasquali, A., Christian, C., de Mink, S.E., Ubeda, L.: A high-resolution multiband survey of Westerlund 2 with the Hubble Space Telescope. I. Is the massive star cluster double? Astron. J. **150**, 78 (2015). doi:10.1088/0004-6256/150/3/78, 1506.08887

Zeidler, P., Preibisch, T., Ratzka, T., Roccatagliata, V., Petr-Gotzens, M.G.: The VISTA Carina Nebula survey. II. Spatial distribution of the infrared-excess-selected young stellar population. Astron. Astrophys. **585**, A49 (2016). doi:10.1051/0004-6361/201424376, 1510.01631

Chapter 2
Numerical Simulations of Cluster Formation

Patrick Hennebelle

Abstract We review the physical processes and the numerical simulations, which have been performed to address the question of the formation of stellar clusters. Starting with a description of hydrodynamical and isothermal simulations, we then discuss and describe the influence of the radiative feedback, magnetic field, ionising radiation and protostellar jets. Each of these processes has recently been introduced in simulations of cluster formation and turn out to play a significant role, by reducing the star formation efficiency or the star formation rate, or by influencing the shape of the initial mass function. In each case, we start the discussion by describing the most important effects, which are expected and give the relevant analytical expressions, which have been inferred. We then discuss the numerical simulations, which have been performed to investigate their effects.

2.1 Introduction

As emphasised in this book, stellar clusters are amongst the most important structures of the universe. They largely reveal how stars form, in particular that most stars do not form in isolation and strongly influence the evolution of galaxies (see, e.g., Lada and Lada 2003; Longmore et al. 2014).

The physical processes responsible for their formation and evolution are believed to be self-gravity, turbulence, magnetic field and radiative processes. Moreover stellar feedback is most likely playing a crucial role on their evolution. Their exact respective influences remain, however, largely uncertain. Here we review our current understanding of the cluster formation and the effect of the different processes. Related recent works include the reviews by Kruijssen (2013) and Krumholz et al. (2014).

Apart for physical processes, the other crucial aspects are the initial conditions, which eventually leads to cluster formation. This may have recently comparatively received less attention and typically to investigate the formation of clusters, most

P. Hennebelle (✉)
CEA Saclay, 91191 Gif sur Yvette, France
e-mail: patrick.hennebelle@cea.fr

S. Stahler (ed.), *The Birth of Star Clusters*, Astrophysics and Space Science Library 424, DOI 10.1007/978-3-319-22801-3_2

of the recent works have been considering simple initial conditions for which the cloud is out of equilibrium and prone to collapse. In these works onto which we concentrate below, it is thus assumed that cluster formation is a very dynamical process, that occurs much faster than in the quasi-static scenario for star formation (e.g. Shu et al. 1987).

In the second section, we describe the isothermal and hydrodynamical simulations, which have been performed to investigate cluster formation. We start by presenting some elementary concepts, such as the Jeans mass and the freefall time, important to understand the simulation results. We also discuss the main numerical techniques employed in this field, namely the smooth particle hydrodynamics, the adaptive mesh refinement and the moving mesh approach. In the third section, we review the recent studies, which have been undertaken to investigate the impact of the radiative feedback. The questions of how massive stars form and how fragmentation is modified by radiative feedback are particularly important. The effects that magnetic field has onto to the formation of clusters are discussed in Sect. 2.4. It is argued that the most important impact magnetic field may have during collapse, may be due to its ability to brake the inner part of the cloud, that is to say to reduce its angular momentum. The fifth section is dedicated to the influence of the ionising radiation emitted by massive stars. Analytical estimates and numerical simulations show that it is very significant except for massive, strongly bound clouds for which its influence may be somehow reduced. Finally, the role that protostellar jets may have on clusters is discussed.

2.2 Isothermal Hydrodynamical Simulations

Because of their simplicity isothermal, hydrodynamical simulations have been the first calculations performed to investigate the problem of stellar cluster formation. Even nowadays these simulations remain largely employed as they remain much easier to perform but also because of the largest number of computational grid points, they can afford, therefore leading to better statistics. As seen below, the results they produced must be regarded with great care as they often lead to erroneous conclusions.

2.2.1 Some General Considerations

In order to interpret the complex large-scale calculations, it is necessary to introduce a few important quantities, such as Jeans length, Jeans mass and freefall time as they play a central role. More detailed introduction can be found in textbook such as Stahler and Palla (2005).

2.2.1.1 Ratio of Thermal and Gravitational Energies

It is instructive to start by computing the ratio between the thermal energy $E_{\rm therm} = \frac{M}{(\gamma-1)m_p} k_b T$ and the gravitational energy $E_{\rm grav} = (3/5)M^2 G/R$, where M is the cloud mass, R its radius, m_p the mean mass per particle, T the temperature, k_b and G are, respectively, the Boltzmann and the gravitational constants, and γ is the adiabatic index, which depends on the internal degrees of freedom of the constituents. For a polytropic cloud, the thermal pressure is given by $P = K\rho^{\Gamma}$, where Γ is an effective adiabatic exponent that depends on the cooling processes. With these expressions, we get

$$\frac{E_{\rm therm}}{E_{\rm grav}} \propto R^{4-3\Gamma}. \tag{2.1}$$

While intuitively, it is clear that if the thermal energy is large with respect to the gravitational one, any collapse will be prevented, applying the virial theorem shows that the equilibrium value is expected to be $1/2$. This expression stated by Eq. (2.1) clearly shows that $\Gamma = 4/3$ is a critical case below, which thermal pressure is unable to support the cloud against gravitational collapse because the ratio between support and gravitational energy drops with the radius. While this is in particular true for the isothermal case, $\Gamma = 1$, gravitational collapse will be stopped by thermal pressure if the gas is unable to cool efficiently both for a monoatomic gas ($\Gamma \simeq \gamma = 5/3$) and for a diatomic one ($\Gamma \simeq \gamma = 7/5$).

2.2.1.2 Jeans Length, Jeans Mass and Freefall Time

The Jeans length (Jeans 1905) is easily derived by performing a linear analysis of the self-gravitating fluid equations. Let us consider a cloud of density ρ_0, radius R and sound speed C_s. A linear analysis leads to the dispersion relation

$$\omega^2 = C_s^2 k^2 - 4\pi G\rho_0, \tag{2.2}$$

which reveals that when the wave number, k, is smaller than $\sqrt{4\pi G\rho_0}/C_s$, the waves cannot propagate and perturbations are amplified. From this we obtain the Jeans length, λ_J,

$$\lambda_J = \sqrt{\frac{\pi C_s^2}{G\rho_0}}, \tag{2.3}$$

where G is the gravitational constant. The Jeans length can be physically understood in the following way. Self-gravity tends to induce contraction in a time scale of the order of $1/\sqrt{G\rho_0}$. On the other hand, thermal pressure tends to reestablish uniform

density in a sound crossing time, R/C_s. If $1/\sqrt{G\rho_0} < R/C_s$, then the waves cannot erase the pressure fluctuations induced by the gravitational contraction before the whole cloud collapses.

The Jeans mass is naturally defined as the mass contained in a volume of typical size λ_J. The Jeans mass is generally determined as

$$\begin{aligned} M_J &= \frac{4\pi}{3}\rho_0(\lambda_J/2)^3 \\ &= \frac{\pi^{5/2}}{6}\frac{C_s^3}{(G^3\rho_0)^{1/2}}, \end{aligned} \tag{2.4}$$

though there is no fundamental justification for this choice within a factor of a few.

In general, it is not possible to analytically compute the time for a cloud to collapse. However, in the ideal case of a cold spherical cloud with uniform density, one can calculate it exactly. The result, known as the freefall time, is

$$\tau_{\rm ff} = \sqrt{\frac{3\pi}{32G\rho_0}}. \tag{2.5}$$

The typical density is a prestellar dense core is of the order of 10^{4-6} cm^{-3} (e.g. Ward-Thompson and André 2007) while stellar densities are typically 20 orders of magnitude larger, therefore from Eqs. (2.5) and (2.3), it is clear that the typical spatial and temporal scales involved in this problem vary enormously. This certainly constitutes the most severe difficulty encountered in the context of star formation and implies that appropriate numerical techniques must be used.

2.2.2 Numerical Techniques

Two techniques are usually employed, namely the smooth particle hydrodynamics (SPH) and the adaptive mesh refinement (AMR). The first one (e.g. Springel 2005) is a Lagrangian technique, which consists to follow the fluid particles and therefore provides a natural and simple way to adapt the numerical resolution in dense regions. The AMR (e.g. Teyssier 2002) is an Eulerian approach in which the spatial resolution can be locally increased by introducing new grid elements, when it is necessary to satisfy some specified criteria such as resolving the Jeans length. These two techniques present advantages and disadvantages. Tight comparisons have been performed between them, for example, by Agertz et al. (2009). More recently, a moving mesh has been developed (Springel 2010). In this code, the mesh moves with the flow. It is thus continuously stretched and constitutes an interesting Lagrangian scheme. While grid methods tend to perform better when dealing with hydrodynamical instabilities (such as the Kelvin–Helmholtz instability), in the

context of star formation and strongly self-gravitating flows, they tend to produce similar results and show convergence (e.g. Commerçon et al. 2008) when enough resolution is employed. In any case, it is necessary to maintain code diversity and intercomparison in order to assess the results.

Finally, sink particles that mimic the formation of stars are usually used. Such Lagrangian entities (e.g. Krumholz et al. 2004; Federrath et al. 2010b; Bleuler and Teyssier 2015) can accrete the surrounding gas and interact with it through gravity. Different schemes have been employed to treat them, as, for example, a simple density threshold, a Jeans criteria or a local virial analysis. The comparisons between the various schemes which have been undertaken (Federrath et al. 2010b; Bleuler and Teyssier 2015) reveal that these different choices can lead to very substantial differences. This issue is even more severe when stellar feedback is considered since it depends on the stellar masses very non-linearly.

2.2.3 General Setups

Two typical setups are used in cluster formation calculations, which generally consider clouds of hundreds to thousands of solar masses (e.g. Bate et al. 2003; Girichidis et al. 2011).

The first setup presents an initial shape, which is usually spherical and a density profile, which goes from a uniform density to an r^{-2} dependence (Girichidis et al. 2011). The problem is largely determined by the values of the thermal and turbulent energies, which are typically a few percents of the gravitational energy or less for the former and a factor of a few for the latter. A *turbulent* velocity field, which has a powerspectrum close to the Kolmogorov one and random phases, is initially used.

The second setup (e.g. Klessen and Burkert 2000; Offner et al. 2009) considers a periodic computational box in which some periodic external forcing is applied, first without gravity and then, once statistical stationarity is achieved, self-gravity is consistently treated.

One major difference between these two approaches is that in the first one, the large-scale cloud is globally collapsing while in the second one, the periodic boundaries prevent such a global infall, though local infall certainly develops. As a consequence, dense cores can be more easily identified implying that the accretion reservoir from which the stars eventually build their masses are better defined.

To mimic the dust opacity, a barotropic equation of state is sometimes employed leading, for example, to $c_s^2 = c_{s,0}^2(1 + (n/n_c)^{2/3})$ with $n_c \simeq 10^{10}$ cm^{-3} (note that the exponent $2/3 = 5/3 - 1$ is valid until the internal rotation level of H_2 is not excited after which it should typically be equal to $2/5 = 7/5 - 1$). As described below, calculations including radiative transfer and heating by the stars have been performed as well and modify the results very substantially though due to very large computing overheads, the statistics obtained so far remains limited.

2.2.4 *Result of Hydrodynamical Simulations*

The numerical simulations of massive, self-gravitating, turbulent clumps result in complex clouds, which present large density contrasts and a hierarchy of sub-clumps and filaments. Figure 2.1 (left panel) shows a snapshot of such simulations. A stellar cluster has formed in the centre. Because of this complexity, the confrontation with observations is not straightforward. Since one of the major goal of these studies is to explain the observed Initial Mass Function (IMF, Chabrier 2003; Kroupa 2002), many works have been confronting their results with it. However, some recent works have also attempted to understand the large-scale structures of gaseous protoclusters which are likely the progenitors of evolved stellar clusters.

2.2.4.1 Formation of Gaseous Protocluster

Various observations have attempted to identify probable gaseous progenitors of stellar clusters (see, e.g., Fall et al. 2010) and improved statistics have been recently obtained by Urquhart et al. (2014), thanks to various surveys such as ATLASGAL. An important property of these objects is that they present a mass-size relation $M \simeq 3000\,M_\odot\ R^{1.7}$, where R is the effective radius in pc. Pfalzner et al. (2016) proposed that this could be at the origin of the observed mass-size relation of the young embedded clusters (e.g. Lada and Lada 2003), that present similar trend but

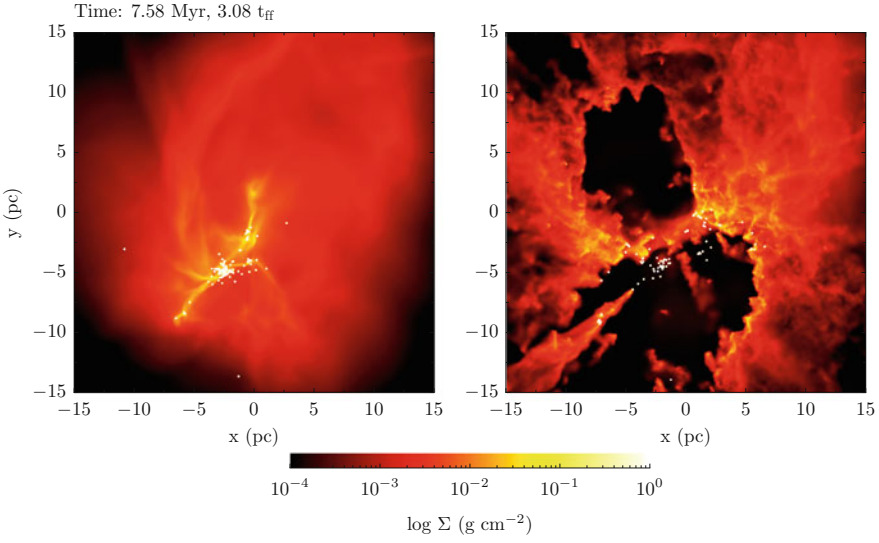

Fig. 2.1 Column density of a $10^4\ M_\odot$ collapsing clouds. *Left*: no ionising radiation (isothermal hydrodynamical simulations). *Right*: ionising radiation has been included since about 2.2 Myr (adapted from Dale et al. (2013))

with a mean mass roughly 4–5 lower. This factor is sometimes interpreted as a possible gas to star conversion efficiency. In an attempt to interpret this relation, various ideas have been proposed.

The role of gas accretion in the driving of turbulence inside the gaseous protocluster and resulting virial equilibrium has been stressed by Hennebelle (2012), Lee and Hennebelle (2016a,b). The underlying idea is that the energy brought by accretion is able to trigger turbulence and that a virial equilibrium is established. Both numerical simulations and analytical models have been performed. Detailed analysis shows that the gaseous radius and the stellar cluster radius are tightly linked though the correspondence is not perfect (and depends on the exact definitions retained for the two radii). The mass-size relation is well reproduced both in the simulations and the analytical models provide the velocity dispersion of the parent clump out of which the gaseous cluster forms present a velocity dispersion that is itself not so far from virial.

Parmentier and Pfalzner (2013) modelled the cluster as a spherical collapsing clump. Considereing the collapse and the formation of stars in the clump, they obtained a mass-size relation as well as a stellar efficiency that nicely reproduced the observed ones. In particular, they inferred $\Sigma_* \propto \Sigma^2$, where Σ_* is the column density of stars and Σ the one of the gas.

More recently Li (2017) emphasised the role played by the turbulent energy dissipation, which combined with virial velocities for self-gravitating objects, leads to a mass-size relation that closely follows the observed one.

To what extent these ideas are exclusive from each others and in which circumstance they would be valid remain to be understood. A major step for future works will be to produce from simulations a distribution of gaseous clusters that reproduce the whole observed distribution. Since this requires the simultaneous treatment of large and small scales, including feedback processes and N-body dynamics, this constitutes a real challenge.

2.2.4.2 Fragmentation Within Clusters

Numerical simulations performed with SPH (e.g. Jappsen et al. 2005; Smith et al. 2008; Bate 2009a, 2012) or using AMR (Girichidis et al. 2011) tend to produce mass distributions, which present similarities with the IMF, that is to say they present a powerlaw at high masses, which has an index compatible with the Salpeter value and a peak at some smaller mass. While the index of the high-mass part appears to be seemingly robust (although the distributions are not always clearly powerlaws), the position of the peak varies as expected with the initial conditions (for example, Bate and Bonnell (2005) show that it depends on the thermal energy) and the equation of state (e.g. Jappsen et al. 2005). The dependence on the initial density profiles found by Girichidis et al. (2011) is very drastic. For example, starting with a uniform density profile leads to the formation of many objects that mimics the IMF (though peaking at too small mass). On the other hand, starting with an r^{-2} density profile, a single object is generally obtained. This is most likely a consequence of the tidal

forces although no quantitative analysis has been performed so far. In general, these simulations tend to find that the peak of the mass distribution is too small compared to the peak of the IMF (which is typically equal to 0.3 $M_{\odot}$). For example, Bate et al. (2003) conclude that too many brown dwarfs (typically a factor 3) form in his simulations.

One potential difficulty with some of these calculations has to do with the core mass function that is most of the time not discussed. Given the very striking similarity between the dense core mass function and the initial mass function (e.g. André et al. 2010), this is certainly an important issue to address irrespectively of their causal relations.

Generally speaking, the physical mechanism responsible for producing the stellar masses (or more precisely the sink masses) in this type of calculations is not clearly assessed (see, e.g., Offner et al. (2013) for a recent review on the various theories for the origin of IMF). For example, Bate (2012) argues that it is due to competitive accretion. The main argument is that the most massive stars at the end of the simulations are the ones, which have accreted longer. Moreover, the accretion often ends after the star undergoes a dynamical interaction and is therefore ejected from the densest part of the parent cloud. Let us stress that the first part of this argument is also compatible with the massive stars having a larger accretion reservoir available as suggested by Hennebelle and Chabrier (2008). This is because bigger cores require more time to collapse. On the other hand, the SPH simulations performed by Smith et al. (2008) show a clear correlation between the initial masses within the gravitational well and the final sink masses up to a few local freefall times (see Chabrier and Hennebelle (2010) for a quantitative analysis), suggesting that the initial prestellar cores do not fragment into many objects. As time goes on, the correlation becomes weaker but seems to persist up to the end of their run. Massive stars, on the other hand, are weakly correlated with the mass of the potential well in which they form. Whether their mass was contained into a larger, more massive well, with which the final sink mass would be well correlated remains an open issue, which needs to be further investigated.

Another important aspect to explain for star formation theories is the binary distribution of stars (e.g. Duquennoy and Mayor 1991). Given that binaries entail the masses of the two companions and their separations, the statistics are more demanding than for the mass distribution and only few recent studies (Bate 2009b, 2014; Myers et al. 2014) have been attempting to reproduce the observed distributions statistically. It is concluded that the observed binary distribution is reasonably well reproduced.

2.3 Radiative Feedback

We now turn to the influence of radiative feedback which is emitted by the stars and contribute to heat the gas within the surrounding envelope and to resist the gravitational infall through radiative pressure. We exclude at this stage any discussion of

ionising radiation that will be considered later. Indeed, this latter has appeared to be a major physical process particularly regarding the formation of massive stars. First, the radiative pressure becomes so intense that for a long time it was believed that the formation of stars more massive that 20 $M_\odot$ was prevented. Second, the heating it provides, substantially increases the temperature and therefore increases the Jeans mass, which therefore modifies substantially the fragmentation of the cloud.

2.3.1 Some Simple Arguments

Before discussing some of the quantitative results obtained in large-scale numerical simulations, it is useful to infer a few analytical results, which illustrates some of the effects at play in the numerical calculations.

2.3.1.1 The Radiation Pressure Problem

The first estimates of the largest stellar mass that can possibly be assembled are due to Larson and Starrfield (1971) and Kahn (1974). The principle of their analysis is to compare the radiative pressure of a massive stellar embryo to the ram pressure induced by the gravitational collapse of its surrounding massive cloud, in its inner and outer parts. If the luminosity of the central star becomes high enough, the radiation pressure may become important and prevent further accretion onto the central object. Since the radiation pressure is acting on the dust grains, one has to assume that the frictional coupling between the gas and the dust is sufficiently strong so that forces acting on the dust grains are transmitted to the gas.

In the inner part of the collapsing cloud, the temperature becomes high and the dust grains evaporate. There is thus a dust shell whose inner edge is located at the radius, r, where the grains evaporate. At this sublimation radius, the radiation pressure is $L_\star/4\pi r^2 c$, where $L_\star$ is the stellar luminosity and c the speed of light. The dynamical pressure is ρu^2, where ρ is the density and u the infall speed which is given by $u^2 \simeq 2GM_\star/r$, where G is the gravitational constant and $M_\star$ the mass of the protostar. This leads to the ratio of radiative to ram pressures

$$\Gamma = \frac{L_\star/4\pi r^2 c}{\rho u^2} \simeq 1.3 \times 10^{-11} \, \frac{L_\star/L_\odot}{(M_\star/M_\odot)^{1/2}} \, r^{1/2}. \tag{2.6}$$

Using an analytic estimate for the temperature inside the cloud and based on the assumption that the grains evaporate at a temperature of $\sim$1 500 K, Larson and Starrfield (1971) estimate the radius of the shell to be

$$r \simeq 2.4 \times 10^{12} \frac{(L_\star/L_\odot)^{1/2}}{(M_\star/M_\odot)^{1/5}} \, \mathrm{cm} \simeq 3.3 \, \frac{(L_\star/10^3 \, L_\odot)^{1/2}}{(M_\star/8 \, M_\odot)^{1/5}} \, \mathrm{AU}. \tag{2.7}$$

It follows from Eqs. (2.6) to (2.7) that

$$\Gamma \simeq 2 \times 10^{-5} \frac{(L/L_\odot)^{6/5}}{(M/M_\odot)^{3/5}}. \tag{2.8}$$

For a stellar mass of 20 $M_\odot$, corresponding to a luminosity of about 4×10^4 $L_\odot$, Γ roughly equals unity. Therefore, according to Larson and Starrfield (1971), the mass at which radiative pressure impedes accretion is around 20 $M_\odot$.

A more accurate estimate has been done by Wolfire and Cassinelli (1987) by using the optical properties and composition of the mixture of dust grains proposed by Mathis et al. (1977). Assuming an accretion rate of 10^{-3} $M_\odot$ yr^{-1} in a 100 $M_\odot$ cloud, Wolfire and Cassinelli (1987) show that Γ is larger than one for any reasonable value of the radiation temperature. They conclude that building a massive star with the "standard" dust grain mixture is difficult and requires reducing the grain abundance by large factors (∼4–8). They thus propose, as a solution to the high-mass star formation problem, that the dust abundance could be locally decreased by an external shock or an internal ionisation front.

More recently, Kuiper et al. (2010) have also performed 1D calculations for various core masses and confirm largely the results of these early works. In particular, they cannot form objects more massive than 20 $M_\odot$ even in very massive cores.

2.3.1.2 The Issue of Fragmentation

Radiative feedback has been found to play an important role in reducing the fragmentation by Krumholz et al. (2007), Bate (2009a) and Commerçon et al. (2011). Generally speaking the reason is that the gas is heated due to the intense accretion luminosity and thus the temperature is higher than what is typically obtained by using a barotropic equation of state. Although no simple estimate of the efficiency in reducing the fragmentation has been provided, this effect is found to be substantial in many studies (see below). For example, Bate (2009a) concludes that the number of brown dwarfs may be lower by a factor of about ≃3 in the radiative calculations.

Another possible consequence, though not firmly established yet, is that the universality of the peak of the IMF could be due to the heating by the stars themselves. This is based on a scaling argument proposed by Bate (2009a). The argument is as follows.

In the optically thick regime, the temperature around a star is given by $L_* \simeq 4\pi\sigma r^2 T^4$ while a Jeans length in this region is given by the relation $c_s^2 = kT/m_p \simeq GM/\lambda_J$ that is to say the thermal support is roughly equal to the gravitational energy for a mass $M \simeq (4\pi/3)\rho\lambda_J^3$. This leads to the relation

$$\lambda_J^{5/2} \simeq \frac{3kL_*^{1/4}}{(4\pi)^{5/4} G m_p \sigma^{1/4}} \rho^{-1}. \tag{2.9}$$

The Jeans mass which is simply estimated as $M_J \simeq (4\pi/3)\rho\lambda_J^3$ is then found to be

$$M_J = (4\pi/3)^{-1/5}(k/Gm_p)^{6/5}L_*^{1/10}(4\pi\sigma)^{-1/10}\rho^{-1/5}. \tag{2.10}$$

Thus instead of getting a density dependence $\rho^{-1/2}$ as in the isothermal case, one gets $M_J \propto \rho^{-1/5}$, which is much shallower dependence seemingly leading to an IMF, which is less dependent on the cloud parameters. Although it constitutes an interesting idea, various aspects of the scheme need further explanations. For example, the first generation of stars that formed in a molecular cloud is not affected by this heating and therefore would have different characteristics unless this effect starts operating while the stars are still forming (for example, by modifying the Jeans mass that would otherwise be accreted by the central star). Another question is the fraction of the gas in the molecular cloud, which is affected by this heating. As this effect strongly depends on the distance to the stars, the pieces of gas which are too far from stars are not heated significantly.

2.3.2 Result of 2D Multi-Wavelength Simulations

The issue of radiative pressure preventing the formation of stars more massive than 20 $M_\odot$ has been solved when it has been possible to perform 2D simulations in which the radiation and the dynamics are treated self-consistently. In these studies, it has been assumed that the radiation arises from both the accretion and the stellar luminosity. While the former is dominant during the earliest phases of the collapse, the latter becomes more important at more advanced stages. One of the main motivations of these calculations was to demonstrate that the presence of a centrifugally supported optically thick disk, inside which the radiative pressure would be much reduced, allows to circumvent the radiation pressure problem. The first numerical simulations have been performed by Yorke and Sonnhalter (2002) in the frequency dependent case (using 64 intervals of frequency) and in the grey case (one single interval of frequency). The cloud they consider is centrally peaked, has a mass of 60 $M_\odot$, a thermal over gravitational energy ratio of about 5% initially, and is slowly rotating. After $\sim 10^5$ yr, the central core has a mass of about 13.4 $M_\odot$ and the surrounding cloud remains nearly spherical. After $\sim 2\times 10^5$ yr, the mass of the central core is about 28.4 $M_\odot$ and the cloud starts to depart from the spherical symmetry. In particular, the infall is reversed by radiative forces in the polar region while the star continues to accrete material through the equator where the opacity is much higher. This is known as the "flashlight effect". Once the stellar mass has grown to about 33.6 $M_\odot$, the central star is no longer accreting although 30 $M_\odot$ of gas is still available within the computational grid. The infall is then reversed in every directions indicating that the radiative forces are effectively preventing further accretion. If instead of a multi-frequency treatment, the grey approximation is made, the early evolution is similar but becomes notably different after $\sim 2.5\times 10^5$ yr.

In particular, there is no evidence of any flow reversal. Instead the material flows along a thin disklike structure, supported in the radial direction by both centrifugal and radiative forces. At the end of the simulation, the mass of the central star is about 20.7 $M_{\odot}$.

In Kuiper et al. (2010) bidimensional simulations have been performed using an hybrid scheme for the radiative transfer. While the gas emission is treated using the flux-limited diffusion and the grey approximation, direct multi-frequency irradiation from the central star is also included. In particular, they stress the importance of spatially resolving the dust sublimation front. In the simulations that do not resolve it well, the accretion quickly stops while it continues when the sublimation front is well described. This is because the radiation is more isotropic when the dust sublimation front is not properly resolved, leading to a weak flashlight effect. In the simulations of Kuiper et al. (2010) objects of mass much larger than $\simeq$20 $M_{\odot}$ form. For example, for a 480 $M_{\odot}$ clump, they form an object of 150 $M_{\odot}$, which is still accreting.

2.3.3 Result of 3D Simulations with Radiative Feedback

The first 3D-calculations of a massive collapsing core in which radiative feedback is self-consistently taken into account have been performed by Krumholz et al. (2007, 2009). They use a flux-limited and grey approximation to treat the radiative transfer. The most striking aspect they report is certainly the development of the Rayleigh–Taylor instability in the radiatively triggered expanding bubble. As a consequence of the non-linear development of this instability, fingers of dense material can channel through the low density radiatively dominated cavity and reach the central object. They therefore identify three modes of accretion in their simulations, accretion through the disk (the flashlight effect), accretion through the cavity wall and accretion through dense Rayleigh–Taylor unstable fingers. A quantitative estimate reveals that the latter route accounts for about 40% of the accretion.

These results have been questioned by Kuiper et al. (2012) who performed bidimensional calculations with a flux-limited scheme similar to the one used by Krumholz et al. (2009) and the hybrid scheme, which is used in Kuiper et al. (2010). The results turn out to be quite different. In the first case, a radiatively dominated bubble is launched but it quickly stops and falls back towards the equatorial plane. In the second case, the bubble keeps expanding leading to a radiatively driven outflow. One of the important consequences is thus that accretion occurs exclusively through the disk. As these simulations are bidimensional, it is unclear whether they completely rule out the development of the Rayleigh–Taylor instability, which could be largely seeded by the non-linear fluctuations induced by the turbulence in 3D (Rosen et al. 2016). They nevertheless suggest that the dynamics of the radiatively dominated cavity is largely determined by the treatment of the radiative

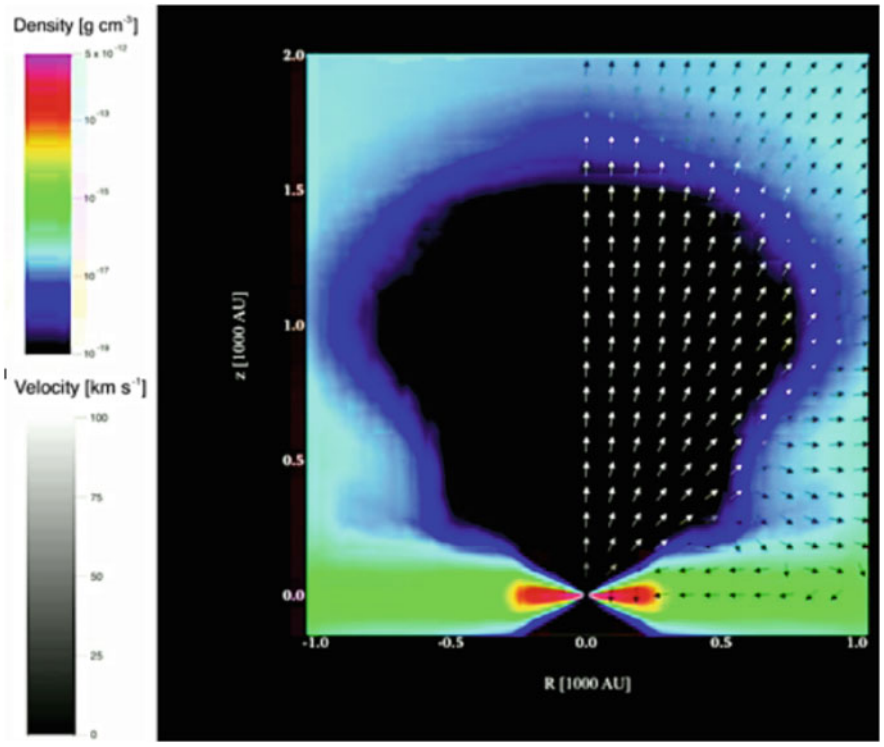

Fig. 2.2 A radiatively driven outflow driven from a massive protostar (adapted from Kuiper et al. (2010)). Accretion is still proceeding from the equatorial plane through the accretion disk

feedback in particular its frequency dependence. Figure 2.2 shows the propagation of a radiatively driven outflow and illustrates the flashlight effect.

As recalled previously, the second drastic problem in the context of massive star formation is how to avoid fragmenting the massive cores in many objects. For example in the simulations that have been performed by Dobbs et al. (2005), the 30 solar mass core they simulate, fragments in about 20 low mass objects. This prevents the formation of high mass objects. While it remains possible that large mass objects could be formed in very massive clumps through competitive accretion (e.g. Bonnell et al. 2004), it is important to treat in any case, the physics of the fragmenting cores properly, which is the task that the studies described below have addressed.

Tridimensional calculations have been performed by Krumholz et al. (2007) using the grey approximation for the radiative transfer. Their initial conditions (aimed at reproducing the model of McKee and Tan (2003)) consist in a centrally peaked 100 $M_{\odot}$ cloud with a density profile proportional to r^{-2}. The initial turbulence within the cloud is sufficient to ensure an approximate hydrostatic equilibrium. Turbulent motions first delay the onset of collapse but, as the turbulence decays, the cloud starts to collapse. Comparison is made with runs for which an

isothermal equation of state is used. In particular, Krumholz et al. (2007) find that, when the radiative transfer is taken into account, the gas temperature inside the cloud is higher than in the isothermal case, by factors up to 10. As a consequence, the cloud is fragmenting much less when radiation is taken into account than when isothermal assumption is used. It is important to re-iterate at this stage that centrally condensed cores are less prone to fragmentation than cores having flatter density profiles as shown by Girichidis et al. (2011). Indeed the radiative hydrodynamical simulations performed by Commerçon et al. (2011) clearly show that cores, which initially have a flat density profile, are undergoing significant fragmentation as shown by the top left and bottom left panels of Fig. 2.3 even so radiative feedback is treated self-consistently.

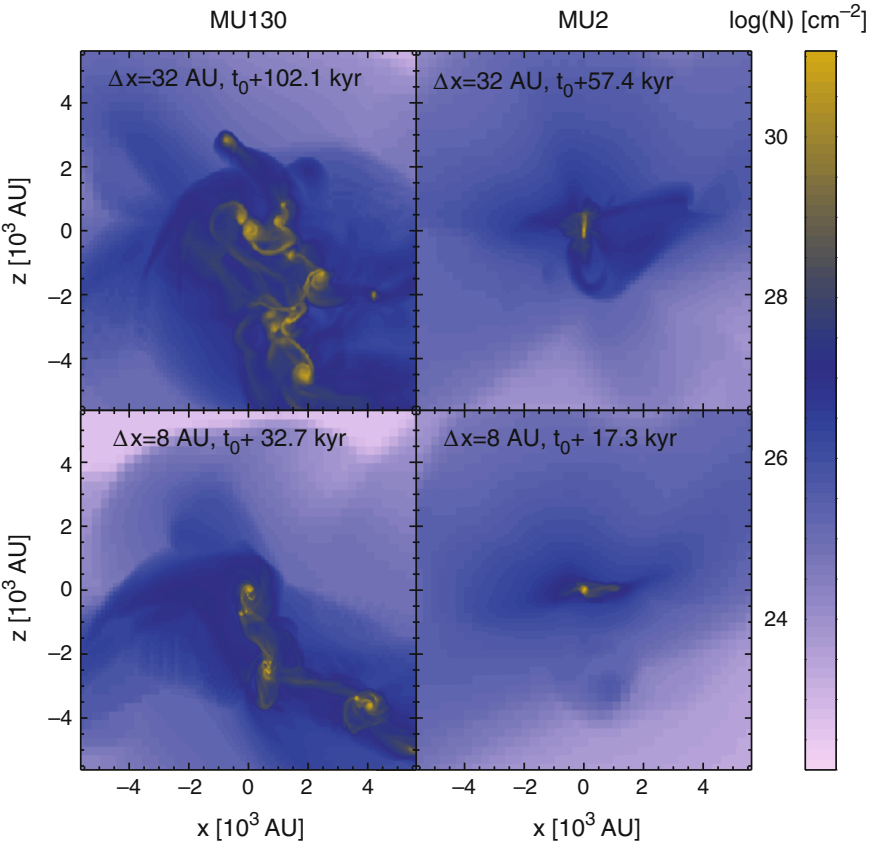

Fig. 2.3 Column density within central part of massive collapsing cores. *Left*: hydrodynamical case, the core is largely fragmenting even though radiative feedback is treated. *Right*: RMHD simulation (initial mass-to-flux of 2), the fragmentation is entirely suppressed due to the combination of magnetic field and radiative feedback (Commerçon et al. 2011)

2.4 Impact of the Magnetic Field

For a long time, magnetic field was ignored in numerical simulations because the numerical schemes were not good enough to handle supersonic MHD turbulence and because MHD simulations are much more demanding than hydrodynamical ones. Thanks to the recent progress of the numerical algorithms (e.g. Gardiner and Stone 2005; Fromang et al. 2006), magnetic field tends now to be routinely taken into account. Numerous studies have confirmed the expectation that it should play a determinant role in the star formation process. As described below, it indeed has unanticipated serious consequences, which largely determines the outcome of star formation. However, while it was believed that its main impact was to reduce the star formation rate in galaxies (e.g. Shu et al. 1987), the magnetic intensities, which have been measured seem too low to affect it at the level, which was anticipated (Crutcher 2012).

2.4.1 The Lorentz Force and Its Consequences

Before describing the results, which have been inferred from large-scale simulations, we start with simple analytical considerations and with a description of low mass core calculations as they are much simpler.

2.4.1.1 Magnetic Support

Unlike the thermal pressure, the Lorentz force, $\mathbf{j}\times\mathbf{B}$, where $\mathbf{j}$ is the electric current, is non-isotropic. In particular, it vanishes along the field lines. An easy way to estimate the magnetic support is to compute the ratio of the magnetic over gravitational energies. For simplicity let us consider again a spherical and uniform cloud of mass M, volume V, radius R, threaded by a uniform magnetic field of strength B. The magnetic flux within the cloud, ψ, is equal to $\psi = \pi R^2 B$. As long as the magnetic field remains well coupled to the gas (see next section), the magnetic flux threading the cloud will remain constant along time. The ratio of magnetic over gravitational energies for uniform density cloud threaded by a uniform magnetic field is

$$\frac{E_{\rm mag}}{E_{\rm grav}} = \frac{B^2 V}{8\pi} \times \frac{2R}{5GM^2} \propto \frac{B^2 R^4}{M^2} \propto \left(\frac{\psi}{M}\right)^2 . \tag{2.11}$$

Remarkably, the ratio of magnetic over gravitational energies is independent of the cloud radius. This implies that if the cloud contracts or expands, the relative importance of these two energies remains the same. This is unlike the thermal energy of an isothermal gas, which becomes smaller and smaller compared to the gravitational energy as the cloud collapses (e.g. Eq. (2.1)). It is clear from Eq. (2.11),

that there is a critical value of the magnetic intensity for which the gravitational collapse is impeded even if the cloud was strongly compressed. Indeed if the energy of the magnetic field dominates the gravitational energy, it will be impossible for gravity to bend the field lines and collapse will be prevented. Mouschovias and Spitzer (1976) have calculated accurately the critical value of the mass-to-flux ratio using the virial theorem and numerical calculations of the cloud bidimensional equilibrium. A cloud, which has a mass-to-flux ratio smaller (larger) than this critical value cannot collapse and is called subcritical (supercritical). It is usual to define $\mu = (M/\psi)/(M/\psi)_{\rm crit}$. Large values of μ correspond to small magnetic fields and thus supercritical clouds.

2.4.1.2 Magnetic Braking

Due to the generation of torsional Alfvén waves, which propagate and transfer angular momentum from the cloud to the intercloud medium (Mouschovias and Paleologou 1981; Shu et al. 1987), the magnetic field is able to efficiently brake interstellar clouds. To estimate the time scale over which this process is occurring, let us consider an intercloud medium of density $\rho_{\rm icm}$ and let us assume that the magnetic field is parallel to the rotation axis. The waves propagate at the Alfvén speed, $V_a = B/\sqrt{4\pi\rho_{\rm icm}}$ along a cylinder parallel to the magnetic field. Significant braking will arise when the waves have transmitted to the intercloud medium a substantial fraction of the cloud angular momentum. This is the case, when the waves have reached a distance from the cloud, l, such that $l \times \rho_{\rm icm} \simeq R \times \rho_0$. That is to say the waves have been able to transfer angular momentum to a mass of intercloud medium comparable to the mass of the cloud. This gives an estimate for the magnetic braking time, in case where the magnetic field and the rotation axis are aligned:

$$\tau_{\rm br} \simeq \frac{R}{V_a}\frac{\rho_0}{\rho_{\rm icm}}. \tag{2.12}$$

The braking time increases when $\rho_{\rm icm}$ decreases because if the intercloud medium has a low inertia, its angular momentum is small.

The numerical calculations of the collapse of magnetised cores, which have been recently performed (e.g. Allen et al. 2003; Price and Bate 2007; Mellon and Li 2008; Hennebelle and Fromang 2008) indeed reveal that magnetic braking is playing a very strong impact on disk formation. These authors conclude that even for relatively weak fields, the formation of big massive disks that form in the hydrodynamical case can be suppressed at least in the early phase of the collapse though Joos et al. (2012) found that the problem is less severe when the magnetic field is inclined with respect to the rotation axis or when turbulence is included (Seifried et al. 2011; Joos et al. 2013). This is because the magnetic field is strongly amplified during the collapse and transports very efficiently the angular momentum (e.g. Galli et al. 2006). As discussed below, magnetic braking turns out to also play

an important role in the context of massive cores and therefore cluster formation. Magnetised models have received some support from the comparisons between high resolution observations of low mass cores and synthetic ones performed using various calculations (Maury et al. 2010). Observational data are in better agreement with magnetised models than with purely hydrodynamical ones. The main difference comes from the presence of a big massive disk in the latter case.

Due to the magnetic braking and also to the generation of a strong toroidal component of the magnetic field induced by the differential rotation at the scale of few hundreds of AU, it has been found in the context of low mass cores, that magnetic field drastically reduces the fragmentation (Machida et al. 2005; Hennebelle and Teyssier 2008).

2.4.2 Results of Large-Scale MHD Simulations

2.4.2.1 MHD Barotropic Calculations

Using the SPH techniques, Price and Bate (2009) performed MHD calculations (in fact including the radiative transfer) at pc scales. One of their important conclusions is that magnetic field tends to reduce the star formation rate, that is the amount of mass converted into stars per units of time, by a factor on the order of two. This is mainly because in these simulations, it exerts significant support onto the diffuse gas (see also Vazquez-Semadeni et al. 2011). This conclusion has also been obtained by Padoan and Nordlund (2011), who performed a series of isothermal runs in which turbulence is maintained supersonic applying forcing in the Fourier space. The reason for this effect has not been analysed in great details so far but it may have to do with the impact magnetic field has onto the density probability distribution as argued by Hennebelle and Chabrier (2013). As shown, for example, by Molina et al. (2012), magnetic field tends to reduce the width of the density PDF because it reduces the density enhancement in shocks.

Simulations of massive cores have been performed by Hennebelle et al. (2011). They have run a set of barotropic simulations for various magnetic intensities. The initial conditions consist in 100 $M_\odot$ cores with a smooth initial density profile and a turbulent velocity field (with a ratio of turbulent and gravitational energies of about 20%). The fragmentation is delayed and reduced when the magnetic flux is strong enough (typically for mass-to-flux smaller than 5). The number of objects decreases up to typically only a factor of two for the strongest magnetisation that was explored. Thus, it appears that magnetic field in itself cannot suppress the fragmentation in many objects. The reason of this limited impact is largely due to the magnetic diffusion induced by the turbulent velocity field, which reduces the magnetic field in the central part of the collapsing core where fragmentation is taking place. Similar conclusion has been reached by Peters et al. (2010) who even included photo-ionisation from the central star.

Simulations of $10^3\ M_\odot$ magnetised forming clusters have also been performed by Wang et al. (2010) and Li et al. (2010). Since they also include jets, these simulations will be described later in Sect. 2.6.

2.4.2.2 MHD Radiative Calculations

A few simulations of massive collapsing clumps which treat both the magnetic field and the radiative transfer have been performed recently.

In their calculations, Price and Bate (2009) show that the magnetic field and the radiative feedback are complementary. While as discussed above, magnetic field tends to support the diffuse gas at large scale, radiative feedback significantly heats the dense clumps and limits their fragmentation in many objects.

The first simulations that include both MHD and radiative feedback in the context of massive star formation, that is to say following the collapse up to AU scales, have been recently performed by Commerçon et al. (2011). These simulations show that the combination of magnetic field and radiative feedback is indeed extremely efficient in suppressing the fragmentation. The reason is that magnetic field and radiative feedback are in a sense interacting (Commerçon et al. 2010) and their combination leads to effects that are much stronger than expected. This is because, as pointed out by Hennebelle et al. (2011) magnetic field, even in the presence of turbulence, leads to efficient magnetic braking, which reduces the amount of angular momentum in the central part of the cloud where fragmentation is taking place. Thus, the accretion is initially much more focused in a magnetised core than in an hydrodynamical core when turbulence is included because in hydrodynamical simulations, a large amount of angular momentum prevents the gas to fall in the central object. Consequently, the accretion luminosity which is $\propto M\dot{M}/R$ is much higher because the mass of the central object and the accretion rate onto the central object are larger. Also the radius at which accretion is stopping is smaller (since there is less angular momentum). Consequently, the temperature in magnetised cores is much higher than in hydrodynamical cores making them much more stable against fragmentation. This is illustrated in Fig. 2.4, which shows the temperature as a function of density in four cases. The first panel shows the case of a cloud with no turbulence and no magnetic field, which is purely spherical initially. In this case, the flow is extremely focused and falls directly in a single central object. The second panel shows the temperature distribution for a turbulent and unmagnetised cloud while the third and fourth panels show this distribution for two magnetic intensities. Clearly the hydrodynamical case with turbulence has the lowest temperatures while the most magnetised case (fourth panel) presents much higher temperatures, which are comparable to the one obtained in the purely spherical case (first panel) that is naturally focused.

Radiative MHD simulations of collapsing massive cores have also been performed by Myers et al. (2013) (see also Myers et al. 2014). These calculations largely confirm that the combination of magnetic field and radiative feedback reduces significantly the fragmentation of massive cores, even leading sometimes to a unique massive object.

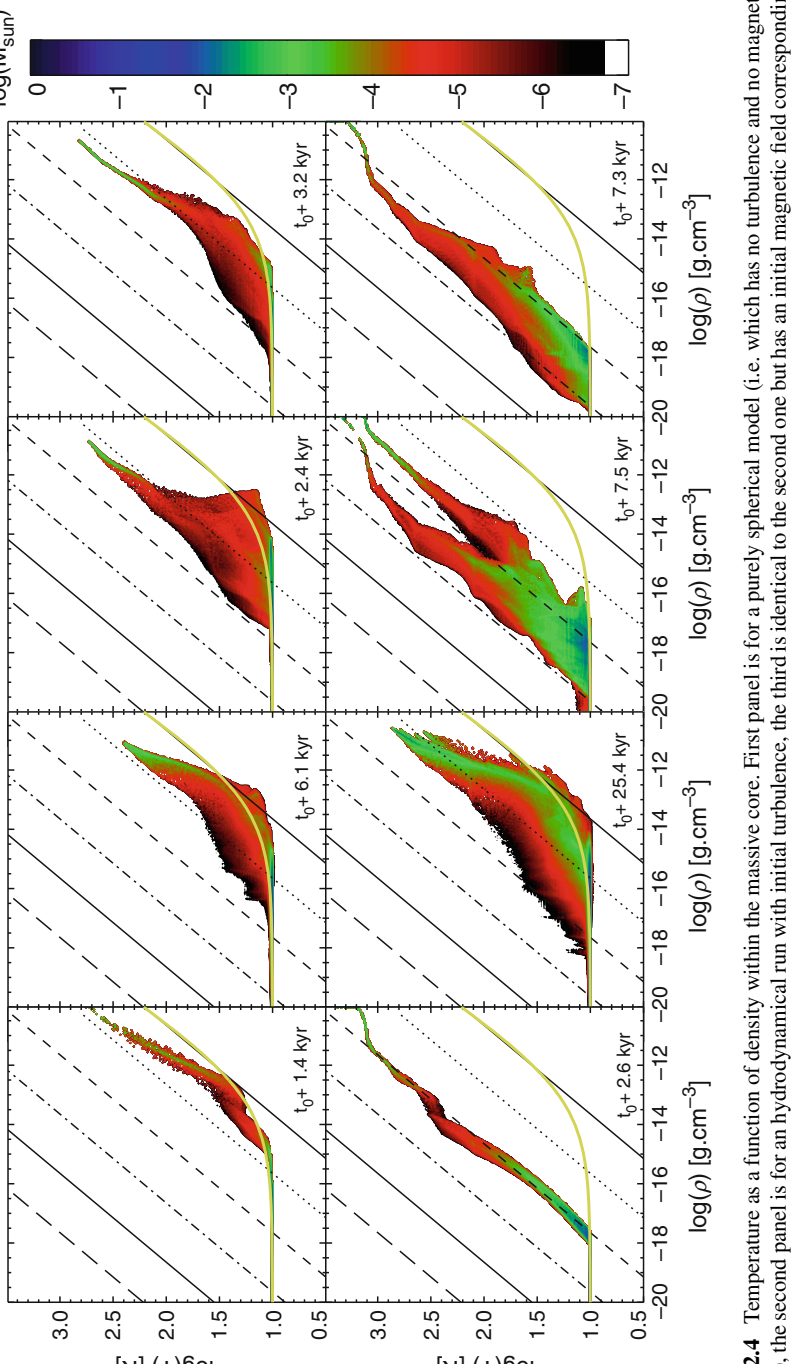

Fig. 2.4 Temperature as a function of density within the massive core. First panel is for a purely spherical model (i.e. which has no turbulence and no magnetic field), the second panel is for an hydrodynamical run with initial turbulence, the third is identical to the second one but has an initial magnetic field corresponding to mass-to-flux of 5 initially. The fourth has a mass-to-flux of 2 (Commerçon et al. 2011)

2.5 Impact of HII Radiation

Massive stars emit a large amount of ionising radiation, which exert a considerable influence on the surrounding gas and constitute a major source of feedback. It contributes at the scale of clusters and molecular clouds, to limit their star formation efficiency (see, for example, Krumholz et al. (2014) for a recent review). Ionising radiation has two major effects. First of all, by ionising the gas, it reduces the amount of material, which may form stars. Second of all, since the temperature of the ionised gas is on the order of 7000 K, the pressure of the ionised gas is generally dominant and it therefore tends to expand, sweeping the dense ISM and injecting momentum.

2.5.1 Analytical Estimates

Before to proceed with the numerical simulations, it is useful to present some of the analytical estimates, which have been performed by various authors (e.g. Spitzer 1978; Whitworth 1979; Williams and McKee 1997; Matzner 2002).

As the ionising radiation is emitted from the star, it propagates in the surrounding medium up to the point, where it is absorbed by an atom of hydrogen (strictly speaking helium must also be considered). However, protons and electrons tend to recombine and this gives rise to an equilibrium described by (e.g. Spitzer 1978)

$$\frac{4\pi}{3} r_s^3 n_e n_H \alpha = S, \tag{2.13}$$

where r_s is the radius of the ionised region, also called the Strömgren sphere, n_e is the electron density, n_H the proton density, S the number of ionising photons emitted per units of time by the central star and α is the recombination coefficient. This radius has been expressed in the convenient form by Matzner (2002)

$$r_s = 2.9 \left(\frac{N_H}{1.5 \times 10^{22}\,\mathrm{cm}^{-2}} \right)^{-1} \left(\frac{S}{10^{49}\,\mathrm{s}^{-1}} \right)^{1/3} \left(\frac{M}{10^6\,M_\odot} \right)^{1/6} \mathrm{pc}, \tag{2.14}$$

where N_H and M are the column density and mass of the cloud in which the HII region propagates.

Once the ionisation front has reached r_s, the propagation of the radiation stops. However, due to the high pressure of the ionised gas, the ionised region starts expanding. Since this lowers the mean density of the ionised gas, this makes the recombination rate smaller and therefore the Strömgren radius increases enhancing the mass of ionised gas. A complete description of this expansion phase is difficult to perform analytically but it is possible to investigate the regime for which the radius, r_{II}, is large with respect to r_s. As shown in Spitzer (1978) and Matzner (2002), in

this regime, $r_{II} \propto t^{4/7}$. More precisely, Matzner (2002) obtained

$$r_{II} = 19 \tag{2.15}$$

$$\left(\frac{t}{3.7\,\mathrm{Myr}}\right)^{4/7} \left(\frac{N_H}{1.5\times10^{22}\,\mathrm{cm}^{-2}}\right)^{-3/7} \left(\frac{S}{10^{49}\,\mathrm{s}^{-1}}\right)^{1/7} \left(\frac{M}{10^6\,M_\odot}\right)^{1/7} \mathrm{pc}, \tag{2.16}$$

The momentum of the shell, p_{II}, is given by the product of the shell mass, $4/3\pi r_{II}^3 n_0$, and its velocity, $\dot{r}_{II}$, which following Matzner (2002) leads to

$$p_{II} = 2.2\times10^5\times \tag{2.17}$$

$$\left(\frac{t}{3.7\,\mathrm{Myr}}\right)^{9/7} \left(\frac{N_H}{1.5\times10^{22}\,\mathrm{cm}^{-2}}\right)^{-3/14} \left(\frac{S}{10^{49}\,\mathrm{s}^{-1}}\right)^{4/7} \left(\frac{M}{10^6\,M_\odot}\right)^{1/14} M_\odot\,\mathrm{km\,s}^{-1}.$$

It is worth noting that for a flux of 10^{49} s^{-1} (typical for O stars), the total momentum injected is comparable to the one injected during a supernova explosion (e.g. Cioffi et al. 1988) although a major difference is that the momentum injection is more impulsive during supernovae events and lasts a few million years for massive star ionising radiation.

The mass evaporated by the HII radiation can be estimated by the momentum divided by the sound speed of the ionised gas (see also Whitworth 1979), which leads to

$$M_{\mathrm{dest}} = 1.2\times10^4\phi_{II}\times \tag{2.18}$$

$$\left(\frac{t}{3.7\,\mathrm{Myr}}\right)^{9/7} \left(\frac{N_H}{1.5\times10^{22}\,\mathrm{cm}^{-2}}\right)^{-3/14} \left(\frac{S}{10^{49}\,\mathrm{s}^{-1}}\right)^{4/7} \left(\frac{M}{10^6\,M_\odot}\right)^{1/14} M_\odot,$$

where ϕ_{II} is a geometrical coefficient, which depends whether the HII regions are embedded or of blister type.

Therefore, from these estimates, we see that HII regions have a very significant impact on the molecular clouds injecting a very significant amount of momentum and ionising a large amount of gas. It must, however, be stressed that the approach developed here does not include gravity. In particular, in a strongly self-gravitating cloud, the infalling material may impede the expansion of the ionised gas by bringing a continuous flux of high density gas. A simple criteria on the accretion rate, $\dot{M}$, has been proposed by Walmsley (1995)

$$\dot{M} > \left(\frac{4\pi SGMm_H^2}{\alpha}\right)^{1/2}. \tag{2.19}$$

To obtain this relation, we start with Eq. (2.14). Then using the expression for the accretion rate $\dot{M} = 4\pi n_H m_H R^2 v$ where $v \simeq (GM/R)^{1/2}$, to express n_H, one obtains the critical accretion rate (within a factor $\sqrt{3}$). For a 60 $M_\odot$ O5 star, Walmsley

(1995) estimated the critical accretion rate to be of about $10^{-4}\ M_\odot\ \mathrm{yr}^{-1}$ and about $4 \times 10^{-6}\ M_\odot\ \mathrm{yr}^{-1}$ for a 17 $M_\odot$ B0 star. More detailed analytical calculations of HII region development around accreting stars have been performed by Keto (2003).

2.5.2 Simulations with HII Radiation

Various simulations including ionising radiation have been performed at different scales and using various setups.

Most of these works have been focusing on the expansion of an HII regions into a molecular clouds (see, e.g., Mellema et al. 2006; Dale and Bonnell 2011; Dale et al. 2012, 2013; Geen et al. 2015, 2016 and of masses on the order of 10^4 to $10^6\ M_\odot$). The three main questions which have received most attention are the efficiency of ionising radiation to destroy the cloud, the possibility that it triggers star formation (i.e. positive feedback) and whether it can inject turbulence.

Regarding this last point (which is directly linked to Eqs. (2.17), Mellema et al. (2006) and Walch et al. (2012) conclude that it can trigger significant random motion interpreted as turbulence. A similar conclusion is reached by Gritschneder et al. (2009) and Tremblin et al. (2012), who use a plane-parallel illumination. In particular, Gritschneder et al. (2009) show that the kinetic energy is increased by a few in the presence of the ionising flux they impose.

The efficiency of the ionising radiation in setting the efficiency of star formation regions has been investigated by Walch et al. (2012) and in a series of papers by Dale and Bonnell (2011), Dale et al. (2012, 2013), Geen et al. (2015), Geen et al. (2016), Gavagnin et al. (2017). While Walch et al. (2012) note that the flux emitted by an O7 stars (with an ionising flux equal to $10^{49}\ \mathrm{s}^{-1}$) is very destructive onto a $10^4\ M_\odot$ cloud, Dale and Bonnell (2011), Dale et al. (2012, 2013), Geen et al. (2015, 2017) find that a key parameter turns out to be the escape velocity from the self-gravitating cloud. When it is smaller than about $10\,\mathrm{km\,s}^{-1}$, that is to say more or less the sound speed of the ionised gas, c_{II}, the ionising radiation leads to a strong cloud evaporation and destruction. Figure 2.1 (right panel) shows a snapshot of a $10^4\ M_\odot$ molecular cloud in which the ionising stars have been radiating for about 2.2 Myr. The comparison with the isothermal cloud is striking. A large amount of dense gas has been ionised and is flowing out of the molecular cloud. On the other hand, when the escape velocity is larger than this value, the ionising radiation has a limited impact onto the cloud. For typical cloud parameters, this occurs for clouds whose mass is of the order of $10^6\ M_\odot$. Interestingly, they note that the ionising radiation has a limited influence onto the dense filaments and clumps within molecular clouds, likely because of the efficiency of the recombination in high density material (as shown by Eq. (2.14)). This may limit the influence of ionising radiation although the exact result may require a very detailed calculations. Indeed, the possibility that HII regions could propagate anisotropically along the more diffuse regions remains in many cases.

At small scales, i.e. from a few hundreds of AU to a fraction of pc, a series of simulations of collapsing massive cores have been performed (e.g. Peters et al. 2010, 2011) precisely to investigate the mutual influence between ionising radiation and the dense accreting envelope. They conclude that in spite of the large accretion, the ionising radiation could indeed, after a confinement phase, eventually propagate and escape along the pole leading to bipolar cavities and may even contribute to the formation of outflows.

The question as to whether the ionising radiation can have a positive feedback onto the star formation activity is tightly related to the question of the efficiency and has been discussed as well. Walch et al. (2012) note that before the ionising radiation starts evaporating the cloud, there is a short phase during which it compresses the gas and could trigger some star formation. The question should, however, be formulated with care. While it is established that ionising radiation can trigger the formation of pillars (e.g. Williams et al. 2001; Tremblin et al. 2012), it is not clear whether it implies that more stars would actually form in the presence of ionising radiation and the simulation performed by Dale and Bonnell (2011), Dale et al. (2012, 2013) suggests that it may not be the case. Moreover even the IMF may not be drastically changed (e.g. Dale et al. 2012).

2.6 Impact of Protostellar Jets

When a star forms, it is now well established that an outflow and a fast jet are launched, the ejection rate being roughly proportional to the accretion rate (e.g. Frank et al. (2014) for a recent review). These ejections certainly influence the nearby gas and in particular the cluster to which the stars is belonging (e.g. Krumholz et al. 2014) mainly because of the large amount of momentum that they may eject in the gas, possibly maintaining a high level of turbulence.

2.6.1 Analytical Estimate

Since the launching of the jets occurs at very small scales, presumably in the vicinity of the star, it is not possible to simulate their acceleration self-consistently. Moreover, the exact mechanism responsible for the launching of jets (and outflows) remains controversial although magnetically driven models have received particular attention. Consequently, there are large uncertainties on how exactly the jets and the outflows should be modelled. Note that MHD collapse simulations have been somehow successful in generating self-consistently outflows (e.g. Wang et al. 2010; Hennebelle et al. 2011), however, these large-scale ejections are not strong enough to represent the fast jets, presumably launched at small scales.

The essence of the analytical estimates which are used in cluster simulations is as follows. When protostars accrete, the gravitational energy must be released and

leads to an accretion luminosity

$$L_{\rm acc} = \frac{GM_*\dot{M}_*}{R_*}. \tag{2.20}$$

If a fraction, f, of this energy is carried out through the ejected material, this implies that

$$\dot{M}_{\rm out} v_{\rm out}^2 = \frac{fGM_*\dot{M}_*}{R_*}, \tag{2.21}$$

and therefore

$$v_{\rm out}^2 = f\frac{GM_*}{R_*}\frac{\dot{M}_*}{\dot{M}_{\rm out}}, \tag{2.22}$$

leading to

$$v_{\rm out} \simeq 300 f^{1/2} \left(\frac{\dot{M}_*}{\dot{M}_{\rm out}}\right)^{1/2} \left(\frac{M_*}{M_\odot}\right)^{1/2} \left(\frac{R_*}{3R_\odot}\right)^{-1/2} {\rm km\,s^{-1}}, \tag{2.23}$$

where $v_{\rm out}$ and $M_{\rm out}$ are the velocity and the mass of the ejected material. The total momentum is thus simply $v_{\rm out}M_{\rm out}$ and the mean momentum divided by the total mass of the star formed is given by

$$V_{\rm out} = v_{\rm out}\frac{M_{\rm out}}{M_*} \simeq 300 f^{1/2} \left(\frac{\dot{M}_{\rm out}}{\dot{M}_*}\right)^{1/2} \left(\frac{M_*}{M_\odot}\right)^{1/2} \left(\frac{R_*}{3R_\odot}\right)^{-1/2} {\rm km\,s^{-1}}, \tag{2.24}$$

where $M_{\rm out}/M_* = \dot{M}_{\rm out}/\dot{M}_*$. Matzner and McKee (2000) estimate $V_{\rm out}$ to be on the order of 20–40 km s^{-1}.

2.6.2 *Simulations with Jets*

Simulations of clusters including jet launching have been performed both at pc scales (Li and Nakamura 2006; Nakamura and Li 2007; Cunningham et al. 2009; Carroll et al. 2009; Wang et al. 2010) and within collapsing massive cores (e.g. Cunningham et al. 2011).

At pc scales, Li and Nakamura (2006) and Nakamura and Li (2007) (see also Federrath 2015) consider a clump of about a 10^3 $M_\odot$ and both isotropic and collimated outflows. They obtain a stationary state in which the turbulence maintained by outflows can effectively counteract gravity and prevent the clump to collapse in a freefall time. Wang et al. (2010) (see also Federrath 2015) performed

a series of simulations in which they include progressively more physical processes starting with no initial turbulence, no magnetic field and no outflows. They show in particular that the star formation rate is reduced by a factor of a few each time one of these processes is added. When the three are included (and for a substantial supercritical magnetic field), the star formation rate can easily be 10 times lower than the value obtained where they are not considered.

The question as to whether turbulence can be efficiently triggered by protostellar outflows has been thoroughly investigated by Cunningham et al. (2009) and Carroll et al. (2009). They find that in a turbulent medium, even if not magnetised, the outflows efficiently couple to the surrounding gas and sustain turbulence. The resulting energy powerspectrum is somewhat stiffer than classical powerspectra obtained in large-scale driven turbulence (e.g. Kritsuk et al. 2007; Federrath et al. 2010; Hennebelle and Falgarone 2012).

Jets have also been found to influence the IMF (or more precisely the *sink* initial mass function). For example, Li et al. (2010) found that jet driving tends to lower the characteristic mass of the IMF, a result also inferred by Federrath et al. (2014). This is likely a consequence of the accreted mass being lost in the flow as well as the capacity of the outflow to reduce further accretion onto the stars/sinks. Finally, higher Mach number and strong shock induced by the outflows, certainly lead to similar trends.

The influence of jets has also been studied during the collapse of massive cores by Cunningham et al. (2011). They found that outflows quickly evacuate polar cavities along which radiation escapes, therefore its influence onto the dense gas is reduced, in particular temperature is somehow smaller and the IMF produced in these simulations (Krumholz et al. 2012) resemble the observed IMF.

Finally, Myers et al. (2014) have performed simulations of clusters, which include jets and radiative feedback for various magnetisation. They confirm that magnetic field tends to reduce fragmentation by a factor of about 2, leading to stars about 2 times more massive on average. The binary properties appear to be reasonably reproduced for the most magnetised runs (having a mass-to-flux ratio of 2).

2.7 Conclusion

Significant progresses have been made during the last decade regarding our understanding of the stellar cluster formation. The set of physical processes taken into account makes the numerical simulations much more realistic. The resolution is also much better though probably still a significant source of inaccuracy and uncertainties.

As discussed in the chapter, radiative feedback, magnetic field, ionising radiation and protostellar jets are all playing important role on the formation of clusters. Their respective influence is, however, different and the effect they have on the three most fundamental quantities in the context of cluster formation, namely the

star formation efficiency, the star formation rate and the initial mass function must be clearly distinguished. We now summarise the recent finding regarding these important questions, stressing what seems now well established and what remains unclear.

2.7.1 The Star Formation Efficiency

The most important process responsible for setting the star formation efficiency, that is to say the fraction of the cloud mass eventually converted into stars, appears to be the ionising radiation (e.g. Whitworth 1979; Matzner 2002; Dale et al. 2013). This is most certainly true for clouds of mass on the order of $10^{4-5}\ M_\odot$. Due to the gravitation infall and to the high escape velocity, it is, however, unclear whether this is true for more massive clouds or more generally for very compact ones. For these clouds, radiative pressure is likely important (e.g. Kim et al. 2016). One source of uncertainty regarding this question is numerical resolution important to describe how the ionising radiation propagates at small scales as in the studies by Peters et al. (2010) but also because numerical resolution is necessary to get a good description of the individual stars, which form. Indeed, ionising radiation is a very non-linear function of the stellar mass.

2.7.2 The Star Formation Rate

The star formation rate, that is to say the mass of gas converted into stars per solar mass and per freefall time, appears to be controlled by turbulence, magnetic field and protostellar outflows (e.g. Wang et al. 2010). For typical conditions, they seem to all contribute to a factor of a few. The typical accretion time is then reduced by a factor on the order of 10 when these three processes are included. One of the most important limitations here may be the limited knowledge of the protostellar flows, whose intensities remain largely uncertain.

2.7.3 The Initial Mass Function

The fundamental mechanism responsible for setting the initial mass function remains controversial (see, e.g., Offner et al. 2013). Good agreement between the sink mass function (Bate 2009a) and the observed IMF has been claimed. The results seem, however, to depend heavily on the radiative feedback, the outflows and the magnetic field (Krumholz et al. 2012; Myers et al. 2014). Radiative feedback may tend to produce too massive stars and one may need outflow cavities to alleviate its effect. Magnetic field also tends to produce more massive stars (mainly because

of magnetic braking). How are these dependences compatible with the apparent invariance of the IMF (Hennebelle 2012)? A major source of uncertainties are clearly the initial conditions that should be varied to verify how sensitively is the IMF relying on them. The other important limitation is once again the numerical resolution particularly because the radiative feedback varies very stiffly with the mass.

References

Agertz, O., Moore, B., Stadel, J., et al.: Mon. Not. R. Astron. Soc. **380**, 963 (2009)
Allen, A., Li, Z.-Y., Shu, F.: Astrophys. J. **599**, 363 (2003)
André, P., Men'shchikov, A., Bontemps, S., et al.: Astron. Astrophys. **102**, 518L (2010)
Bate, M., Bonnell, I., Bromm, V.: Mon. Not. R. Astron. Soc. **339**, 577 (2003)
Bate, M.: Mon. Not. R. Astron. Soc. **392**, 1363 (2009)
Bate, M.: Mon. Not. R. Astron. Soc. **397**, 232 (2009)
Bate, M.: Mon. Not. R. Astron. Soc. **419**, 3115 (2012)
Bate, M.: Mon. Not. R. Astron. Soc. **442**, 285 (2014)
Bate, M., Bonnell, I.: Mon. Not. R. Astron. Soc. **356**, 1201 (2005)
Bleuler, A., Teyssier, R.: Mon. Not. R. Astron. Soc. **445**, 4015 (2015)
Bonnell, I., Vine, S., Bate, M.: Mon. Not. R. Astron. Soc. **349**, 735 (2004)
Carroll, J., Frank, A., Blackman, E., et al.: Astrophys. J. **695**, 1376 (2009)
Chabrier, G.: Publ. Astron. Soc. Pac. **115**, 763 (2003)
Chabrier, G., Hennebelle, P.: Astrophys. J. **79**, 725L (2010)
Cioffi, D. McKee, C., Bertschinger, E.: Astrophys. J. **334**, 252 (1988)
Commerçon, B., Hennebelle, P., Audit, E., Chabrier, G., Teyssier, R.: Astron. Astrophys. **482**, 371 (2008)
Commerçon, B., Hennebelle, P., Audit, E., et al.: Astron. Astrophys. **3**, 510L (2010)
Commerçon, B., Hennebelle, P., Henning, T.: Astrophys. J. **9**, 742L (2011)
Crutcher, R.: Annu. Rev. Astron. Astrophys. **50**, 29 (2012)
Cunningham, A., Frank, A., Carroll, J., et al.: Astrophys. J. **692**, 816 (2009)
Cunningham, A., Klein, R., Krumholz, M., et al.: Astrophys. J. **740**, 107 (2011)
Dale, J., Bonnell, I.: Mon. Not. R. Astron. Soc. **414**, 321 (2011)
Dale, J., Ercolano, B., Bonnell, I.: Mon. Not. R. Astron. Soc. **424**, 377 (2012)
Dale, J., Ercolano, B., Bonnell, I.: Mon. Not. R. Astron. Soc. **430**, 234 (2013)
Dobbs, C., Bonnell, I., Clark, P.: Mon. Not. R. Astron. Soc. **360**, 2 (2005)
Duquennoy, A., Mayor, M.: Astron. Astrophys. **248**, 485 (1991)
Fall, M., Krumholz, M., Matzner, C.: Astrophys. J. **710**, 142 (2010)
Federrath, C., Roman-Duval, J., Klessen, R., et al.: Astron. Astrophys. **512**, 81 (2010)
Federrath, C., Banerjee, R., Clark, P., Klessen, R.: Astrophys. J. **713**, 269 (2010b)
Federrath, C., Schrön, M., Banerjee, R., Klessen, R.: Astrophys. J. **797**, 19 (2014)
Federrath, C.: Mon. Not. R. Astron. Soc. **450**, 4035 (2015)
Frank, A., Ray, T., Cabrit, S.: (2014). arXiv:1402.3553
Fromang, S., Hennebelle, P., Teyssier, R.: Astron. Astrophys. **457**, 371 (2006)
Galli, D., Lizano, S., Shu, F., Allen, A.: Astrophys. J. **647**, 374 (2006)
Gardiner, T., Stone, J.: J. Comput. Phys. **205**, 509 (2005)
Gavagnin, E., Bleuler, A., Rosdahl, J., Teyssier, R.: (2017). arXiv:170107982
Geen, S., Hennebelle, P., Tremblin, P., Rosdahl, J.: Mon. Not. R. Astron. Soc. **454**, 4484 (2015)
Geen, S., Hennebelle, P., Tremblin, P., Rosdahl, J.: Mon. Not. R. Astron. Soc. **463**, 3129 (2016)
Geen, S., Soler, J., Hennebelle, P.: (2017). arXiv:170310071
Girichidis, P., Federrath, C., Banerjee, R., Klessen, R.: Mon. Not. R. Astron. Soc. **413**, 2741 (2011)

Gritschneder, M., Naab, T., Walsch, S., et al.: Astrophys. J. **694**, L26 (2009)
Hennebelle, P., Fromang, S.: Astron. Astrophys. **477**, 9 (2008)
Hennebelle, P., Teyssier, R.: Astron. Astrophys. **477**, 25 (2008)
Hennebelle, P., Chabrier, G.: Astrophys. J. **684**, 395 (2008)
Hennebelle, P.: Astron. Astrophys. **545**, 147 (2012)
Hennebelle, P., Chabrier, G.: Astrophys. J. **770**, 150 (2013)
Hennebelle, P., Commerçon, B., Joos, M., et al.: Astron. Astrophys. **528**, 72 (2011)
Hennebelle, P., Falgarone, E.: A&RAv **20**, 55 (2012)
Jappsen, A., Klessen, R., Larson, R., et al.: Astron. Astrophys. **435**, 611 (2005)
Jeans, J.: Astrophys. J. **22**, 93 (1905)
Joos, M., Hennebelle, P., Ciardi, A.: Astron. Astrophys. **543**, 128 (2012)
Joos, M., Hennebelle, P., Ciardi, A., Fromang, S.: Astron. Astrophys. **554**, 17 (2013)
Kahn, F.: Astron. Astrophys. **37**, 149 (1974)
Keto, E.: Astrophys. J. **599**, 1196 (2003)
Kim, J.-G., Kim, W.-T., Ostriker, E.: Astrophys. J. **819**, 137 (2016)
Klessen, R., Burkert, A.: Astrophys. J. Suppl. Ser. **128**, 287 (2000)
Kritsuk, A., Norman, M., Padoan, P., Wagner, R.: Astrophys. J. **665**, 416 (2007)
Kroupa P.: Science **295**, 82 (2002)
Kruijssen, J.: (2013). arXiv:1304.4600
Krumholz, M., Klein, R., McKee, C.: Astrophys. J. **611**, 399 (2004)
Krumholz, M., Klein, R., McKee, C.: Astrophys. J. **656**, 959 (2007)
Krumholz, M., Klein, R., McKee, C., Offner, S., Cunningham, A.: Science **323**, 754 (2009)
Krumholz, M., Klein, R., McKee, C.: Astrophys. J. **754**, 71 (2012)
Krumholz, M., Bate, M., Arce, H., et al.: (2014). arXiv:1401.2473
Kuiper, R., Klahr, H., Beuther, H., Henning, T.: Astrophys. J. **722**, 1556 (2010)
Kuiper, R., Klahr, H., Beuther, H., Henning, T.: Astron. Astrophys. **537**, 122 (2012)
Lada, C., Lada, E.: Annu. Rev. Astron. Astrophys. **41**, 57 (2003)
Larson, R., Starrfield, S.: Astron. Astrophys. **13**, 190 (1971)
Lee, Y.-N., Hennebelle, P.: Astron. Astrophys. **591**, 30 (2016)
Lee, Y.-N., Hennebelle, P.: Astron. Astrophys. **591**, 31 (2016)
Li, Z.-Y., Nakamura, F.: Astrophys. J. **640**, L187 (2006)
Li, Z.-Y., Wang, P., Abel, T., Nakamura, F.: Astrophys. J. **720**, 26 (2010)
Li, G.-X.: Mon. Not. R. Astron. Soc. **465**, 667 (2017)
Longmore, S., Kruijssen, J., Bally, J., et al.: (2014). arXiv:1401.4175
Machida, M., Matsumoto, T., Hanawa, T., Tomisaka, K.: Mon. Not. R. Astron. Soc. **362**, 382 (2005)
Matzner, C., McKee, C.: Astrophys. J. **545**, 364 (2000)
Matzner, C.: Astrophys. J. **566**, 302 (2002)
McKee, C.F., Tan, J.C.: Astrophys. J. **585**, 850 (2003)
Mathis, J., Rumpl, W., Nordsieck, K.: Astrophys. J. **217**, 425 (1977)
Maury, A., André, P., Hennebelle, P., et al.: Astron. Astrophys. **512**, 40 (2010)
Molina, F., Glover, S., Federrath, C., Klessen, R.: Mon. Not. R. Astron. Soc. **2**, 680 (2012)
Mellema, G., Arthur, S., Henney, W., et al.: Astrophys. J. **647**, 397 (2006)
Mellon, R., Li, Z.-Y.: Astrophys. J. **681**, 1356 (2008)
Mouschovias, T., Spitzer, L.: Astrophys. J. **210**, 326 (1976)
Mouschovias, T., Paleologou, E.: Astrophys. J. **246**, 48 (1981)
Myers, A., McKee, C., Cunningham, A.: Astrophys. J. **766**, 97 (2013)
Myers, A., Klein, R., Krumholz, M.: Mon. Not. R. Astron. Soc. **439**, 3420 (2014)
Nakamura,F., Li, Z.-Y.: Astrophys. J. **662**, 395 (2007)
Offner, S., Klein, R., McKee, C., Krumholz, M.: Astrophys. J. **703**, 131 (2009)
Offner, S., Clark, P., Hennebelle, P., et al.: (2013). arXiv:1312.5326
Padoan, P., Nordlund, A.: Astrophys. J. **730**, 40 (2011)
Parmentier, G., Pfalzner, S.: Astron. Astrophys. **549**, 132 (2013)
Pfalzner, S., Kirk, H., Sills, A., et al.: Astron. Astrophys. **586**, 68 (2016)

Peters, T., Banerjee, R., Klessen, R., et al.: Astrophys. J. **711**, 1017 (2010)
Peters, T., Banerjee, R., Klessen, R., et al.: Astrophys. J. **729**, 72 (2011)
Price, D., Bate, M.: Mon. Not. R. Astron. Soc. **377**, 77 (2007)
Price, D., Bate, M.: Mon. Not. R. Astron. Soc. **398**, 33 (2009)
Rosen, A., Krumholz, M., McKee, C., Klein, R.: Mon. Not. R. Astron. Soc. **463**, 2553 (2016)
Seifried, D., Banerjee, R., Klessen, R., Duffin, D., Pudritz, R.: Astrophys. J. **417**, 1054 (2011)
Shu, F.H., Adams, F.C., Lizano, S.: Annu. Rev. Astron. Astrophys. **25**, 23 (1987)
Smith, R., Clark, P., Bonnell, I.: Mon. Not. R. Astron. Soc. **391**, 1091 (2008)
Spitzer, L.: Physical processes in the interstellar medium (1978). ppim.book
Springel, V.: Mon. Not. R. Astron. Soc. **364**, 1105 (2005)
Springel, V.: Mon. Not. R. Astron. Soc. **401**, 791 (2010)
Stahler, S., Palla, F.: The formation of stars (2005). fost.book
Teyssier, R.: Astron. Astrophys. **385**, 337 (2002)
Tremblin, P., Audit, E., Minier, V., et al.: Astron. Astrophys. **546**, 33 (2012)
Urquhart, J., Moore, T., Csengeri, T., et al.: Mon. Not. R. Astron. Soc. **443**, 1555 (2014)
Vazquez-Semadeni, E., Banerjee, R., Gómez, G., et al.: Mon. Not. R. Astron. Soc. **414**, 2511 (2011)
Walch, S., Whitworth, A., Bisbas, T., et al.: Mon. Not. R. Astron. Soc. **427**, 625 (2012)
Walmsley, M.: Rev. Mex. Astron. Astrofis. Conf. Ser. **1**, 137 (1995)
Wang, P., Li, Z.-Y., Abel, T., Nakamura, F.: Astrophys. J. **709**, 27 (2010)
Ward-Thompson, D., André, P.: In: Reipurth, B., Jewitt, D., Keil, K. (eds.) Protostars and Planets V, vol. 951, p. 33. University of Arizona Press, Tucson (2007)
Williams, J., McKee, C.: Astrophys. J. **476**, 166 (1997)
Williams, R., Ward-Thompson, D., Whitworth, A.: Mon. Not. R. Astron. Soc. **327**, 788 (2001)
Whitworth, A.: Mon. Not. R. Astron. Soc. **186**, 59 (1979)
Wolfire, M., Cassinelli, J.: Astrophys. J. **319**, 850 (1987)
Yorke, H., Sonnhalter, C.: Astrophys. J. **569**, 846 (2002)

Chapter 3
Massive Young Clusters Near the Galactic Center

Jessica R. Lu

Abstract In this chapter, I review studies of the three massive young clusters at the Galactic Center—Arches, Quintuplet, and the Young Nuclear Cluster. These clusters reside in an extreme environment and are ideal laboratories for studying how such environments influence the star and cluster formation process and subsequent cluster evolution. The emphasis in this chapter is on the observational constraints on the cluster properties including the stellar content, initial mass function, orbit and birth location, and internal dynamics. I place these clusters into the context of our understanding of star formation. I also describe observational methodologies needed for studies of these clusters and I finish with open questions that can be addressed with both current and future observational facilities.

3.1 Introduction: Three Massive Young Clusters

Three of the most massive young star clusters in the Galaxy are located near the Galactic Center: the Arches Cluster, the Quintuplet Cluster, and the Young Nuclear Star Cluster (Fig. 3.1). They reside in the Central Molecular Zone (CMZ), which is a region of dense molecular gas totalling $\sim 10^8\ M_\odot$ and extending to a radius of 100−200 pc from the central supermassive black hole (Morris and Serabyn 1996; Molinari et al. 2011). The gas in the CMZ from which the clusters formed has higher temperatures, densities, magnetic fields, and turbulent pressures than molecular clouds in the disk of the Milky Way (Kruijssen and Longmore 2013; Henshaw et al. 2016). Thus these three clusters are of particular import in studies of star formation as they probe a different set of initial conditions and environments than disk clusters. With masses of $\sim 2 \times 10^4\ M_\odot$, these clusters are important contributors, if not the dominant ones, to the total star formation presently taking place in the CMZ. This preponderance of rich clusters has also raised the possibility that the dominant mode of star formation in the CMZ might differ from that in the Galactic disk (Kruijssen and Longmore 2013).

J.R. Lu (✉)
University of California, Berkeley, CA, USA
e-mail: jlu.astro@berkeley.edu

S. Stahler (ed.), *The Birth of Star Clusters*, Astrophysics and Space Science Library 424, DOI 10.1007/978-3-319-22801-3_3

Fig. 3.1 Three massive young clusters reside in the central molecular zone of the Milky Way: the Arches Cluster, the Quintuplet Cluster, and the Young Nuclear Star Cluster centered on the supermassive black hole. This color composite image was constructed from a combination of infrared images from the NICMOS camera on the Hubble Space Telescope and the IRAC camera on Spitzer. The image is oriented such that the Galactic plane is horizontal across the image. Image credit: NASA, ESA, D. Wang, S. Stolovy

In the following chapter, we present background on the discovery and early studies of the Arches, Quintuplet, and the Young Nuclear Cluster (YNC) in Sect. 3.2. The current census of the stellar content and constraints on the cluster ages are discussed in Sect. 3.3. The internal structure and dynamics of each cluster is presented in Sect. 3.4. Constraints on the present-day and initial stellar mass function are discussed in Sect. 3.5. A short primer on recent developments in the observational and modeling methodologies is presented in Sect. 3.7. The Galactic Center young massive clusters are placed into a theoretical context in Sect. 3.8 where we consider whether the star formation process differs in the Galactic Center environment. Finally some of the open questions for future studies of the massive young clusters at the Galactic Center are presented in Sect. 3.9.

3.2 Discovery and Early History

The Galactic Center region is subject to tens of magnitudes of visual extinction; thus, the discovery of the three massive young clusters at the Galactic Center awaited the advent of infrared astronomy and infrared surveys. The initial discovery of the Galactic Center in stellar light used a single-element infrared photometer and was significantly aided by the presence of the Young Nuclear Cluster (hereafter, the YNC) in the central parsec (Becklin and Neugebauer 1968). However, the individual luminous stars in the YNC were only resolved with the advent of infrared arrays (Rieke and Low 1973; Becklin and Neugebauer 1975; Allen et al. 1983), and even later were spectroscopically recognized to be massive young stars (Allen et al. 1990;

Krabbe et al. 1991; Blum et al. 1995, e.g.,). The character and dynamics of the YNC are strongly affected by the presence of the Galactic Black Hole (GBH) upon which the YNC is centered, and by the far more massive nuclear stellar cluster of older stars having a broad range of ages (Schödel et al. 2009, 2014; Do et al. 2015; Martins et al. 2007). Although there was a growing recognition between the 1970s and 1990s that a supermassive black hole might be present at the Galactic Center, the presence of the YNC led some to question the existence of the GBH because of the expectation that its tidal force would prevent gravitational collapse of even very dense cloud cores (Sanders 1992). To this day, the formation of the YNC remains a challenging, unsolved problem, although inroads have been made toward finding ways in which the star formation might have occurred there (see Sect. 3.8).

The other Arches and Quintuplet Clusters were not recognized until much later. Located, respectively, at 26 and 32 parsecs from the GBH in projection, the Arches and Quintuplet Clusters became evident only after near-infrared surveys allowed investigators to distinguish them from the dense background of bulge stars. The Quintuplet stood out originally because its five namesake stars are all very luminous, cool emitters with blackbody temperatures in the range 600–900 K, causing them to stand out prominently at wavelengths beyond 3 μm (Okuda et al. 1987, 1989, 1990; Nagata et al. 1990). It is now recognized that these stars are young, post-main-sequence Wolf–Rayet stars enshrouded with carbon-enriched dust and with a spectral type of WC (Figer et al. 1999b). The Arches Cluster wasn't discovered until the mid-1990s, when the emission-line character of many of its stars called attention to it (Nagata et al. 1995; Cotera et al. 1996). The name "Arches" refers to the Arc-shaped HII region with complex filamentary substructure that bends around the cluster (Morris and Yusef-Zadeh 1989; Lang et al. 2001). The tremendous Lyman-continuum output of the Arches Cluster (see Sect. 3.3) is very likely responsible for ionizing the surface of the molecular cloud underlying the Arches HII region (Colgan et al. 1996; Lang et al. 2001; Figer et al. 2002) (Fig. 3.2).

Fig. 3.2 Zoomed infrared images of the Arches Cluster (*left*), Quintuplet Cluster (*middle*), and the Young Nuclear Cluster (*right*). The extreme stellar density and patchy extinction are evident. This false-color image shows infrared light ranging from 1 to 1.6 μm from the NICMOS camera on the Hubble Space Telescope. The centers of both the Arches and YNC are so dense that only a handful of the brightest young stars can be individually resolved with HST and ground-based adaptive optics images on 8–10 m class telescopes are required. The images are oriented with North up and East to the left and are 80″ (3.2 pc at a distance of 8 kpc) on a side

3.3 Stellar Content and Cluster Ages

The presence of hot, massive stars, including OB main-sequence stars, OB giants, OB supergiants, and post-main-sequence Wolf–Rayet stars, in all three clusters is a clear indication that they are younger than 10 Myr. The ages of the three massive clusters are similar enough that there were early questions of whether a single starburst event occurred at the Galactic Center in which all of them formed. However, more detailed studies of the clusters' stellar content show that the ages are sufficiently different that they must have formed separately at three different times. It is notable that all three of these clusters have comparable total masses, on the order of $10^4\ M_\odot$. Thus, the total number of massive stars is large enough that the subsets of OB and WR stars and the ratios of different sub-classes (i.e., nitrogen-enriched vs. carbon-enriched WR stars, OB vs. WR stars) can be used as a means of age dating the clusters. Further age indicators include the location of the main-sequence turn-off and the most massive stars on the Hertzsprung–Russell diagram (Rosslowe and Crowther 2015). One should note that age dating clusters from only evolved stars, even with spectroscopy, is highly uncertain due to uncertainties in the models of stellar evolution and atmospheres and, most especially, the impact of binary mass-transfer on stellar evolution. These clusters' stellar content and ages are critical inputs into estimations of the initial mass function (see Sect. 3.5), which is a key output of the star formation process and can be used to constrain star and cluster formation theories (see Sect. 3.8). In this section, the clusters' stellar content and age determinations are described in order from youngest to oldest (Table 3.1).

Arches The Arches Cluster contains an estimated 160 O stars, including at least two OIf+ supergiants and 13 Wolf–Rayet stars of type WN7-9h, that have been identified spectroscopically and are packed largely within its virial radius of 0.76 ± 0.12 pc (Figer et al. 2002; Najarro et al. 2004; Martins et al. 2008; Harfst et al. 2010). The hydrogen-rich WN stars have luminosities ranging up to $2 \times 10^6\ L_\odot$, and implied initial masses exceeding $60\ M_\odot$ and ranging up to $120\ M_\odot$ (Martins et al. 2008). The WN stars are apparently still in their hydrogen-burning stage and have ages estimated by Martins et al. (2008) to be 2–3 Myr based on their spectral features and their location in the Hertzsprung–Russell diagram. Although the O supergiants could, in principle, have ages up to 4 Myr, it is more likely that the stars in this cluster are coeval, given that intense star formation in such a small

Table 3.1 Properties of Young Clusters at the Galactic Center

Cluster	D_{BH} (pc)	Mass ($M_\odot$)	Age (Myr)	Age w/binary (Myr)	Radius[a] ($''$)	(pc)
Arches	26	10^4	2.5 ± 0.5	3.5 ± 0.7	70	2.8
Quintuplet	32	10^4	3.0 ± 0.5	4.8 ± 1.1		
YNC	0	10^4	6 ± 2		24	0.96

[a]Projected distance where clusters members have been identified ($d = 8$ kpc)

volume would rapidly disperse gas. Therefore, the Arches Cluster age has converged to values of 2.5 ± 0.5 Myr (Martins et al. 2008; Figer et al. 1999a, 2002; Blum et al. 2001; Habibi et al. 2013). One note of caution is that the growing recognition of the importance of both binary evolution in massive stars and mass loss by strong stellar winds led (Schneider et al. 2014) to conclude from their Monte Carlo simulations that the most massive 9 ± 3 stars in the Arches are rejuvenated binary products. They therefore determine the age of the Arches Cluster to be 3.5 ± 0.7 Myr when the influence of binaries is accounted for.

The intermediate- and low-mass stellar content of the Arches cluster has proven more difficult to characterize given the high and variable extinction, stellar crowding, and confusion with the large number of field stars. Several attempts have been made to statistical identify members by using multi-band photometry from HST NICMOS, WFC3-IR, or ground-based adaptive optics imagers to construct a color-magnitude diagram (CMD) from the region of the cluster and to subtract off a corresponding offset field position (Figer et al. 1999a; Stolte et al. 2002, 2005; Kim et al. 2006; Espinoza et al. 2009; Shin and Kim 2015). However, the pre-main-sequence turn on point of the CMD is not clearly distinguishable with this approach. More recent studies employ proper motions to separate cluster members from contaminating field stars using ground-based adaptive optics observations (Stolte et al. 2010; Clarkson et al. 2012; Hosek et al. 2015; Stolte et al. 2015). The pre-main-sequence appears to be visible; but the current photometric precision of the AO data prevents this feature from being used to constrain the age of the cluster. Finally, roughly 10% of Arches members between 5 and 15 $M_{\odot}$ show significant infrared excess at K' (2.2 μm) and L' (3.8 μm). Several of these IR-excess sources have been confirmed as young stars with circumstellar disks based on the presence of CO emission in spectroscopy at 2.3 μm (Stolte et al. 2010). The disk fraction is broadly consistent with an age of 2–4 Myr when compared with other massive young clusters in the Milky Way and the LMC (Stolte et al. 2015).

Quintuplet Like the Arches Cluster, the Quintuplet is well-populated with WR stars, with 21 known altogether, but with a wider range of spectral types, including WN6, WN9-10h, WC8-9, and the five Quintuplet namesake stars, which are dust-enshrouded WC8-9 stars in high-mass binaries with colliding winds that give rise to spiral patterns (Figer et al. 1999b; Tuthill et al. 2006; Liermann et al. 2009, 2012). In addition, 60 O stars have been identified (Liermann et al. 2009), and one red supergiant is present in the central region of the cluster (Glass et al. 1990). On the basis of the mix of spectral types, (Liermann et al. 2012) estimate the age of the Quintuplet to be 3.0 ± 0.5 Myr, consistent with earlier estimates (Figer et al. 1999b; Liermann et al. 2010). Some consideration of the evolutionary effects of binary stars was included in the Liermann et al. (2012) age estimate, but Schneider et al. (2014) arrived at a somewhat older estimate of 4.8 ± 1.1 Myr by arguing for the greater importance of binary evolution and stellar winds than had previously been assumed, and concluding that the most massive 8 ± 3 stars in the Quintuplet are rejuvenated binary products. The presence of the red supergiant is potentially problematical for the younger age estimates because of the time needed for a star to evolve to that

stage. Considering only single star evolution, Vanbeveren et al. (1998) conclude that WR stars and red supergiants can be simultaneously present only for clusters in the age range from 4 to 5 Myr.

One additional piece of evidence that the Quintuplet is older than the Arches Cluster is that it is more dispersed. The core radius of the Quintuplet is 0.65 ± 0.09 pc (Hußmann et al. 2012), whereas that of the Arches Cluster is much smaller: 0.14 ± 0.05 pc (Espinoza et al. 2009). Although the initial cluster radii are unknown, these clusters are expected to evaporate on a time scale comparable to the age of the Quintuplet Cluster as a result of the strong tidal forces near the Galactic Center (Kim et al. 1999), so their central densities decline and core radii grow with time (Mauerhan et al. 2010; Dong et al. 2012; Habibi et al. 2014; Dong et al. 2015).

Interpreting the cluster luminosity functions or color-magnitude diagrams to determine age is also highly degenerate with metallicity. Fortunately, the metallicity at the Galactic Center is predominantly solar to slightly super-solar. The metallicity of the Quintuplet Cluster has been measured at roughly solar iron abundance and twice solar for α elements (Najarro et al. 2009). However, these measurements were conducted on hot, evolved stars whose stellar atmosphere models are still somewhat uncertain (Georgy et al. 2013; Leitherer et al. 2014).

YNC The Young Nuclear Cluster (YNC) in the central parsec around the supermassive black hole contains more than 100 hot stars including 23 Wolf–Rayet (WR) stars, six OB supergiants with narrow emission lines, and OB main-sequence or giant stars for the remainder (Allen et al. 1990; Krabbe et al. 1991, 1995; Blum et al. 1995; Tamblyn et al. 1996; Najarro et al. 1997; Ghez et al. 2003; Paumard et al. 2006; Bartko et al. 2010; Do et al. 2013; Feldmeier-Krause et al. 2015). The most massive and luminous of the OB stars have a spectral type of O7 or later, consistent with an age range of 3–8 Myr (Martins et al. 2007; Paumard et al. 2006; Feldmeier-Krause et al. 2015). The YNC is challenging to study as it is inter-mixed with the old nuclear star cluster that is more massive by several orders of magnitude and both clusters are centered on the supermassive black hole. YNC members have all been identified spectroscopically. Using the population synthesis models for single stars, the ratio of WR stars to OB stars favors an age closer to either 4 Myr or 8 Myr; but, this depends on the adopted IMF (Lu et al. 2013). There are a few of red supergiants (RSGs) that may belong to the YNC, including the most luminous M1 supergiant IRS 7. The presence of RSGs has been interpreted to favor an age between 6.5*and*10 Myr (Becklin and Neugebauer 1968, 1975; Pott et al. 2008; Paumard et al. 2014) as only lower mass stars of $M < 25\,M_{\odot}$ likely experience this cool phase on the post-main-sequence. However, note that the Quintuplet Cluster also hosts a RSG despite its age of 3–5 Myr.

The lower-mass stellar content of the YNC has yet to be studied due to the need for spectroscopy to find each cluster member. Thus pre-main-sequence turn-on dates will be the domain of future observatories such as the James Webb Space Telescope and the next-generation of 20–40 m ground-based telescopes equipped with adaptive optics.

3.4 Structure and Dynamics

A unique aspect of the young star clusters in the Galactic Center is the strong tidal field and dense environment in which they reside. The tidal forces come from the supermassive black hole, the old nuclear star cluster, and the inner bulge and disk, which all have rapidly rising stellar density profiles with decreasing radius (Launhardt et al. 2002; Portail et al. 2017). These tidal forces may impact the star formation efficiency, early dynamical evolution, and the rate of dissolution of these clusters (Kim et al. 1999, 2000; Kim and Morris 2003). This section presents the current state of our understanding of the radial distribution of stars and the internal kinematics of the cluster and how they have been used to measure the outer tidal radius and the orbit of the cluster around the Galactic Center.

Arches and Quintuplet Proper motion studies of both the Arches and Quintuplet using adaptive optics measurements have allowed investigators to establish the membership of these clusters, which have been extremely important for constraining their properties, given the very high density of unrelated bulge and disk stars projected against them. The number of known high-probability members is now ∼450 in the Arches Cluster and ∼1440 in the Quintuplet (Stolte et al. 2015; Hosek et al. 2015). The proper motions have also revealed the clusters' bulk motions, and when combined with radial velocity measurements, have provided strong constraints on the Galactic orbits and formation sites of these clusters, as described below and in Sect. 3.8.

The Arches Cluster is apparently one of the densest clusters in the Galaxy. Its central density has been estimated to be $2 \pm 0.4 \times 10^5\ M_\odot\ \mathrm{pc}^3$ (Espinoza et al. 2009). Investigations utilizing proper motions to cleanly identify cluster members have found that, despite theoretical predictions, there is no obvious tidal truncation radius in the outskirts of the cluster (Hosek et al. 2015). A significant population of cluster members can be found out to at least 2.8 pc (Fig. 3.3), which is the limit of the field of view of the current data sets. Beyond ∼0.1 pc, the surface density profile is well described by a power-law, $\Sigma \propto r^{-\Gamma}$ stars $\mathrm{pc}^{-}2$, with a slope of $\Gamma = 2.06 \pm 0.17$ (Hosek et al. 2015). This lack of tidal truncation may indicate that the cluster has not had a recent periapse passage between 0.2 and 1 Myr and that those stars that have escaped remain on a similar orbit. Future measurements of the internal velocity dispersion and N-body simulations of the Arches dynamical evolution are needed to fully interpret this finding. The Quintuplet Cluster's surface density profile is less well measured; however, it appears to be at least a factor of 4 less dense in the core than the Arches Cluster (Habibi 2014). An analysis of new Hubble Space Telescope (HST) data of comparable quality to the Arches data is underway.

YNC The YNC has a much more shallow surface density profile on the sky than the Arches and Quintuplet, with $\Gamma \sim 1$ (Do et al. 2013, 2017), and a sharp decrease in the stellar density beyond ∼0.4 pc (Støstad et al. 2015). The YNC also has kinematically distinct substructures including (1) a *thin disk* containing

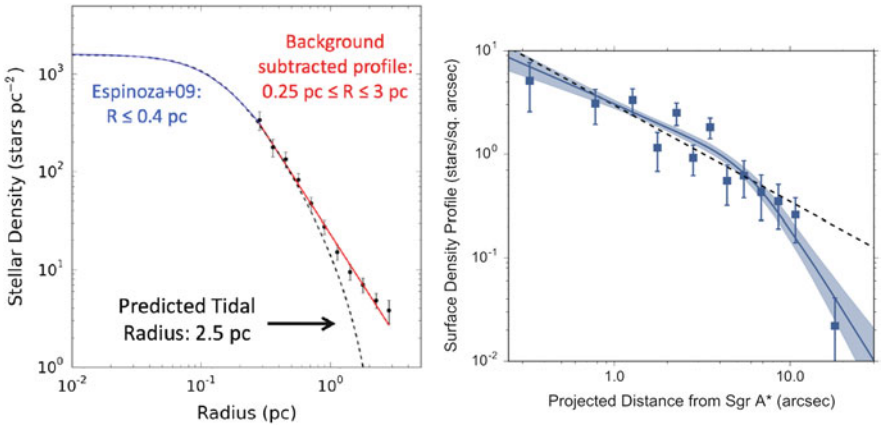

Fig. 3.3 The Arches (*left*) and YNC (*right*) cluster surface density profile. The Arches Cluster has a peak projected radial density of $\sim$ 1500 stars pc^{-}2 for stars of $M > 2.5\,M_{\odot}$ and extends as a power-law out to at least 3 pc, well beyond the predicted tidal truncation radius. The YNC density peak is $\sim$5 times higher than the Arches for stars with $M > 8\,M_{\odot}$. The YNC has a flatter profile that abruptly turns over at $\sim$10″ (0.4 pc). This *left panel* has been adopted and modified from Hosek et al. (2015). The *right panel* is reproduced from Do et al. (2017)

15 %, (2) an *off-disk* population with a broad range of inclinations containing 65 %, (3) an isotropic group of *S-stars* within 0.8″ with high-eccentricities containing 20 % (Ghez et al. 2008; Bartko et al. 2010; Yelda et al. 2014). The thin disk extends from 0.8″ to 3.2″ (0.03–0.13 pc) and has an opening angle of $\sim 8° \pm 1°$ or a scale height of $h/r = 0.1 \pm 0.01$ (Levin and Beloborodov 2003; Yelda et al. 2014). The orbital periods of the stars in the YNC are sufficiently short and the astrometric measurements sufficiently precise that some of the orbital parameters for individual stars are constrained. For stars on the thin disk, the eccentricity distribution is significantly different from 0 with an average of $< e > \sim 0.3$ (Yelda et al. 2014). In contrast, the eccentricity distribution of the S-star cluster is more thermalized with many high-eccentricity stars (Gillessen et al. 2017). The off-disk population is less well constrained, but extends from $\sim$3″ and outward. Additional substructures within this more nebulous population (e.g., warped disks) have been proposed but are currently of low significance (Bartko et al. 2009; Fritz et al. 2010). The kinematic substructures and the sharp outer edge of the YNC indicate that this cluster formed in situ and did not form far from the SMBH and migrate to its current location (Berukoff and Hansen 2006; Lu et al. 2009; Yelda et al. 2014; Støstad et al. 2015; Feldmeier-Krause et al. 2015).

Mass Segregation In discussions of cluster structure, one must always be aware of the impact of mass segregation. The previous radial profiles represent the average value for stars above $\sim 2.5\,M_{\odot}$. In the Arches Cluster, there is clear evidence of mass segregation with the brightest and most massive stars (H-band $\lesssim$ 17, $M > 13\,M_{\odot}$) showing a steeper drop-off with radius (Hosek et al. 2015). Unfortunately, the YNC membership currently doesn't extend beyond 8 $M_{\odot}$ and this, combined with the

complex dynamical substructures, makes mass segregation difficult to characterize. However, extreme mass segregation can significantly impact the interpretation of the cluster structure, enclosed mass, and dynamical evolution and care must be taken to incorporate this effect.

3.5 Present-Day and Initial Mass Functions

The distribution of stellar masses, known as initial mass function (IMF), is one of the fundamental outcomes of the star formation process. And yet, the question of whether the IMF is universal or not and how it varies with environment is still much debated (Bastian et al. 2010; van Dokkum and Conroy 2010). Most measurements of the IMF in the solar neighborhood show a mass function of the form

$$\frac{dN}{dm} \propto m^{-\alpha} \quad \text{where} \quad \begin{cases} \alpha = 2.3 & \text{for } 0.5\,M_\odot < m < 120\,M_\odot \\ \alpha = 1.3 & \text{for } 0.08\,M_\odot < m < 0.5\,M_\odot \\ \alpha = 0.3 & \text{for } 0.008\,M_\odot < m < 0.08\,M_\odot; \end{cases} \tag{3.1}$$

as originally proposed by Salpeter (1955) at the high-mass end and Kroupa (2001) at the low-mass end, although alternative forms such as a log-normal distribution have been proposed (Chabrier 2003; Bastian et al. 2010; Dib et al. 2017). The Galactic Center clusters are ideal laboratories for testing competing theories of star formation as they probe a more extreme environment and are sufficiently massive to populate the full range of stellar masses. Ultimately, the initial mass function of the Galactic Center clusters should be compared to other clusters in the Milky Way disk of similar mass and age in a well-controlled experiment that can be used to constrain star formation theories.

Although the clusters at the Galactic Center are young, they are still old enough to have experienced stellar and dynamical evolution that can significantly alter the initial mass function (IMF) into the observed present-day mass function (PDMF). Thus measurements of the IMF depend critically on knowledge of the cluster age, present-day internal dynamics, mass segregation, tidal truncation, and orbital history of the cluster to convert from a PDMF to an IMF. While we have not yet achieved such a complete picture of the IMF for the three Galactic Center clusters, there is already intriguing evidence that the initial mass function does vary in the Galactic Center. The current status of PDMF and IMF measurements for each of the clusters is described below.

YNC The YNC is in the most extreme environment in the Milky Way and thus is an excellent location to search for variations in the IMF of stars produced during cluster formation. Initial findings appeared to indicate an extremely top-heavy mass function, favoring the formation of very massive stars, for stars above $M > 8\,M_\odot$ (Bartko et al. 2010). However, more detailed analysis of spectroscopic observations

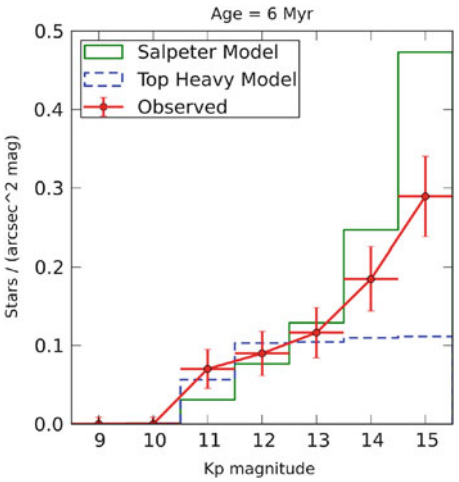

Fig. 3.4 The K_p-band (2.2 μm) luminosity function for the Young Nuclear Cluster (*red*) as compared with the best-fit model with a top-heavy IMF (*blue*) and a Salpeter IMF (*green*). Figure is reproduced from Lu et al. (2013)

used to distinguish young and old stars indicates that the IMF is only moderately top-heavy (Lu et al. 2013). Observations of young stars between ∼8 and 60 $M_\odot$ show that the mass function is consistent with a single power-law with $\alpha = 1.7 \pm 0.2$ compared to a Salpeter IMF slope of α ∼2.35 (Fig. 3.4). Further support for an IMF that favors massive stars may also be the over-abundance of magnetars (Muno et al. 2005), young neutron stars with extremely strong magnetic fields typically associated with massive progenitors ($M > 40\,M_\odot$ Figer et al. 2005; Gaensler et al. 2005; Muno et al. 2006), and a lack of normal pulsars that typically trace progenitor masses from 8 to 20 $M_\odot$ (Dexter and O'Leary 2014). Unfortunately, most of the IMF estimates in young star clusters near the solar neighborhood do not probe above $M > 8\,M_\odot$, which makes precise comparisons difficult.

One method for measuring the low-mass end of the IMF is through the X-ray emission of accretion or coronally active low-mass stars (e.g., Feigelson et al. 2002; Barnes 2003). Early observations from the Chandra X-ray Observatory indicated that the observed X-ray flux in the central parsec was deficient by a factor of 10 relative to the expected X-rays from a cluster with a normal IMF such as the Orion Nebula Cluster (Nayakshin and Sunyaev 2005). Our understanding of X-ray emission from pre-main-sequence stars has improved dramatically over the past decade and new X-ray data has been obtained that is several orders of magnitude more sensitive; thus the time is ripe for a new analysis of the low-mass end of the IMF from the X-ray perspective.

Studies of the IMF in the YNC couple tightly with studies of the cluster structure and dynamics as the more top-heavy the mass function is, the more quickly the disk can evolve and dynamically produce a wider range of eccentricities and inclinations from an initially circular disk (Alexander et al. 2007; Lu et al. 2013; Yelda et al. 2014). The current eccentricity distribution for on-disk stars, which peaks at $e \sim 0.3$, is just consistent a population formed at $e = 0$ *if* the IMF is slightly top-heavy.

Improvements in the IMF measurements for the YNC will require more sensitive spectroscopy, which may be available from the James Webb Space Telescope (JWST) and the next-generation of ground-based Extremely Large Telescopes (ELT) equipped with adaptive optics. Continued astrometric monitoring will also improve our ability to assign the individual young stars to the three kinematic substructures and compare the mass function between the groups. This is perhaps one of the most important methods for determining how the Young Nuclear Cluster formed and evolved into its present-day state.

Arches and Quintuplet The Arches and Quintuplet present-day mass function measurements extend to lower masses than the YNC since membership does not necessarily depend on spectroscopic observations. However, converting these clusters from a PDMF into an IMF is complicated by their rapid dynamical evolution. Mass segregation combined with possible tidal stripping can significantly alter this conversion process (Kim et al. 2000; Portegies Zwart et al. 2007; de Grijs 2009; Harfst et al. 2010). The most recent measurements of the present-day mass function using photometry alone yield a PDMF that appears to be roughly consistent with a Salpeter IMF above $M > 10\,M_{\odot}$ within the central 0.4 pc of both clusters (Stolte et al. 2002; Espinoza et al. 2009; Harfst et al. 2010; Habibi et al. 2013). Attempts have been made to convert the present-day mass function measurements into constraints on the initial mass function at the time of formation by comparing to N-body simulations of clusters in the Galactic Center potential with internal dynamical evolution and mass loss (Kim et al. 2000; Portegies Zwart et al. 2007; Harfst et al. 2010), with most models yielding an IMF consistent with the "universal" value (Fig. 3.5).

The lower end of the mass function, below where individual stars have been detected or resolved, has also been constrained with two different techniques. First, the total enclosed mass of the Arches Cluster has been estimated with measurements of the internal velocity dispersion using high-precision astrometric observations from the W.M. Keck Observatory adaptive optics system The velocity dispersion of $\sigma = 5.4 \pm 0.4$ translates into a constraint on the enclosed mass measurement of $M_{\rm encl} = 0.9 \times 10^4\,M_{\odot}$ within a radius of 0.4 pc (Clarkson et al. 2012). Interestingly, if you sum the individual observed stars at higher masses and use a Salpeter or Kroupa (2001) mass-function to project down to lower masses, the predicted enclosed mass is discrepant with the enclosed mass determined from the velocity dispersion (Fig. 3.6). The conversion from velocity dispersion to enclosed mass does depend on an assumption that the cluster is virialized. However, the most likely deviation from virial is that the cluster is expanding due to gas expulsion or external tidal forces, and this would lead to an overly large dispersion, in contrast with what is observed. Therefore, the most likely interpretation of the velocity dispersion constraint is that the mass function deviates from a Kroupa IMF with either a higher-mass peak or a flatter slope, with more massive stars than the field IMF.

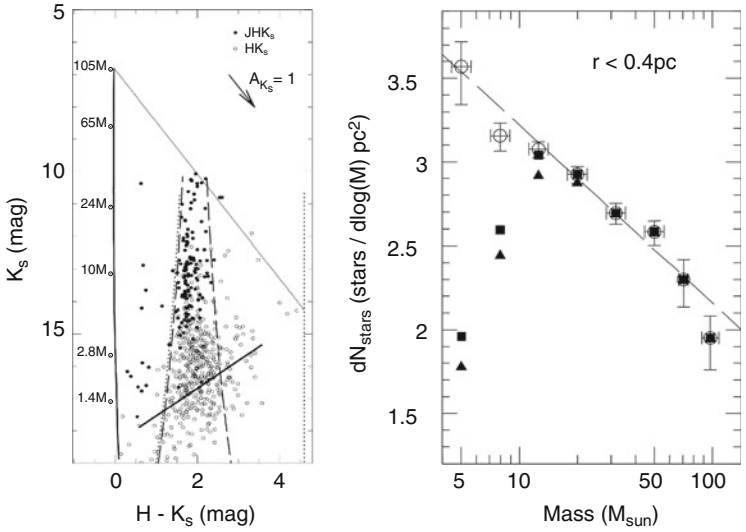

Fig. 3.5 The Arches color—magnitude diagram (*left*) and mass function (*right*) reproduced and modified from Espinoza et al. (2009). The CMD contains both field and cluster stars and cluster members were selected photometrically using color cuts defined by the *dashed lines*. Also shown are a 2.5 Myr unreddened isochrone, the reddening vector, and the 50. The mass function is shown for completeness-corrected data in *circles* with large corrections, noted as *open circles*, below 10 $M_\odot$. The resulting mass function slope for this photometrically selected sample is consistent with a Salpeter slope

Second, the low-mass end of the mass function has also been constrained by examining the residual light after subtracting off the more massive resolved stars (Shin and Kim 2015, 2016). In contrast with findings from the velocity dispersion, the residual light appears consistent with a Kroupa IMF below 1–2 $M_\odot$. However, the integrated light measurements depend on statistical subtraction of the field contribution and assume perfect subtraction of the PSF, which are both sources of significant uncertainty given the large and spatially variable reddening present toward the cluster and control fields.

Major limitations on current estimates of the mass functions in the Arches and Quintuplet Clusters include the lack of cluster membership, limited sensitivity to individual low-mass stars, and uncertainties in the conversion between luminosity and mass due to differential extinction and a possibly variable extinction law. The addition of proper motions is essential to identifying cluster members at lower mass and at larger radii with high completeness. Programs are underway to combine astrometry from ground-based adaptive optics systems on the most-crowded cluster centers with Hubble Space Telescope IR data on outskirts of the cluster, which should yield precise measurements of the PDMF down to $\sim$1 $M_\odot$. Future observations with JWST and the ELTs may push this lower mass limit down into the brown dwarf regime.

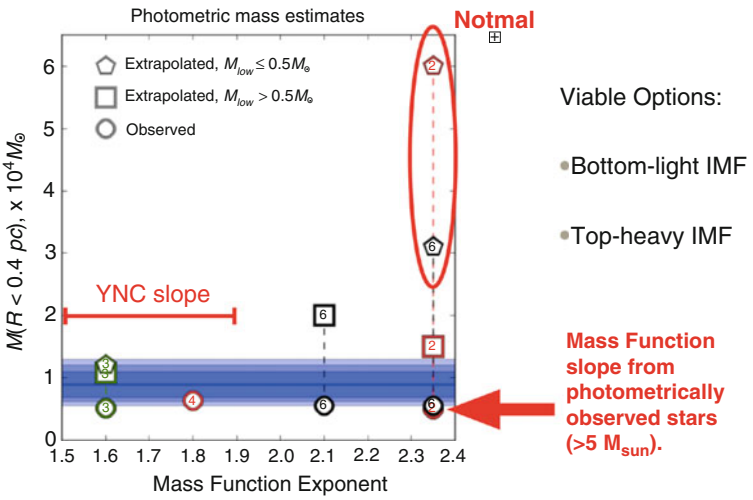

Fig. 3.6 A comparison of the Arches Cluster mass estimates from both photometric and kinematic measurements. The total enclosed mass determined from measurements of the internal velocity dispersion is shown as a *blue band*. Mass estimates from counting individual stars in photometric bins are shown with symbols for the directly observed mass (*circles*) and extrapolated mass (*squares, pentagons*) for different IMF high-mass slopes and low-mass cutoffs. The "normal" IMFs are disallowed and the Arches IMF likely has either a flatter high-mass slope (similar to the YNC) or a low-mass cutoff that is significantly above the 0.5 $M_\odot$ cutoff found in the solar neighborhood. This figure has modified from the original Fig. 11 of Clarkson et al. (2012)

3.6 Cluster Orbits and Birth Locations

Unlike young clusters in the Milky Way disk, the Arches and Quintuplet clusters have traversed a significant fraction of their orbit. Thus they may have migrated through significantly different environments with weaker or stronger tidal fields than their present-day location indicates. In other words, they weren't born where they are today and accurate knowledge of their birth location is needed to interpret observations. The same may be true for the YNC—it may have been born elsewhere and migrated into its current location. Current measurements of the cluster orbits and birth locations are presented below. The impact of this birth location on the star formation process is described in more detail in Sect. 3.8.

YNC The Young Nuclear Cluster is centered on the supermassive black hole and extends to $\sim$ 0.4 pc with a fairly sharp truncation as described in Sect. 3.4. The lack of a trail of young stars out at larger radii indicates that young stars most likely formed in situ rather than migrating in from larger radii. Proposed formation scenarios for the YNC are discussed in more detail in Sect. 3.8.

Arches and Quintuplet The birth site of the Arches and Quintuplet is not well known as the clusters are old enough to have traveled at least once around the

Galaxy. One method that has been employed to determine their birth sites is using proper motions and radial velocities to constrain the orbit that the clusters are on. The velocity of the Arches Cluster has been measured from a combination of spectroscopy and proper motions yielding a 3D space motion of $232 \pm 30\,\mathrm{km\,s^{-1}}$ with respect to the field population assuming a distance of 8 kpc (Stolte et al. 2008). The Quintuplet's 3D velocity has been similarly measured as $167 \pm 15\,\mathrm{km\,s^{-1}}$ (Stolte et al. 2015) relative to the field. The direction of the two velocity vectors are similar and are mostly aligned with the plane of the Milky Way with very little motion along the line-of-sight. Some caution is required regarding current estimates of the absolute proper motion for the clusters since it is measured with respect to the non-cluster stars in the field of view and then corrected using a model of the field population. However, measuring and modeling the field population is still difficult and an active area of investigation (Portail et al. 2017).

The 3D motions, combined with the 2D positions on the plane of the sky, have been used to model the orbits of the two clusters. The line-of-sight distance is unknown for both clusters; except that strong interactions between the gas clouds and the clusters, as evidenced by photo-ionization fronts, indicate that the clusters are likely in the central molecular zone within 200 pc of the center. Thus certain classes of orbits can be ruled out, including circular orbits (Fig. 3.7 Stolte et al. 2008, 2014). The lack of a tidal truncation radius in the observed surface density profile for the Arches Cluster may also indicate that only those orbits that place the Arches in front of the SMBH are permitted (Hosek et al. 2015). However, a more complete N-body simulation with an accurate gravitational potential for the Galactic bulge, inner disk, bar, and nuclear cluster is needed to verify this finding.

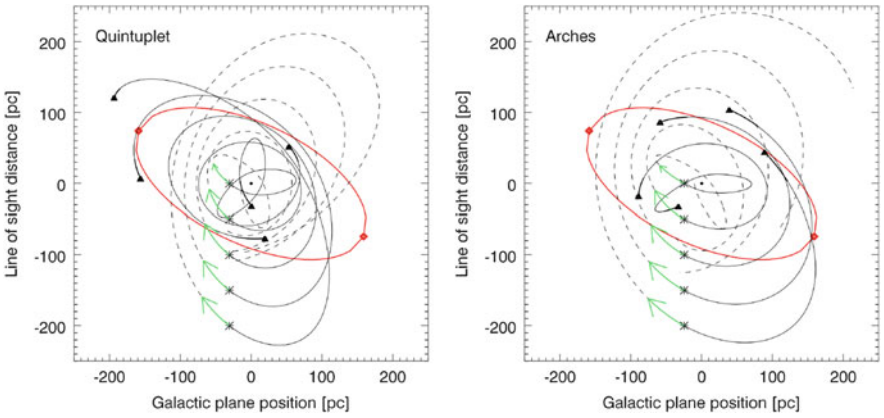

Fig. 3.7 Possible orbits for the Arches and Quintuplet based on the 2D position on the sky and the 3D space motion. The figure is reproduced from Stolte et al. (2010) and is based on data from Stolte et al. (2008); Clarkson et al. (2012); Stolte et al. (2010). The orbit is viewed from above the Galactic plane with the present-day positions at various line-of-sight distances marked as *asterisks*. The *red ellipse* shows the outermost x2 orbits, which is also the location of the molecular ring/streams (Molinari et al. 2011) and may be the birth site of both the Arches and Quintuplet (Stolte et al. 2014)

3.7 Observational Methodology

Key ingredients for observations of the Galactic Center young massive clusters include the following:

- Infrared images and spectra are necessary to penetrate the high extinction ($A_V \sim 30$) toward the Galactic Center.
- High spatial resolution is essential for overcoming crowding and resolving individual stars and stellar systems down to low masses.
- Cluster membership is best obtained with high-precision proper motion for the Arches and Quintuplet and with integral-field unit spectroscopy for the YNC.
- High-precision, multi-band photometry is needed to refine extinction laws and maps of the spatially varying extinction.
- The relationship between the apparent magnitude and the stellar mass should be calibrated using spectroscopy of well-modeled (e.g., main-sequence) stars. This helps remove degeneracies with age and distance that arise when only fitting photometry.
- Accurate stellar evolution and atmosphere models that include moderate resolution at infrared wavelengths are also needed.
- Constraining the cluster properties such as the IMF slopes, cluster age, cluster distance, and total extinction requires modeling and optimization routines that properly capture the uncertainties in the data, incompleteness, and correlations between the parameters. Bayesian inference methods work well.

State-of-the-art observations of the Galactic Center clusters currently come from large ground-based telescopes equipped with either (1) adaptive optics systems that deliver diffraction limited IR images for photometry and astrometry and spectroscopy for spectral types and radial velocities over smaller fields of view ($\sim 20''$), or (2) HST IR images that provide precise photometry and astrometry at slightly lower spatial resolution but over wider fields ($\sim 2'$). The astrometric precision required to identify cluster members is better than 0.2 mas yr^{-1}, which can be achieved in <1 year with NIRC2 at Keck (Lu 2008).

One procedure for modeling the observed clusters is laid out in Fig. 3.8. While this procedure is conceptually simple, it has rarely been implemented in a manner where all parameters are modeled simultaneously as it is computationally expensive and systematic errors in the models can lead to biased results (Lu et al. 2013).

3.8 Star Formation: Is it Peculiar?

The young stellar population in the Galactic Center is only one half of the puzzle of whether star formation in the Galactic Center differs significantly from star formation in the solar neighborhood or throughout the Milky Way disk. The other half to investigate is the molecular gas and molecular clouds and how their

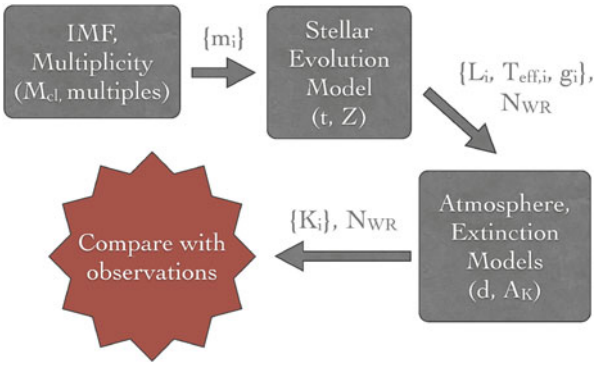

Fig. 3.8 A schematic of the necessary ingredients for modeling the initial mass function of a star cluster. Synthetic clusters are generated using a mass function and multiplicity distributions to predict a set of stellar and system masses, $\{m_i\}$. Using stellar evolution models for a certain age, t, and metallicity, Z, the masses are converted to luminosity, effective temperature, and gravity $\{L_i, T_{\mathrm{eff},i}, \log(g_i)\}$. Note that post-main-sequence massive stars such as Wolf–Rayet stars are very difficult to model; however, the number of Wolf–Rayet stars is a reliable product of the models. Atmosphere models, extinction laws, and filter transmission functions are used to convert these quantities into apparent magnitudes. Finally, the synthetic clusters are compared to observations and this process can be repeated to optimize the cluster properties, including the IMF

properties are different from similar clouds in the Milky Way disk. New data with the JVLA and ALMA and large surveys with SMA and APEX have confirmed that the central molecular zone has more extreme properties such as higher temperatures, pressures, and magnetic fields (e.g., Pillai et al. 2015; Ginsburg et al. 2016), and that star formation is suppressed compared with gas of a similar density in the Milky Way disk (Kruijssen et al. 2014; Kauffmann et al. 2016). Star formation theory and simulations frequently show changes to the mass function slopes and turn-over points when initial gas conditions are changed to such a degree (e.g., Morris 1993; Bonnell et al. 2004; Krumholz and McKee 2008). However, in this section, we focus on the stellar output of the star formation process and we interpret it in the context of understanding whether the IMF varies a little, a lot, or not at all in the extreme environment at the Galactic Center.

Arches and Quintuplet The Arches and Quintuplet most likely formed in the central molecular zone given that there is abundant evidence of giant molecular clouds apparently in different stages of star formation such as Sgr B2 (Longmore et al. 2013). The molecular clouds in this region have significantly different properties from those in the Milky Way disk and may, in fact, be more representative of molecular cloud properties in high-redshift galaxies with extreme pressures, densities, temperatures, ambient radiation fields, and cosmic-ray fluxes (Morris and Serabyn 1996). The distribution of molecular clouds in the Central Molecular Zone are not random and show evidence for dynamical order in the form of a ring or streamers (Molinari et al. 2011) along the outermost x2 family of bar orbits (Binney et al. 1991), where the long-axis bar orbits and the short-axis bar orbits intersect.

There have been suggestions that the Arches and Quintuplet fall on the same ring-like structure (Longmore et al. 2013); however, the current reported velocities are somewhat inconsistent with this picture (Stolte et al. 2014). Further observations are needed of both the gas and stars to understand the connection between the Arches and Quintuplet and other star-forming clouds in the CMZ.

YNC The currently favored formation scenario for the Young Nuclear Cluster is in situ formation, where the stars formed in their current location, from one or more molecular clouds that rapidly fell into the central parsec (Vollmer and Duschl 2001; Nayakshin et al. 2007). Alternative scenarios that have been proposed include the formation of a young massive cluster at much larger radii that spirals in via dynamical friction and is tidally disrupted in the central parsec (Gerhard 2001; McMillan and Portegies Zwart 2003). The supporting observational evidence that favors in situ scenarios over infall scenarios is the steep radial profile with an outer break of the observed massive young stars (Levin and Beloborodov 2003; Nayakshin and Sunyaev 2005).

The in situ formation scenario naturally produces a disk of young stars as infalling molecular gas settles into a thin disk (Morris 1993; Nayakshin and Sunyaev 2005; Levin and Beloborodov 2003; Bonnell and Rice 2008; Wardle and Yusef-Zadeh 2008; Hobbs and Nayakshin 2009). In principle, a gaseous disk could have built up slowly over time and, once it reached a critical mass, collapsed vertically under its own self-gravity. A slow-gas-buildup scenario is unlikely to produce a significant population of off-disk stars. Subsequent dynamical evolution also appears insufficient to explain the observed high ratio of off-disk to disk stars and non-zero eccentricities both on and off the disk; although work is still ongoing in this area (Gualandris et al. 2012; Ulubay-Siddiki et al. 2013; Šubr and Haas 2014; Haas and Šubr 2016). Thus, the molecular material from which the YNC formed most likely fell in rapidly (Bonnell and Rice 2008; Mapelli et al. 2008). The simulations that most closely resemble the observed data so far are those involving the infall of two molecular clouds that collide producing gas on a thin inner disk and many more gas streamers at larger radii that have a large range of orientations (Nayakshin et al. 2007; Vollmer et al. 2004; Alig et al. 2011).

The in situ formation scenarios do not easily explain the origin of the S-stars concentrated in the central $0.5''$ or 0.02 pc. At these close distances, the tidal forces are simply too strong for a molecular cloud to collapse and form a star. Numerous scenarios for migrating the S-stars from the young disk into tighter orbits around the black hole have been explored (e.g., Alexander et al. 2007; Perets and Alexander 2008; Löckmann et al. 2009; Perets and Gualandris 2010). Madigan et al. (2014) have analyzed the dynamics of the B-type main-sequence stars and show that the brightest S-stars could have been formed in the disk of young stars and migrated in, while the fainter S-stars are too numerous to have come from the disk alone and require some other injection mechanism or star formation event to explain their existence. The origin and fate of the S-stars and their relation to both the YNC and hypervelocity stars observed flying away from the Galactic Center is an important area of current research (Brown et al. 2009).

Finally, the YNC is only the most recent episode of star formation in the central parsec (Morris 1993). Based on spectroscopic studies, it appears that 80% of the mass in the nuclear star cluster is older than 5 Gyr (Pfuhl et al. 2011). While the YNC may represent the current state of star formation, it does not contribute much in the way of total mass of the nuclear cluster. Further studies of the mass-function of the old nuclear cluster are needed as it holds fossil information about the long-term history of the IMF.

3.9 Open Questions

Many of the most pressing questions in star and cluster formation can be addressed with observations of the Galactic Center young massive clusters. Specific next steps are described in detail in the above sections. They are summarized and prioritized here:

1. Is the star formation process fundamentally different in the extreme environment of the Galactic Center as evidenced by changes in the initial mass function and multiplicity properties?
2. Where were the individual clusters born and how does their birth location relate to other major features such as the $r \sim 100$ pc gas stream/ring, the circumnuclear disk, and the SMBH?
3. What is the orbit for the Arches and Quintuplet Cluster and how close do they approach the SMBH?
4. How close in time where the Arches, Quintuplet, and YNC born and was this flurry of cluster formation unique or do comparable-mass older and younger clusters also exist.
5. Can we measure the tidal radius, mass segregation, and internal dynamical state of the Arches and Quintuplet in order to constrain models of cluster evolution in a strong tidal field?
6. How did the kinematic substructures in the YNC (disk, off-disk, and S-star cluster) form and evolve and are the stellar populations different in each group?
7. Does the central molecular zone enhance or suppress star formation relative to the Galactic disk?
8. Is the distribution of cluster masses born in the Galactic Center environment significantly different than in the Galactic disk?
9. How does the formation and evolution of the YNC couple with the growth of the SMBH and the nuclear star cluster?
10. Where do the young hypervelocity stars come from and how frequently are they ejected in different directions?

Many of these questions can be partially or completely address with high-spatial-resolution infrared imaging and spectroscopy, including precise multi-band photometry, long time-baseline astrometry, and spectral resolution sufficient to measure radial velocities and spectral types. Such observations typically require

large ground-based telescopes equipped with adaptive optics or, in the less-dense outskirts of the cluster, HST and JWST. While the Gaia mission will provide high-precision astrometry, it is largely blind to stars in the Galactic Center as they are too heavily extinct in Gaia's optical band pass. However, Gaia will be instrumental in defining an absolute astrometric reference that high-resolution infrared astrometry can tie into in order to measure the Arches and Quintuplet Cluster orbits. Additionally, the future WFIRST mission will place many of the cluster observations, which can be done with a few HST and JWST pointings, into a broader context and allow us to search for lower-mass or slightly older star clusters that don't stand out photometrically but can be identified astrometrically. With the advent of the next-generation of extremely large telescopes, the IMF can be determined down to very low-mass stars and brown dwarfs and in-depth multiplicity studies can be conducted. The Galactic Center will remain an interesting environment in which to study star and cluster formation for the foreseeable future.

References

Alexander, R.D., Begelman, M.C., et al.: Astrophys. J. **654**, 907 (2007)
Alig, C., Burkert, A., et al.: Mon. Not. R. Astron. Soc. **412**, 469 (2011)
Allen, D.A., Hyland, A.R., et al.: Mon. Not. R. Astron. Soc. **244**, 706 (1990)
Allen, D.A., Hyland, A.R., et al.: Mon. Not. R. Astron. Soc. **204**, 1145 (1983)
Barnes, S.A.: Astrophys. J. **586**, 464 (2003)
Bartko, H., Martins, F., et al.: Astrophys. J. **697**, 1741 (2009)
Bartko, H., Martins, F., et al.: Astrophys. J. **708**, 834 (2010)
Bastian, N., Covey, K.R., et al.: Annu. Rev. Astron. Astrophys. **48**, 339 (2010)
Becklin, E.E., Neugebauer, G.: Astrophys. J. **151**, 145 (1968)
Becklin, E.E., Neugebauer, G.: Astrophys. J. Lett. **200**, L71 (1975)
Berukoff, S.J., Hansen, B.M.S.: Astrophys. J. **650**, 901 (2006)
Binney, J., Gerhard, O.E., et al.: Mon. Not. R. Astron. Soc. **252**, 210 (1991)
Blum, R.D., Depoy, D.L., et al.: Astrophys. J. **441**, 603 (1995)
Blum, R.D., Schaerer, D., et al.: Astron. J. **122**, 1875 (2001)
Bonnell, I.A., Rice, W.K.M.: Science **321**, 1060 (2008)
Bonnell, I.A., Vine, S.G., et al.: Mon. Not. R. Astron. Soc. **349**, 735 (2004)
Brown, W.R., Geller, M.J., et al.: Astrophys. J. **690**, 1639 (2009)
Chabrier, G.: Publ. Astron. Soc. Pac. **115**, 763 (2003)
Clarkson, W.I., Ghez, A.M., et al.: Astrophys. J. **751**, 132 (2012)
Colgan, S.W.J., Erickson, E.F., et al.: Astrophys. J. **470**, 882 (1996)
Cotera, A.S., Erickson, E.F., et al.: Astrophys. J. **461**, 750 (1996)
de Grijs, R.: Astrophys. Space Sci. **324**, 283 (2009)
Dexter, J., O'Leary, R.M.: Astrophys. J. Lett. **783**, L7 (2014)
Dib, S., Schmeja, S., et al.: Mon. Not. R. Astron. Soc. **464**, 1738 (2017)
Do, T., Ghez, A., et al.: In: Crocker, R.M., Longmore, S.N., Bicknell, G.V. (eds.) IAU Symposium. The Multi-Messenger Astrophysics of the Galactic Centre, vol. 322, pp. 222–230 (2017)
Do, T., Kerzendorf, W., et al.: Astrophys. J. **809**, 143 (2015)
Do, T., Lu, J.R., et al.: Astrophys. J. **764**, 154 (2013)
Dong, H., Mauerhan, J., et al.: Mon. Not. R. Astron. Soc. **446**, 842 (2015)
Dong, H., Wang, Q.D., et al.: Mon. Not. R. Astron. Soc. **425**, 884 (2012)
Espinoza, P., Selman, F.J., et al.: Astron. Astrophys. **501**, 563 (2009)
Feigelson, E.D., Garmire, G.P., et al.: Astrophys. J. **572**, 335 (2002)

Feldmeier-Krause, A., Neumayer, N., et al.: Astron. Astrophys. **584**, A2 (2015)
Figer, D.F., Kim, S.S., et al.: Astrophys. J. **525**, 750 (1999a)
Figer, D.F., McLean, I.S., et al.: Astrophys. J. **514**, 202 (1999b)
Figer, D.F., Najarro, F., et al.: Astrophys. J. Lett. **622**, L49 (2005)
Figer, D.F., Najarro, F., et al.: Astrophys. J. **581**, 258 (2002)
Fritz, T.K., Gillessen, S., et al.: Astrophys. J. **721**, 395 (2010)
Gaensler, B.M., McClure-Griffiths, N.M., et al.: Astrophys. J. Lett. **620**, L95 (2005)
Georgy, C., Ekström, S., et al.: Astron. Astrophys. **558**, A103 (2013)
Gerhard, O.: Astrophys. J. Lett. **546**, L39 (2001)
Ghez, A.M., Duchêne, G., et al.: Astrophys. J. Lett. **586**, L127 (2003)
Ghez, A.M., Salim, S., et al.: Astrophys. J. **689**, 1044–1062 (2008)
Gillessen, S., Plewa, P.M., et al.: Astrophys. J. **837**, 30 (2017)
Ginsburg, A., Henkel, C., et al.: Astron. Astrophys. **586**, A50 (2016)
Glass, I.S., Moneti, A., et al.: Mon. Not. R. Astron. Soc. **242**, 55P (1990)
Gualandris, A., Mapelli, M., et al.: Mon. Not. R. Astron. Soc. **427**, 1793 (2012)
Haas, J., Šubr, L.: Astrophys. J. **822**, 25 (2016)
Habibi, M.: Starburst clusters in the Galactic center. Ph.D. thesis, Argelander Institut für Astronomie, Universität Bonn (2014)
Habibi, M., Stolte, A., et al.: Astron. Astrophys. **556**, A26 (2013)
Habibi, M., Stolte, A., et al.: Astron. Astrophys. **566**, A6 (2014)
Harfst, S., Portegies Zwart, S., et al.: Mon. Not. R. Astron. Soc. **409**, 628 (2010)
Henshaw, J.D., Longmore, S.N., et al.: Mon. Not. R. Astron. Soc. **457**, 2675 (2016)
Hobbs, A., Nayakshin, S.: Mon. Not. R. Astron. Soc. **394**, 191 (2009)
Hosek, M.W. Jr., Lu, J.R., et al.: Astrophys. J. **813**, 27 (2015)
Hußmann, B., Stolte, A., et al.: Astron. Astrophys. **540**, A57 (2012)
Kauffmann, J., Pillai, T., et al.: (2016). arXiv e-prints
Kim, S.S., Figer, D.F., et al.: Astrophys. J. Lett. **653**, L113 (2006)
Kim, S.S., Figer, D.F., et al.: Astrophys. J. **545**, 301 (2000)
Kim, S.S., Morris, M.: Astrophys. J. **597**, 312 (2003)
Kim, S.S., Morris, M., et al.: Astrophys. J. **525**, 228 (1999)
Krabbe, A., Genzel, R., et al.: Astrophys. J. Lett. **382**, L19 (1991)
Krabbe, A., Genzel, R., et al.: Astrophys. J. Lett. **447**, L95 (1995)
Kroupa, P.: Mon. Not. R. Astron. Soc. **322**, 231 (2001)
Kruijssen, J.M.D., Longmore, S.N.: Mon. Not. R. Astron. Soc. **435**, 2598 (2013)
Kruijssen, J.M.D., Longmore, S.N., et al.: Mon. Not. R. Astron. Soc. **440**, 3370 (2014)
Krumholz, M.R., McKee, C.F.: Nature **451**, 1082 (2008)
Lang, C.C., Goss, W.M., et al.: Astrophys. J. Lett. **551**, L143 (2001)
Launhardt, R., Zylka, R., et al.: Astron. Astrophys. **384**, 112 (2002)
Leitherer, C., Ekström, S., et al.: Astrophys. J. Suppl. Ser. **212**, 14 (2014)
Levin, Y., Beloborodov, A.M.: Astrophys. J. Lett. **590**, L33 (2003)
Liermann, A., Hamann, W., et al.: Astron. Astrophys. **524**, A82+ (2010)
Liermann, A., Hamann, W.-R., et al.: Astron. Astrophys. **494**, 1137 (2009)
Liermann, A., Hamann, W.-R., et al.: Astron. Astrophys. **540**, A14 (2012)
Löckmann, U., Baumgardt, H., et al.: Mon. Not. R. Astron. Soc. **398**, 429 (2009)
Longmore, S.N., Kruijssen, J.M.D., et al.: Mon. Not. R. Astron. Soc. **433**, L15 (2013)
Lu, J.R.: Exploring the origins of the young stars in the central parsec of the Galaxy with stellar dynamics. Ph.D. thesis, University of California, Los Angeles (2008)
Lu, J.R., Do, T., et al.: Astrophys. J. **764**, 155 (2013)
Lu, J.R., Ghez, A.M., et al.: Astrophys. J. **690**, 1463 (2009)
Madigan, A.-M., Pfuhl, O., et al.: Astrophys. J. **784**, 23 (2014)
Mapelli, M., Moore, B., et al.: Mon. Not. R. Astron. Soc. **383**, 1223 (2008)
Martins, F., Genzel, R., et al.: Astron. Astrophys. 468, 2007, 233
Martins, F., Hillier, D.J., et al.: Astron. Astrophys. **478**, 219 (2008)
Mauerhan, J.C., Morris, M.R., et al.: Astrophys. J. Lett. **713**, L33 (2010)

McMillan, S.L.W., Portegies Zwart, S.F.: Astrophys. J. **596**, 314 (2003)
Molinari, S., Bally, J., et al.: Astrophys. J. Lett. **735**, L33 (2011)
Morris, M.: Astrophys. J. **408**, 496 (1993)
Morris, M., Serabyn, E.: Annu. Rev. Astron. Astrophys. **34**, 645 (1996)
Morris, M., Yusef-Zadeh, F.: Astrophys. J. **343**, 703 (1989)
Muno, M.P., Clark, J.S., et al.: Astrophys. J. Lett. **636**, L41 (2006)
Muno, M.P., Lu, J.R., et al.: Astrophys. J. **633**(1), 228 (2005)
Nagata, T., Woodward, C.E., et al.: Astron. J. **109**, 1676 (1995)
Nagata, T., Woodward, C.E., et al.: Astrophys. J. **351**, 83 (1990)
Najarro, F., Figer, D.F., et al.: Astrophys. J. Lett. **611**, L105 (2004)
Najarro, F., Figer, D.F., et al.: Astrophys. J. **691**, 1816 (2009)
Najarro, F., Krabbe, A., et al.: Astron. Astrophys. **325**, 700 (1997)
Nayakshin, S., Cuadra, J., et al.: Mon. Not. R. Astron. Soc. **379**, 21 (2007)
Nayakshin, S., Sunyaev, R.: Mon. Not. R. Astron. Soc. **364**, L23 (2005)
Okuda, H., Shibai, H., et al.: In: Peimbert, M., Jugaku, J. (eds.) IAU Symposium. Star Forming Regions, vol. 115, p. 556 (1987)
Okuda, H., Shibai, H., et al.: In: Morris, M. (ed.) IAU Symposium. The Center of the Galaxy, vol. 136, p. 281 (1989)
Okuda, H., Shibai, H., et al.: Astrophys. J. **351**, 89 (1990)
Paumard, T., Genzel, R., et al.: Astrophys. J. **643**, 1011 (2006)
Paumard, T., Pfuhl, O., et al.: Astron. Astrophys. **568**, A85 (2014)
Perets, H.B., Alexander, T.: Astrophys. J. **677**, 146–159 (2008)
Perets, H.B., Gualandris, A.: Astrophys. J. **719**, 220 (2010)
Pfuhl, O., Fritz, T.K., et al.: Astrophys. J. **741**, 108 (2011)
Pillai, T., Kauffmann, J., et al.: Astrophys. J. **799**, 74 (2015)
Portail, M., Gerhard, O., et al.: Mon. Not. R. Astron. Soc. **465**, 1621 (2017)
Portegies Zwart, S., Gaburov, E., et al.: Mon. Not. R. Astron. Soc. **378**, L29 (2007)
Pott, J.-U., Eckart, A., et al.: Astron. Astrophys. **487**, 413 (2008)
Rieke, G.H., Low, F.J.: Astrophys. J. **184**, 415 (1973)
Rosslowe, C.K., Crowther, P.A.: Mon. Not. R. Astron. Soc. **447**, 2322 (2015)
Salpeter, E.E.: Astrophys. J. **121**, 161 (1955)
Sanders, R.H.: Nature **359**, 131 (1992)
Schneider, F.R.N., Izzard, R.G., et al.: Astrophys. J. **780**, 117 (2014)
Schödel, R., Feldmeier, A., et al.: Astron. Astrophys. **566**, A47 (2014)
Schödel, R., Merritt, D., et al.: Astron. Astrophys. **502**, 91 (2009)
Shin, J., Kim, S.S.: Mon. Not. R. Astron. Soc. **447**, 366 (2015)
Shin, J., Kim, S.S.: Mon. Not. R. Astron. Soc. **460**, 1854 (2016)
Stolte, A., Brandner, W., et al.: Astrophys. J. Lett. **628**, L113 (2005)
Stolte, A., Ghez, A.M., et al.: Astrophys. J. **675**, 1278 (2008)
Stolte, A., Grebel, E.K., et al.: Astron. Astrophys. **394**, 459 (2002)
Stolte, A., Hußmann, B., et al.: Astrophys. J. **789**, 115 (2014)
Stolte, A., Hußmann, B., et al.: Astron. Astrophys. **578**, A4 (2015)
Stolte, A., Morris, M.R., et al.: Astrophys. J. **718**, 810 (2010)
Støstad, M., Do, T., et al.: Astrophys. J. **808**, 106 (2015)
Tamblyn, P., Rieke, G.H., et al.: Astrophys. J. **456**, 206 (1996)
Tuthill, P., Monnier, J., et al.: Science **313**, 935 (2006)
Ulubay-Siddiki, A., Bartko, H., et al.: Mon. Not. R. Astron. Soc. **428**, 1986 (2013)
Šubr, L., Haas, J.: Astrophys. J. **786**, 121 (2014)
van Dokkum, P.G., Conroy, C.: Nature **468**, 940 (2010)
Vanbeveren, D., De Loore, C., et al.: Astron. Astrophys. Rev. **9**, 63 (1998)
Vollmer, B., Beckert, T., et al.: Astron. Astrophys. **413**, 949 (2004)
Vollmer, B., Duschl, W.J.: Astron. Astrophys. **377**, 1016 (2001)
Wardle, M., Yusef-Zadeh, F.: Astrophys. J. Lett. **683**, L37 (2008)
Yelda, S., Ghez, A.M., et al.: Astrophys. J. **783**, 131 (2014)

Chapter 4
The Lifecycle of Clusters in Galaxies

Angela Adamo and Nate Bastian

Abstract We review many of the basic properties of star cluster systems, and focus in particular on how they relate to their host galaxy properties and ambient environment. The cluster mass and luminosity functions are well approximated by power-laws of the form $Ndm \propto M^{\alpha} dm$, with $\alpha \sim -2$ over most of the observable range. However, there is now clear evidence that both become steeper at high masses/luminosities, with the value of the downward turn dependent on environment. The host galaxy properties also appear to affect the cluster formation efficiency (Γ—i.e. the fraction of stars that form in bound clusters), with higher star-formation rate density galaxies having higher Γ values. Within individual galaxies, there is evidence for Γ to vary by a factor of 3–4, likely following the molecular gas surface density, in agreement with recent predictions. Finally, we discuss cluster disruption and its effect on the observed properties of a population, focussing on the age distribution of clusters. We briefly discuss the expectations of theoretical and numerical studies, and also the observed distributions in a number of galaxies. Most observational studies now find agreement with theoretical expectations, namely nearly a constant cluster age distribution for ages up to $\sim$100 Myr (i.e. little disruption), and a drastic steepening above this value caused by a combination of cluster disruption and incompleteness. Rapid cluster disruption for clusters with ages $<$100 Myr is ruled out for most galaxies.

A. Adamo (✉)
The Oskar Klein Centre, Department of Astronomy, AlbaNova, Stockholm University, SE-106 91 Stockholm, Sweden
e-mail: adamo@astro.su.se

N. Bastian
Astrophysics Research Institute, Liverpool John Moores University, 146 Brownlow Hill, Liverpool L3 5RF, UK
e-mail: N.J.Bastian@ljmu.ac.uk

S. Stahler (ed.), *The Birth of Star Clusters*, Astrophysics and Space Science Library 424, DOI 10.1007/978-3-319-22801-3_4

4.1 Introduction

Galactic and extragalactic star-forming regions show that the vast majority of stars are formed in clustered environments, i.e. in the densest cores of giant molecular clouds (GMCs). Clustering is a common feature observed in local star-forming regions, caused by the fractal properties of the ISM under the effect of turbulence (Elmegreen and Efremov 1997). As a result, star-formation appears to be a hierarchical process, with GMC complexes on large scales ($\sim$1 kpc), and young star clusters (YSCs) at the bottom of the hierarchy forming the densest and only bound structures (Elmegreen 2011; Hopkins 2013a). Turbulence is one of the driving mechanisms which governs star-formation. Because turbulence is a scale-free process, both gas and stars follow continuum density distributions that are described by lognormal functions. Stars will form only in regions which have gas densities above a certain threshold (Kainulainen et al. 2014), and only a fraction of these stars will be formed in systems dense enough to be gravitationally bound (Bressert et al. 2010). Throughout this chapter we will focus on YSCs that are gravitationally bound, i.e. systems that are older than a dynamical time, which separates bound clusters from unbound associations (e.g. Gieles and Portegies Zwart 2011). We will also only address properties of clusters with ages less than a few hundred Myr. YSCs typically contain 10^2–10^7 stars, and have effective radii between 1–10 pc, often leading to systems with densities exceeding that observed in globular clusters (Portegies Zwart et al. 2010).

YSCs are easily detected with the resolving power of the Hubble Space Telescope (HST), in star-forming galaxies as distant as $\sim$100 Mpc (e.g. Adamo et al. 2010a; Fedotov et al. 2011) and many may remain bound for billions of years. Hence they can keep records of the star-formation history (SFH) of their host galaxy. Indeed, globular clusters (GCs), remnants of the extreme star-formation process that occurred in a much younger Universe, are likely the ancient counterparts of the YSCs we observe in local galaxies (e.g. Kruijssen 2014). In this contribution we will focus on the statistical and physical properties which characterise YSCs and their relation to star-formation more generally. In particular we will discuss how the galactic environment of the parent galaxy influences the YSC population within it.

Potentially, YSCs can bridge the divide between the sub-pc scales of star-formation and the kpc scales of galaxy formation and evolution. They can be used as tracers of star-formation in space and time, provided that we have a full understanding of their formation, evolution, and disruption as a function of the galactic environment.

4.2 Cluster Populations

While much can be learned by studying individual clusters in exquisite detail, many works have focussed on entire cluster populations to see (1) the full range of properties that clusters can have and their statistical distributions, and (2) how these distributions relate to each other, (3) how the host environment affects the initial distributions and how they evolve with time.

Photometry can be used to estimate the age, mass, and extinction of a cluster by comparing the observed cluster luminosity and colours to simple stellar population (SSP) models (where all stars have the same age and metallicity within some small tolerance). Most studies to date have focussed on the UV and optical parts of the spectrum, where the changes in the overall spectral energy distribution of the cluster change most rapidly as a function of age (although see Gazak et al. 2013 for a near-IR photometric age indicator). Hence, by obtaining imaging in the U, B, V, and I bands, and including a narrow band filter like Hα to break the age-extinction degeneracy, we can estimate the basic parameters of tens or hundreds of clusters at once (c.f., Anders et al. 2004). Alternatively, UV and optical spectroscopy of massive clusters can be used to infer more accurate ages, and hence masses and extinctions, along with estimates of the cluster radial velocity and metallicity. However, this only allows for the study of single (or tens, with multi-slit observations) clusters, making large samples prohibitively expensive to obtain (e.g. Trancho et al. 2007; Konstantopoulos et al. 2009). One caveat, however, to these types of studies, is that by using traditional SSP models, an implicit assumption is made that the initial mass function of stars within each cluster is fully sampled. However, this is only strictly valid for the most massive clusters $>10^5$–$10^6\,M_\odot$. For lower mass clusters, stochastic sampling of the IMF can have dramatic affects on the estimated ages, masses, and extinctions (e.g. Fouesneau and Lançon 2010), or even whether or not a cluster is detected Silva-Villa and Larsen 2011. As such, care must be taken when interpreting the results for lower mass clusters. Often a lower mass limit of $5000\,M_\odot$ is adopted.[1] Additionally, throughout this chapter, and for most studies in the literature, it is assumed that clusters are well approximated as an SSP (i.e. they have negligible spreads in age and abundance within them), which appears to be good approximation (e.g. Longmore et al. 2014).

4.2.1 Cluster Formation

In this section we will provide a statistical description of the main YSC population properties and how they are intrinsically linked to star-formation more generally and to the properties of their parent galaxies. The interested reader can find an excellent

[1] Although stochastic effects are still present to some level at this mass for young ages.

review of the most recent theories and observational evidence on cluster formation in the work by Longmore et al. (2014).

4.2.1.1 The Cluster Mass and Luminosity Functions

During the past two decades, numerous observational studies have provided clear evidence that the initial cluster mass function (ICMF) can be well described by a power-law distribution $dN/dM \sim M^{\alpha}$, with index $\alpha \sim -2$ (e.g. Zhang and Fall 1999; Bik et al. 2003; Hunter et al. 2003; de Grijs et al. 2003). This same distribution is also found for the youngest (i.e. embedded) clusters/associations (e.g. Lada and Lada 2003). The index of the ICMF can be understood in the framework of the hierarchical properties of the ISM, which makes star-formation a scale-free process due to supersonic motions in the presence of turbulence and self-gravity (Elmegreen 2006; Hopkins 2013b) . For this reason, the high mass end of the stellar IMF, most of the cluster mass range, and upper end of the GMC mass functions are reasonably approximated by power-laws, with similar indices (-2 ± 0.3, Kennicutt and Evans 2012).

The ICMF appears to be sampled stochastically within galaxies, so it is desirable to observe a large and massive cluster population in merging galaxies with high star-formation rates (see Sect. 4.2.1.3). However, when we look at cluster formation in dwarf galaxies, the change can be quite drastic. In these systems, star and cluster formation is a sporadic event, and during peaks of star-formation, dwarf galaxies can form very massive clusters or potentially, few or no clusters (Billett et al. 2002; Cook et al. 2012). In spiral galaxies, on the other hand, star-formation is largely constant over a large time range. In these systems, cluster populations are often continuous in their age and mass distributions.

However, the mass range over which the power-law has been fitted varies from study to study, hence a direct comparison between galaxies has been somewhat limited. Nevertheless, from recent studies, it is becoming increasingly clear that the ICMF of some galaxies has a turn-down at high masses, the exact location of which varies from galaxy to galaxy, and even within a single galaxy (Larsen 2009; Bastian et al. 2012). The Antennae merger system, for example, has a power-law ICMF with index close to -2 within a mass range from 10^4 to 10^6 $M_{\odot}$ (Zhang and Fall 1999), with any turn-down being above 10^6 $M_{\odot}$ (Portegies Zwart et al. 2010). It is interesting to notice that, in spiral galaxies, YSC masses rarely reach the range typically observed in merger systems, although there are some exceptions (e.g. NGC 6946, Larsen et al. 2001).

However, Larsen (2009) showed that the ICMF of the Milky Way cannot be reconciled with a power-law function within the same mass range as for the Antennae, namely 10^2 to 10^7 $M_{\odot}$. It is more likely that the upper mass end of the ICMF of the Milky Way is closer to $\sim 10^5$ $M_{\odot}$. This value is not a sharp truncation, but the probability that a cluster can form with a mass significantly larger than this

value rapidly approaches zero. A Schechter (1976) function,

$$\frac{dN}{dM} \propto (M/\mathrm{M}_\star)^\alpha \exp(M/\mathrm{M}_\star), \tag{4.1}$$

is a valid approximation of this distribution because it can describe, simultaneously, the power-law distribution with index α (generally taken to be -2) for clusters with masses below a characteristic mass, $\mathrm{M}_\star$, and an exponential distribution for higher masses. Gieles et al. (2006a,b), Gieles (2009) and Larsen (2009) have shown that a Schechter function is a better approximation of the high mass cluster distribution than a pure power-law function for a sample of dwarf and spiral galaxies.

The characteristic mass, $\mathrm{M}_\star$, appears to vary as function of galactic environment. Larsen (2009) suggested that spirals have $\mathrm{M}_\star \sim 1-2\times10^5\,M_\odot$, while the Antennae has most likely a higher truncation mass ($\mathrm{M}_\star \sim 10^6\,M_\odot$). The presence of an upper mass limit or a truncation mass in the ICMF suggests that the host galaxies will unlikely be able to produce clusters with masses, $M \gg \mathrm{M}_\star$. However, it is important to bear in mind that cluster formation is a stochastic process and that the ICMF is stochastically populated. The truncation mass is only a value above which it becomes unlikely (but not impossible) to form clusters.

The presence of such an upper limit in the ICMF could be linked to the ability of the galaxy to form massive GMCs. It is known that shear and streaming motions in spiral systems destroy GMCs, while in environments like the Antennae, the external pressure exerted on the gas makes it possible to form very massive GMCs and GMC complexes. Since clusters form in GMCs (and must have masses less than their progenitor GMCs) the difference in GMC masses observed, for example, in the Milky Way and in the Antennae may explain why the Milky Way is unlikely to form clusters more massive than a few times $10^5\,M_\odot$ (Larsen 2009). A recent high-spatial resolution study of the GMC population in the grand-design spiral M 51 has revealed how GMC properties change as function of the galactic environment (Colombo et al. 2014). In particular, the maximum mass of the GMCs is tightly related to the dynamical environment of M 51, with higher masses found in the central regions and spiral arms and less massive ones in the inter-arm regions. Kruijssen (2014), using both theoretical arguments and observations, proposed that the maximum GMC mass is linked to the Toomre mass and therefore to the gas surface density within the region. The Toomre mass is also a fairly good prediction of the characteristic ICMF mass, $\mathrm{M}_\star$, assuming star-formation and cluster formation efficiency are known.

In support of the environmental dependency of the truncation mass of the ICMF, Bastian et al. (2012) found a different truncation mass of the cluster population in an inner and outer region ($\mathrm{M}_\star^{\mathrm{in}} \sim 1.6\times10^5$ and $\mathrm{M}_\star^{\mathrm{out}} \sim 0.5\times10^5\,M_\odot$) of another grand-design spiral galaxy, M 83. Similar results have been found for NGC 4041(Konstantopoulos et al. 2013). The difference of the truncation mass in the inner and outer field can be explained by the difference in the gas surface density within the two regions. Using the same data as Bastian et al. (2012), Chandar et al. (2010a,b, 2014) reported that the mass functions of the cluster population in

these two regions follow a pure power-law distribution, with index −2, in the inner region, but is significantly steeper (over a similar mass range) in the outer region. When approximating an ICMF as a single power-law, this is the type of behaviour expected if a truncation is present. Hence, the two studies appear to be consistent, finding evidence of a truncation (or at least a steepening) at high masses.

Larsen (2006) has shown that the number of clusters populating the high mass bins is small and it is usually dominated by the size of the cluster population. If the truncation mass is about $10^4\ M_\odot$ then a cluster population of a few hundred clusters could be enough to statistically distinguish between a pure power-law ICMF without upper limits and a Schechter ICMF. An order of magnitude higher truncation mass ($\sim\ 10^5\ M_\odot$) requires a much more numerous cluster population (a factor of 10 higher) to populate significantly the high mass bins. Therefore it is statistically challenging to trace an upper mass truncation in local galaxies and large cluster populations are needed if standard histograms are used. Instead, cumulative distributions or statistics that use just the brightest/most massive clusters do a better job at finding whether a truncation is present, in the limit of relatively small cluster populations (Maíz Apellániz and Úbeda 2005; Maschberger and Kroupa 2009).

It is worth mentioning that the globular cluster mass function is also better fitted by an evolved Schechter function (it takes into account the effect of the temporal evolution of cluster masses, Jordán et al. 2007). These authors also found that the truncation mass of the globular cluster mass function is positively correlated to the total B band luminosity (stellar mass) of the host galaxy. Dynamical friction cannot alone explain the observed trend, therefore it must be linked to the physical properties of the galaxy at the moment a significant fraction of their globular cluster population was formed (Kruijssen 2015).

While the ICMF is the underlying physical distribution that we wish to understand, observational works often focus on the cluster luminosity function (CLF), as this does not require one to estimate the age of each cluster (a necessary step in order to apply the age dependent mass-to-light ratio from SSP models). As for the ICMF, most studies have found that the CLF is well approximated by a power-law with an index of $\sim\ -2$ over much of the observed range. However, a number of works have found that the CLF is *steeper* than the ICMF (e.g. Larsen 2002). Gieles et al. (2006a,b) showed that if the ICMF has a truncation at the high mass end, this will manifest itself as a break (change of index) in the CLF, with the distribution becoming steeper at the high luminosity end. Such a steepening has been seen in a number of works (e.g. Gieles et al. 2006b; Santiago-Cortés et al. 2010; Bastian et al. 2012; Konstantopoulos et al. 2013; Whitmore et al. 2014).

An additional expectation if the ICMF has a truncation at the high mass end and the star-formation is constant over hundreds of Myr, is that the median age of clusters will vary as a function of luminosity, with the brightest clusters being preferentially younger than fainter clusters. This trend is expected because, statistically, the galaxy forms the most massive clusters close to the $M_\star$, therefore they will have similar masses but their luminosity will fade because of stellar evolution. For a pure power-law, on the other hand, one would expect that the

median age of a sample of clusters is independent of the luminosity. Larsen (2009) and Gieles (2010) exploited this fact and found that brighter clusters were preferentially younger than older clusters, in agreement with expectations if the ICMF is truncated at the high mass end.

The ICMF can be approximated by a power-law distribution with an index −2 and is stochastically sampled. For many cluster populations the upper end of the mass distribution is better described by an exponential decrease above some characteristic mass, $M_\star$. Observational evidence and theoretical models suggest that the galactic environment can affect the upper mass end of the ICMF. The chances that the galaxy may form a cluster more massive than $M_\star$ are low but not null. Spiral and dwarf galaxies have $M_\star \sim 10^5\, M_\odot$ while this value increases significantly for cluster populations within galactic mergers and starbursts.

4.2.1.2 The Size-of-Sample Effect

With the advent of the Hubble Space telescope it was possible to study YSCs not only in the nearby Magellanic Clouds but also in more distant galaxies, probing a much larger range of environments and star-formation rates (SFRs). As the number of samples increased it became evident that the formation of massive star clusters was not only confined to the early universe (i.e. the globular clusters) but that the majority of local star-forming galaxies host YSC populations (similar to some extent to the globular clusters but much younger and less dynamically evolved). Whitmore (2000) showed that the V-band luminosity of the brightest cluster in a galaxy scales with the number of YSCs in the galaxy (left panel, Fig. 4.1). He also suggested that the relation could be explained if the clusters were sampled from power-law luminosity (mass) distribution with index ~ -2. The nature of this scaling relation became clearer when Larsen (2002) linked the luminosity of the brightest cluster observed in the galaxy (and the total number of clusters within the population) with the present SFR of the system (see right panel in Fig. 4.1).

Although the formation of clusters must be governed by clear physical processes, with the final cluster properties (e.g. mass and radius) set by the initial conditions and subsequent evolution, cluster populations appear to be stochastically sampled from an underlying parent distribution, the ICMF. Hence, for higher SFRs, more clusters (i.e. larger populations) are formed. A more numerous population has a higher probability to sample the cluster mass (luminosity) function at the high mass (brighter) end. This property of the cluster population is referred to as a size-of-sample effect in the literature, and is the underlying driver of the observed $M_V^{\rm brightest}$ vs SFR relation. However, we note that such an effect only dominates a population where the ICMF is not sampled far above the characteristic (Schechter) mass. In

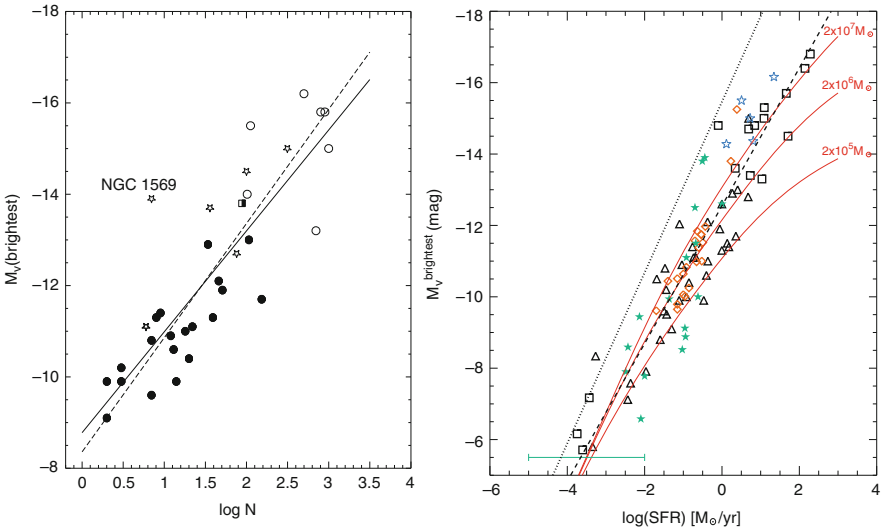

Fig. 4.1 *Left panel*: Number of clusters detected in each galaxy versus the V band absolute luminosity of the brightest cluster within the galaxy. The *dashed line* is the best fit to the data, excluding NGC 1569, while the *solid line* is the expected relation if cluster luminosity distribution is described by a power-law, with an index of -2 (from Whitmore 2000). *Right panel*: The luminosity of the brightest cluster plotted against the star-formation rate (SFR) of the host galaxy. This plot contains a compilation of all data available in the literature. The *dashed line* is the best fit to the sample of galaxies plotted as triangles (Larsen 2002). *Squares* are the sample added by Bastian (2008). *Blue stars* are the sample of luminous blue compact galaxies studied by Adamo et al. (2011). The *orange diamonds* show the sample contributed by Whitmore et al. (2014). The *green stars* and the *horizontal line* represent dwarf galaxies using data compiled from the literature (see text for a detailed description of the data). Additionally, we show the expected relation for an underlying power-law ICMF ($\alpha = -2$) as a *dotted line* (for $\Gamma = 1$, i.e. 100% of stars form in clusters) and three relations showing Schechter distributions for the ICMF with three different $M_\star$ values (assuming $\Gamma = 0.1$). The plot is taken from Adamo et al. (2015)

fact, the $M_V^{\rm brightest}$ vs SFR relation implies a steeper ICMF than often found in cluster studies (i.e. an index of $-2.3 - 2.5$ rather than -2—e.g. Whitmore 2000), implying that a truncation is beginning to affect the relation. *While it may appear on face value that this relation may undermine evidence of a truncation or break in the mass/luminosity distributions (Sect. 4.2.1.1), the two are consistent given that many galaxies do not sample the ICMF up to the (if present) truncation mass.* In Fig. 4.1 we show the expected relation between $M_V^{\rm brightest}$ and the SFR if the underlying mass distribution is described as a Schechter function with three different values of $M_\star$ (2×10^5, 2×10^6, 2×10^7 $M_\odot$). The implication is that $M_\star$ is related to the SFR, which is expected from theory (e.g. Kruijssen 2014). We refer the reader to Larsen (2010) for a more in-depth discussion of this topic.

The scatter in the $M_V^{\rm brightest}$ vs SFR relation can be understood as being due to the errors associated with the measurements along with the stochastic sampling

of the underlying ICMF (e.g. Bastian 2008, see also da Silva et al. 2014). For most galaxies the SFR was estimated through its Hα flux, which is a measure of the current ($<$ 8 Myr) SFR of the host galaxy. In some post-starburst galaxies, however, the current SFR is not a good representation of the star-forming event that formed the highest mass or most luminous clusters. In extreme starbursts, the most massive cluster formed can be the brightest cluster in the galaxy for hundreds of Myr, especially if the SFR has a sharp decline like in post-merger stages or in dwarf galaxies. Therefore, the use of the brightest young (i.e. a cluster that is directly related to the measured star-formation rate) cluster will reduce the scatter.

It is interesting to note that if one assumes that all stars form in clusters (i.e. 100% cluster formation efficiency) then we would have expected the observed populations to follow the dotted line in the right panel of Fig. 4.1. Using simulated cluster populations by stochastically sampling a Schechter ICMF, Bastian (2008) showed that the observed $M_V^{\rm brightest}$-SFR relation can be reproduced only if a small fraction of the star-formation is happening in bound clusters ($\sim 8 \pm 3\%$—see also Gieles 2010). Adamo et al. (2011), following these results, discussed the possibility that the scatter at high SFR could also be caused by a varying cluster formation efficiency in different galaxies. It is also worth mentioning that many of the highest SFR galaxies either lie at distances where crowding effects may affect the luminosity of single clusters or are in highly extinguished systems (i.e. luminous IR galaxies). On the other hand, if we look at the lowest SFR regimes the scatter is similar, implying that such biases do not strongly influence the results (see Randriamanakoto et al. (2013) for a further discussion).

The $M_V^{\rm brightest}$ vs SFR plot contains the values of about 60 dwarfs (total B band luminosity fainter than -18 mag, green stars and green horizontal bar) which have been searched for clusters[2] (Fig. 4.1). Of this sample about 50 % of the dwarfs do not have compact bound clusters above the detection limits and about 40% have clusters (according to the definition of Cook et al. 2012) younger than 100 Myr. The galaxies with available cluster photometry and SFRs have been included in Fig. 4.1. A green horizontal bar at the bottom of the plot shows the range in SFR of the dwarf galaxies which do not have bound clusters (Cook et al. 2012). Some galaxies with similar SFRs have formed clusters where others have not. It is still under debate if this is an effect of the galactic environment where star-formation is happening or whether it is just an effect of the stochastic process at very low SFR regimes (e.g. Cook et al. 2012).

[2]The green filled stars are a collection of cluster studies in dwarf galaxies of galactic B band luminosity $M_B > -18$ mag Kobulnicky and Johnson 1999; Billett et al. 2002; Rafelski and Zaritsky 2005; Annibali et al. 2009; Goddard et al. 2010; Popescu and Hanson 2010; Annibali et al. 2011; Cook et al. 2012; de Grijs et al. 2013. This sample also contains two systems which have been omitted from Larsen (2002) catalogue, i.e. NGC 1569 and NGC1705. These two dwarf starbursts are now included with revised measurement of the galactic SFR (Pasquali et al. 2011; Annibali et al. 2009, respectively).

The $M_V^{brightest}$-SFR (or number of clusters in a population) relation shows one of the characteristics of cluster populations, that they are dominated by size-of-sample effects. In higher star-formation rate regimes, galaxies form more numerous cluster populations which increases the probability to sample the cluster mass (luminosity) function to higher masses (brightness).

4.2.1.3 The Cluster Formation Efficiency on Global Scales

In this section we discuss a relevant aspect of cluster formation and its link to the star-formation process. As mentioned in the Introduction, there do not appear to be distinct "clustered" and "distributed" modes of star-formation. Star-formation is a clustered process, hierarchical in space and time. Clusters are part of this continuous process and stand out because of their relaxation-dominated dynamics (gravitationally bound structures) emerging at the density peaks within the hierarchy of star formation—not because of preexisting cloud boundaries (Elmegreen 2006). Massive YSCs usually host a large population of very massive stars, therefore ionising radiation and feedback from clusters may have important effects on galactic scales.[3] To quantify the impact that clusters have on their parent galaxies and at which rate they are formed, it is necessary to probe which fraction of the total stellar mass produced during a star formation event is found in bound YSCs and whether this fraction varies between different galaxies and environments.

Some of the first ultraviolet (UV) high-spatial resolution images of starburst galaxies provided by HST showed that YSCs dominate the morphological appearance at these wavelengths and significantly contribute (>20%) to the total UV flux of the galaxy (Meurer et al. 1995). Larsen and Richtler (2000) developed a more quantitative approach to the clustering properties of a star-forming galaxy. They used the fraction of luminosity contributed by the YSCs with respect to the total luminosity of the galaxy, in a specific band, i.e. in the UV, $\Gamma_L(U)$. The authors found that $\Gamma_L(U)$ increases as function of the averaged SFR density of the host galaxy. In Fig 4.2 (left panel), we show the original sample by Larsen and Richtler extended to higher SFR regimes by the luminous blue compact galaxy sample of Adamo et al. (2011). The scatter in the data is large but the trend is clear. *For increasing SFR density, the fraction of stars born in bound clusters is higher.*

The data have not been corrected for any internal reddening (which should not affect the $\Gamma_L(U)$ estimates). Therefore, there are numerous underlying factors that go into this simple observational relation and their effects have not yet been clearly traced (e.g. the role of a varying SFR). However, the observed increasing trend

[3] It is currently unclear whether the efficiency of feedback from massive stars is higher if the stars are part of a cluster, rather than being relatively isolated (i.e. in an association) and acting largely on their own.

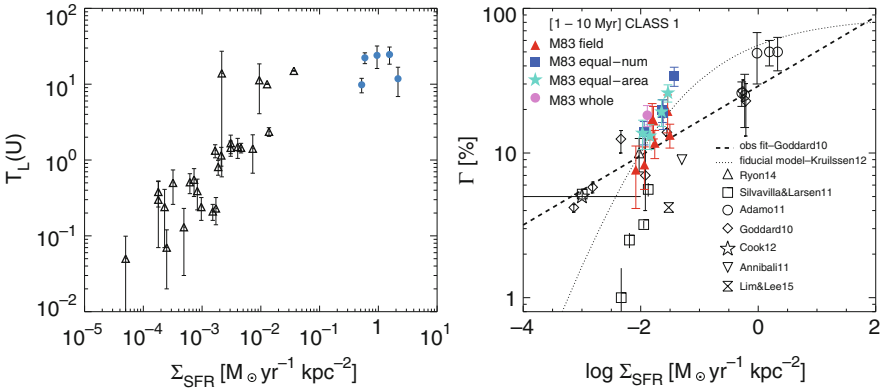

Fig. 4.2 *Left plot*: The fraction of *U* band light contributed by YSCs to the total *U* band luminosity of the galaxy versus the star-formation rate density of the host galaxy. Original data from Larsen and Richtler (2000) are plotted as *black triangles*. The *blue solid dots* (data from Adamo et al. 2011) extend the relation to much higher SFR density regimes (plot readapted from Adamo et al. 2011). *Right plot*: Cluster formation efficiency (Γ) versus star-formation rate densities. The original plot and dataset by Goddard et al. (2010) have been updated with all the data available in the literature (see inset). The *dashed line* is a fit to the Goddard et al.'s data while the *dotted line* is a fiducial model provided by Kruijssen (2012). *Filled dots* are data from a recent study of the cluster formation efficiency in M 83 on sub-galactic scales. This plot will appear in Adamo et al. (2015). See text for more information

hints at a tight physical connection between the cluster formation event and the galactic environment where the clusters are forming. In the previous section we have discussed the size-of-sample effect. If this process would be the only driving mechanism in cluster formation, then we should expect the ratio between the amount of stars formed in clusters and the SFR over the age range of the clusters (this is the meaning of the quantity $T_L(U)$) to be constant. The increasing trend suggests that the cluster formation efficiency (CFE or Γ) scales positively with the SFR density of the galaxy, or in other words, that the amount of stars born in bound clusters is not a constant fraction but changes as function of the galactic environment.

A way to probe this statement is to directly look at the cluster formation efficiency in different galaxies. Bastian (2008) defines Γ as the ratio between the cluster formation rate (CFR) and the SFR. The CFR is usually estimated using the total stellar mass in YSCs over a certain age range. Because of observational limits, the total observed stellar mass in clusters more massive than the limits is used to normalise the ICMF and extrapolate the missing mass hidden below the detection limits, assuming a power-law distribution with index −2 (down to 100 $M_\odot$). The SFR is usually derived using indirect tracers like Hα, FUV, and 24 μm or averaged SFH from direct stellar counts. It is important that the age ranges over which CFR and SFR are estimated are consistent.

In Fig 4.2 (right panel), we present a compilation of data available in the literature for which Γ has been measured. The original sample showing the first

evidence of an increasing Γ over 5 order of magnitude in SFR densities was originally published by Goddard et al. (2010). The sample has now been extended to a large variety of galactic environments. The linear fit proposed by Goddard et al. to describe the observed trend (dashed line in the plot) has been replaced by the fiducial model (dotted line) proposed by Kruijssen (2012). The latter model predicts the fraction of star-formation that ends up being gravitationally bound by combining different physical processes, i.e. the gas density distribution of the ISM in a galaxy disc, the critical density above which stars form, gas evacuation by star-formation and feedback, and the resulting star-formation efficiency. The flattening at the very high SFR density regimes is produced by the fact that the density of the gas in that regime is so high that nearly only bound structures form. The Γ-$\Sigma_{\rm SFR}$ relation, which reflects the more fundamental Γ-$\Sigma_{\rm gas}$ relation, shows how the galactic environment affects the clustering properties of the star-formation process.

4.2.1.4 The Cluster Formation Efficiency on Local Scales: The Case of M 83

Silva-Villa et al. (2013) looked for the first time at possible variation of Γ within different regions of the same galaxy, M 83. They find evidence, using the cluster sample from two HST pointings, that Γ declines as a function of galactocentric distances from the centre of the galaxy.

This analysis has now been extended to the whole galaxy, thanks to a complete survey of the M 83 disk with the exquisite resolution power of the HST (Silva-Villa et al. 2014). In Fig. 4.3 we show how Γ declines as a function of distance from the centre of the galaxy (Adamo et al. 2015). Γ has been estimated within annuli of the same area. The detection limits used to estimate the observed total stellar mass in clusters (the amount in clusters less massive than this limit is inferred assuming a power-law ICMF) is a function of the age range considered. The SFR compared to clusters younger than 10 Myr has been estimated from Hα images, while the SFR for clusters with ages between 10 and 50 Myr is derived from direct stellar counts. Note the systematic decrease in Γ as a function of galactocentric distance. To reinforce the link with the underlying galactic environment we overplot the azimuthally averaged gas surface density measured in each annulus. The correspondence between the radial variation of Γ and gas surface density profiles was quantitatively predicted by the model of Kruijssen (2012, yellow triangles in Fig. 4.3), where the fraction of stars bound in clusters is a function of the molecular gas surface density, which is near-linear at low ($\Sigma \leq 50\ M_{\odot}$) surface densities. *Hence, we conclude that the fraction of stars that are formed in bound clusters depends on the local and global environment, and ranges from* $\sim$ 3% *(or less) in quiescent dwarf galaxies up to* $\sim$ 50% *or more in intense starbursts.*

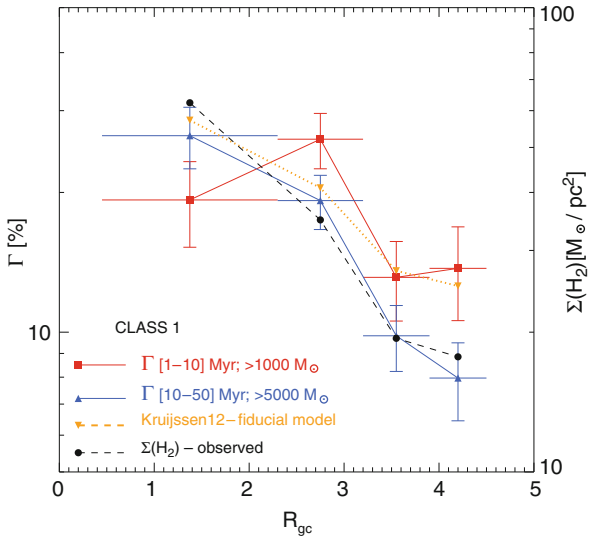

Fig. 4.3 The cluster formation efficiency as function of galactocentric distances in the spiral galaxy M 83. The bins have been selected to have equal area. For clusters younger than 10 Myr (*red solid line with squares*) the SFR has been derived using Hα as indicator. For clusters in the age range 10–50 Myr (*blue solid line with triangles*) the SFR has been derived from resolved stellar populations. Errors on Γ take into account stochastic effects of the ICMF and 0.2 dex in the estimates of the ages and masses of individual clusters. *Horizontal bars* show the width of the bin. The *black dashed line* shows the azimuthally averaged gas surface density (right y-axis) in each bin. Taken from Adamo et al. (2015)

Observations and theoretical models have found that the clustering properties of the stellar population change as a function of the galactic environments. Higher SFR densities produce on average larger Γ, i.e. a larger fraction of the star-formation is happening in bound clusters.

4.3 The Cluster Age Distribution and Cluster Disruption

Early work with HST led to the exciting conclusion that major starburst events within galaxies result in the formation of hundreds of massive, globular cluster progenitors (e.g. Holtzman et al. 1992; Miller et al. 1997). Hence the age distribution of clusters held extraordinary potential to derive the star-formation history of galaxies, or at least their major star-forming episodes. However, it was known that clusters do not survive forever, but rather lose mass through a variety of processes, discussed in more detail below (e.g. Spitzer 1987). Correcting for this cluster mass

loss or disruption has become a point of major contention in the field. Below, we outline the basic physical properties, expectations, debate on the empirically derived disruption laws, and summarise the current observational state of the field.

4.3.1 Expectations from Theory and Parameterisations

Once a cluster forms, a number of processes cause the cluster to lose mass (i.e. lose stars from the cluster to the surroundings), eventually leading to its entire disintegration. If the cluster forms, and the gas left over from the non-100% star-formation efficiency makes up a significant amount of the mass of the cluster (i.e. the gravitational potential is still dominated by the gas), then the removal of this gas, on a short timescale, may cause the cluster to lose much of its stellar mass, potentially disrupting the entire cluster (e.g. Lada et al. 1984), in a process known as "infant mortality". Recent observations (e.g.) as well as numerical simulations (e.g. Kruijssen et al. 2012) suggest, however, that massive clusters are not strongly affected by this process (see Longmore et al. (2014) for a full review), so we shall not deal with this process in detail here. However, we note that for massive clusters, even if gas expulsion does modify the cluster, the cluster will be back in equilibrium within 5–20 Myr (Longmore et al. 2014).

A potentially much more severe disruption process is caused by the interaction of young clusters with GMCs in their vicinity. Since clusters are born in gas rich environments, this effect will be strongest at young ages and will decrease as the cluster moves away from its natal star-forming region (Elmegreen 2010; Kruijssen et al. 2011). This process is often referred to as the "cruel cradle effect". If the density of GMCs is high, the gravitational shocks imparted by the GMCs on the young clusters are expected to be strong. Sufficiently strong shocks could disrupt any cluster in a single encounter, leading to mass-independent cluster disruption. Under less extreme conditions, the mass loss on the cluster is expected to be proportional to the cluster density, with lower density clusters easier to destroy. Since, YSCs do not, in general, display a mass-radius relation (e.g. Larsen 2004), this means that this process should be proportional to mass, so higher mass clusters should live longer.

If a cluster survives long enough to escape from its natal gas-rich environment, it will still lose mass due to (1) the gravitational tidal field of its host galaxy, (2) encounters with GMCs, (3) stellar evolution, and (4) two-body relaxation (an internal process—although governed by the external tidal field—Gieles and Bastian 2008). The relative strength of the first two processes depends on the environment. It is beyond the scope of this chapter to discuss these processes in detail, and we refer the interested reader to the excellent review by Portegies Zwart et al. (2010) as well as the detailed discussions provided by Lamers et al. (2010) on the tidal field and Kruijssen et al. (2011) on tidal shocks (c.f., their Fig. 8). In principle, one can tune the above processes to make them all (nearly) independent of mass (e.g. Fall et al. 2009), however, the first two will always remain strongly environmentally

dependent. *The basic outcome of theory is that in most environments, more massive clusters should survive for longer and that in environments with high GMC density and/or strong tidal fields cluster dissolution should happen more rapidly (for a given cluster mass).*

4.3.2 Analysing Cluster Populations

Throughout this section we will only discuss *mass-limited samples*. It is possible to use *luminosity-limited samples*, e.g. Boutloukos and Lamers (2003), however, it complicates the analysis. Many apparent contradictions in the field can be traced to the use of luminosity-limited samples being analysed as if they were mass limited. We will discuss the behaviour of luminosity-limited samples when necessary.

We will, following on from previous works, approximate the cluster age distributions as power-laws, normalised to the linear range of the age bin, namely of the form $d\mathrm{N}/dt \sim t^{-\zeta}$. In this form, if the cluster formation rate is constant and no disruption acts on the population, then the distribution should be flat (i.e. constant) with age, $\zeta = 0$. If disruption affects a population, then the distribution should become steeper at older ages, as young clusters have not undergone much mass-loss relative to older clusters. However, if a sample is luminosity limited, this also steepens the age distribution, and can lead to erroneous conclusions regarding the role of cluster disruption in shaping the observed population.[4]

In the literature, two empirical disruption laws have been advocated, *mass independent disruption* (MID—e.g. Whitmore et al. 2007) and *mass dependent disruption* (MDD—e.g. Lamers et al. 2005). As their names suggest, the two scenarios propose different dependencies of the cluster mass on the cluster lifetime. They also predict different roles of the galactic environment. That is, the MID scenario assumes that cluster disruption has little or no dependence on environment, while the MDD predicts a strong dependence on environment. We refer the reader to the review contained in Bastian et al. (2012) for a more thorough discussion of the models.

These two disruption laws produce clear differences in the expected age distribution (see Lamers (2009) for an in-depth discussion). Briefly, the MID scenario predicts that because cluster disruption is independent of cluster mass and the local environment, all age distributions should be similar (modulo SFH effects), following a single power-law with index, $\zeta \sim 0.9$ (e.g. Whitmore et al. 2007). At what age this rapid decline should stop, is still an open question. For the MDD scenario, due to the dependence of cluster disruption on the local environment, we would expect to see a range of age distributions, additionally we should see not a single power-law,

[4] If a sample is luminosity limited, the age distribution for the case of no disruption and a constant cluster formation rate is expected to decrease with $\zeta = 0.65, 0.9$ if the sample is limited in the V or U-bands, respectively Gieles 2010.

but rather multiple parts to the distribution. At young ages, when disruption has not acted strongly yet (modulo "infant mortality" and the "cruel cradle effect") the age distribution should be flat ($\zeta \sim 0$). This should then steepen at older ages, as cluster disruption begins eating into the population.

Theoretically, cluster disruption is quite well understood, with the rate of cluster disruption, for a given mass, dependent on the ambient environment. If the tidal fields are strong or large numbers of GMCs are present, the lifetimes of clusters should be significantly shorter than in environments with weak tidal fields or few GMCs. In the case of strong disruption, the age distribution of clusters should be steeper than in the case of little or no disruption.

4.3.3 Numerical Results

Kruijssen et al. (2011, 2012, hereafter K12) ran a series of galaxy scale gravitational and hydrodynamical models of quiescent and merging spiral galaxies. In these simulations, clusters were allowed to form from the gas if the local density exceeded some threshold density. The gas in this region was then converted to stars in clusters, and the clusters were sampled from a power-law mass function with index, −2. The evolution of these clusters were then followed in a sub-grid model, taking into account their galactic environment and the dissolution effects discussed above. All of their cluster mass-loss algorithms were calibrated to direct N-body simulations of clusters with stellar evolution in a tidal field.

The authors found that in gas-rich mergers, cluster disruption could indeed proceed largely independent of the cluster mass. However, in their quiescent spirals, cluster disruption was a much slower process, showing a clear environmental dependence, along with a dependence on the cluster mass. In Fig. 4.4 we show the median age distribution of the cluster population of twelve of the K12 quiescent spiral galaxies as filled black squares, and the grey shaded region shows the full distribution found in the models.

Each of the galaxies in the K12 simulation shows the same overall trend. A near-flat part of the distribution (i.e. where disruption is not strongly affecting the population) and then a downwards curve. Since we have a mass limited and complete sample, this effect is entirely due to disruption. Environments where disruption is faster will have age distributions that bend earlier, compared to environments where disruption proceeds slower. Unfortunately, incompleteness also can cause the downward bend at old ages, so care must be taken when analysing observed age distributions.

Hence, the results from these numerical simulations agree with the expectations from analytical theory (e.g. Lamers et al. 2005; Lamers and Gieles 2006). The

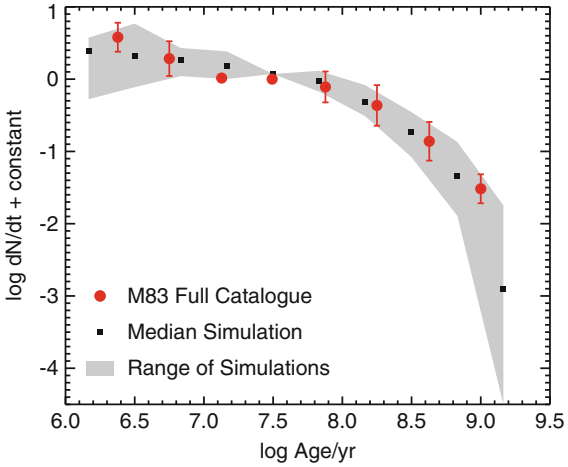

Fig. 4.4 A comparison of age distributions from the numerical simulations (*solid squares* represent the median simulations and the *shaded region* shows the full range of the simulations) of cluster populations in spiral galaxies (Kruijssen et al. 2012) and the observed cluster population of M83 (Silva-Villa et al. 2014). Both distributions are normalised at 30 Myr, to allow a direct comparison. We show the full cluster catalogue (applying a lower mass limit of 5000 $M_{\odot}$) and the error bars represent the differences between two similar fields (F1 and F5) where the disruption timescale should be comparable. The up-turn in the observational data at young ages (<10 Myr) may be due to some amount of cluster disruption (i.e. infant mortality/cruel cradle effect) or the inclusion of associations in the catalogue

models of Renaud and Gieles (2013) largely confirm the results of Kruijssen et al. (2011, 2012) simulations for the gas-poor part of the parameter space where they overlap—as the former have not included gas (GMCs) in their simulations so they find weaker cluster disruption than in the gas-rich environments included by the latter simulations. While the theory behind cluster disruption appears to be on strong footing with little debate, the observational picture is more complicated, and has been the subject of an ongoing debate within the literature (MID vs. MDD). Below we discuss the observed age distributions of clusters in different environments, and compare studies done by different groups.

Numerical simulations and analytic theory predict that the age distribution for quiescent spirals should show a flat portion, from young ages to ∼100–300 Myr, followed by a steeper portion where cluster disruption is dominating the population.

4.3.4 *Observational Results on the Cluster Age Distribution*

There has been a significant amount of work done on cluster populations in the Galaxy, as well as nearby galaxies, especially since the advent of HST. However, the past decade has also witnessed a significant amount of controversy regarding this topic, which in turn has strongly impacted the discussion of the lifetimes of clusters. As discussed above, if the lifetimes of clusters are short (tens of Myr or less), then the overall population age distribution will be steep, at least over the timeframe where disruption is occurring. If, on the other hand, clusters are stable when they form, and survive for hundreds of Myr, then the age distribution is expected to be shallow. However, as we will see, a single power-law is not a good description of many of the cluster populations studied to date, so we will be paying particular attention to the age range over which the fit was carried out.

It is also important to remember that the overall SFH of the galaxy can influence the age distribution of the clusters (see, e.g., Bastian et al. 2009). If the SFR of a galaxy has been increasing the age distribution will become steeper, whereas it will become flatter (or even inverted) if the SFR has been decreasing. Clearly, the assumption of a constant SFR for merging or starburst galaxies is questionable, whereas this should be a better assumption when looking at the full cluster population in more quiescent spirals.

In this section we look at a number of results from the literature, and study a handful of cluster systems in detail as case studies.

4.3.4.1 The Open Cluster Population in the Milky Way

Our knowledge of the open cluster population of the Galaxy is surprisingly incomplete. Piskunov et al. (2006) suggest that we are only complete out to a distance of ∼800 pc from the sun. This limit is important, as samples of clusters out to, e.g. ∼ 2 kpc are incomplete, and behave as luminosity-limited samples. An example of such a behaviour can be seen when comparing the age distribution of open clusters in Lada and Lada (2003—based on the catalogue of Battinelli and Capuzzo-Dolcetta 1991) with that of Lamers et al. (2005) or Piskunov et al. (2006). Lada and Lada (2003) find that the number of clusters per *logarithmic* bin is roughly constant with age, which suggests that the $d\mathrm{N}/dt \propto t^{-1}$, i.e. $\zeta = 1.0$. The authors conclude that up until ∼ 100 Myr, 90% of clusters disrupt every decade of age, i.e. very strong cluster disruption. However, the catalogue used included clusters out to 2 kpc, hence was effectively luminosity limited.

In comparison, Lamers et al. (2005, also see Piskunov et al. 2006) found that the age distribution was largely flat to an age of ∼ 100 Myr and then rapidly decreased, if a mass-limited sample was used, including only clusters within 800 pc of the Sun. The authors used the MDD framework discussed above to conclude that a cluster with a mass of $10^4 M_\odot$ will (on average) survive for 1.7 Gyr in the solar neighbourhood. Hence, it appears that in the solar neighbourhood, stellar clusters

are long lived entities, in agreement with expectations given the relatively weak tidal field and the scarcity of massive and dense GMCs.

4.3.4.2 The Cluster Population of M31

A recent survey that deserves special consideration is the *Panchromatic Hubble Andromeda Treasury* (PHAT) survey, which covers a 0.5 deg^2 area of M31, extending from the central regions out $\sim$ 20 kpc (Dalcanton et al. 2012). Johnson et al. (2012) have analysed the "1st year data" of the survey, which covers five "bricks" (collections of HST imaging footprints) from the inner to the outermost regions of the galaxy, and presented integrated luminosities in six filters for 601 clusters identified in their sample. Fouesneau et al. (2014) used this sample to estimate the ages, masses, and extinctions of the clusters using stochastic SSP models and a Bayesian analysis method. They then construct age distributions for three radial bins at 6, 10, and 15 kpc, and find a flat distribution ($\zeta \sim 0$) for the first $\sim$70–100 Myr, after which the distribution declines rapidly, with $\zeta = 1.15$. Remarkably, each of the three fields shows the same distribution. The rapid decrease after 100 Myr is due to a combination of their completion limit (i.e. the sample becomes luminosity limited after this age) and cluster disruption. However, it is clear that there is little evidence for rapid cluster disruption within M31 (at these radii) for at least the first 100 Myr. As was found for the solar neighbourhood, and in numerical simulations, it appears that once a cluster forms, it is a long lived entity in the Andromeda galaxy.

While the full survey is expected to add an additional $\sim$2000 clusters to the sample, and will place the results on an even stronger statistical footing, it is clear from the current data that the population follows the expected trends, and that rapid cluster disruption within the first 100 Myr is inconsistent with the data.

4.3.4.3 The Cluster Population of the LMC

The LMC is the nearest galaxy to us with a significant young cluster population, and as such has been the subject of numerous studies. Here we only focus on results from the past $\sim$5 years, given the controversy that has emerged on the issue of the age distribution in this galaxy. Chandar et al. (2010a) used the cluster catalogue of Hunter et al. (2003) and re-estimated each cluster's age, mass, and extinction. The authors find that for ages between 1 and 1000 Myr, the age distribution can be well described by a single power-law with $\zeta = 0.8$. Unfortunately, the data used for their analysis has not been made publicly available, so it is not possible to confirm the results. Chandar et al. also find a relatively large population of massive ($>10^4\ M_\odot$) young ($<$10 Myr) clusters in their sample, i.e. eight R136 type clusters. Given the ease of detecting these kinds of objects, and their lack of appearance in other studies, it seems likely that these are misfit clusters, leading to an overestimation of the number of such very young massive clusters in the LMC.

Baumgardt et al. (2013) collated all major publicly available catalogues of clusters in the LMC, removing a significant amount of double detections (often within the same catalogue) and re-estimated each cluster's age, mass, and extinction. The authors only include clusters older than 10 Myr. These authors find a significantly different distribution than that reported in Chandar et al. (2010a), namely a flat age distribution to ages of 200–300 Myr ($\zeta \sim 0.3$), followed by a steep decline (again caused by a combination of disruption and incompleteness). de Grijs et al. (2013) independently collated cluster studies of the LMC, and found results consistent with Baumgardt et al. (2013) and inconsistent with Chandar et al. (2010a).

Comparing the Chandar et al. and Baumgardt et al. distributions, it appears that some difference is caused by the choice of binning, with the youngest age bin of the Chandar et al. study forcing the fit to steeper values, as the age range between 10–100 Myr is largely flat in their sample. This highlights the danger of adopting a single value for the binning of data, showing that at least multiple bin widths need to be considered, or, preferably, better statistical analyses such as maximum likelihood comparisons. We have carried out a maximum likelihood fit on the Baumgardt et al. sample, fitting the age distribution over different age intervals (for mass-limited samples, $M > 5000\ M_{\odot}$). For the age interval from 10 to 100 Myr, we confirm that Baumgardt et al. value of $\zeta = 0.35$. Once older ages are included, the age distribution begins dropping rapidly (likely due to a combination of disruption and incompleteness). Fitting the full range from 10 to 1000 Myr, we find $\zeta = 0.9$, in good agreement with Chandar et al.

The obvious interpretation of these results is that a single power-law fit to the data is not a good representation to the cluster population of the LMC. For ages younger than 100 Myr, there appears to be no evidence for rapid disruption (c.f. Baumgardt et al. 2013; de Grijs et al. 2013). For older ages, disruption and incompleteness are likely causing the steepening of the age distribution.

4.3.4.4 The Cluster Population of M83

Due to its proximity and large amount of HST/WFC3 coverage, the spiral galaxy, M83, has been targeted by a number of recent cluster studies. An additional importance of this galaxy is that due to its distance (∼4.5 Mpc), it is possible to sample different environments within the same galaxy (with a reasonable amount of observing time), while still semi-resolving the clusters. Hence, it is an excellent environment to test the environmental dependence of cluster disruption.

Chandar et al. (2010b) studied the first of seven fields, F1 (see Fig. 4.5) with multi-wavelength HST/WFC3 imaging, covering the inner region of the galaxy. Using similar methods to those discussed above, they found $\zeta = 0.9$ from 1 to 1000 Myr, for a single power-law fit. Bastian et al. (2012) reanalysed F1, and overall, found excellent agreement with both the cluster catalogue and derived properties, and also the age distribution, finding $\zeta = 0.85$ over the same age range. The main differences between the catalogues were restricted to young objects (< 10 Myr) as it is difficult to distinguish between bound clusters and unbound associations at these

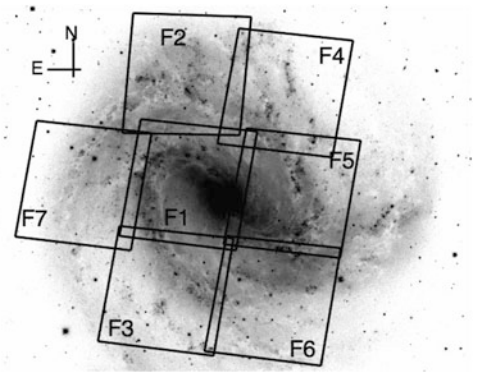

Fig. 4.5 An R-band image of M83 with the seven HST/WFC3 fields superimposed and labelled (taken from Silva-Villa et al. 2014)

ages (e.g. Gieles and Portegies Zwart 2011). Bastian et al. simply adopted more conservative criteria for identifying clusters, although this is largely a subjective distinction. Hence, the Bastian et al. sample provides lower limits at young ages, while the Chandar et al. sample provides upper limits for the age distribution. For ages older than 10 Myr, the two populations gave nearly identical results.

However, Bastian et al. also studied a second field, F2 (see Fig. 4.5) using the same techniques, and found that the age distribution was significantly shallower ($\zeta = 0.4$–0.5). This is expected if cluster disruption is environmentally dependent, as further from the galaxy centre, the tidal field and the number of GMCs have dropped considerably, meaning that clusters are likely to survive for longer (e.g. Lamers et al. 2010; Kruijssen et al. 2011). Bastian et al. (2011) showed that even in colour-space (i.e. before an age dating is done) the clusters in F2 are significantly redder in $U-B$ than those in F1, showing that they have older ages (extinction cannot cause the observed colour differences).

Chandar et al. (2014) also studied F2, and found results consistent with those of Bastian et al. (2011, 2012). However, the authors suggest that the differences between the two fields is only at the 2–3σ level. Chandar et al. (2014) data are public so we can look into this issue in detail. One difference between the Chandar et al. (2010a,b, 2014) results was that in 2014, only clusters older than 10 Myr were included in the analysis. However, if younger clusters are included so that we analyse the age range of 5–300 Myr (as the two fields were treated equally, the distinction between clusters and associations should not affect the results), the two fields have very different distributions. The age distribution of F1 is much steeper than F2, with $\zeta_{F1} = 0.85 \pm 0.15$ and $\zeta_{F2} = 0.15 \pm 0.15$ (in agreement with the independent analysis done by Silva-Villa et al. 2014). Using a KS-test, we find that the two samples have a probability of $<1\times10^{-5}$ of being drawn from the same parent distribution.

Hence, it appears that all catalogues of M83 studied to date agree that the cluster population closer to the galaxy centre is different than in the outer parts, in the way predicted by environmental dependent cluster disruption theories. Results suggesting otherwise were largely caused by the choice of age range over which the fit was carried out.

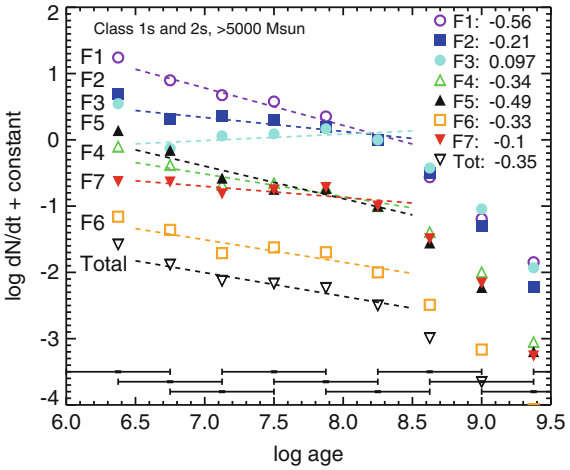

Fig. 4.6 The age distribution of clusters and associations in seven (slightly overlapping) fields (each one HST/WFC3 pointing). The *lines* indicate the best fit slope ($-\zeta$) over the range indicated (for mass-limited samples), and the values are listed in the panel. F1 covers the central part of the galaxy, and has the steepest slope, while the fields that cover the outskirts of the galaxy (e.g. F2 and F7) display significantly shallower slopes. This clearly shows the environmental dependence of cluster disruption. The drop at $\sim$200 Myr is a combination of incompleteness and cluster disruption (taken from Silva-Villa et al. 2014)

Finally, Silva-Villa et al. (2014) have studied all seven fields, using the same techniques, and found that ζ varies from 0.8 in the central regions to $\sim$0 in the outer regions. Their age distributions for the seven fields are shown in Fig. 4.6. The authors found excellent agreement when comparing their results to the Chandar et al. (2010a,b, 2014) and Bastian et al. (2012) results. The Silva-Villa et al. full catalogue is shown in Fig. 4.4 in comparison with the simulations of Kruijssen et al. (2012). Note the excellent agreement with the simulations, which explicitly predict that cluster disruption is dependent on both the environment and the initial cluster mass.

We conclude that the age distribution in M83 is clearly dependent on location within the galaxy. The inner regions of the galaxy are characterised by relatively steep age distributions, indicative of heavy disruption. However, in the outer regions of the galaxy the age distributions are significantly shallower (in some cases, nearly flat). As discussed in Bastian et al. (2012) (and above) this is in excellent agreement with predictions of environmentally dependent cluster disruption (MDD).

4.3.4.5 Other Cluster Population Studies from the Literature

While we have focussed on a handful of cluster populations in detail, a number of other studies have found clear evidence that the age distribution of clusters depends systematically on the ambient environment. Galaxies with strong tidal fields and/or

large GMC populations have steeper age distributions, while galaxies, like the SMC, where cluster disruption is not expected to be a strong effect, have flat distributions. In Table 4.1 we show the results of other recent works from the literature as well as for the galaxies discussed in the previous sections. We also highlight the age range over which the fit was carried out. The selected ages range, as discussed above, strongly affect the resulting fits, as the inclusion of unbound associations at young ages and/or the inclusion of ages older than the completeness limit allows, can lead to significantly steeper distributions than is physically present.

Table 4.1 List of measurements of the cluster age distribution in different galaxies, focussing, with the exception of the Antennae galaxies, on systems where the SFH should have been largely constant over the age range measured

Galaxy	Age range	ζ	Reference
SMC	20–1000 Myr	0.0 ± 0.1[a]	Gieles et al. (2007)
M31	5–100 Myr	$0 - 0.15$	Fouesneau et al. (2014)
NGC 2997	10–100 Myr	0.1 ± 0.2	Ryon et al. (2014)
M51	10–300 Myr	0.15 ± 0.2	Hwang and Lee (2010)
Solar neighbourhood	5–300 Myr	0.3 ± 0.15	Lamers et al. (2005)
LMC	10–100 Myr	0.3 ± 0.15	Baumgardt et al. (2013)
M33	10–100 Myr	0.3 ± 0.2[b]	Gieles and Bastian (2008)[c]
NGC 4041	5–200 Myr	0.4 ± 0.2	Konstantopoulos et al. (2013)
NGC 1566	5–300 Myr	0.5 ± 0.15	Hollyhead et al. (2016)
NGC 4449	5–500 Myr	0.5 ± 0.15[b]	Annibali et al. (2011)
NGC 7793	10–500 Myr	0.55 ± 0.2	Silva-Villa and Larsen (2011)
NGC 1313	10–500 Myr	0.6 ± 0.1	Silva-Villa and Larsen (2011)
M83	10–500 Myr	0.25 ± 0.1	Silva-Villa and Larsen (2011)
M83 F1	1–1000 Myr	0.9 ± 0.2	Chandar et al. (2010b)
M83 F2	10–1000 Myr	0.5 ± 0.2	Chandar et al. (2014)
M83 F2	5–300 Myr	0.15 ± 0.15	Chandar et al. (2014) catalogue
M83 (F1-F7)	10–300 Myr	$0 - 0.6$	Silva-Villa et al. (2014)
M83 (full sample)	10–300 Myr	0.35 ± 0.15	Silva-Villa et al. (2014)
Antennae	5–500 Myr	0.85 ± 0.15	Whitmore et al. (2007, 2010)

Throughout, we have assumed a power-law type profile of the form $dN/dt \sim t^{-\zeta}$ over the age range listed

[a]Note the difference between this result and Chandar et al. (2006) who effectively used a luminosity-limited sample, hence found a much steeper age distribution. The Gieles et al. result was independently confirmed by de Grijs and Goodwin (2008)

[b]Based on the upper envelope of the age-mass relation (see Gieles and Bastian 2008)

[c]Similar results have also been found by Sarajedini and Mancone (2007), Fan and de Grijs (2014), and de Meulenaer et al. (2015). However, Sarajedini and Mancone (2007) used a luminosity-limited sample, hence they erroneously interpreted their steep distribution as being caused by disruption, correcting for this leads to $\zeta \sim 0.4$

From this growing list of studies it is clear that the age distribution of clusters is not universal, but rather depends strongly on the ambient environment. However, care must be taken when fitting the distributions, as approximating the full age distribution by a single power-law over the full observed range can lead to erroneous conclusions.

There has been a significant amount of debate in the literature on the form of the age distribution of cluster populations, which in turn has led to uncertainties in the role of cluster disruption in shaping the population. Publicly available catalogues have been used to compare results between different teams and galaxies, and now clearly show ($P_{\rm KS} < 10^{-5}$) that the age distribution varies strongly as a function of environment, with some galaxies (or regions) having flat ($\zeta \sim 0$) distributions (i.e. little disruption) while others display evidence of steep declines ($\zeta \sim 1$), indicative of strong disruption. Environments with weak tidal fields and/or low numbers of GMCs show flatter age distributions, consistent with analytical and numerical expectations.

4.4 Conclusions and Future Outlook

Recent work on cluster populations has found an increasing level of connectedness between the population properties and those of the host galaxy. It appears that the fraction of star-formation that happens in bound clusters (Γ) increases with the surface density of star-formation (which is likely just a proxy for the surface density of dense gas within a galaxy), ranging from $5 to 10\%$ for quiescent spirals and dwarf galaxies to $\sim$30–50% in starbursts. Even within a single galaxy, Γ can vary by a factor of four or more. An interesting implication of this is that star-formation in clusters may have been much more common in the early Universe, during the epoch of globular cluster formation. While the cluster initial mass function is well described by a power-law with index -2 over much of the observed range, an increasing number of studies have found that there is a truncation (or break) at high-masses, the point of which, $M_\star$, is also dependent on the host galaxy properties. Recent theoretical work (Kruijssen 2014) has linked $M_\star$ with the mass of the most massive GMCs within a galaxy (controlled by the Toomre-mass), hence galaxies like merging gas-rich systems which can produce massive GMC complexes are able to form more massive clusters, hence have higher values of $M_\star$. Finally, cluster populations have been used to study the process of cluster disruption, with the age distribution of clusters being sensitive to the rate at which clusters are destroyed. A clear trend of the age distribution with galaxy properties (with gas-rich high mass galaxies having steep age distributions, and quiescent galaxies having flat distributions) has been found by a number of studies. For most galaxies, rapid

disruption of young (<100 Myr) clusters is not supported by the data, and that the lifetimes of clusters are strongly related to their ambient environment.

Many of the studies and results presented here are based on a limited number of observations, or a small sample of cluster populations. Hence, large surveys focussing on individual galaxies (such as the M31 *Panchromatic Hubble Andromeda Treasury* (PHAT) survey—Dalcanton et al. 2012) or large galaxy samples (e.g. Legacy Extragalactic UV Survey—Calzetti et al. 2015) will allow detailed tests of the relations presented here as well as our theoretical framework to understand them. How does Γ vary within galaxies, both in space and time? Are there environments where cluster formation is actively suppressed? Or environments that encourage the formation of only a handful of massive clusters instead of sampling from an underlying parent distribution that favours the formation of many low-mass clusters (i.e. like that observed in most galaxies)?

On the cluster disruption side, the influence of environment on the lifetime of clusters is clear, and is expected for all scenarios of cluster dissolution. However, the role of cluster mass is still uncertain. The dominant cluster disruption mechanism in many galaxies is interactions with passing GMCs. The effect of the passage is proportional to the cluster density, hence if there is not a specific mass-radius relation for young clusters, cluster disruption is expected to be dependent on cluster mass (with high mass clusters surviving longer). Hence, deriving the cluster mass-radius relation in a sample of galaxies, and at a range of ages, will be very useful. Looking for changes in the cluster mass function (at the low mass end) as a function of age within a population is also a potential way to estimate the dependence of mass on disruption, however, incompleteness and sample selection affect the low-mass end of any observed sample preferentially, making the distinction between selection effects and physical properties challenging. Larger samples of cluster populations, however, may be able to address this question statistically.

Finally, one of the outstanding questions of cluster research is how, exactly, do the young massive clusters observed today relate to the ancient globular clusters observed around all major galaxies. Can we simply apply our understanding of cluster formation locally, and scale to the conditions of the early Universe? Much theoretical progress has been made in linking globulars and young massive clusters (e.g. Kravtsov and Gnedin 2005; Kruijssen 2014), however, many open issues remain.

Acknowledgements We gratefully acknowledge comments and suggestions by Diederik Kruijssen, Søren Larsen, Linda Smith, Steven Stahler, Jenna Ryon, Esteban Silva-Villa, Iraklis Konstantopoulos, Mark Gieles, and Daniella Calzetti which significantly improved the manuscript. NB is partially funded by a Royal Society University Research Fellowship.

References

Adamo, A., Östlin, G., Zackrisson, E., et al.: Mon. Not. R. Astron. Soc. **407**, 870 (2010)
Adamo, A., Östlin, G., Zackrisson, E.: Mon. Not. R. Astron. Soc. **417**, 1904 (2011)
Adamo, A., Kruijssen, J.M.D., Bastian, N., Silva-Villa, E., Ryon, J.: Mon. Not. R. Astron. Soc. **452**, 246 (2015). http://adsabs.harvard.edu/abs/2015MNRAS.452..246A
Anders, P., Bissantz, N., Fritze-v. Alvensleben, U., de Grijs, R.: Mon. Not. R. Astron. Soc. **347**, 196 (2004)
Annibali, F., Tosi, M., Monelli, M., et al.: Astron. J. **138**, 169 (2009)
Annibali, F., Tosi, M., Aloisi, A., van der Marel, R.P.: Astron. J. **142**, 129 (2011). http://adsabs.harvard.edu/abs/2011AJ....142..129A
Bastian, N.: Mon. Not. R. Astron. Soc. **390**, 759 (2008)
Bastian, N., Trancho, G., Konstantopoulos, I.S., Miller, B.W.: Astrophys. J. **701**, 607 (2009)
Bastian, N., Adamo, A., Gieles, M., et al.: Mon. Not. R. Astron. Soc. **417**, L6 (2011)
Bastian, N., Adamo, A., Gieles, M., et al.: Mon. Not. R. Astron. Soc. **419**, 2606 (2012)
Battinelli, P., Capuzzo-Dolcetta, R.: Mon. Not. R. Astron. Soc. **249**, 76 (1991)
Baumgardt, H., Parmentier, G., Anders, P., Grebel, E.K.: Mon. Not. R. Astron. Soc. **430**, 676 (2013)
Bik, A., Lamers, H.J.G.L.M., Bastian, N., Panagia, N., Romaniello, M.: Astron. Astrophys. **397**, 473 (2003)
Billett, O.H., Hunter, D.A., Elmegreen, B.G.: Astron. J. **123**, 1454 (2002)
Boutloukos, S.G., Lamers, H.J.G.L.M.: Mon. Not. R. Astron. Soc. **338**, 717 (2003)
Bressert, E., Bastian, N., Gutermuth, R., et al.: Mon. Not. R. Astron. Soc. **409**, L54 (2010)
Calzetti, D., Lee, J. C., Sabbi, E., et al.: Astron. J. **149**, 51 (2015)
Chandar, R., Fall, S.M., Whitmore, B.C.: Astrophys. J. **650**, L111 (2006)
Chandar, R., Fall, S.M., Whitmore, B.C.: Astrophys. J. **711**, 1263 (2010a)
Chandar, R., Whitmore, B.C., Kim, H., et al.: Astrophys. J. **719**, 966 (2010b)
Chandar, R., Whitmore, B. C., Calzetti, D., O'Connell, R.: Astrophys. J. **787**, 17 (2014)
Colombo, D., Hughes, A., Schinnerer, E., et al.: Astrophys. J. **784**, 3 (2014)
Cook, D.O., Seth, A.C., Dale, D.A., et al.: Astrophys. J. (751), 100 (2012)
Dalcanton, J.J., Williams, B.F., Lang, D., et al.: Astrophys. J. Suppl. Ser. **200**, 18 (2012)
da Silva, R.L., Krumholz, M.R., Fumagalli, M., Fall, S.M.: Mon. Not. R. Astron. Soc. **438**, 2355 (2014)
de Grijs, R., Anders, P., Bastian, N., et al.: Mon. Not. R. Astron. Soc. **343**, 1285 (2003)
de Grijs, R., Goodwin, S.P.: Mon. Not. R. Astron. Soc. **383**, 1000 (2008)
de Grijs, R., Goodwin, S.P., Anders, P.: Mon. Not. R. Astron. Soc. **436**, 136 (2013)
de Grijs, R., Anders, P., Zackrisson, E., Östlin, G.: Mon. Not. R. Astron. Soc. **431**, 2917 (2013)
de Meulenaer, P., Narbutis, D., Mineikis, T., Vansevičius, V.: Astron. Astrophys. **581**, A111 (2015)
Elmegreen, B.G.: Astrophys. J. **648**, 572 (2006)
Elmegreen, B.G.: Astrophys. J. **712**, L184 (2010)
Elmegreen, B.G.: EAS Publ. Ser. **51**, 31 (2011)
Elmegreen, B.G., Efremov, Y.N.: Astrophys. J. **480**, 235 (1997)
Fall, S.M., Chandar, R., Whitmore, B.C.: Astrophys. J. **704**, 453 (2009)
Fan, Z., de Grijs, R.: Astrophys. J. Suppl. Ser. **211**, 22 (2014)
Fedotov, K., Gallagher, S.C., Konstantopoulos, I.S., et al.: Astron. J. **142**, 42 (2011)
Fouesneau, M., Lançon, A.: Astron. Astrophys. **521**, A22 (2010)
Fouesneau, M., Johnson, L.C., Weisz, D.R., et al.: Astrophys. J. **786**, 117 (2014)
Gazak, J.Z., Bastian, N., Kudritzki, R.-P., et al.: Mon. Not. R. Astron. Soc. **430**, L35 (2013)
Gieles, M.: Mon. Not. R. Astron. Soc. **394**, 2113 (2009)
Gieles, M.: Galaxy Wars: Stellar Populations and Star Formation in Interacting Galaxies, vol. 423, p. 123 (2010)
Gieles, M., Larsen, S.S., Scheepmaker, R.A., et al.: Astron. Astrophys. **446**, L9 (2006a)
Gieles, M., Larsen, S.S., Bastian, N., Stein, I.T.: Astron. Astrophys. **450**, 129 (2006b)

Gieles, M., Lamers, H.J.G.L.M., Portegies Zwart, S.F.: Astrophys. J. **668**, 268 (2007)
Gieles, M., Bastian, N.: Astron. Astrophys. **482**, 165 (2008)
Gieles, M., Portegies Zwart, S.F.: Mon. Not. R. Astron. Soc. **410**, L6 (2011)
Goddard, Q.E., Bastian, N., Kennicutt, R.C.: Mon. Not. R. Astron. Soc. **405**, 857 (2010)
Hollyhead, K., Adamo, A., Bastian, N., Gieles, M., Ryon, J.E.: Mon. Not. R. Astron. Soc. **460**, 2087 (2016). http://adsabs.harvard.edu/abs/2016MNRAS.460.2087H
Holtzman, J.A., Faber, S.M., Shaya, E.J., et al.: Astron. J. **103**, 691 (1992)
Hopkins, P.F.: Mon. Not. R. Astron. Soc. **428**, 1950 (2013)
Hopkins, P.F.: Mon. Not. R. Astron. Soc. **430**, 1653 (2013)
Hunter, D.A., Elmegreen, B.G., Dupuy, T.J., Mortonson, M.: Astron. J. **126**, 1836 (2003)
Hwang, N., Lee, M.G.: Astrophys. J. **709**, 411 (2010)
Johnson, L.C., Seth, A.C., Dalcanton, J.J., et al.: Astrophys. J. **752**, 95 (2012)
Jordán, A., McLaughlin, D.E., Côté, P., et al.: Astrophys. J. Suppl. Ser. **171**, 101 (2007)
Kainulainen, J., Federrath, C., Henning, T.: Science **344**, 183 (2014)
Kennicutt, R.C., Evans, N.J.: Annu. Rev. Astron. Astrophys. **50**, 531 (2012)
Konstantopoulos, I.S., Bastian, N., Smith, L.J., et al.: Astrophys. J. **701**, 1015 (2009)
Konstantopoulos, I.S., Smith, L.J., Adamo, A., et al.: Astron. J. **145**, 137 (2013)
Kravtsov, A.V., Gnedin, O.Y.: Astrophys. J. **623**, 650 (2005)
Kruijssen, J.M.D.: Mon. Not. R. Astron. Soc. **426**, 3008 (2012)
Kruijssen, J.M.D.: Class. Quantum Grav. **31**, 244006 (2014)
Kruijssen, J.M.D.: Mon. Not. R. Astron. Soc. **454**, 1658 (2015)
Kruijssen, J.M.D., Pelupessy, F.I., Lamers, H.J.G.L.M., Portegies Zwart, S.F., Icke, V.: Mon. Not. R. Astron. Soc. **414**, 1339 (2011)
Kruijssen, J.M.D., Maschberger, T., Moeckel, N., et al.: Mon. Not. R. Astron. Soc. **419**, 841 (2012)
Kobulnicky, H.A., Johnson, K.E.: Astrophys. J. **527**, 154 (1999)
Lada, C.J., Margulis, M., Dearborn, D.: Astrophys. J. **285**, 141 (1984)
Lada, C.J., Lada, E.A.: Annu. Rev. Astron. Astrophys. **41**, 57 (2003)
Lamers, H.J.G.L.M.: Astrophys. Space Sci. **324**, 183 (2009)
Lamers, H.J.G.L.M., Gieles, M.: Astron. Astrophys. **455**, L17 (2006)
Lamers, H.J.G.L.M., Gieles, M., Bastian, N., et al.: Astron. Astrophys. **441**, 117 (2005)
Lamers, H.J.G.L.M., Baumgardt, H., Gieles, M.: Mon. Not. R. Astron. Soc. **409**, 305 (2010)
Larsen, S.S.: Astron. J. **124**, 1393 (2002)
Larsen, S.S.: Astron. Astrophys. **416**, 537 (2004)
Larsen, S.S.: (2006). arXiv:astro-ph/0606625
Larsen, S.S.: Astron. Astrophys. **494**, 539 (2009)
Larsen, S.S.: R. Soc. Lond. Philos. Trans. Ser. A **368**, 867 (2010)
Larsen, S.S., Richtler, T.: Astron. Astrophys. **354**, 836 (2000)
Larsen, S.S., Brodie, J.P., Elmegreen, B.G., et al.: Astrophys. J. **556**, 801 (2001)
Longmore, S.N., Kruijssen, J.M.D., Bastian, N., et al.: Protostars and Planets VI, vol. 291 (2014)
Maíz Apellániz, J., Úbeda, L.: Astrophys. J. **629**, 873 (2005)
Maschberger, T., Kroupa, P.: Mon. Not. R. Astron. Soc. **395**, 931 (2009)
Meurer, G.R., Heckman, T.M., Leitherer, C., et al.: Astron. J. **110**, 2665 (1995)
Miller, B.W., Whitmore, B.C., Schweizer, F., Fall, S.M.: Astron. J. **114**, 2381 (1997)
Pasquali, A., Bik, A., Zibetti, S., et al.: Astron. J. **141**, 132 (2011)
Piskunov, A.E., Kharchenko, N.V., Röser, S., Schilbach, E., Scholz, R.-D.: Astron. Astrophys. **445**, 545 (2006)
Popescu, B., Hanson, M.M.: Astrophys. J. **724**, 296 (2010)
Portegies Zwart, S.F., McMillan, S.L.W., Gieles, M.: Annu. Rev. Astron. Astrophys. **48**, 431 (2010)
Rafelski, M., Zaritsky, D.: Astron. J. **129**, 2701 (2005)
Randriamanakoto, Z., Escala, A., Väisänen, P., et al.: Astrophys. J. **775**, L38 (2013)
Renaud, F., Gieles, M.: Mon. Not. R. Astron. Soc. **431**, L83 (2013)
Ryon, J.E., Adamo, A., Bastian, N., et al.: Astron. J. **148**, 33 (2014)
Santiago-Cortés, M., Mayya, Y.D., Rosa-González, D.: Mon. Not. R. Astron. Soc. **405**, 1293 (2010)

Sarajedini, A., Mancone, C.L.: Astron. J. **134**, 447 (2007)
Schechter, P.: Astrophys. J. **203**, 297 (1976)
Silva-Villa, E., Larsen, S.S.: Astron. Astrophys. **529**, A25 (2011)
Silva-Villa, E., Adamo, A., Bastian, N.: Mon. Not. R. Astron. Soc. **436**, L69 (2013)
Silva-Villa, E., Adamo, A., Bastian, N., Fouesneau, M., Zackrisson, E.: Mon. Not. R. Astron. Soc. **440**, L116 (2014)
Spitzer, L.: Dynamical Evolution of Globular Clusters, 19 pp. Princeton University Press, Princeton (1987). http://adsabs.harvard.edu/abs/1987degc.book.....S
Trancho, G., Bastian, N., Miller, B.W., Schweizer, F.: Astrophys. J. **664**, 284 (2007)
Whitmore, B.C.: (2000). arXiv:astro-ph/0012546
Whitmore, B.C., Chandar, R., Fall, S.M.: Astron. J. **133**, 1067 (2007)
Whitmore, B.C., Chandar, R., Schweizer, F., et al.: Astron. J. **140**, 75 (2010)
Whitmore, B.C., Chandar, R., Bowers, A.S., et al.: Astron. J. **147**, 78 (2014)
Zhang, Q., Fall, S.M.: Astrophys. J. **527**, L81 (1999)

Chapter 5
Multiwavelength Studies of Young OB Associations

Eric D. Feigelson

Abstract We discuss how contemporary multiwavelength observations of young OB-dominated clusters address long-standing astrophysical questions: Do clusters form rapidly or slowly with an age spread? When do clusters expand and disperse to constitute the field star population? Do rich clusters form by amalgamation of smaller subclusters? What is the pattern and duration of cluster formation in massive star forming regions (MSFRs)? Past observational difficulties in obtaining good stellar censuses of MSFRs have been alleviated in recent studies that combine X-ray and infrared surveys to obtain rich, though still incomplete, censuses of young stars in MSFRs. We describe here one of these efforts, the MYStIX project, that produced a catalog of 31,784 probable members of 20 MSFRs. We find that age spread within clusters is real in the sense that the stars in the core formed after the cluster halo. This is consistent with some recent astrophysical models involving merging star-forming filaments. Cluster expansion is seen in the ensemble of (sub)clusters, and older dispersing populations are found across MSFRs. Long-lived, asynchronous star formation is pervasive across MSFRs.

5.1 Historical Discussions of Star Cluster Formation

Galactic Plane star clusters, well known to classical astronomers like second century Claudius Ptolemy and tenth century Abd al-Rahman al-Sufi, were catalogued in the eighteenth to nineteenth centuries by Charles Messier and William and John Herschel. As astrophysical explanations for astronomical phenomena rose to prominence around the turn of the twentieth century, it was natural that the processes giving rise to clusters were investigated. We address here several astrophysical themes of long-standing importance where, even today, theory is not well-constrained by observation.

E.D. Feigelson (✉)
Department of Astronomy & Astrophysics, Pennsylvania State University, University Park, PA 16802, USA
e-mail: edf@astro.psu.edu

S. Stahler (ed.), *The Birth of Star Clusters*, Astrophysics and Space Science Library 424, DOI 10.1007/978-3-319-22801-3_5

The historically oldest issue is the argument that most stars are born in clusters that expand and disperse to comprise the field star population. In a 1917 discussion of Kapteyn's "systems of stars which travel together in parallel paths," Charlier (1917), director of Lund Observatory in Sweden, argues

> that the stars which now belong to such a system are only the insignificant remnant of a large cluster which at one time constituted a compact system in space.

Such questions could be investigated computationally, both by integrating difficult differential equations and by Monte Carlo N-body calculations, in the 1970s. In an important study, Tutukov (1978) wrote:

> It is generally believed that ... stars [form] in small groups which dissolve comparatively quickly during very early stages of evolution, practically at the moment of their formation. ... It is natural to suppose that the gas not utilized for star formation was blown away by hot stars, probably due to the ionizing radiation and stellar wind. If the mass of gas is higher than the mass of stars and the kinetic energy of the gas exceeds the binding energy of the cluster, then the disruption of a young cluster seems inevitable.

The issue of stellar dispersal arose again when early type stars were discovered far from their natal clouds away from the Galactic Plane. Greenstein and Sargent (1974) noted:

> The kinematical behavior of these stars is, however, quite strange ... The stars are not kinematically relaxed; they are apparently observed soon after formation and ejection. ... [This reveals] a fundamental problem that far too many, hot, high-velocity, apparently normal stars exist.

Some of these stars are clearly runaway stars ejected at high velocities from hard binary interactions, but others some dispersed up to ∼200 pc from the Plane could not easily be traced to rich clusters (de Wit et al. 2005). In a catalogue of stellar members in OB associations within 3 kpc, Garmany and Stencel (1992) found that massive OB stars are commonly spread over large (∼200 pc) regions; these did not appear to be high-velocity runaways.

Another long-standing issue concerns the mechanism by which rich star clusters form. Aarseth and Hills (1972) sought to evaluate two alternatives views: simultaneous formation of a monolithic rich cluster and its possible later construction from pre-existing subclusters. They wrote:

> The density distribution of stars in a stellar cluster usually gives every appearance of being smoothing varying and non-clumpy. On the face of it, this is a bit surprising since elementary considerations from [Jeans gravitational collapse] star-formation theory suggest that a cluster should initially be subdivided into a hierarchy of subclusters. ... The subdivision process terminates when the cloud becomes opaque enough for the collapse time-scale to catch up with the cooling time-scale ... [so] that a cluster is initially composed of a hierarchy of subclusters.

Stellar subgroups were empirically found in a number of nearby rich OB associations by Blaauw (1964). But it was unclear whether the primary process is fragmentation of an initially homogeneous cluster, or incomplete consolidation of smaller subclusters into a unified structure. The latter view came to the fore when molecular clouds were discovered to be highly inhomogeneous due to supersonic

turbulence (Mac Low and Klessen 2004). Maps obtained with the Herschel satellite far-infrared imaging show that even the coldest and densest cloud structures mostly have clumpy and filamentary structure (André et al. 2010).

A third contentious issue is the duration of star formation in molecular clouds. Various researchers argue, on both physical and observational grounds, that cluster formation is rapid, although a small number of stars may form over an extended period before the principal starburst (Elmegreen 2000; Palla and Stahler 2000; Hartmann et al. 2012). Others suggest that regulation of star formation by magnetically induced turbulence in molecular clouds and feedback from nascent stars prevents large-scale free-fall gravitational collapse and rapid cluster formation (Mac Low and Klessen 2004; Bate 2009; Krumholz and Tan 2007; Krumholz et al. 2012). The evidence outlined above for widely distributed early type stars suggests that star formation in massive star forming regions is long-lived, so that earlier generation of massive stars have time to drift outward from still-active star forming regions.

5.2 The Observational Challenges

It is now clear that most stars form in rich clusters. The cluster luminosity function in the Milky Way Galaxy and nearby galaxies demonstrates that the majority of stars form in clusters with 10^2–10^4 stars (Lada and Lada 2003) and, during galactic starburst episodes, superclusters of 10^5 stars may dominate. But even the fundamental physical properties, processes and timescales of cluster formation and early evolution are observationally poorly established. Cogent arguments have been made that clusters form quickly (Elmegreen 2000) and slowly (Tan et al. 2006), that they form as a unified structure or are assembled from merging subclusters (McMillan et al. 2007; Bate 2009), that they form in spherical cloud cores or in filamentary cloud structures (Rathborne et al. 2006; André et al. 2010). Timescales for cluster formation and early dynamical evolution are poorly constrained by observation. Attempts to measure the ages of constituent stars of nearby clusters by fitting their location in Hertzsprung–Russell diagrams (HRDs) to theoretical evolutionary tracks is beset with observational difficulties, so that it is unclear whether the observed spreads in HRDs represent true age spreads (Preibisch 2012).

The reasons for the failure to test competing astrophysical models of cluster formation can arguably be placed on practical observational difficulties in defining their member stars. Much progress has been made in studying the progenitor molecular clouds through, for example, maps of coolant molecular lines with millimeter array telescopes and far-infrared imaging of continuum dust emission with the Herschel satellite. The environmental effects of the hot OB stars can also be traced across the Galactic Plane: ionized gas is easily mapped at radio wavelengths, and heated dust produces PAH band emission mapped with infrared space telescopes. But the actual stellar populations of star clusters beyond distances $\sim$1 kpc are poorly known. Indeed, hardly any members have been identified in most of the massive Galactic star forming regions that would be called “extragalactic giant H II regions” were they to be present in nearby galaxies (Figer 2008).

Acquiring a reliable census of members of star clusters beyond $d \sim 1$ kpc faces several challenges. The most devastating is contamination by uninteresting older Galactic field stars along the line-of-sight. At Galactic latitude $b \sim 0°$ and longitudes in the inner quadrants, field stars have 10–100 times higher surface density than the cluster members over most of the cluster extent at near-infrared magnitudes around the peak of the Initial Mass Function. Interstellar absorption can reach $A_V \sim 30$ mag along the line-of-sight to the cluster and can vary by tens of magnitude within the star forming region due to the local molecular cloud. Detection of faint infrared stars is difficult amid the nebular H II region emission from heated dust.

As a result of these problems, the census of young star cluster members has often been restricted to nearby lower-mass clusters or to special subpopulations of massive clusters: the inner cluster core where the surface density rises above the field stars; OB stars that are brighter and bluer than ambient stars and easily confirmed with optical spectroscopy; and pre-main sequence stars with photometric infrared excesses (IRE) from dust protoplanetary disks. The IRE criterion is often used to define the population of "young stellar objects" (YSOs) but it is restricted to disk-bearing pre-main sequence stars (Class I–II). In many clusters, the bulk of the stars have lost their disks and are thus photometrically indistinguishable from contaminant field stars in the infrared bands. Inferences regarding star formation histories may be flawed due to the IRE sample bias towards younger systems with hot inner accretion disks.

However, a technique has emerged in recent years that overcomes, to some degree, these observational difficulties and biases. Sensitive and high-resolution imaging of star forming regions with NASA's Chandra X-ray Observatory, sensitive in the 0.5–8 keV (25–1.5 Å) X-ray band, can detect reasonable fractions of young cluster populations out to distances of several kiloparsecs with reasonable exposure times. A typical 100 ks exposure with Chandra's Advanced CCD Imaging Spectrometer of a typical rich cluster at $d \sim 2$–3 kpc will reveal 1000 or more cluster members, perhaps 5–20% of the full Initial Mass function (IMF). Most importantly, the X-ray image captures only a minute fraction of the Galactic field stars that contaminate the infrared images so badly. The main contaminant of X-ray images is quasars seen through the Galactic Plane, and these are readily removed due to their lacking infrared counterparts. X-ray emission in pre-main sequence arises from magnetic flaring activity, similar to that of the Sun but with much more powerful and frequent flares (Feigelson and Montmerle 1999). The flaring X-ray emission has a sufficiently "hard" X-ray spectrum that these stars can be detected through high column densities of intervening interstellar material, equivalent to $A_V \sim 100$ mag in some cases. Finally, X-ray selection is complementary to IRE selection because it most efficiently captures disk-free (Class III) stars.

The remainder of this chapter discusses a particular effort called MYStIX (Massive Young Stellar complexes study in Infrared and X-rays) that combines Chandra X-ray, UKIRT near-infrared, and Spitzer Space Telescope mid-infrared surveys of 20 OB-dominated star forming regions at distances $0.4 < d < 4$ kpc

(Feigelson et al. 2013). After complicated data analysis with statistical procedures designed to reduce contaminants, a sample of ∼31,000 MYStIX Probable Complex Members (MPCMs) is generated. While far from a complete stellar census, the samples are typically much larger than previously available and appear to be reasonably free from contaminating field stars. After a brief description of the MYStIX observational effort (Sect. 5.3) and a new stellar chronometer based on X-ray/infrared photometry (Sect. 5.4), we summarize some of the characteristics of these star clusters (Sect. 5.5). A variety of results are then outlined (Sect. 5.7): the morphology of stellar clustering and maps of stellar surface density, histories of star formation in MSFRs, and direct measurement of cluster expansion.

MYStIX is only one of several similar X-ray/infrared surveys that include: Chandra Carina Complex Project (Townsley et al. 2011), Chandra Cyg OB2 Legacy Survey (Wright et al. 2014), Star Formation in Nearby Clouds (Getman et al. 2017), NGC 6611 (Guarcello et al. 2007), Eagle Nebula (Guarcello et al. 2010), NGC 1893 (Prisinzano et al. 2011), DR 15 (Rivera-Gálvez et al. 2015), NGC 6231 (Damiani et al. 2016; Kuhn et al. 2017), NGC 7538 (Sharma et al. 2017), and others.

5.3 The MYStIX Project

The MYStIX effort seeks to construct an improved census of stars in rich clusters and their environs in 20 MSFRs near the Sun. Populations that are not dominated by an O or early-B star are omitted; thus, MYStIX omits nearby small star forming regions like the Taurus-Auriga, ρ Ophiuchi, and Chamaeleon complexes. Table 5.1 lists the MYStIX star forming regions with approximate distance from the Sun and spectral type of the dominant star. The accompanying Fig. 5.1 shows the location of the MYStIX regions on a diagram of the Milky Way Galaxy with the Sun at the middle. The MYStIX targets do not constitute a complete sample in any way, but

Table 5.1 MYStIX star forming regions

Region	D_{kpc}	*	Region	D_{kpc}	*
Orion Neb	0.4	O7	NGC 6334	1.7	O8:
Flame Neb	0.4	O8:	NGC 6357	1.7	O3
W 40	0.5	O:	Eagle Neb	1.8	O9
RCW 36	0.7	O8	M 17	2.0	O4
NGC 2264	0.9	O7	W 3	2.0	O5
Rosette Neb	1.3	O4	W 4	2.0	...
Lagoon Neb	1.3	O4	Carina Neb	2.3	O2
NGC 2362	1.5	O9I	Trifid Neb	2.7	O7
DR 21	1.5	...	NGC 3576	2.8	O:
RCW 38	1.7	O5	NGC 1893	3.6	O5

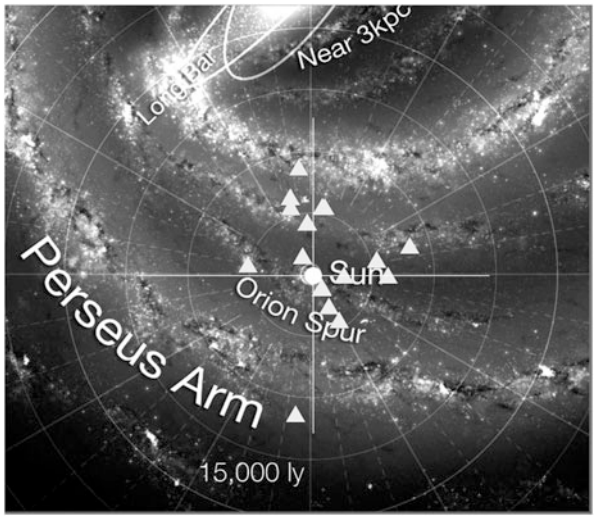

Fig. 5.1 Galactic location of MYStIX star forming regions (triangles)

rather were selected by practical considerations: they must have sufficiently deep coverage by the Chandra and Spitzer satellite images.

Simply stated, the MPCM samples are the sum of probable complex members extracted from X-ray sources in the Chandra X-ray Observatory images, IRE sources from UKIRT near-infrared observations (often part of the UKIDSS Galactic Plane Survey) and the Spitzer Space Telescope mid-infrared observations, and published OB stars confirmed by published optical spectroscopy. But the actual procedure for constructing the MPCM samples is complicated by the need to reduce the often-overwhelming contamination of Galactic field stars combined with spatially variable cloud absorption and nebular emission. Challenges overcome include:

X-ray source lists were obtained using the *ACIS Extract* package and associated software developed for the Chandra ACIS instrument at Penn State (Kuhn et al. 2013a; Townsley et al. 2014). This allows detection of sources with as few as 3–5 photons on-axis, even in the presence of crowding and diffuse X-ray emission. Contamination from extragalactic X-ray sources and field X-ray stars was reduced by a naive Bayes classifier based on various properties of the sources and their infrared counterparts (Broos 2013). The reliability of these sources is validated by the high fraction associated with stars exhibiting other pre-main sequence properties (Kuhn et al. 2013a, 2017).

Near-infrared source lists were obtained with the UKIDSS pipeline software modified to accommodate very crowded Galactic plane fields with nebulosity (King et al. 2013).

Mid-infrared source lists were obtained with the Spitzer IRAC team software modified to accommodate crowding and nebulosity (Kuhn et al. 2013b).

X-ray/infrared counterpart identifications were based on a probabilistic calculation of proximate sources that accounts for the magnitude distribution expected for true complex members, in order to reduce false associations with fainter field stars (Naylor et al. 2013).

Infrared excess stars were extracted based on a complicated decision tree of criteria designed to reduce the often-heavy contamination by field red giants and false sources associated with nebular knots (Povich et al. 2013).

The classified X-ray sources, IRE stars, and published OB stars were then combined into the MPCM catalog of 31,784 stars in the 20 regions of Table 1 (Broos 2013). The MYStIX papers, and their electronic tables of intermediate and final samples, are collected at the Web site http://astro.psu.edu/mystix.

The MPCM sample is far from a complete census. The X-ray samples are generally limited to stars with masses above $\sim$ 0.5 $M_{\odot}$, and thus miss the peak of the IMF of low-mass members. Various biases are present in the sample as well (see Appendix B of Feigelson et al. (2013)). Nonetheless, the MPCM samples are the largest for most of the star forming regions under consideration. Tests of the sample reliability were made using the well-studied NGC 2264 population; $\sim$80% of previously identified Hα and optically variable stars were recovered, and dozens of new members are proposed (Feigelson et al. 2013).

Figures 5.2 and 5.3 illustrate the MPCM samples for four MYStIX star forming regions. The regions have complex structures though with some similar behaviors.

Lagoon Nebula (M 8) In this MSFR, we see two major clusters: the poorly characterized NGC 6523 cluster to the east with the famous massive star Herschel 36; and the well characterized NGC 6530 cluster in a large cavity to the west. As one proceeds westward, the fraction of IRE stars (red circles in Fig. 5.2) decreases; it is not immediately clear whether this is an age gradient or a selection effect due to the difficulty of finding IRE stars in the bright PAH nebulosity of the western region. A clump of stars is also seen to the far-southeast associated with a bright rimmed cloud; it includes the luminous embedded star M 8E.

NGC 6334 This is a large MSFR elongated along the Galactic Plane with both heavy absorption and complex bright nebular emission that precluded generation of a reliable stellar census in the past. The 1667-member MPCM sample shows several distinct clusters, some dominated by young IRE stars and others by older X-ray selected stars (Feigelson et al. 2009). The morphology might represent a star formation wave from the southwest to the northeast, but older clusters are sometimes superposed on younger clusters and a distributed young star component is also present. A selection of likely protostars, based on MYStIX sources with ascending infrared spectral slopes or ultra-hard X-ray spectra, shows a distribution of very young stars tracing the curved molecular filament to the northeast (Romine et al. 2016).

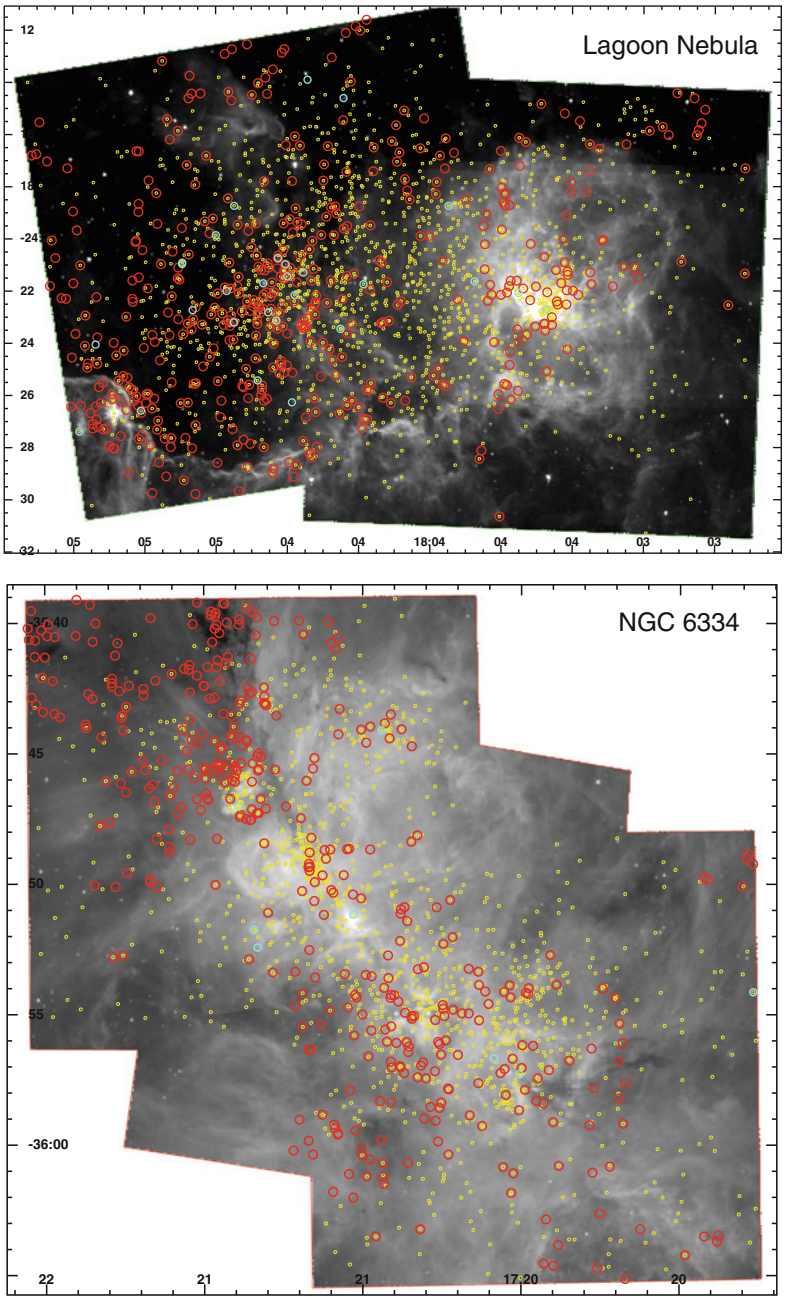

Fig. 5.2 Spatial location of MYStIX Probable Complex Members (MPCMs) for the Lagoon Nebula and NGC 6334 fields (Broos 2013). Infrared excess stars are noted by *red circles*, X-ray selected stars by *yellow dots*, and published OB stars by *cyan circles*. The stars are superposed on Spitzer IRAC 8.0 μm maps. Each Chandra field subtends $17' \times 17'$

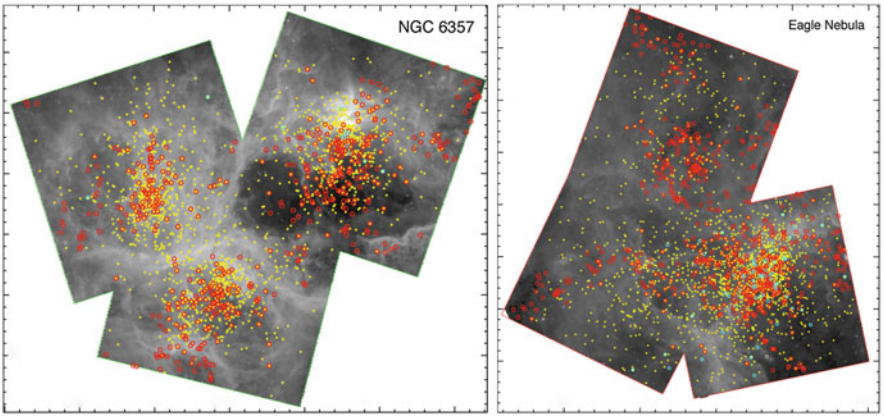

Fig. 5.3 The MPCMs in the NGC 6357 and Eagle Nebula complexes superposed on Spitzer IRAC 8 μm maps (Broos 2013). *Yellow dots* are X-ray selected members, *red circles* are infrared-excess members, and *cyan symbols* are published OB stars

NGC 6357 This region has 2,235 MPCMs, very few of which had previously been identified by optical or infrared surveys even though this is a very active star forming region in the Carina spiral arm. Three very rich clusters are seen; Pismis 24 to the northwest has several $\sim$ 100 $M_{\odot}$ O3 stars. In each cluster, we can see spatial displacements between the infrared and X-ray selected subsamples. The IRE selection method is ineffective around the brightest nebular emission of the northwest H II region. Two dozen new absorbed ($4 < A_V < 24$ mag) candidate OB stars are identified in the MYStIX catalog in this region (Povich et al. 2017).

Eagle Nebula (M 16) Here the southwestern rich cluster is dominated by disk-free X-ray selected members, while the sparser subclusters to the north and west are dominated by disk-bearing IRE members. As in most MYStIX regions, the X-ray selected stars outnumber the IRE stars, implying that the star formation has endured for many millions of years beyond the typical longevity of infrared-emitting disks.

5.4 A New Stellar Chronometer

To reveal the spatiotemporal history of star formation in MYStIX regions, it would be very desirable to obtain reliable ages of different (sub)clusters of MPCM stars. Two pre-main sequence chronometers are traditionally used: a star's location in the HRD compared to theoretical evolutionary tracks; and the presence of a star's infrared-emitting circumstellar disk (Haisch et al. 2001; Richert et al. 2017). But neither are very effective for MSFRs. HRD locations

are not available because the stars are often too reddened to readily obtain optical spectra, and in any case several extraneous problems render HRD-derived ages uncertain (Preibisch 2012). Disk fractions or classification (Class 0-I-II-III) derived from infrared photometry are inaccurate and difficult to calibrate. For example, IRE populations are reduced by local H II region contamination, differences in infrared-to-X-ray sensitivities can systematically bias disk fraction comparisons between MYStIX regions, and individual disk dissipation timescales range over 0.5–5 Myr or more. A potentially accurate chronometer based on oscillations of intermediate-mass stars has been proposed (Zwintz et al. 2014), but it can be applied only to a handful of bright well-studied stars, not to thousands of faint MSFR stars.

In the MYStIX context, Getman and colleagues have developed a new, surprisingly simple chronometer for pre-main sequence stars that can be applied to a reasonable fraction of MPCM stars (Getman et al. 2014a). It is based on the long-standing empirical correlation between X-ray luminosity L_x, produced by magnetic reconnection flares, and stellar mass M in pre-main sequence stars. This $L_x - M$ relation is best calibrated in the Taurus-Auriga population (Telleschi et al. 2007). The astrophysical cause of this correlation is poorly understood (presumably related to magnetic dynamos in fully convective stellar interiors), but it accounts for much of the 10^4 range of L_x in young stellar populations. MYStIX L_x measurements, after correction for soft X-ray absorption from intervening interstellar gas, thus give mass estimates for each star. MYStIX also gives measures photospheric luminosities $L_{\rm bol}$; Getman et al. use dereddened J band magnitudes M_J as a proxy for $L_{\rm bol}$. M values inferred from L_x and measured M_J values combined with standard theoretical evolutionary tracks give stellar age estimates for each star, nicknamed Age_{JX}. Each Age_{JX} value may be inaccurate, but obtaining the median Age_{JX} for a spatially defined subsample of young stars appears to be effective for elucidating histories of star formation within and between clusters.

5.5 Identifying (Sub)Clusters

The MYStIX fields are mostly centered on rich OB associations with optically bright H II region, often with names like "Rosette Nebula" and "Lagoon Nebula" that date to the nineteenth century. But examination of the MPCM spatial distributions shows considerable diversity in clustering behavior—a simple dichotomy between rich clusters and distributed star formation is clearly inadequate. Global statistics of spatial point processes, such as Ripley's K function and the related two-point correlation function (Illian et al. 2008), are not directly useful as they are strongly affected by the richest clusters and do not reflect the diversity of patterns within a single field. Defining stellar "clusters" or "groups" by surface density enhancements (Feigelson et al. 2011) also has the disadvantage of requiring an arbitrary threshold.

We therefore proceeded to locate "clusters" using a parametric statistical regression approach known as "mixture models" (McLachlan and Peel 2000). Here we require that cluster structure has a specific mathematical form corresponding an isothermal sphere or ellipsoid (Kuhn et al. 2014a). A likelihood function giving the probability that the observed celestial locations of MPCM stars correspond to a specified mixture of isothermal ellipsoids. When a flat "distributed" stellar population is added, a model with k clusters has $6k + 1$ parameters. The best fit model is obtained by maximum-likelihood estimation for a range of k, and the optimal number of clusters is obtained by maximizing the Akaike Information Criterion, a well-accepted penalized likelihood measure for model selection. Note that the method permits hierarchical structures with one ellipsoid lying within or overlapping another ellipsoid. Model fits are generally excellent with no strong features in the residual spatial maps. The resulting spatial decompositions for the NGC 6357 and Eagle Nebula MYStIX fields are shown in Fig. 5.4.

The result of this analysis is the assignment of each of the ∼31,000 MPCM stars to one of 142 (sub)clusters or to a distributed population (Kuhn et al. 2014a). Since each subcluster has an assumed isothermal ellipsoid internal structure, parameters such as core radii and ellipticity can be calculated. Two measures of absorption are available for each (sub)cluster: the median $J - H$ color index and the sample median of the individual median energies of the X-rays from the constituent stars. For example, the Eagle Nebula has 12 statistically significant subclusters (Fig. 5.4) with sample populations ranging from 7 to 451 MPCM stars, core radii from 0.07 to 1.0 pc, ellipticities from 7% to 64%, and absorptions from $A_V \sim 5$ to 16 mag. Note that the sample sizes are not unbiased measures of the true stellar populations, as they depend on the circumstantial exposure times of the Chandra and Spitzer observations, region distance, and absorption.

Two additional critical properties of subclusters can be derived. First, the age of each subcluster can be estimated from the median Age_{JX} values of the constituent stars (Sect. 5.4). Ages for the Eagle (sub)clusters range from 0.8 to 2.4 Myr. Second, the total stellar population can be inferred by scaling the sample X-ray luminosity function (truncated at different limiting X-ray sensitivities) to the full-sampled X-ray luminosity function of the Orion Nebula Cluster (Kuhn et al. 2014b). The total populations inferred from X-ray luminosity functions agree well with a parallel analysis based on dereddened J band magnitudes scaled to a standard Initial Mass Function.

Combining the estimated total population with the (sub)cluster structural parameters like core radius, unbiased estimates can be made of important quantities such as total stellar mass (in $M_\odot$), central surface densities (in stars/pc^2), central volume densities (in stars/pc^3), characteristic crossing, and relaxation times (in Myr) (Kuhn et al. 2015).

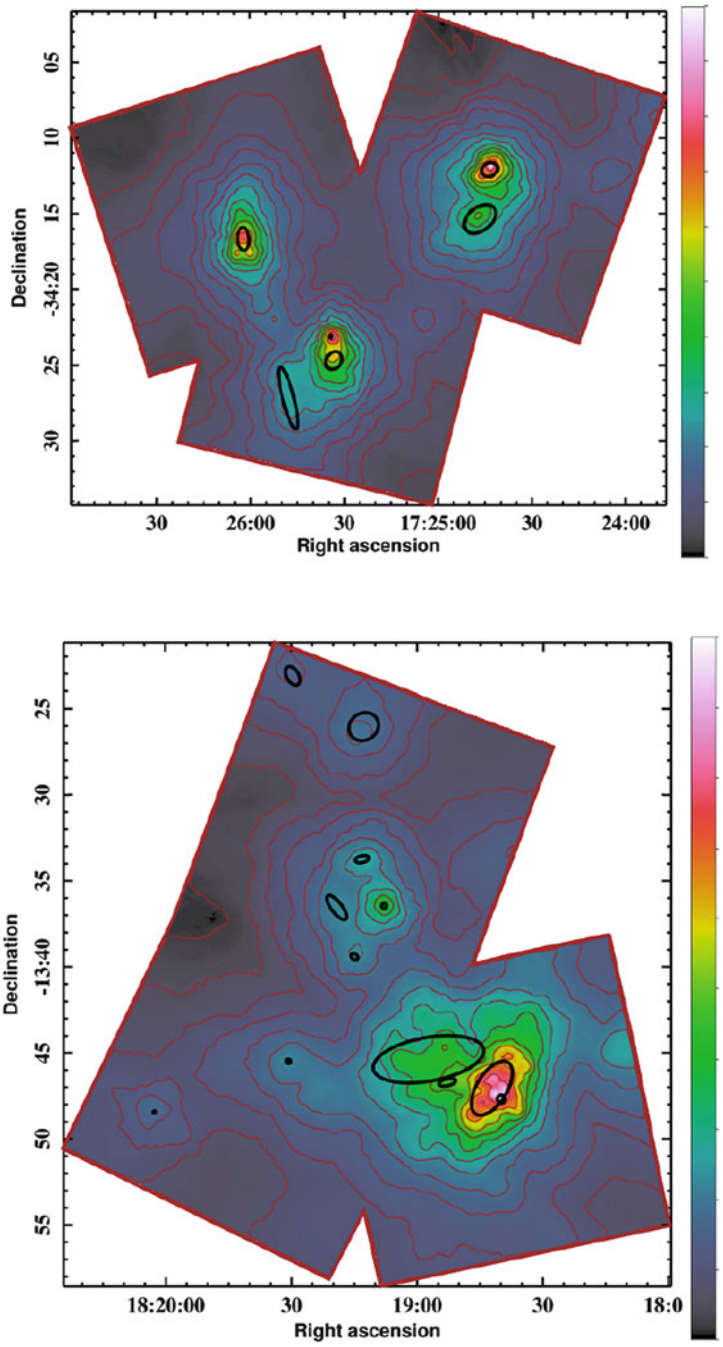

Fig. 5.4 Statistically defined subclusters in the NGC 6357 and Eagle Nebula complex are shown as *black ellipses* superposed on smoothed maps of the MPCM stellar distribution

5.6 Spatial Distribution of Stars Across Star Forming Regions

Comparisons of MPCM stellar spatial distributions in maps like Figs. 5.3 and 5.4 can be misleading due to inhomogeneity in sensitivity. This particularly affects the X-ray measurements. First, within each Chandra ACIS field the sensitivity is highest at the field center and degrades by a factor of ∼3 as one approaches the field edges due to the coma of the high-resolution X-ray mirrors. Second, Chandra fields are often mosaics of overlapping exposures; due to the low background of the ACIS detector, sensitivity scales linearly with exposure time. Third, the Chandra exposure times are not scaled with the square of the MYStIX region distance, so the X-ray luminosity function (and, through the empirical L_x-Mass relationship) and mass function are truncated at different levels.

However, as outlined in Sect. 5.5, these problems can be overcome (Kuhn et al. 2014b). We first "flatten" the intra-ACIS sensitivity variation by omitting the faint sources near the field center. The stellar surface densities are then normalized to the full IMF assuming all regions have the same intrinsic X-ray luminosity function. Although the lower mass stars missed by Chandra cannot be individually identified, the surface densities can be scaled upward to compensate for the different truncation levels. Note it is more difficult to corrected the maps for variations in the surface densities of IRE sources, which are deficient in the brightest H II nebular regions.

The result is Fig. 5.5 a remarkable new view of the stellar distributions in massive star forming clouds (Kuhn et al. 2014b). The densities correspond to the full intrinsic stellar populations down to the M∼ 0.08 $M_\odot$ limit shown on a uniform physical scale (see the 5 pc scale bar) and a uniform color scale in stars/pc^2 (see color calibration bar). We find, for example, that both the embedded clusters and the revealed massive cluster of the Rosette Nebula region have low surface densities of 10^1 stars/pc^2. But the RCW 38, Orion Nebula Cluster, and M 17 clusters have extremely high central surface densities around 10^4 stars/pc^2.

Diversity, rather than consistency, is the premier result from these surface density maps. The main Rosette Nebula cluster NGC 2244 must be in a completely different dynamical state than the RCW 38 or W 40 clusters; and indeed, this may be related to the complete absence of mass segregation in NGC 2244 (Wang et al. 2008). Until these maps were compared, it was not realized that RCW 38 (which is badly contaminated in the IR bands due to nebulosity) has the densest collection of stars of any cluster in the nearby Galaxy. It thus provides an excellent laboratory to study dynamical effects of close stellar encounters (Pflamm-Altenburg and Kroupa 2006; Pfalzner and Kaczmarek 2013).

The MYStIX maps showing of a wide range of central surface densities, $< 10^1$ to $\sim 3 \times 10^4$ stars/pc^2 (Fig. 5.5), stands in conflict with the findings of Bressert and colleagues who report that young stellar clusters exhibit a characteristic central surface density distribution with mean around 20 stars/pc^2 (Bressert et al. 2010). Their study is limited to nearby molecular clouds where clusters are generally small and, most importantly, their sample is limited to IRE stars and thus miss

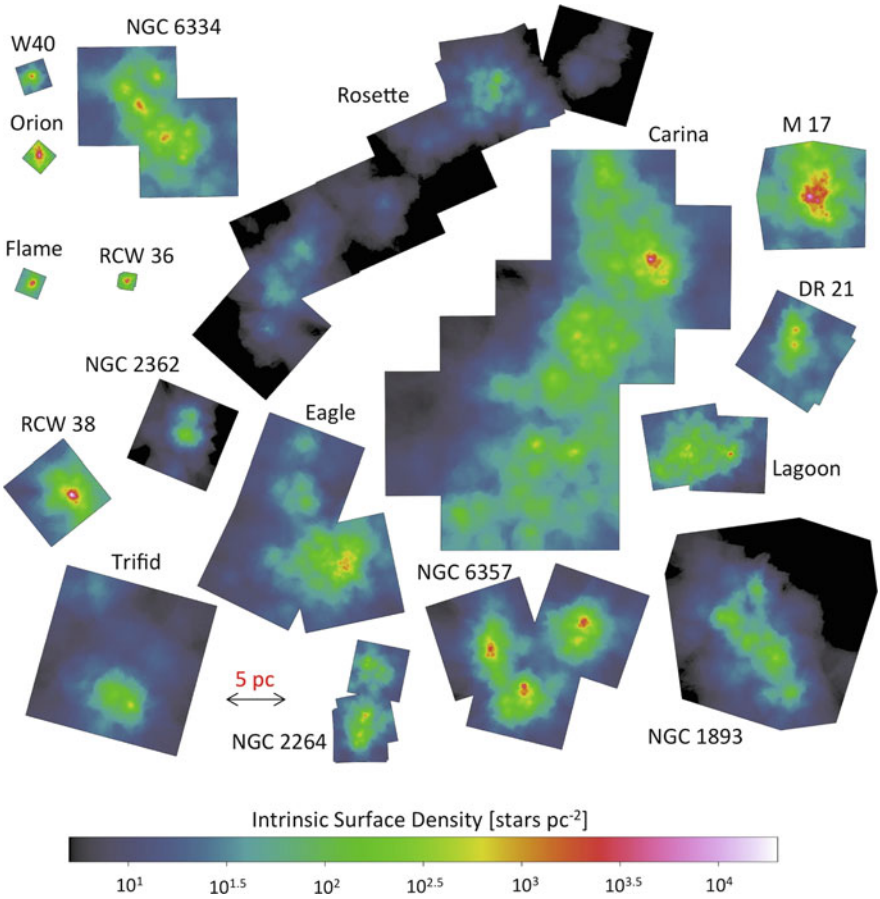

Fig. 5.5 Montage of maps of surface density of X-ray selected stars in MYStIX regions, shown to the same physical scale in parsecs (Kuhn et al. 2014b). These intrinsic surface densities have been corrected for variations of X-ray sensitivities within and between fields, with density values scaled to the full IMF

the disk-free X-ray selected stars that dominate many star forming regions. The MYStIX findings on stellar surface densities, although still subject to limitations and biases, are probably more reliable than the more constrained IRE-only results.

5.7 Observational Constraints on Astrophysical Questions

We now discuss how the MYStIX project—specifically the MPCM sample of 31,747 young stars in 142 (sub)clusters associated with 20 MSFRs—addresses the astrophysical questions outlined in Sect. 5.1 that concern the origin and early

evolution of star clusters. The questions are pursued by searching for spatial and statistical patterns among the various physical quantities measured or inferred for the (sub)clusters. One must recognize that the MPCM sample is constructed in complicated ways with unavoidable incompleteness and biases (Feigelson et al. 2013); however, each MYStIX region is analyzed in the same fashion and corrections to alleviate sensitivity and contamination effects can be applied in consistent ways.

5.7.1 Cluster Expansion and Dispersal

The MYStIX dataset shows many cases of the expected range of cluster structures: compact clusters embedded in their molecular cores, larger clusters following molecular gas ejection, and older stars dispersing into the field population.

Direct evidence for cluster expansion is shown in Fig. 5.6 (Kuhn et al. 2014a, 2015). The first panel shows that MYStIX (sub)cluster core radii systematically increase as clusters range from heavily absorbed to lightly absorbed. The X-ray median energy range is roughly equivalent to $0 < A_V < 40$; the same result is seen using $J - H$ as an absorption measure. The other panels show the relationships between core radii or central density and median Age_{JX} values for the subclusters. Here we see roughly a factor of 10 increase in radius, and a factor of 1000 decrease in central core density, as (sub)clusters age from $\sim$ 0.5 to 4 Myr. This is roughly consistent with dynamical calculations of cluster expansion following gas expulsion, although some models assume initial conditions that predict more rapid expansion at earlier times (Banerjee and Kroupa 2013; Pfalzner and Kaczmarek 2013).

Evidence of this expansion has been presented by Pfalzner and colleagues (Pfalzner 2009; Pfalzner and Kaczmarek 2013) using samples of Galactic and extragalactic young clusters obtained from the literature. They report a "universal sequence" relating cluster size, central density and age indicative of cluster

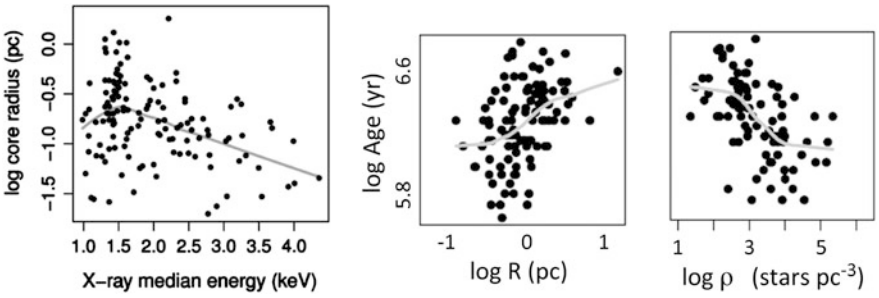

Fig. 5.6 Expansion of young clusters. *Left:* Subcluster core radius *vs.* X-ray median energy, a measure of interstellar absorption with nonparametric regression curve (Kuhn et al. 2014a). *Center and right:* Bivariate scatter diagrams showing subcluster radius and central density *vs.* Age_{JX} with nonparametric regression curve (Kuhn et al. 2015)

expansion from a uniform compact state. Their "loose clusters," similar to MYStIX clusters, expand ∼10-fold from 2 to 20 Myr.

Pre-MYStIX studies had reported that X-ray selected stars, including early-type OB stars, were often dispersed from the molecular cores that active form stars today (Feigelson et al. 2009). In the Carina complex, half of the X-ray stars lie outside the regions dominated by the Trumpler 14-15-16 clusters and the South Pillars clouds (Feigelson et al. 2011). This pattern is seen in most MYStIX regions. Dispersed stellar surface densities range from near-zero to tens of stars/pc^2 in the different regions (Kuhn et al. 2014a, 2015). Age_{JX} analysis shows that, in nearly all cases, the dispersed stars are older (typically 3 to >5 Myr) than the MYStIX (sub)clusters (Getman et al. 2014a).

These findings give confidence in the long-standing argument (Charlier 1917) that young clusters often quickly dissipate to constitute the field star population. However, the MYStIX photometric observations cannot distinguish the physical process: do individual stars slowly drift away, are individual stars ejected at high velocity by stellar interactions in the cluster core, or do clusters release all of their stars simultaneously as they become gravitationally unbound?

5.7.2 Cluster Formation by Merging Subclusters

The MYStIX (sub)cluster sample gives ample opportunity to reveal merging of smaller subclusters as an important process of building up large equilibrated clusters as predicted in models of cluster formation in turbulent molecular clouds (Bate 2009). Yet direct evidence for subcluster merging is not self-evident in the MYStIX data, but indirect evidence is emerging.

First, consider the geometric properties of MYStIX (sub)clusters without inclusion of physical quantities such as age and mass (Kuhn et al. 2014a). As exemplified in NGC 6357 and the Eagle Nebula decompositions in Fig. 5.4, some rich clusters are consistent with simple smooth ellipsoidal stellar distributions, while others are clumpy and require several ellipsoids to be adequately modeled. Figure 5.7 is a diagram of the ellipsoidal structures in 15 MYStIX regions placed into a heuristic classification of simple, linear chain, core-halo, and complex clumpy classes (Kuhn et al. 2014a). As in Sect. 5.6, we see a wide diversity of clustering morphologies produced by massive molecular clouds.

It is tempting to interpret the morphological classes as an evolutionary sequence where star formation begins as linear chains in filamentary clouds, passes through a clumpy stage as subclusters merge, and ends with core-halo and simple structures that may be in dynamical equilibrium. However, when Age_{JX} values are examined for these morphological classes, no evidence for an evolutionary sequence is found (Kuhn et al. 2015). Perhaps linear morphologies (like DR 21 and NGC 2264) disperse rather than merge into simpler spherical morphologies (like W 40 and the three clusters of NGC 6357). However, it seems physically reasonable to suggest that the dense but clumpy configuration of M 17 will equilibrate into a unified rich cluster.

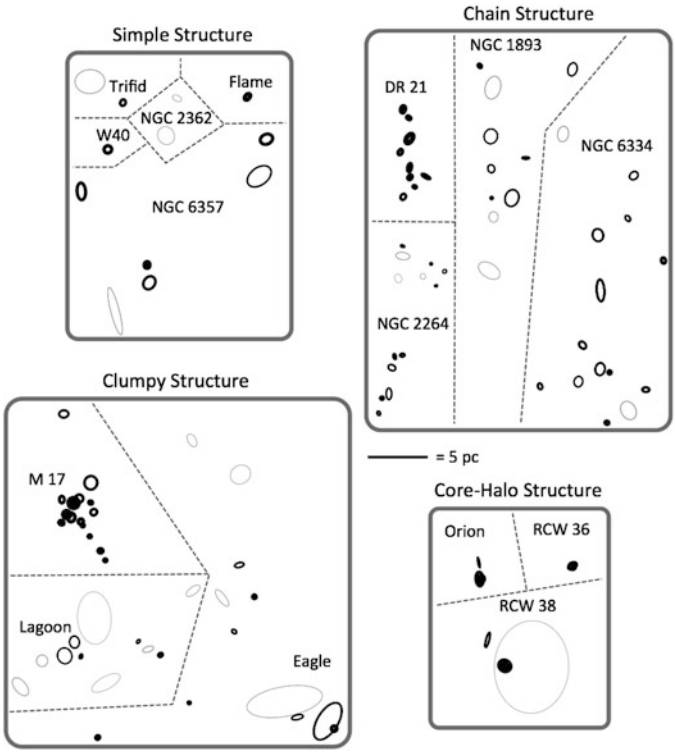

Fig. 5.7 Heuristic classification of the star formation complex morphology of 15 MYStIX regions based on the ellisoidal subcluster spatial decomposition (Kuhn et al. 2014a). Regions are shown on the same physical scale (see the 5 pc calibration bar), and line thickness is scaled to the subcluster stellar surface density of each subcluster

A second failure to detect (sub)cluster merging is from a scatter plot of total stellar population vs. Age_{JX} for MYStIX (sub)clusters. No indication of cluster population growth is seen (Kuhn et al. 2015). It is possible that the statistical decomposition of stellar clustering into 142 isothermal ellipsoids masquerades a growth effect.

A third test, however, gives a hint of cluster growth. A strong anti-correlation between (sub)cluster central star densities and core radii naturally appears in ensembles of young clusters. A relationship $\rho \propto r_c^{-3}$ is expected from a collection of clusters of uniform and constant mass seen at different phases of expansion. The MYStIX sample shows $\rho \propto r_c^{-2.6\pm0.1}$ over the range $0.03 \leq r_c \leq 1$ pc and $1.5 \leq \log \rho \leq 5$ stars/pc^3 (Kuhn et al. 2015). This relationship appears shallower than a -3 powerlaw index, indicating that larger clusters have somewhat higher masses than smaller clusters. This suggests that MYStIX subclusters undergo

growth from mergers or continued star formation as they expand. Note this stands in contrast to Pfalzner's "leaky clusters" that lose mass as they expand (Pfalzner 2009).

A fourth consideration gives a hint that merging may be needed to form the richest young clusters. With the exception of W 3 Main (Feigelson and Townsley 2008), there is no obvious case in the nearby Galaxy of a very rich (thousands of stars) with a dynamically relaxed appearance that is still embedded in its cloud. The typical embedded cluster found in the MYStIX study has is not very rich (tens to hundreds of stars) and often with a clumpy morphology. If rich clusters formed rapidly and monolithically as proposed by in some theoretical studies (Elmegreen 2000; Palla and Stahler 2000; Hartmann et al. 2012), then perhaps more should be found in embedded environments. But a model where rich clusters form by the merging of smaller structures (Mac Low and Klessen 2004; Bate 2009) is consistent with the paucity of very rich embedded clusters.

Finally, an intriguing line of evidence supports a "global hierarchical collapse" model for cluster formation (Vásquez-Semadeni et al. 2017). In this calculation, subclusters and gas fall towards the center of a growing cluster over an extended period, replenishing material for continuing star formation in the cluster core. Older stars which formed in subclusters prior to reaching the cluster center have higher velocity dispersions and populate the outer regions of the cluster. The result is a core-halo age gradient where stars in the core appear younger (that is, formed later) than stars in the halo. Stars in the richer MYStIX clusters with Age_{JX} age estimates (Sect. 5.4) show exactly this age gradient. The two clearest cases are shown in Fig. 5.9 (Sect. 5.7.3), and the phenomenon is shown to be statistically significant in the collective sample of other rich MYStIX clusters (Getman et al. 2017b).

5.7.3 Duration of Star Formation

The MYStIX and related studies give unequivocal evidence that long-lived star formation is pervasive, both across MSFRs and within rich clusters. The acquisition of Age_{JX} estimates for dozens of spatially well-defined (sub)clusters allows us to study the history of star formation across MYStIX star forming regions. Getman and colleagues find a clear and consistent pattern: more heavily absorbed clusters have younger ages than lightly absorbed clusters (Getman et al. 2014a). This is shown for two MYStIX regions in Fig. 5.8, RCW 36 with a "simple" structure and Rosette Nebula with a "complex" structure. In RCW 36 the ages range from 0.9 to 1.9 Myr, while in Rosette they range from 1 to 4 Myr. Ages are also available for stars that are not assigned to clusters; these distributed stars always show older ages than absorbed clusters.

These results confirm with widespread belief that clusters are formed inside dusty molecular cores (high $J - H$ color environments) and later expel their molecular material (low $J - H$ environments). But there were few quantitative measures of this expectation prior to the MYStIX analysis. Previous demonstrations of age gradients were based on spatial correlations between Class I-II-III (disk-bearing to disk-free)

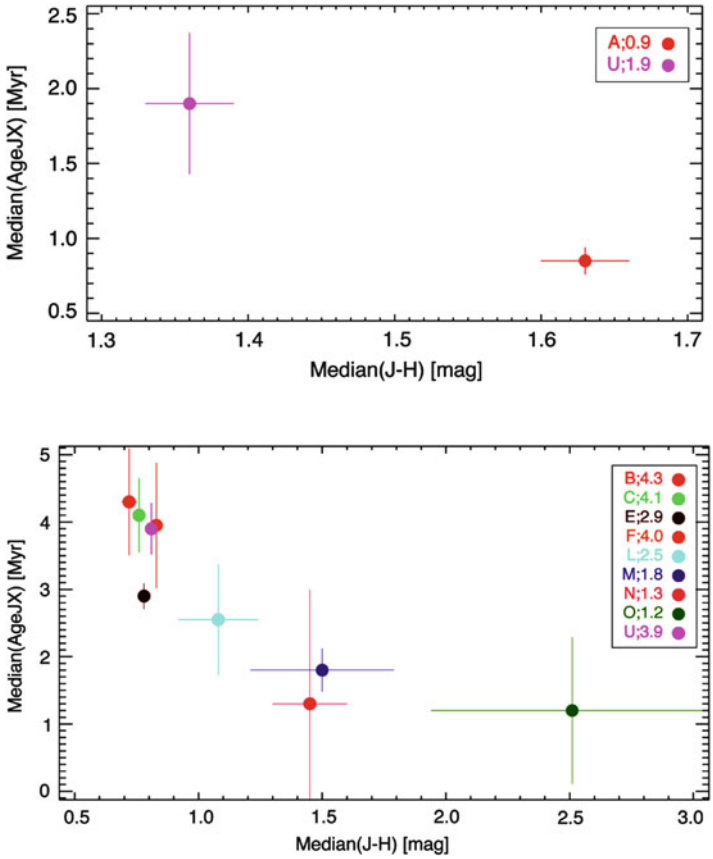

Fig. 5.8 Age differences for selected MYStIX subclusters as a function of $J - H$ color index, a measure of cloud absorption, in the RCW 36 and Rosette Nebula fields (Getman et al. 2014a). Each point refers to subclusters identified in Kuhn et al. (2014a). The "U" designation refers to unclustered stars

populations and absorption in the W 40 and Rosette Nebula regions (Kuhn et al. 2010; Ybarra et al. 2013). Both of these quantities are not calibrated to age in Myr, and the situation is often not so simple; in the Orion L1541 cloud, for example, two clusters dominated by older disk-free stars are lightly obscured while one is heavily obscured (Pillitteri et al. 2013).

A more surprising result is the age spread, and spatial age gradient, found by Getman and colleagues *within* two nearby rich clusters, in addition to the gradients found earlier *between* (sub)clusters (Getman et al. 2014b). The cluster cores are much younger than the cluster outer regions (Fig. 5.9). In the Flame Nebula cluster, stars within 0.2 pc of the center are 0.2 Myr old while stars 1 pc from the center are 1.6 Myr old. In the Orion Nebula cluster, the age ranges from 1.2 to 2.0 Myr. This measurement is based entirely on analysis of solar-type stars, and thus does not conflate age and mass segregation.

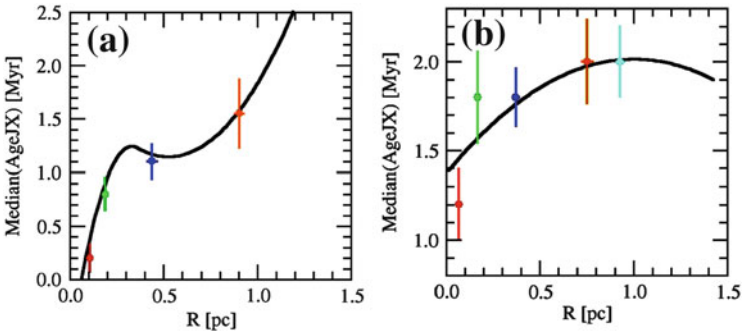

Fig. 5.9 Age differences within the (a) Flame Nebula cluster and (b) Orion Nebula Cluster showing that stars in the cores are younger than stars in the halos (Getman et al. 2014b)

The result is startling because naive models for cluster formation (based on Jeans gravitational collapse in an isothermal cloud core) expect that star fill form first in the dense center, and thus would later appear to have the oldest, not the youngest stars. Other models tend to homogenize the younger and older stars during a subcluster merging process (Bate 2009). More complex cluster formation scenarios might explain the observed phenomenon; for example, the older stars may have kinematically dispersed from the core, and/or the core may have been supplied with infalling molecular gas to allow star formation after the gas was depleted in the halo (Getman et al. 2014b). The global hierarchical collapse model of Vásquez-Semadeni et al. (2017) is a quantitative calculation of such effects that reproduces the MYStIX intra-cluster age gradients reported by Getman et al. (2014b, 2017b).

But the MYStIX intracluster age gradient also resolves a long-standing controversy concerning apparent stellar age spreads in HRDs (Preibisch 2012). The age spread appears to be real, at least in part, because it represents a spatial segregation of older and younger stars. Thus models based on rapid cluster formation in a single collapse time (Elmegreen 2000) are not consistent with the findings.

5.8 Final Comments and Future Research

We emerge with some optimism that a frustrating period is ending when models for clustered star formation were largely unconstrained by empirical results concerning the outcomes of star formation processes (properties of the young stellar populations) to complement empirical results on the inputs to star formation processes (molecular cloud properties). A multiwavelength approach provides the key: X-ray surveys to isolate the pre-main sequence population from the contaminating field star population and to avoid strong nebular emission; near-infrared imaging replacing optical observations to penetrate regions of high absorption; and mid-infrared photometry to discriminate the important subpopulation of disk-bearing young stars from often-overwhelming Galactic field star contamination.

The diversity of clustering patterns found in MYStIX regions (Fig. 5.7) points to the importance of studying star formation in multiple environments. The observational strategy of MYStIX can easily be extended to more star forming regions in the nearby (roughly distances < 3 kpc) Galaxy. Results are now emerging from Chandra X-ray Observatory observations of ~ 20 regions with distances ≤ 1 kpc dominated by intermediate-mass BA stars (Getman et al. 2017), and both Chandra and XMM-Newton missions have observed the nearest star forming regions around 0.14–0.3 kpc.

It is more difficult to extend such study to the lowest mass stars that dominate the IMF ($0.1 < M < 0.5$ $M_{\odot}$), and to the richest star forming regions of the Galaxy lying $\sim$5–12 kpc from the Sun. Million-second Chandra exposures are needed to acquire sufficient X-ray sensitivity, and infrared follow-up requires both high resolution and high sensitivity. Fortunately, the Chandra satellite is in good health since launch in 1999 and is likely to last for a considerable time into the future. Infrared technologies are continuously improving: the VISTA Via Lactea project gives wide-field, multi-epoch photometry of large portions of the Galactic Plane (Minniti et al. 2010); the KMOS and MOSFIRE multi-object spectrographs offer efficient spectroscopic capabilities on 8-meter class telescopes; and the James Webb Space Telescope will greatly advance infrared imaging and spectroscopy in a few years. These observational capabilities give confidence that fruitful interactions between theory and observations can become the norm in the study of clustered star formation.

Acknowledgements This review rests on the labor and talents of the MYStIX team, particularly Patrick Broos, Konstantin Getman, Michael Kuhn, Tim Naylor, Matthew Povich, and Leisa Townsley. Many of the astrophysical results appear in the dissertation of Michael Kuhn and work led by Kostantin Getman; the author is especially grateful for their collaborative energy and thoughtful analysis. The MYStIX Project was principally supported at Penn State by NASA grant NNX09AC74G and AR7-18000X, NSF grant AST-0908038, and SAO/CXC grant AR7-18002X and ACIS Team contract SV-74018.

References

Aarseth, S.J., Hills, J.G.: Astron. Astrophys. **21**, 255 (1972)
André, P., Men'shchikov, A., Bontemps, S., et al.: Astron. Astrophys. **518**, LL102 (2010)
Banerjee, S., Kroupa, P.: Astrphys. J., **764**, 29 (2013)
Bate, M.R.: Mon. Not. R. Astron. Soc. **392**, 590 (2009)
Blaauw, A.: Ann. Rev. Astron. Astrophys. **2**, 213 (1964)
Bressert, E., Bastian, N., Gutermuth, R., et al.: Mon. Not. R. Astron. Soc. **409**, L54 (2010)
Broos, P.S., Getman, K.V., Povich, M.S., et al.: Astrophys. J. Suppl. **209**, 32 (2013)
Charlier, C.V.L.: Observatory **40**, 387 (1917)
Damiani, F., Micela, G., Sciortino, S.: Astron. Astrophys. **596**, #A82 (2016)
de Wit, W.J., Testi, L., Palla, F., Zinnecker, H.: Astron. Astrophys. **437**, 247 (2005)
Elmegreen, B.G.: Astrophys. J. **530**, 277 (2000)

Feigelson, E.D., Montmerle, T.: Ann. Rev. Astron. Rev. **37**, 363 (1999)
Feigelson, E.D., Townsley, L.K.: Astrophys. J. **673**, 354 (2008)
Feigelson, E.D., Martin, A.L., McNeill, C.J., et al.: Astron. J. **138**, 227 (2009)
Feigelson, E.D., Getman, K.V., Townsley, L.K., et al.: Astrophys. J. Suppl. **194**, 9 (2011)
Feigelson, E.D., Townsley, L.K., et al.: Astrophys. J. Suppl. **209**, 26 (2013)
Figer, D.F.: IAU Symposium, vol. 250, p. 247 (2008)
Garmany, C.D., Stencel, R.E.: Astron. Astrophys. Suppl. **94**, 211 (1992)
Getman, K.V., Feigelson, E.D., Kuhn, M.A., et al.: Astrophys. J. **787**, 108 (2014)
Getman, K.V., Feigelson, E.D., Kuhn, M.A.: Astrophys. J. **787**, 109 (2014)
Getman, K.V., Broos, P.S., Kuhn, M.A., et al.: Astrophys. J. Suppl. **229**, #28 (2017)
Getman, K.V., Feigelson, E.D., Kuhn, M.A.: Astrophys. J. (2017b, submitted)
Greenstein, J.L., Sargent, A.I.: Astrophys. J. Suppl. **28**, 157 (1974)
Guarcello, M.G., Prisinzano, L., Micela, G., et al.: Astron. Astrophys. **462**, 245 (2007)
Guarcello, M.G., Micela, G., Peres, G., et al.: Astron. Astrophys. **521**, AA61 (2010)
Haisch, K.E. Jr., Lada, E.A., Lada, C.J.: Astrophys. J. Lett. **553**, L153 (2001)
Hartmann, L., Ballesteros-Paredes, J., Heitsch, F.: Mon. Not. Royal Astro. Soc. **420**, 1457 (2012)
Illian, J., Pentinnen,A., Stoyan, H., Stoyan, D.: Statistical Analysis and Modeling of Spatial Point Patterns. Wiley, Chichester (2008)
King, R.R., Naylor, T., Broos, P.S., et al.: Astrophys. J. Suppl. **209**, 28 (2013)
Krumholz, M.R., Tan, J.C.: Astrophys. J. **654**, 304 (2007)
Krumholz, M.R., Klein, R.I., McKee, C.F.: Astrophys. J. **754**, 71 (2012)
Kuhn, M.A., Getman, K.V., Feigelson, E.D., et al.: Astrophys. J. **725**, 2485 (2010)
Kuhn, M.A., Getman, K.V., Broos, P.S., et al.: Astrophys. J. Suppl. **209**, 27 (2013)
Kuhn, M.A., Povich, M.S., Luhman, K.L., et al.: Astrophys. J. Suppl. **209**, 29 (2013)
Kuhn, M.A., Feigelson, E.D., Getman, K.V., et al.: Astrophys. J. **787**, 107 (2014)
Kuhn, M.A., Feigelson, E.D., Getman, K.V.: Astrophys. J. **802**, #60 (2014)
Kuhn, M.A., Feigelson, E.D., Getman, K.V., Sills, A., et al.: Astrophys. J. **812**, #131 (2015)
Kuhn, M.A., Medina, N., Getman, K.V., et al.: Astron. J. **154**, 87 (2017)
Lada, C.J., Lada, E.A.: Ann. Rev. Astron. Astrophys. **41**, 57 (2003)
Mac Low, M.-M., Klessen, R.S.: Rev. Mod. Phys. **76**, 125 (2004)
McLachlan, G., Peel, D.: Finite Mixture Models. Wiley, Chichester (2000)
McMillan, S.L.W., Vesperini, E., et al.: Astrophys. J. Lett. **655**, L45 (2007)
Minniti, D., Lucas, P.W., Emerson, J.P., et al.: New Astron. **15**, 433 (2010)
Naylor, T., Broos, P.S., Feigelson, E.D.: Astrophys. J. Suppl. **209**, 30 (2013)
Palla, F., Stahler, S.W.: Astrophys. J. **540**, 255 (2000)
Pillitteri, I., Wolk, S.J., Megeath, S.T., et al.: Astrophys. J. **768**, 99 (2013)
Pfalzner, S.: Astron. Astrophys. **498**, L37 (2009)
Pfalzner, S., Kaczmarek, T.: Astron. Astrophys. **559**, A38 (2013)
Pflamm-Altenburg, J., Kroupa, P.: Mon. Not. R. Astron. Soc. **373**, 295 (2006)
Povich, M.S., Kuhn, M.A., Getman, K.V., et al.: Astrophys. J. Suppl. **209**, 31 (2013)
Povich, M.S., Busk, H.A., Feigelson, E.D., et al.: Astrophys. J. **838**, 61 (2017)
Preibisch, T.: Res. Astron. Astrophys. **12**, 1 (2012)
Prisinzano, L., Sanz-Forcada, J., Micela, G., et al.: Astron. Astrophys. **527**, AA77 (2011)
Rathborne, J.M., Jackson, J.M., Simon, R.: Astrophys. J. **641**, 389 (2006)
Richert, A.J., Getman, K.V., Feigelson, E.D., et al.: Astrophys. J. (submitted)
Rivera-Gálvez, S., Román-Zúñiga, C.G., Jiménez-Baión, E., et al.: Astron. J. **150**, 191 (2015)
Romine, G., Feigelson, E.D., Getman, K.V., et al.: Astrophys. J. **833**, 193 (2016)
Sharma, S., Pandey, A.K., Ojha, D.K., et al.: Mon. Not. R. Astron. Soc. **467**, 2943 (2017)
Tan, J.C., Krumholz, M.R., McKee, C.F.: Astrophys. J. Lett. **641**, L121 (2006)
Telleschi, A., Güdel, M., Briggs, K.R., et al.: Astron. Astrophys. **468**, 425 (2007)
Townsley, L.K., Broos, P.S., Corcoran, M.F., et al.: Astrophys. J. Suppl. **194**, #1 (2011)
Townsley, L.K., Broos, P.S., Garmire, G.P., et al.: Astrophys. J. Suppl. **213**, 1 (2014)
Tutukov, A.V.: Astron. Astrophys. **70**, 57 (1978)

Vásquez-Semadeni, E., González-Samaniego, A., Conín, P.: Mon. Not. R. Astron. Soc. **467**, 1313 (2017)
Wang, J., Townsley, L.K., Feigelson, E.D., et al.: Astrophs. J. **675**, 464 (2008)
Wright, N.J., Drake, J.J., Guarcello, M.G., et al.: (2014). arXiv:1408.6579
Ybarra, J.E., Lada, E.A., Román-Zúñiga, C.G., et al.: Astrophys. J. **769**, 140 (2013)
Zwintz, K., Fossati, L., Ryabchikova, T., et al.: Science **345**, 550 (2014)

Chapter 6
Formation of Very Young Massive Clusters and Implications for Globular Clusters

Sambaran Banerjee and Pavel Kroupa

Abstract How Very Young Massive star Clusters (VYMCs; also known as "starburst" clusters), which typically are of $\gtrsim 10^4 M_\odot$ and are a few Myr old, form out of Giant Molecular Clouds is still largely an open question. Increasingly detailed observations of young star clusters and star-forming molecular clouds and computational studies provide clues about their formation scenarios and the underlying physical processes involved. This chapter is focused on reviewing the decade-long studies that attempt to computationally reproduce the well-observed nearby VYMCs, such as the Orion Nebula Cluster, R136 and NGC 3603 young cluster, thereby shedding light on birth conditions of massive star clusters, in general. On this regard, focus is given on direct N-body modelling of real-sized massive star clusters, with a monolithic structure and undergoing residual gas expulsion, which have consistently reproduced the observed characteristics of several VYMCs and also of young star clusters, in general. The connection of these relatively simplified model calculations with the structural richness of dense molecular clouds and the complexity of hydrodynamic calculations of star cluster formation is presented in detail. Furthermore, the connections of such VYMCs with globular clusters, which are nearly as old as our Universe, is discussed. The chapter is concluded by addressing long-term deeply gas-embedded (at least apparently) and substructured systems like W3 Main. While most of the results are quoted from existing and up-to-date literature, in an integrated fashion, several new insights and discussions are provided.

To be published in *The Origin of Stellar Clusters*, ed. S. Stahler (Springer).

S. Banerjee (✉)
AIfA/HISKP, University of Bonn, Auf dem Hügel 71, 53121 Bonn, Germany
e-mail: sambaran@astro.uni-bonn.de; sambaran.banerjee@gmail.com

P. Kroupa
HISKP, University of Bonn, Auf dem Hügel 71, 53121 Bonn, Germany
e-mail: pavel@astro.uni-bonn.de

S. Stahler (ed.), *The Birth of Star Clusters*, Astrophysics and Space Science Library 424, DOI 10.1007/978-3-319-22801-3_6

6.1 Introduction

Very Young Massive Clusters (hereafter VYMCs) refer to a sub-category of star clusters which are $\gtrsim 10^4 M_\odot$ heavy (i.e., massive) and a few Myr old in age, typically 1–3 Myr (i.e., very young).[1] A number of such star clusters are observed in the molecular gas-dominated spiral arms (e.g., the NGC 3603 Young Cluster) and in the central molecular zone (e.g., the Arches and the Quintuplet clusters) of our Galaxy. They are also found in nearby disk galaxies of the local group (e.g., the R136 cluster of the Large Magellanic Cloud) and in "starburst galaxies" (e.g., in the Antennae Galaxies). An age $\lesssim 3$ Myr would imply that all of the massive stellar members of a VYMC are in their main sequences (MSs). The key importance of VYMCs is that being newly hatched, the details of their structure and internal kinematics can constrain the conditions under which massive star clusters, which are globular clusters at their infancy (Marks and Kroupa 2012; Kruijssen 2014), form. This allows one to distinguish between the different scenarios of massive cluster formation (Longmore et al. 2014). Note that the above mass and age limits defining VYMCs are meant to be generally true (see also Portegies Zwart et al. 2010) but not absolutely rigorous, to allow some well-studied young systems, like the ONC ($\approx 10^3 M_\odot$), to be counted in as VYMCs.

Morphologically, VYMCs are often found as the richest core-halo member cluster of extended cluster complexes/stellar associations, e.g., the ONC (Alves and Bouy 2012). Young stellar systems are also found as extended associations of OB stars, e.g., the Cygnus OB2 (Kuhn et al. 2014; Wright et al. 2014). It is also common to find them surrounded by HII (ionized hydrogen) gas (e.g., NGC 3603 and R136; Pang et al. 2013). As for the sizes, the half-light radii of VYMCs are $\lesssim 1$ pc, i.e., they are typically a factor of three more compact than Galactic globular clusters. This is consistent with VYMCs being infant globular clusters as their subsequent evolution due to mass segregation, dynamical encounters among stars and stellar binaries and stellar evolution would expand them. A handful of systems are found near-embedded in gas and highly compact; RCW 38 is a classic example where the HII-gas appears to have just begun releasing itself from the cluster (see below), exposing only the cluster's central part (DeRose et al. 2009). Interestingly, several VYMCs are found to contain multiple density centres, i.e., substructures, despite having an overall spherical core-halo morphology (Kuhn et al. 2014; Zeidler et al. 2015; Gennaro et al. 2017).

How (near) spherical parsec-scale VYMCs form out of vast, irregular molecular-hydrogen clouds is being widely debated for at least the past 10 years. Even without invoking any specific formation scenario, it can be said that dynamical relaxation

[1] These objects are also popularly called "starburst" clusters. We prefer to call them Very Young Massive Clusters based on their characteristic properties, instead of referring to their likely starburst origin. The latter criterion may coincide with the origins of other types of massive clusters, e.g., globular clusters. VYMCs constitute the youngest sub-category of Young Massive Clusters (YMCs; Portegies Zwart et al. 2010).

(i.e., statistical energy exchange among stars) must play a critical role in shaping the spherical core-halo structure of a VYMC. Hence, any formation channel for VYMCs must allow enough room for dynamical relaxation of the final (at an age of 1–3 Myr) stellar assembly. The overall two-body relaxation time, that determines the secular (near dynamically stable) evolution, is typically several Gyr for a VYMC, which is much longer than its age. Hence, the present-day morphology of a VYMC is primarily dictated by what is called "violent relaxation" (Spitzer 1987). The latter process refers to the energy redistribution among stars due to mutual encounters and rapid changes of the gravitational potential, leading to (near) dynamical equilibrium or "virialization" of the system, which happens in the timescale of stellar orbits (or in the dynamical timescale; Spitzer 1987; Heggie and Hut 2003),[2] i.e., typically in a fraction of a Myr. The observed *lack* of an age range among the members of the youngest star clusters (see, e.g., Bastian and Silva-Villa 2013; Hollyhead et al. 2015) implies that these stars must have formed in a burst and integrated into a cluster over a short period of time.

Currently, there exist apparently at least two distinct scenarios for the formation of VYMCs. The "monolithic" or "episodic" or "in situ" (top-down) scenario implies the formation of a compact star cluster in an essentially single but highly active star-formation episode (a "starburst"). The infant cluster of pre-main-sequence (PMS) and main sequence (MS) stars remains embedded in its parent molecular gas cloud. The latter eventually gets ionized by the UV radiation from the massive stars and receives energy from stellar mass outflows and due to coupling with stellar radiation. Such energy injection eventually causes the embedding gas to become gravitationally unbound from the system and to disperse in a timescale typically comparable to the dynamical time of the stellar system, i.e., too fast for the stars to adjust with the corresponding depletion of the potential well. This causes the stellar system to expand violently and lose a fraction of its stars depending on its initial mass and concentration (Lada et al. 1984; Adams 2000; Boily and Kroupa 2003a,b; Baumgardt and Kroupa 2007). The remaining system may eventually regain virial or dynamical equilibrium (re-virialization); hence a given VYMC may or may not be in equilibrium depending on the time taken to re-virialize and the epoch of its observation (Banerjee and Kroupa 2013). Such a monolithic or top-down cluster formation scenario has successfully explained the details of well-observed VYMCs, e.g., ONC (also the Pleiades; Kroupa et al. 2001), R136 (Banerjee and Kroupa 2013) and the NGC 3603 young cluster (Banerjee and Kroupa 2014).

Alternatively, VYMCs are thought to have formed "bottom-up" through hierarchical merging of less massive subclusters (Longmore et al. 2014). Several of such subclusters fall onto each other and coalesce to form the final VYMC. The gravitational potential of the background molecular gas within which these subclusters appear makes the infall faster (the so-called conveyor belt mechanism;

[2]This timescale is commonly represented by the orbital "crossing time" which is the time taken to traverse the spatial scale of the system (say, its half-mass diameter) by a particle moving radially with the dispersion speed.

Longmore et al. 2014). The observational motivation for such a scenario is the apparent substructures in OB associations and even in VYMCs with overall core-halo configurations (Kuhn et al. 2014).

As of now, star formation has been studied in hydrodynamic calculations involving development of seed turbulences, in cubical/spherical gas clouds, into high-density filaments where star formation occurs as a result of gravitational collapse and fragmentation (Klessen et al. 1998; Bate and Bonnell 2004; Girichidis et al. 2011). In all such smoothed-particle-hydrodynamic (SPH) calculations, a hydrodynamic "sink particle"[3] is physically associated with a proto-star. In these computations, clusters of proto-stars are formed within high-density filaments and/or filament junctions, which then fall collectively into the gravitational potential well of the cloud to form larger (gas-embedded) clusters (e.g., in Bate 2009 and Girichidis et al. 2011). Different groups have reached the state of the art of such calculations by including different details of the relevant physical processes but for mass scales much lighter than VYMCs. Such SPH calculations, requiring very high particle resolution, are prohibitive for the mass range of VYMCs ($> 10^4 M_\odot$).

High-resolution (reaching the "opacity limit") SPH computations have so far been done forming stars in spherical gas clouds of up to $\approx 500 M_\odot$ only (Klessen et al. 1998; Bate and Bonnell 2004; Bate 2009; Girichidis et al. 2011, 2012; Bate 2012) but without any feedback and hence self-regulation mechanism, which is critical in determining the star formation efficiency (SFE). Radiation-magnetohydrodynamic (MHD) calculations including stellar feedback (radiation and matter outflows) to the star-forming gas have also been carried out from proto-stellar scales (Machida and Matsumoto 2012; Bate et al. 2014) up to $\approx 50 M_\odot$ gas spheres (Price and Bate 2010). While the latter studies provide insights into the self-regulation mechanisms in the star formation process and point to an SFE near 30%, the scenario of the ultimate dispersal of the residual gas still remains superficial. See Krumholz et al. (2014) for an up-to-date review. Note, however, that the gas must disperse from the region in the molecular cloud where the cluster ultimately assembles, to obtain a gas-free young cluster like what we see today.

Therefore, as it turns out, the majority of the published studies to date related to the formation and evolution of "real-sized" VYMCs treat the gas-dispersal phase by including a time-varying external analytical potential (see Sect. 6.2.2) mimicking the residual gas (e.g., Adams 2000; Kroupa et al. 2001; Baumgardt and Kroupa 2007; Pfalzner and Kaczmarek 2013; Banerjee and Kroupa 2013, 2014). This captures the essential dynamical effects of the gas dispersal. The dynamical evolution of the cluster, however, is treated accurately using direct N-body integration (Aarseth 2003), in most of such works. This approach has successfully explained several well-observed VYMCs, e.g., the Galactic ONC (Kroupa et al. 2001) and NGC 3603 young cluster (Banerjee and Kroupa 2014) and R136 (Banerjee and Kroupa 2013)

[3] A "sink particle" is a dense, self-gravitating region in a fluid field approximated by a point mass for facilitating calculations (Klessen et al. 1998). A sink particle can only grow in mass by accreting matter from its surrounding.

of the LMC. Such studies point to a universal SFE of $\epsilon \approx 33\%$ and a near-sonic dispersal of the residual HII gas (see Banerjee and Kroupa 2013 and the references therein), remarkably reproducing the measured kinematic and structural properties of these clusters.

On the other hand, the dynamical process of coalescence of subclusters into more massive clusters has also been studied recently using direct N-body calculations in both absence (e.g., Fujii et al. 2012) and presence (e.g., Smith et al. 2013) of a background gas potential. The role of this process is also investigated in the context of formation of dwarf galaxies through merger of young massive clusters (Kroupa 1998; Fellhauer and Kroupa 2005; Amaro-Seoane et al. 2014).

The goal of the present chapter is to comprehend the most recent studies on the formation of VYMCs. Although most of these works treat the star-forming gas indirectly as mentioned above, they incorporate the mass and spatial scales appropriate for VYMCs and capture the essential physics at the same time. Extrapolation of the results from hydrodynamical calculations over a large mass range, i.e., from the computationally accessible masses (see above) to the realistic values, is unreliable since the scalings of all the relevant physical processes are not known and also they scale differently. This leaves us with the analytical treatment of the residual gas (Sect. 6.2.2) as the only viable option to directly treat VYMC-scale systems, given the present state of technology.

In Sect. 6.2 of this chapter, we discuss the monolithic formation scenario in greater detail. We focus on those (theoretical) studies that have addressed well-observed VYMCs. The central young cluster HD 97950 (hereafter HD97950) of the Galactic NGC 3603 star-forming region is always of particular interest in this regard since, due to its proximity, it is perhaps the best observed VYMC. Next, in Sect. 6.3, we move on to discuss further on the hierarchical formation of VYMCs. Here, we again focus on HD97950 cluster whose structure is known in detail. This enables us to directly compare the two formation channels and put constraints on the initial conditions in each case. In Sect. 6.5, we conclude this chapter by discussing how VYMCs can be related to embedded clusters.

> Technology, at present, does not permit self-consistent hydrodynamic calculations of star cluster formation, with adequate resolution and including feedback at the same time, for masses relevant for young massive clusters ($\gtrsim 10^4 M_\odot$). While such hydrodynamic calculations are doable with gas clouds of much lower masses (up to $100 M_\odot$s), a large extrapolation is grossly unreliable since the physical processes involved are not all well understood (e.g., gravitational fragmentation, role of magnetic field) and they scale differently. An analytic treatment of the gas combined with N-body calculation of the star cluster is, at present, the only viable way to reach such mass scales.

6.2 Monolithic or Episodic Formation of Very Young Massive Clusters

Before going into any details of modelling, one can obtain preliminary estimates that signifies the role of violent relaxation in the formation of VYMCs. For a self-bound system in dynamical (or virial) equilibrium with total K.E., T, and total P.E., V, the virial condition is satisfied (Spitzer 1987), i.e.,

$$2T = -V. \tag{6.1}$$

For an "explosive" gas expulsion (see Sect. 6.1; Kroupa 2005), i.e., gas removal in a timescale, τ_g, smaller or comparable to the crossing time, τ_{cr}, of the system (see below), T remains nearly unchanged right after the gas is removed although the P.E. drops to V'. The scale length of the system, r_h, usually taken as its half-mass radius, also remains nearly unchanged.

For the overall system to remain bound after the gas expulsion, one must have,

$$T + V' \leq 0. \tag{6.2}$$

If M and M' are the total systemic masses before and just after the mass depletion, respectively, then $V = -GM^2/r_h$ and $V' = -GM'^2/r_h$. Hence, using Eq. (6.1),

$$M'^2 \geq \frac{M^2}{2}, \tag{6.3}$$

or

$$M' \gtrsim 0.7M. \tag{6.4}$$

For the present case, $M = M_{\rm tot}$ is the total mass of the residual gas and the stars in the cluster, before the gas expulsion, and $M' = M_*$ is the total stellar mass after the depletion. Hence,

$$M_* \gtrsim 0.7M_{\rm tot}. \tag{6.5}$$

In other words, for the cluster to survive the gas expulsion, its SFE should be $\epsilon = M_*/M_{\rm tot} \gtrsim 70\%$. This requirement is in contrast with realistic values of SFE which is $\epsilon \lesssim 30\%$ as supported by both observations (Lada and Lada 2003) and theoretical studies (Machida and Matsumoto 2012; Bate et al. 2014; see below). This alone would invalidate the monolithic cluster formation scenario since all clusters would dissolve even for the maximum SFE.

In practice, however, violent relaxation[4] among the stars in the expanding cluster generates a "fallback effect" which retains a fraction of gravitationally bound stars even for SFE $\lesssim$ 30% (also see Boily and Kroupa 2002). The resultant bound fraction, F_b, depends on how efficiently stars in the expanding post-gas-expulsion cluster exchange energy during this relaxation process. Hence, F_b is proportional to the central stellar concentration (total stellar mass vs. size) of the pre-gas-expulsion cluster and to the timescale of the gas expulsion (time over which the expanding system remains in a dense enough phase for efficient energy exchange). In other words, F_b is proportional to the efficiency of violent relaxation which ultimately scales with the stellar number density. The latter is governed by the stellar density of the pre-gas-expulsion cluster. Note that for a given (fractional) rate of gas removal and a pre-gas-expulsion stellar density, the resulting efficiency of violent relaxation limits the expansion of the initial (bound) stellar system and the time in which the bound fraction returns to equilibrium (or the re-virialization time; see Sect. 6.2.3.2).

Figure 6.1 shows the bound fraction as a function of the initial (pre-gas-expulsion) cluster stellar mass, $M_{\rm cl}(0)$, and the effective speed, v_g, at which the gas is expelled; see Brinkmann et al. (2017). v_g directly translates into the gas expulsion timescale (e-folding time; see below), τ_g, since $\tau_g = r_h(0)/v_g$. The observed trend in Fig. 6.1 is what is expected from the above discussion.

6.2.1 *Why is an Episodic or Monolithic Mode of Cluster Formation Necessary?*

The conditions in star-forming molecular clouds in our Galaxy, which can be considered representative of star-forming environments in gas-rich galaxies, do not necessarily imply cluster formation in a single go (see Sect. 6.1). Such molecular regions typically contain compact, interconnected filamentary structures as revealed by detailed observations, e.g., by the *Herschel* space telescope. These observations (André et al. 2014) reveal clusters of proto-stars forming within such high-density filaments (or ridges), which are found to have Plummer-like cross sections with radii of 0.1–0.3 pc, and at their junctions, implying a highly substructured initial condition for newborn stellar associations. This is also consistent with several observed stellar associations that contain individual stellar groups (e.g., the Taurus-Auriga or T-A association; Palla and Stahler 2002) or are highly substructured (e.g., Cygnus OB2; Wright et al. 2014), indicating an amorphous and substructured

[4]In a self-gravitating system which is in dynamical equilibrium, the orbital energy exchange among stars by two-body encounters occur differentially among similar orbits (apart from that in occasional close encounters). This "two-body relaxation" drives the overall quasi-static secular evolution of the system which happens on the timescale of many orbital crossing times. However, if the system is not in equilibrium, the energy exchange happens much faster, in crossing times. Such "violent relaxation" drives the system (or a fraction of it) towards dynamical equilibrium (or energy minimum). See, e.g., Spitzer (1987) for details.

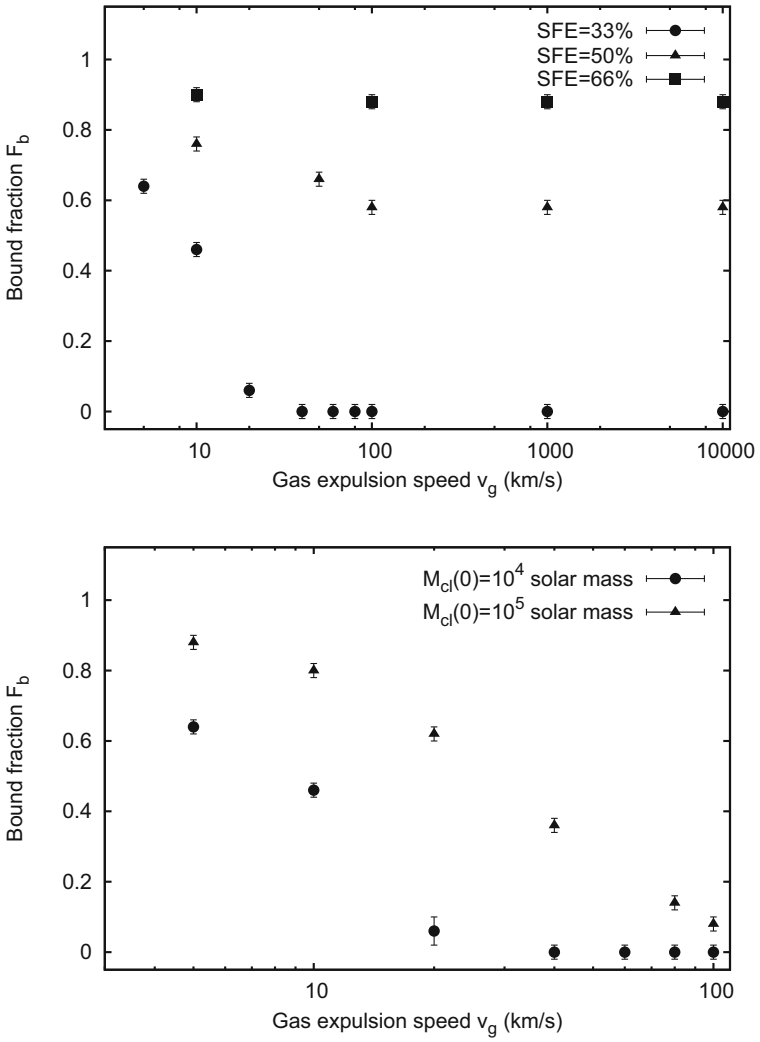

Fig. 6.1 Bound fraction, F_b, of a star cluster as a function of the overall gas removal speed, v_g, with varying star formation efficiency, ϵ ($M_{\rm cl}(0) = 10^4 M_\odot$, $r_h(0) = 0.3$ pc; *top panel*), and initial stellar cluster mass, $M_{\rm cl}(0)$ ($\epsilon = 0.33$, $r_h(0) = 0.3$ pc; *bottom panel*). All the initial clusters follow a Plummer density distribution. These results are obtained from `NBODY6` computations. See text for details. The authors thank Nina Brinkmann (Max-Planck-Institut für Radioastronomie, Bonn) for providing aid in preparing this figure. See Brinkmann et al. (2017)

beginning of a star cluster as is often argued (see, e.g., Longmore et al. 2014). On the other hand, VYMCs are found with near spherical core-halo profiles at a few Myr age which does not add up with the above scenario and calls for a different, episodic regime of cluster formation.

Of course, a stellar assembly cannot appear with 100% SFE since star formation is quenched by stellar radiative and mechanical feedback. Hydrodynamic simulations (e.g., Machida and Matsumoto 2012; Bate et al. 2014) including stellar feedback and observations of embedded stellar assemblies in the solar neighbourhood (Lada and Lada 2003) both indicate SFE $\lesssim$30%. Hence a substantial gas dispersal should accompany such a monolithic cluster formation to expose the gas-free young cluster. Arguably, several VYMCs, despite their near spherical monolithic structure contain substructures in the form of multiple density maxima in their surface stellar density profiles (Kuhn et al. 2014). Here, such systems will also be called monolithic.

The present-day sizes of gas-free massive, young clusters, with half-mass radii, r_h, between 3 and 10 pc is itself indicative of the importance of gas expulsion in the formation of such systems (Pfalzner 2009). Observations suggest that newborn (i.e., embedded) clusters are highly compact—typically with half-mass radii (effective radii) $r_h < 1$ pc (see Sect. 6.2.2.1). It is nearly impossible to expand such compact clusters up to their present-day sizes through purely secular evolution. Figure 6.2 shows the evolution of the effective radii of model clusters with initial masses, $M_{\rm cl}(0)$, between $10^4 M_\odot and 10^5 M_\odot$ and sizes $r_h(0) \lesssim 1.0$ pc, as obtained through direct N-body calculation using the state-of-the-art NBODY6[5] program. Here, the cluster expands only by a factor of few in $\approx$ 100 Myr, due to dynamical interactions and mass loss via stellar evolution; it hardly expands in a few Myr age. Even the least compact clusters (of $r_h(0) \approx 1$ pc) barely catch up with the observed sizes, i.e., the initial clusters would need to be inconsistently large compared to the typical observed sizes of embedded clusters and other dense substructures in molecular clouds. Hence, an additional expansion mechanism is essential to explain the observed cluster sizes.

The strongest support for an episodic mode of star formation is what can be called the "timescale problem" of cluster assembly. Consider a system of stellar clumps (or subclusters) of total mass M_* within a spherical volume of radius R_0, which have zero or small relative speeds (see Sect. 6.3). In other words, they form a "cold" system which can fall in and assemble into a single bound star cluster. An embedding background molecular gas of total mass M_g would accelerate the infall, the so-called conveyor belt mechanism (Longmore et al. 2014). The time, t_{in}, for the subclusters to collide onto each other at the systemic potential minimum is given by

[5] Sverre Aarseth's code NBODY6 and its variants (Aarseth 2012) are presently the most advanced and realistic direct N-body evolution code. The N-body integration engine computes individual trajectories of all the stars using a fourth-order Hermite scheme. Close encounters are dealt with two- and multi-body regularizations. In addition, the code employs the BSE stellar and binary evolution scheme (Hurley et al. 2000) for evolving the individual stars and mass-transferring binaries. The code also includes recipes for tidal interactions and stellar collisions. See Aarseth (2003) for details.

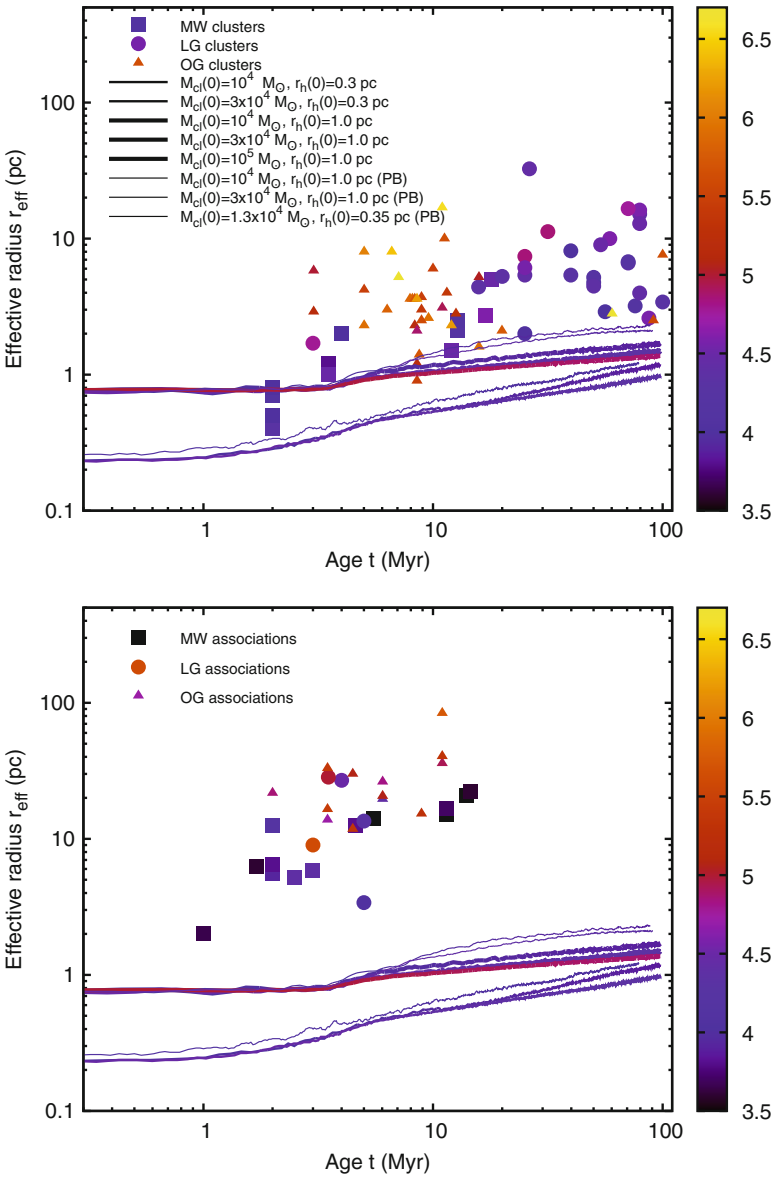

Fig. 6.2 *Top*: Effective radius, $r_{\rm eff}$, vs. age, t, for young massive bound star clusters (YMCs) in the Milky Way, the Local Group, and external galaxies which are distinguished by different filled symbols. The symbols are colour-coded according to the clusters' respective photometric mass, $\log_{10}(M_{\rm phot}/M_{\odot})$. These observed data are from Table 1 of Banerjee and Kroupa (2017, see also the references therein). Overlaid in the panel are the computed curves for the evolution of projected half-mass radius (or effective radius), $r_{\rm eff}(t)$, for model star clusters with initial masses, $M_{\rm cl}(0)$, and half-mass radii, $r_h(0)$, as indicated in the legends (see Table 3 of Banerjee and Kroupa 2017), where "PB" indicates that the computed cluster includes a realistic primordial binary population (see Sect. 2.1 of Banerjee and Kroupa 2017). These computed models are *not* subjected to any

(Banerjee and Kroupa 2015)

$$t_{\rm in} \approx \frac{R_0^{3/2}}{\sqrt{GM_{\rm tot}}} = 0.152 \frac{(R_0/{\rm pc})^{3/2}}{(M_{\rm tot}/10^4 M_\odot)^{1/2}}\ {\rm Myr}, \tag{6.6}$$

where $M_{\rm tot} = M_* + M_g$. Figure 6.3 shows the dependence of $t_{\rm in}$ on typical masses and sizes involved in massive stellar associations.

Note that the above $t_{\rm in}$ estimates the time taken for the subclusters to meet each other *for the first time*, after which they pass through each other to continue in their orbits. The orbital energy of the subclusters is dissipated into the orbital energy of the individual stars during their each mutual passage due to violent relaxation, causing the subclusters' orbits to decay and finally merge into a single cluster in dynamical equilibrium. Hence, the final merger time, $t_{\rm mrg}$, is several $t_{\rm in}$s as found in N-body calculations (Sect. 6.3). Although $t_{\rm in}$ decreases with increasing background gas mass, M_g, this does not necessarily lead to shorter $t_{\rm mrg}$ as the subclusters approach faster and hence take larger number of orbits to dissipate their K.E. As found in N-body calculations, the background gas actually lengthens $t_{\rm mrg}$ (see Sect. 6.3 for the details) for $R_0 \gtrsim 2$ pc. In other words, the conveyor belt process does not necessarily accelerate the assembly of the final cluster. Hence, Fig. 6.3 implies that unless a group of subclusters form too close to each other, i.e., already within the length scale of a compact star cluster (a few pc), it is practically impossible to assemble a VYMC by its young age through sequential mergers of less massive substructures as found in star-forming molecular clouds; see Sect. 6.3 for more details. Therefore, it is far more likely that VYMCs form in cluster- or molecular clump-scale localized high efficiency star formation episodes, i.e., monolithically.

Interestingly, based on the observed velocity fields of gas clouds in the neighbourhood of several starburst clusters, some authors (Furukawa et al. 2009; Fukui et al. 2014, 2016) suggest that these clusters (e.g., Westerlund 2, NGC 3603) form out of intense starbursts triggered during major cloud-cloud collisions. Such conclusions are based on the observed "broad-bridge" features (Haworth et al. 2015) in the velocity-space morphologies of cloud fragments near these VYMCs. A collision between a pair of massive molecular clouds lasts for a short time, typically $\approx$1 Myr. Hence, as before, this points to an episodic formation of these VYMCs

Fig. 6.2 (continued) residual gas expulsion and their evolution is solely due to dynamical processes (two-body relaxation, close encounters and ejections) and stellar evolution. These lead to an overall slow (quasi-static) expansion of the clusters due to the associated dynamical heating and mass loss. These lines are also colour-coded according to the corresponding clusters' instantaneous total bound mass $\log_{10}(M_{\rm cl}(t)/M_\odot)$. As can be seen, if the clusters evolve from compact sizes that is typical for dense substructures in molecular clouds ($r_h(0) \lesssim 1$ pc), their secular expansion substantially falls short of the observed sizes of YMCs. *Bottom*: Here, the curves and the colour-coding are the same as above except that the data for the young massive associations in Table 1 of Banerjee and Kroupa (2017, see also the references therein) are plotted. These panels are reproduced from Banerjee and Kroupa (2017)

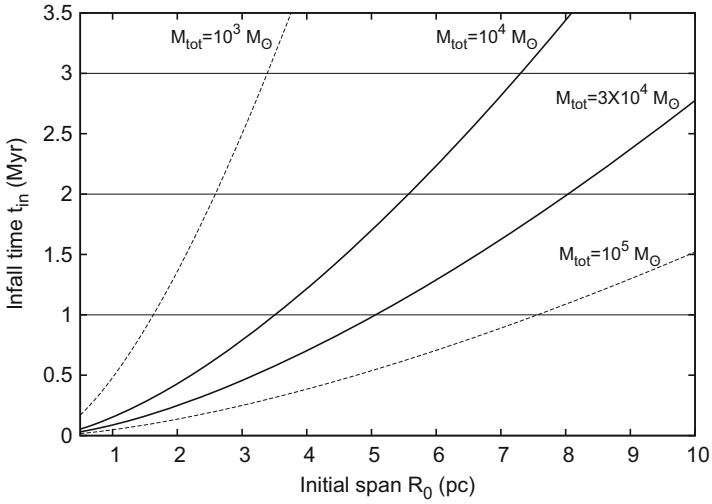

Fig. 6.3 The infall time (or the time of first arrival at orbital pericentre) of the subclusters, $t_{\rm in}$, as a function of the radius, R_0, of the spherical volume over which they are initially distributed. The curves are according to Eq. (6.6) for different systemic mass $M_{\rm tot}$. The highlighted curves for $M_{\rm tot} = M_* = 10^4 M_\odot$ without a residual gas and $M_{\rm tot} = 3M_* = 3 \times 10^4 M_\odot$ correspond to the model calculations for the NGC 3603 young cluster (see Sect. 6.3). This figure is reproduced from Banerjee and Kroupa (2015)

during the cloud–cloud collisions. After the clouds have crossed each other, the depletion of the background potential would lead to an expansion of the newly hatched cluster, as in the case of internal gas expulsion. However, more detailed studies of the internal velocities of such gas clouds as well as further theoretical studies of cloud–cloud collisions (Duarte-Cabral et al. 2011; Takahira et al. 2014) are necessary to establish this scenario.

Finally, one can ask the following question: *What if a VYMC is simply formed in situ but with its current observed size and not being governed by compact molecular filaments or other compact structures of the molecular clouds, eliminating the need of a substantial rapid gas dispersal?* In that case, the cluster must form with a sufficiently high SFE. However, it is unlikely that SFE can be pushed beyond $\approx$30% as observational and theoretical studies suggest (see Sect. 6.2.2.1). Hence, such a scenario is unrealistic. With SFE near 30%, a typical present-day sized star cluster would largely become unbound and/or become too extended, depending on its initial mass. The cluster can, however, survive if the gas is dispersed slowly; in a timescale longer than a few crossing times (Lada et al. 1984). The ambient gas can also be depleted if it is accreted by the (proto-) stars ("gas consumption"; Longmore et al. 2014), without expanding or unbinding the cluster. These processes would, however, take much longer than a few Myr and one would obtain an embedded cluster instead, like W3 Main. Further discussions follow in Sect. 6.5. The flowchart in Fig. 6.4 summarizes the discussions in this section.

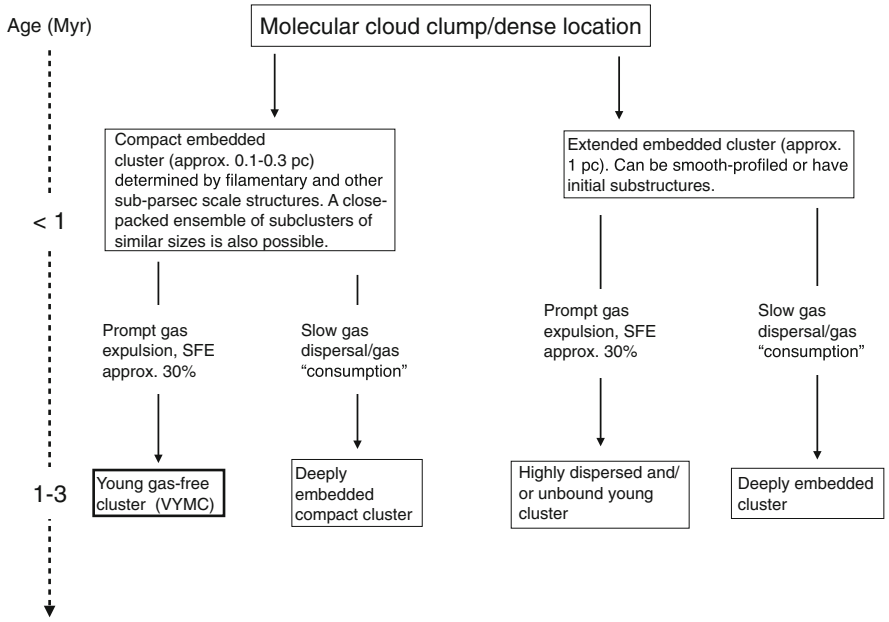

Fig. 6.4 Flowchart showing that exposed young massive clusters of 1–3 Myr age can form through essentially only one channel; a highly compact gas embedded proto-cluster undergoing a substantial (≈70% by mass) and rapid (in a timescale comparable to the crossing time of the proto-cluster) gas removal

The typical present-day density (10^4–$10^5 M_\odot$ pc^{-3}; or size ≈1 pc), age (≈1–3 Myr) and (near) spherical core-halo morphology of gas-free very young massive clusters (VYMCs), like R136, NGC 3603 and the ONC, dictate an episodic or monolithic (or near monolithic) formation of such star clusters, undergoing a violent gas dispersal phase.

6.2.2 An Analytic Representation for Gas Expulsion

The episodic cluster formation scenario involving gas expulsion, which is widely used (Lada et al. 1984; Adams 2000; Kroupa et al. 2001; Boily and Kroupa 2002; Baumgardt and Kroupa 2007; Banerjee and Kroupa 2013, 2014; Pfalzner and Kaczmarek 2013), has been successful in explaining the detailed structure and several well-observed VYMCs. All these studies use a rather straightforward

initial condition of a Plummer star cluster of mass, $M_{\rm cl}(0)$,[6] and half-mass radius, $r_h(0)$, that is embedded in its spherically symmetric natal gas of total mass $M_g(0)$. The latter is assumed to have a constant SFE, ϵ, throughout, i.e., the gas density profile follows the stellar Plummer density profile. The initial system represents a dense molecular gas clump with a recent episode of star formation with efficiency ϵ. The initial mass function (IMF) of the stellar system can be plausibly represented by the canonical mass function (Kroupa 2001; Kroupa et al. 2013) although equal mass stars have also been used in the literature for scalability (e.g., Baumgardt and Kroupa 2007; Pfalzner and Kaczmarek 2013).

As discussed above, the gas component is treated simply as an analytical external (Plummer) potential corresponding to its mass distribution whereas the stellar system is tracked accurately using direct N-body calculations, which captures the essential dynamics of the stellar system. The escape of the gas component is typically modelled as an exponential decay of the gas mass with e-folding time τ_g after a "delay time" τ_d, i.e.,

$$\begin{aligned} M_g(t) &= M_g(0) \quad t \leq \tau_d, \\ M_g(t) &= M_g(0) \exp\left(-\frac{(t-\tau_d)}{\tau_g}\right) \quad t > \tau_d. \end{aligned} \tag{6.7}$$

τ_g is determined by the effective speed, v_g, with which the gas escapes out, i.e., $\tau_g \approx r_h(0)/v_g$. The Plummer radius of the gas distribution is kept fixed at $r_h(0)$. Such an analytic treatment of the gaseous component is justified by Geyer and Burkert (2001) who show that expelling the gas analogously by detailed SPH calculations (using shock heating) and analytically produce similar effect on the stellar system.

Note that the corresponding (clump) SFE is $\epsilon = M_{\rm cl}(0)/(M_{\rm cl}(0) + M_g(0))$ or

$$M_g(0) = M_{\rm cl}(0)\left(\frac{1}{\epsilon} - 1\right) \tag{6.8}$$

6.2.2.1 Parameters for Gas Expulsion

One key parameter in the above model of the initial phase of cluster formation is the initial size of the embedded system given by its half-mass radius $r_h(0)$. While in the literature there is no norm in the choice of the compactness of the gas-filled system, detailed observations of molecular clouds and embedded proto-stars imply highly compact profiles of proto-stellar clusters. As seen in the *Herschel* observations, and more recently using the *ALMA*, proto-stellar associations appear in the highly compact filamentary overdensities and in their junctions (Schneider et al. 2010, 2012; Hill et al. 2011; Hennemann et al. 2012; Tafalla and Hacar 2015) in giant

[6] For monolithic systems we denote here the stellar mass as $M_{\rm cl} \equiv M_*$.

molecular gas clouds (GMCs). The sections of these filaments are very compact; typically $\lesssim 0.3$ pc and peaked at $\approx$0.1 pc (André et al. 2011). The profiles of these filament sections are typically Plummer-like (Malinen et al. 2012). This dictates a plausible, idealized initial embedded cluster to be a highly compact Plummer sphere with $r_h(0) \lesssim 0.3$ pc. Indeed, the embedded associations in the solar neighbourhood (Lada and Lada 2003; Tapia et al. 2011, 2014) and near embedded young clusters, e.g., RCW 38 (DeRose et al. 2009; Kuhn et al. 2014) and the ONC (Kroupa et al. 2001) are all found to have half-mass radii well less than a parsec.

In an independent and semi-analytic study, Marks and Kroupa (2012) have investigated the initial conditions of star clusters that would give rise to the currently observed binary period distribution in several observed clusters. Here, the "inverse dynamical population synthesis" (Kroupa 1995a) is used to infer the initial stellar density (and hence the size) of a given cluster, which would dynamically evolve an initial universal primordial binary period distribution (Kroupa 1995a,b) to the present-day distribution. This study relates the birth mass and the half-mass radius of a star cluster as,

$$\frac{r_h(0)}{\mathrm{pc}} = 0.10^{+0.07}_{-0.04} \times \left(\frac{M_{\rm cl}(0)}{M_\odot}\right)^{0.13\pm0.04}. \tag{6.9}$$

This gives comparable initial (embedded) cluster size as above which depends weakly on the initial mass.

The observed values of SFE in star-forming clouds and embedded associations range widely, from less than a percent (Rathborne et al. 2014) to $\approx$30% for the embedded stellar associations in the solar neighbourhood (Lada and Lada 2003). An appropriate value of SFE is even more unclear from theoretical studies which depends on a number of assumptions and inputs that are adopted in the hydrodynamic calculations. SPH calculations with spherical (or cubical) gas clouds of $<$100–1000s $M_\odot$ without any implementation for stellar feedback, as often done for such masses (e.g., Klessen et al. 1998; Bate and Bonnell 2004; Bate 2009; Girichidis et al. 2011), cannot infer any SFE and would eventually let all of the gas be absorbed into the proto-stars (or sink particles), i.e., give $\approx$100% SFE as an artefact. Self-regulation by stellar matter outflow (wind and jet) and radiation (Adams and Fatuzzo 1996) is crucial to arrive at a realistic SFE. Current state-of-the-art SPH studies (reaching opacity limit and sub-sink-particle resolution) in this direction incorporate seed magnetic field in the star-forming gas and diffusive radiation feedback but are limited to individual proto-stars' scale. Proto-stars or sink particles are found to form with jet outflows where a self-regulated SFE up to $\approx$30% is obtained (Bate et al. 2014; see also Machida and Matsumoto 2012). Recently, an independent analytical study (Banerjee 2014) of formation of clump-cores (that would eventually turn into proto-stars) in gas clumps and of the maximum mass of the cores infers an upper limit of $\approx$30% for the clump SFE. This is consistent with the hydrodynamic calculations with self-regulation and observations in the solar neighbourhood (see above). From their SPH calculations of low-resolution but real-sized (10^5–$10^6 M_\odot$) turbulent molecular clouds, that include radiative feedback

but no magnetic field, Dale et al. (2015), however, find high SFE approaching 100%. This inferred SFE is likely to be an overestimate due to introduction of too low resolution (where a sink particle represents a stellar subcluster) and partial feedback by excluding magnetic field. From this viewpoint, the outcome of the proto-star-scale calculations, as mentioned above, are much more reliable. Pfalzner and Kaczmarek (2013) also find that ≈30% SFE best describes the age-mass and age-size correlation in young clusters of <20 Myr age. It is, therefore, plausible but not entirely obvious to assume that the massive clusters form with the highest possible SFE, an estimate of which is $\epsilon \approx 30\%$, according to the above-mentioned studies. Note that this SFE refers to the clump (i.e., over the spatial scale of a newborn cluster) efficiency; the SFE over an entire GMC is only a few percent.

The values of the timescales governing the gas expulsion timescale, viz., τ_g and τ_d depend on the complex physics of gas–radiation interaction. When the gas starts to escape, it should be ionized by the UV radiation from the massive stars causing efficient coupling of the stellar radiation with the gas which is one of the primary drivers of the gas. Hence, one can plausibly use an average gas velocity of $v_g \approx 10\,\mathrm{km\,s^{-1}}$ which is the sound-speed in ionized hydrogen (HII) gas. For massive clusters, whose escape speed (of the stellar system) exceeds the above v_g, the coupling of stellar radiation with the ionized gas over-pressures the latter and can even make it radiation pressure dominated (RPD) for massive enough clusters. During such RPD phase, the gas is driven at speeds well exceeding its sound-speed (Krumholz and Matzner 2009). Once the expanding gas becomes gas pressure dominated (GPD), the outflow continues with the HII sound speed (Hills 1980). Hence, τ_g as determined by $v_g \approx 10\,\mathrm{km\,s^{-1}}$, is an *upper limit*; it can be shorter depending on the duration of the RPD state. Note that this initial RPD phase is crucial to launch the gas from massive stellar systems whose escape speed exceeds the HII sound speed (Krumholz and Matzner 2009).

As for the delay-time, a widely used representative value is $\tau_d \approx 0.6$ Myr (Kroupa et al. 2001). The correct value of τ_d is again complicated by radiative gas physics. Although stellar input to the parent gas has been studied in some detail for single low mass proto-stars (Bate et al. 2014), the phenomena is much less understood over the global scale of a massive cluster. Nevertheless, an idea of τ_d can be obtained from the lifetimes of Ultra Compact HII (UCHII) regions which can be up to $\approx 10^5$ yr (0.1 Myr; Churchwell 2002). The highly compact pre-gas-expulsion clusters (see above) are a factor of ≈3–4 larger in size ($r_h(0)$) than a typical UCHII region (≈0.1 pc). If one applies a similar Strömgren sphere expansion scenario (see Churchwell 2002 and the references therein) to the compact embedded cluster, the estimated delay-time, τ_d, before a sphere of radius $r_h(0)$ becomes ionized, would also be larger by a similar factor and close to the above representative value. Once ionized (i.e., becomes HII from its predominantly neutral molecular or HI state), the gas couples efficiently with the stellar radiation and launched immediately (see above). High-velocity jet outflows from proto-stars (Patel et al. 2005) aid the gas outflow.

For super-massive clusters ($> 10^6 M_\odot$), i.e., for proto-globular clusters, however, a "stagnation radius" can form within the embedded cluster inside which the

radiation cooling becomes sufficiently efficient to possibly form second-generation stars (Wünsch et al. 2011). Also, as discussed above, the gas-outflow can initially be supersonic which generates shock-fronts. Although shocked, it is unlikely that star formation will occur in such a RPD gas. Later, during the GPD outflow, the flow can still be supersonic in the rarer/colder outer parts of the embedded cluster where the sound speed might be lower than that typical for HII gas. It is, however, unclear whether the cooling in the shocked outer regions would be efficient enough to form stars.

Admittedly, the above arguments do not include complications such as unusual morphologies of UCHIIs and possibly non-spherical ionization front, among others, and only provide basic estimates of the gas-removal timescales. Observationally, Galactic $\approx$1 Myr old gas-free young clusters such as the ONC and the HD97950 imply that the embedded phase is $\tau_d < 1$ Myr for massive clusters. The above popularly used gas-expulsion model does capture the essential dynamical response of the star cluster.

The stellar mass function of the embedded clusters is typically taken to be canonical (Kroupa 2001). Note that the stellar entities here are proto-stars which are yet to reach their hydrogen-burning main sequences. Also, the interplay between gas accretion and dynamical processes (ejections, mergers) in the compact embedded cluster continue to shape the global stellar IMF of the cluster (Klessen et al. 1998). This IMF is often observed to be canonical for VYMCs. This gas accretion and the dynamical processes only influence the massive tail of the IMF and also set the maximum stellar mass (Weidner and Kroupa 2004; Weidner et al. 2013a), as indicated in hydrodynamic calculations (Klessen et al. 1998; Dib et al. 2007; Girichidis et al. 2011). The overall canonical shape of the IMF as determined by the low mass stars, which contribute to most of the stellar mass of the system ($> 90\%$), appears primarily due to gravitational fragmentation alone. There are observational evidences available which suggest that VYMCs posses a canonical IMF below $1 M_\odot$ (Shin and Kim 2015). This justifies the adoption of the canonical IMF for the embedded (proto-) star cluster. In more recent studies (e.g., Banerjee and Kroupa 2013, 2014 discussed below) an "optimal sampling" of the canonical IMF is used (Kroupa et al. 2013) which automatically terminates the IMF at the maximum stellar mass (Weidner and Kroupa 2004).

On a separate note, efficient gas expulsion from star clusters is indirectly supported by the lack of gas in young and intermediate-aged clusters, in general. In particular, a recent survey of the LMC's massive star clusters over wide ranges of mass ($> 10^4 M_\odot$) and age (30–300 Myr) has failed to identify reserved gas in any of these clusters (Bastian and Strader 2014). These clusters would have accreted enough surrounding gas by now for the latter to be detected within them. This implies that star clusters can, in fact, disperse their gaseous component efficiently at any age $<$300 Myr and irrespective of their escape velocities (Bastian and Strader 2014). However, short ($<$1 Myr) bursts of new star formation episodes can lead to long-term continued growth of star clusters as these may accrete gas episodically from the surrounding interstellar medium (Pflamm-Altenburg and Kroupa 2009).

6.2.3 *Matchings with Individual Very Young Massive Clusters*

The best way to validate the monolithic or episodic scenario of VYMC formation is to compare its computed outcome with the details of well-observed VYMCs. There are only a few VYMCs whose profiles are measured from their centres to their halos using ground (primarily the *Very Large Telescope* or VLT) and space based (the *Hubble Space Telescope* or HST) photometry. To obtain a radial mass density profile of a dense assembly, proximity is essential as much as low extinction. This allows reliable estimates of starcounts in well-resolved annuli and also the estimates of the individual stellar masses. Thus (surface) mass density profiles have been obtained only for nearby and kpc-distance Galactic young clusters. The stellar velocity dispersion in a young cluster's central region can also constrain its initial conditions. The (one-dimensional) velocity dispersion can be obtained from stellar radial velocities from multi-epoch spectroscopy. Proper motions of the individual stars, as obtained from multi-epoch high-resolution imaging with sufficient time baseline, can provide the dispersion in the transverse velocity components. The Galactic NGC 3603 young cluster or HD97950, being our nearest starburst cluster, is perhaps the best observed VYMC whose mass density profile (obtained using the VLT; Harayama et al. 2008) and transverse stellar velocity dispersions (obtained using HST with a 10 year baseline; Rochau et al. 2010; Pang et al. 2013) are known out to $\approx$ 3 pc with reasonable accuracy. Being as young as $\approx$1 Myr (Stolte et al. 2004) despite being a gas free cluster, HD97950 acts as a "smoking gun" of formation of massive star clusters.

Table 6.1 shows model N-body computations in the literature and their corresponding parameters which have reproduced well-observed VYMCs (see Table 6.2) beginning from single-cluster initial conditions. The key results from these works will be discussed below. All these studies utilize certain common properties and conditions as below:

- The SFE ϵ $\approx$0.3 and the gas dispersal is determined by $v_g \approx 10\,\mathrm{km\,s^{-1}}$ ($\tau_g/\,\mathrm{Myr} = (r_h(0)/\,\mathrm{pc})/10$) and $\tau_d \approx 0.6\,\mathrm{Myr}$.
- The initial stellar and gas distribution follow the same Plummer profile.

As discussed in Sect. 6.2.2.1, these values and conditions are representatives and idealizations but physically motivated from what we know so far from observations and calculations at smaller scales. Furthermore, in several of them (Kroupa et al. 2001; Banerjee and Kroupa 2014) a primordial binary population is used according to the "birth period distribution" (Kroupa 1995b; Marks et al. 2014). While it is more compute intensive, introducing primordial binaries is more realistic in light of the high multiplicity of PMS stars. In these cases, a 100% primordial binary fraction ($f_{\rm bin}(0) = 1.0$) is used at $t = 0$ (Kroupa 1995a). The orbital period (P) distribution of such binary population spans over a wide range, between $1.0 < \log P < 8.43$ where P is in days (Kroupa 1995b). The binary eccentricities, e, are taken to be thermalized, i.e., distributed as $f(e) \propto e$ (Spitzer 1987). With the dynamical evolution (and also due to the orbital evolution by tidal interaction among PMS

Table 6.1 Initial and gas expulsion parameters, for the computed models beginning with monolithic initial conditions, that reproduce well-observed very young massive clusters (see Sect. 6.2.3)

Model cluster	$M_{\rm cl}(0)/M_\odot$	$M_g(0)/M_\odot$	$r_h(0)$/pc	τ_g/Myr	$\tau_{cr}(0)$/Myr	τ_d/Myr	$f_{\rm bin}(0)$	$Z/Z_\odot$	Reference
ONC-B	4.2×10^3	8.4×10^3	0.21	0.021	0.066	0.6	1.0	1.0	Kroupa et al. (2001)
R136	1.0×10^5	2.0×10^5	0.45	0.045	0.021	0.6	0.0	0.5	Banerjee and Kroupa (2013)
HD97950s	1.0×10^4	2.0×10^4	0.25	0.025	0.029	0.6	0.0	1.0	Banerjee and Kroupa (2014)
HD97950b	1.0×10^4	2.0×10^4	0.25	0.025	0.025	0.6	1.0	1.0	Banerjee and Kroupa (2014)
ONC-A[a]	3.7×10^3	7.4×10^3	0.45	0.045	0.23	0.6	0.0	1.0	Kroupa et al. (2001)
NYC[a]	1.3×10^4	2.6×10^4	0.34	0.034	0.038	0.6	0.0	1.0	Banerjee and Kroupa (2013)

See text for the meanings of the notations

The initial gas mass $M_g(0)$ and the gas expulsion timescale τ_g (see Sect. 6.2.2) are determined by $\epsilon \approx 0.33$ and $v_g \approx 10\,{\rm km\,s^{-1}}$ ($\tau_g = r_h(0)/v_g$), respectively, and $\tau_d \approx 0.6\,{\rm Myr}$ for all these computed models. The models HD97950s/b refer to the ones with initial single-only stars/primordial binaries as computed in Banerjee and Kroupa (2014)

[a]These computed models are not "matching" models but are discussed various in places of this chapter

Table 6.2 Properties of VYMCs, discussed in this chapter, as inferred from observations. "—" implies that the corresponding value or quantity is ambiguous or unknown. The surface profiles known for these clusters (last column) are either stellar number or mass density profiles or both (see below)

Cluster name	Cluster mass ($M_{\rm cl}/M_\odot$)	Age (t/Myr)	Galactocentric distance (R_G/kpc)	Half-light radius (r_h/pc)	Radial profile
ONC	$\approx 10^3$	1–2	$\approx$solar	—	Number
R136	$\approx 10^5$	2–3	—	$\lesssim 1$	—
NGC 3603	$(1.0–1.6)\times 10^4$	≈ 1	$\approx$solar	≈ 0.75	Number/mass

stars or the "eigenevolution"; Kroupa 1995b) of the binary population and eventual disruption of the parent cluster (by the Galactic tidal field), such a primordial binary population naturally transforms to the log-normal period distribution observed for low mass stellar binaries in the solar neighbourhood (Kroupa 1995a). A detailed discussion of the period distribution of primordial binaries, which is currently a widely debated topic (Kroupa et al. 2013; Marks et al. 2014; Leigh et al. 2015), is beyond the scope of this text.

These studies also incorporate stellar evolution and the associated mass loss in the N-body calculations using the semi-analytic `BSE` stellar evolution code (Hurley et al. 2000). The `BSE`, while available as standalone, is integrated with the `NBODY6` direct N-body code (Aarseth 2003). `NBODY6` is currently the most realistic way to associate stellar (and binary) evolution with dynamics. In the following, we discuss the key results from the studies mentioned in Table 6.1. For more details the reader is suggested to consult the respective references.

6.2.3.1 The Orion Nebula Cluster: Structure and Kinematics

Kroupa et al. (2001) provide a comprehensive study of the Orion's main central cluster (the ONC). These authors demonstrate that an appropriate monolithic initial state with the above parameters (Table 6.1) well reproduce the key observed properties of the ONC. An important corollary of this work is that the ONC would dynamically evolve to a cluster similar to Pleiades in $\approx$100 Myr. Hence, a young system like the ONC represents the infant stage of an intermediate age open cluster like the Pleiades. These calculations are done using a version of the `NBODY6` code that includes an analytic time-varying external gas potentials (the `GASEX`; Kroupa et al. 2001) as discussed above. A realistic birth primordial binary population with 100% binary fraction is used in these calculations.

Figure 6.5 shows that the evolution of the core radius, r_c, for the computed models ONC-A and -B (Table 6.1). ONC-B agrees well with the observed r_c for the ONC at $t \approx 1$ Myr age and evolves over to be agreeable with the observed value for Pleiades at $t \approx 100$ Myr. The core-radius evolution of ONC-A, on the other hand, is far less consistent with these observed values.

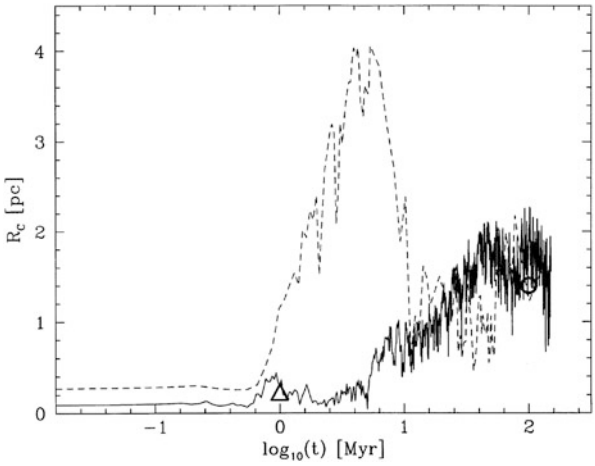

Fig. 6.5 The evolution of the core radius, r_c, in the ONC A (*dashed curve*) and the ONC B (*solid curve*) model clusters as computed by Kroupa et al. (2001). The *open triangle* and *circle* are the observed values of core radius for ONC (Hillenbrand and Hartmann 1998) and Pleiades (Radboud and Mermilliod 1998), respectively. This figure is reproduced from Kroupa et al. (2001)

Notably, model B expands to much larger extent at later times than immediately after its gas expulsion. Such late-time expansion is common for clusters with a mass spectrum and hard primordial binaries. This is driven by the mass loss due to the supernovae of the massive stars that segregate to the cluster's central region by then. The expansion is further assisted by frequent single star-binary close encounters in the cluster's central region that cause ejections of single and binary stars (Banerjee et al. 2012a; Oh et al. 2014) in super-elastic encounters (Heggie 1975; Hills 1975).[7] This boosts the internal K.E. of the cluster's core due to the associated mass loss and encounter recoils. The dynamical heating becomes efficient at late times after the bound fraction of the initial system re-virializes (see beginning of Sect. 6.2) and the most massive stars and the binaries segregate towards the cluster's centre, augmenting their density and hence the encounter rates therein. The evolutionary course of model A is, however, different where the initial expansion due to gas expulsion is more extensive. Being of lower mass and an initially larger radius, model A has lower stellar density and hence less efficient violent relaxation throughout its violent expansion phase (see beginning of Sect. 6.2), allowing it to expand to larger radii and cause the bound fraction to take longer to fall back (c.f. dashed line in Fig. 6.5). The longer duration of expansion and re-collapse covers a good part of the supernova phase ($t \gtrsim 3$ Myr) and makes binary-single/binary-binary encounters much less frequent. Note that for both

[7] According to "Heggie-Hills law", a hard binary (i.e., a binary whose orbital velocity is higher than the relative velocity of its COM and the intruder) statistically becomes harder, i.e., gains binding energy, in a gravitational encounter with a third body. Hence, due to energy conservation, a hard binary-single encounter would cause gain in the COM energy of the recoiling entities in the cost of deepening the binary's potential well. This, in turn, results in an increase of the K.E. in a packed-enough environment, e.g., the central region of a massive star cluster. Close encounters can result in the escape of one or both systems if they recoil exceeding the escape velocity.

models, the primordial binaries and the stars of all masses are distributed initially without any spatial preference, i.e., without any primordial mass segregation. Also, see Sect. 6.2.3.2.

Figure 6.6 shows the computed evolutions of the stellar (surface) number-density profiles. Being consistent with the core-radius evolution, the radial profile for the ONC-B model agrees reasonably with the observed radial stellar density profile of the ONC, out to $\approx$ 3 pc from the centre, at $t \approx 1$ Myr (bottom panel). This is unlike the ONC-A model which is either too dense or too expanded compared to the observed radial profile (top panel).

The evolution of computed one-dimensional velocity dispersion, σ_{1d}, is shown in Fig. 6.7. The frequent abrupt jumps in the computed σ_{1d} at late times is due to binary-single star close encounters which cause ejections of single and binary systems from the cluster. The recoil K.E. in the encounter and the mass loss due to the escape heats up the cluster's core (see above). The long-term boost in σ_{1d} for the ONC-A model between 60 and 100 Myr is an artefact of the method in which σ_{1d} is evaluated in this study which considers only binaries as centres of mass (COMs) but not higher multiplets. The increased σ_{1d} here is caused due to the outer member of a long-lasting triple system that can appear in relatively low density systems. Given that the excursions in σ_{1d} is probabilistic in nature, both A and B models are consistent with the observed values for ONC and Pleiades (c.f. Fig. 6.7).

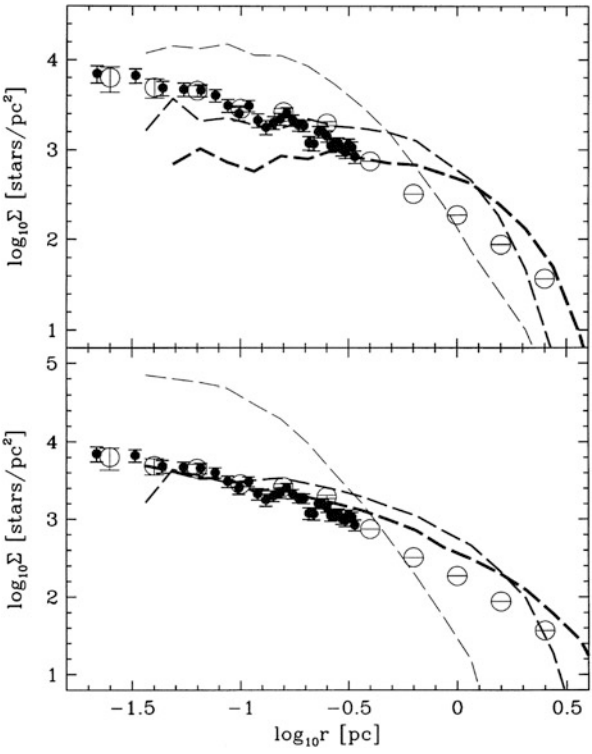

Fig. 6.6 The projected radial stellar number density profile at $t = 0, 0.87$ and 1.1 Myr (in increasing thickness) for the computed clusters ONC A (*top*) and B (*bottom*). The *open circles* are observed data from Hillenbrand (1997) and the *solid circles* are from McCaughrean (private communication). This figure is reproduced from Kroupa et al. (2001)

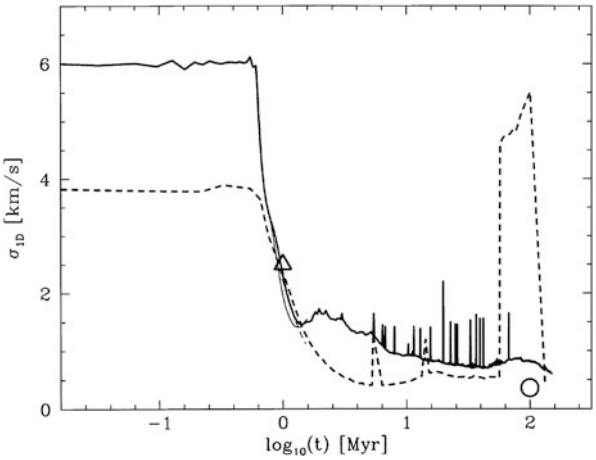

Fig. 6.7 The velocity dispersion of systems within $R \leq 3.2$ pc (*thick curves*) and within $R \leq 2.5$ pc (*thin curves*). The value for the Pleiades is the *open circle* (Radboud and Mermilliod 1998), and the *triangle* is that for the ONC (Jones and Walker 1988). The *dashed* and the *solid lines* are for ONC-A and B models respectively. The vertical excursions at later times are due to energetic binary-star encounters, which eject stars. This figure is reproduced from Kroupa et al. (2001)

Given the overall consistent agreement with the observed core radius, radial stellar density profile and one-dimensional velocity dispersion, ONC-B's initial conditions and parameters (Table 6.1) comprise an appropriate initial state of the ONC. In other words, this model represents a monolithic "solution" of the ONC. It justifies the in situ formation of this VYMC from a single, initially bound stellar association formed in a starburst in a molecular-gas clump, after expelling the majority of the clump's gas ($\approx$ 70% by mass). As a corollary, an ONC-like young star cluster would evolve and expand to a Pleiades-like open cluster as the above calculations show.

6.2.3.2 The Tarantula Cluster (R136): Central Velocity Dispersion

A common criticism put forward against the role of gas expulsion in the formation of VYMCs is the inferred dynamical equilibrium in several VYMCs. The central R136 cluster of the Tarantula Nebula of the LMC is particularly cited in this context (Hénault-Brunet et al. 2012). The inferred total photometric mass of this cluster is $\approx 10^5 M_\odot$ (Crowther 2010) and the age of the bulk of its stars is $\approx$3 Myr (Andersen et al. 2009). Clearly, R136 is quite an outlier by mass in the high side among the well-studied nearby VYMCs (it is also at least twice as massive compared to the Arches cluster).

As a part of the ongoing "VLT-FLAMES Tarantula Survey" (VFTS; Evans et al. 2011), Hénault-Brunet et al. (2012) measured radial/line-of-sight velocities (RV) of *single* O-stars within 1 pc $\lesssim R \lesssim$ 5 pc projected distance from R136's centre. (Strictly, the distances were measured from the most massive cluster member star R136a1. The exact location of the R136's true density centre being unknown, we consider this star be expectedly very close to the cluster's density centre.) They conclude that the RV dispersion, V_r, of the *single* O-stars within this region is $4\,\mathrm{km\,s^{-1}} \lesssim V_r \lesssim 5\,\mathrm{km\,s^{-1}}$. Spectroscopy (with FLAMES) at multiple epochs have been used to eliminate the radial velocities of spectroscopic binaries (Hénault-Brunet et al. 2012), i.e., the above V_r corresponds the COM motion of the stars (and binaries) over the selected region of the cluster. Given the mass of R136, the above V_r is consistent with the cluster being in dynamical equilibrium at the present day.

This is contradictory to the generally accepted notion that young clusters, if emerged from recent gas dispersal, should presently be expanding. This is indeed the case for the ONC (Kroupa et al. 2001). Brandner (2008) demonstrated that young systems show an overall increase in size with age. As noted above (Sects. 6.1 and 6.2), a recently gas-expelled cluster may or may not be in dynamical equilibrium at a given age depending on the effectiveness of violent relaxation in its expanding phase. This, in turn, depends on its initial density. Hence, if initially massive and/or compact enough, a VYMC can as well be in dynamical equilibrium at present even after undergoing a significant amount of gas expulsion.

Figure 6.8 (top panel) shows the evolution of the Lagrange radii for a model of a R136-like massive cluster ($M_{\rm cl}(0) \approx 10^5 M_\odot$), viz., model "R136" in Table 6.1. The initial half-mass radius, $r_h(0) = 0.45$ pc, is chosen according to Eq. (6.9) which is consistent with the size of embedded clusters and that of the sections of dense filaments in molecular gas clouds (see Sect. 6.2.2.1). These Lagrange radii (escaping and bound stars are always included) imply that the R136 cluster, under reasonable conditions (see Sect. 6.2.2.1), would re-virialize well within its current age of 3 Myr. The re-virialization time, in this case, is $\tau_{\rm vir} \approx 1$ Myr and the bound fraction after re-virialization is $F_b \approx 0.6$, implying an efficient violent relaxation phase. This calculation (as well the following one described in this subsection) is done using the `NBODY6` code (see above). No primordial binaries are used in these calculations as $\tau_{\rm vir}$ and F_b would not get affected by binaries significantly. Also, primordial binaries are a significant computational hurdle for direct N-body calculations for such massive clusters (even for Monte Carlo calculations; c.f. Leigh et al. 2015).

As expected, the corresponding computed $V_r \approx 4.5\mathrm{km\,s^{-1}}$ between 1 and 3 Myr age, as appropriate for the remaining bound virialized cluster, is consistent with the observed value for R136 (see above). This is shown in Fig. 6.8 (bottom panel). Note that in Fig. 6.8, the computed evolution of V_r corresponds to stars with (zero-age) mass $> 16 M_\odot$ which correspond to O-type stars that are used to determine the radial velocity dispersion in R136 by Hénault-Brunet et al. (2012). Also, V_r is computed within 1 pc $\lesssim R \lesssim$ 5 pc as observed by the above authors. The initial large fluctuations in V_r for $\tau_d < 0.6$ Myr are due to the initial mass-segregated condition used in this calculation (Banerjee and Kroupa 2013), which results in only a few O-stars within 1 pc $\lesssim R \lesssim$ 5 pc initially. As shown in Banerjee and Kroupa

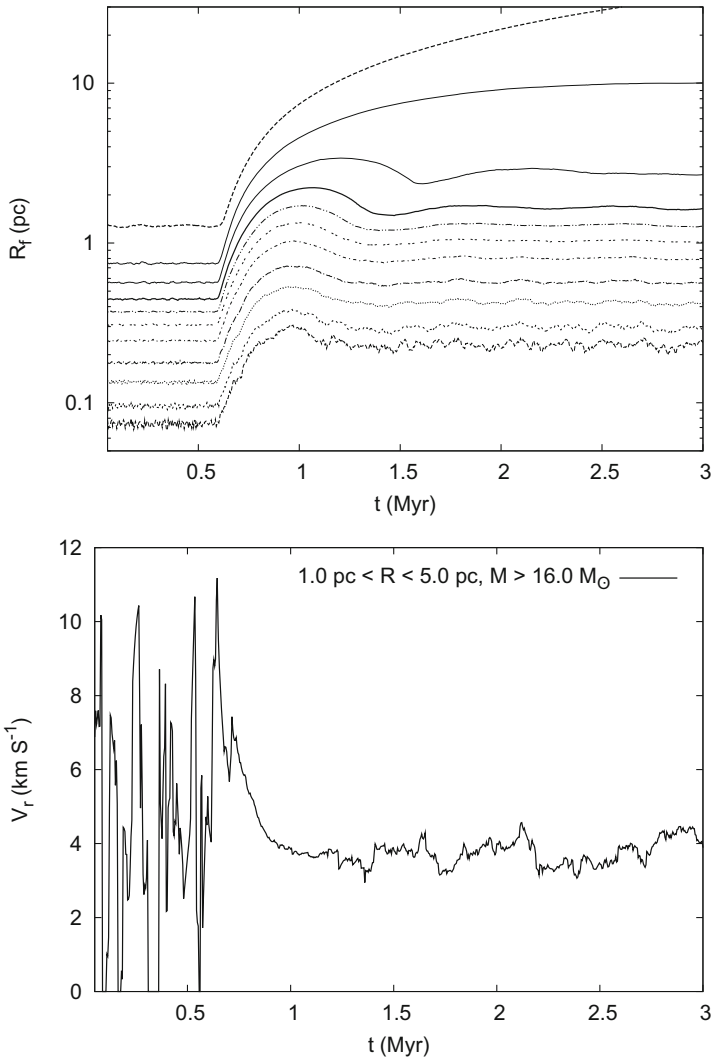

Fig. 6.8 *Top*: The evolution of the Lagrange radii, R_f, for stellar cluster mass fractions f for the computed R136 model in Banerjee and Kroupa (2013) (see Table 6.1). The curves, from *bottom to top*, correspond to $f = 0.01, 0.02, 0.05, 0.1, 0.2, 0.3, 0.4, 0.5, 0.625, 0.7$ and 0.9, respectively. The *thick solid line* is therefore the half-mass radius of the cluster. *Bottom*: The corresponding evolution of the radial velocity (RV) dispersion, V_r, of the O-stars ($M > 16 M_\odot$), within the projected distances 1 pc $< R <$ 5 pc from the cluster centre. These panels are reproduced from Banerjee and Kroupa (2013)

(2013) by comparing initially segregated and non-segregated computed models, primordial mass segregation does not influence the Lagrange radii and the V_r after re-virialization. In models at these initial densities, the mass segregation timescale,

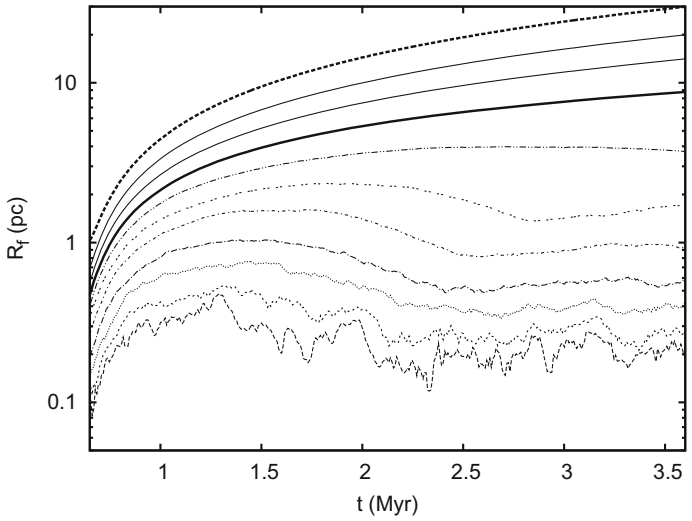

Fig. 6.9 The evolution of the Lagrange radii for the computed NGC3603-like cluster in Banerjee and Kroupa (2013) (see Table 6.1). The legends for the curves are same as in Fig. 6.8. The time axis before the beginning of the gas dispersal (until $\tau_d = 0.6$ Myr) is suppressed. This panel is reproduced from Banerjee and Kroupa (2013)

$\tau_{\rm seg}$, given by (Banerjee et al. 2010)

$$\tau_{\rm seg} \approx 15 \frac{\langle m \rangle}{m_{\rm massive}} \tau_{\rm rh}(0), \tag{6.10}$$

is very short for the massive end of the stellar IMF. In Eq. (6.10), $\tau_{\rm rh}(0)$ is the initial half-mass relaxation time (Spitzer 1987) of a cluster with average stellar mass $\langle m \rangle$.

Figure 6.9 shows the Lagrange radii of a computed model that is a few factors less massive than the R136 model discussed above. This model corresponds to the NBODY6-computed model "NYC" in Table 6.1 whose mass is similar to the NGC 3603 Young Cluster (HD97950). Note that while this model is not a "matching model" for NGC 3603 cluster which are covered in the following subsection (models "HD97950"s/b of Table 6.1), the initial conditions are similar. Unlike the R136 model, the re-virialization time is much longer in this case, viz., $\tau_{\rm vir} \approx 2$ Myr. Hence at its present age of $\approx$1 Myr, an NGC3603-like young cluster would not be in dynamical equilibrium (except in its innermost regions; see Sect. 6.2.3.3), as one generally expects. As discussed in Sect. 6.2.3.1, a smaller $M_{\rm cl}(0)$ and hence less initial stellar density causes the NYC model to take longer to regain dynamical equilibrium with a reduced bound fraction ($F_b \approx 0.3$).

From the above calculations it can be said that "an observed dynamical equilibrium state of a very young stellar cluster does not necessarily dictate that the cluster has not undergone a substantial gas-expulsion phase" (Banerjee and Kroupa 2013). The R136 cluster is very likely a VYMC that is promptly re-virialized after

its gas expulsion owing to its large mass (hence initial density). Admittedly, these conclusions depend on the initial and gas expulsion conditions. As discussed in Banerjee and Kroupa (2013), the above conclusions are immune to reasonable variations in the gas expulsion timescales τ_d and τ_g, as long as $\epsilon \approx 33\%$ which is reasonable for VYMCs (see Sect. 6.2.2.1).

In passing, it is worthwhile to consider the effect if the SFE possibly varies radially across the initial cluster (Adams 2000). In that case, the central region of the cluster is likely to have a higher SFE due to higher density there. The resulting gas removal preferentially from the outer parts of the cluster would cause it to expand less than the corresponding case of a uniform SFE. This would, in turn, shorten $\tau_{\rm vir}$ and increase F_b, i.e., the above conclusions still remain unchanged.

6.2.3.3 NGC 3603 Young Cluster: Structure and Kinematics

Being our nearest starburst cluster, the central young cluster HD97950 of the Galactic NGC 3603 star-forming region is perhaps the best observed VYMC. Due to its proximity ($\approx$7 kpc from the Sun) and brightness (photometric mass $10000 M_\odot \lesssim M_{\rm cl} \lesssim 20000 M_\odot$) its radial stellar mass-density profile for low mass stars (Harayama et al. 2008) (using VLT observations in NIR) and the number-density profile for stars up to $100 M_\odot$ (Pang et al. 2013) are determined, both out to 3 pc ($R \approx 100''$) from its centre. Furthermore, its central velocity dispersion, within $R \lesssim 0.5$ pc($\approx 15''$), and the stellar tangential velocities are determined from proper motion measurements with the HST ($\approx$10-year baseline; Rochau et al. 2010; Pang et al. 2013).

In Banerjee and Kroupa (2014), a set of initial conditions is presented which remarkably reproduce the above structural and kinematic data of the HD97950 cluster, viz., the models "HD97950s/b" of Table 6.1. These computed clusters (using `NBODY6`) have the same initial conditions, except that HD97950b contains a primordial binary population. This binary population is taken to be the birth population (Kroupa 1995b), except that a uniform distribution in $\log_{10} P$ between $0.3 < \log_{10} P < 3.5$ and a mass ratio biased towards unity (ordered pairing; as introduced by Oh and Kroupa 2012) is used for stellar masses $m > 5 M_\odot$. This is motivated by the observed period distribution of O-star binaries in nearby O-star rich clusters (Sana and Evans 2011; Chini et al. 2012). It is currently unclear at which stellar mass and how the orbital period law changes and the above switching of the P-distribution at $m = 5 M_\odot$, therefore, is somewhat arbitrary. Note that for this P-distribution, the primordial binaries are much tighter and hence energetic in dynamical encounters for $m > 5 M_\odot$.

Both the computed models reproduce the HD97950 cluster reasonably but the one with the above primordial binary distribution (i.e., HD97950b) does better in terms of matching the central velocity dispersion. A substantial fraction of tight massive binaries ($\approx 50\%$ in this case) augments the central velocity dispersion due to energetic binary-single interactions (binary heating) and makes it agree better with the observed value in this case (Banerjee and Kroupa 2014). Here, only the HD97950b model is detailed.

Figure 6.10 shows the surface or projected mass density profile Σ_M at $t \approx 1.4$ Myr for the HD97950b model (filled squares joined by solid line). It matches remarkably with the observed profile in HD97950 (filled circles; Harayama et al. 2008). Note that in this comparison a similar stellar mass range and annuli as those for the observed profile are used to construct the density profile from the computed cluster.

Figure 6.11 shows the radial profile of the incompleteness-limited stellar number density Σ_N from the above computed cluster (filled squares joined by solid line) at $t \approx 1.4$ Myr and that obtained from the HST (Pang et al. 2013) (filled triangles) which agree remarkably. Here, the computed stellar distribution is sampled according to the radius and mass-dependent incompleteness fraction particular to this observation (Pang et al. 2013). This mimics the "observation" of the model cluster. Note that in constructing both of these density profiles we include only the most massive member (primary) of a binary which would dominate the detected light from it.

Figure 6.12 (bottom) shows the evolution of the (one-dimensional) dispersion of the stellar velocity components, σ_{1d} (1d = x, y, z), for the HD97950b model for $1.0 M_\odot < m < 100.0 M_\odot$ within $R < 0.5$ pc. The computed σ_{1d}s lie between

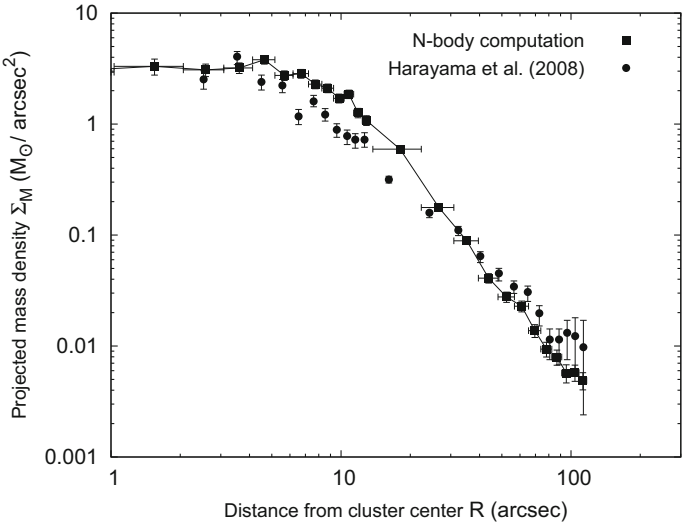

Fig. 6.10 The computed projected mass density profile (*filled squares* and *solid line*) for the stellar mass range $0.5 M_\odot < m < 2.5 M_\odot$ at $t \approx 1.4$ Myr, from the computed model HD97950b ($r_h(0) \approx 0.25$ pc, $M_{cl}(0) \approx 10000 M_\odot$; see Table 6.1) containing an initial primordial binary population (see Sect. 6.2.3.3). This computed profile shows remarkable agreement with the observed profile (Harayama et al. 2008), for the same stellar mass range, of the central young cluster (HD97950) of NGC 3603 (*filled circles*). The angular annuli (the horizontal error bars) used for computing the projected densities are nearly the same as those used by Harayama et al. (2008) to obtain the observed profile. The vertical error bars are the Poisson errors for the individual annuli. This panel is reproduced from Banerjee and Kroupa (2014)

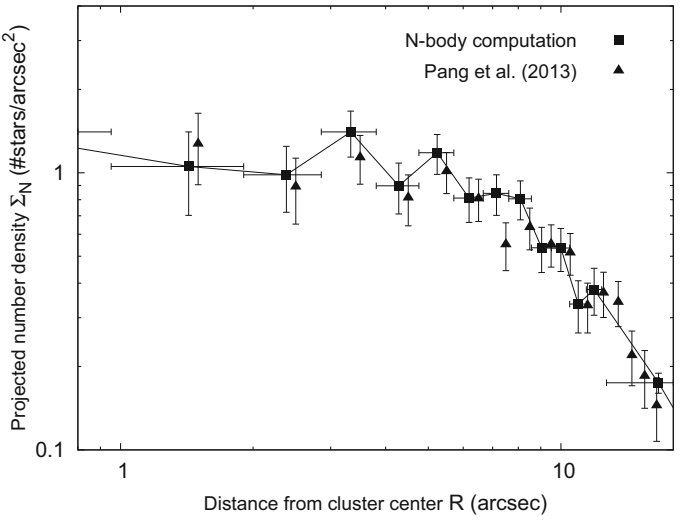

Fig. 6.11 The computed projected stellar number density profile for the calculation HD97950b (Table 6.1; *filled squares* and *solid line*). This shows a remarkable agreement at $t \approx 1.4$ Myr with the same obtained with the stars of HD97950 from the HST/PC chip (up to the central 15″; *filled triangles*; chip data from Pang et al. 2013). In constructing the computed profile, the incompleteness in the detection of the stars is taken into account that depends on the stellar mass (luminosity) and projected angular annuli on the cluster, as given in Pang et al. (2013). In this comparison, similar angular annuli (horizontal error-bars) are used to construct the density profiles. The vertical error bars are the corresponding Poisson errors. This panel is reproduced from Banerjee and Kroupa (2014)

$4.0 < \sigma_{1d} < 7.0\,\mathrm{km\,s^{-1}}$ for $1 < t < 2$ Myr. The corresponding observed one-dimensional velocity dispersions indeed vary considerably with orthogonal directions (Pang et al. 2013) like the computed ones here (see Fig. 6.12; bottom panel) and their variation well matches the above computed range. Figure 6.12 (top) shows the σ_{1d}s corresponding to the stellar mass range $1.7M_\odot < m < 9.0M_\odot$ as in Rochau et al. (2010). The corresponding mean σ_{1d} is consistent with that obtained by Rochau et al. (2010) from HST proper motions. The abrupt vertical excursions in σ_{1d} in Fig. 6.12 (bottom) are due to energetic two- or few-body encounters which are most frequent for the most massive stars and binaries as they centrally segregate the most via two-body relaxation.

Figure 6.13 shows radial profiles of σ_{1d}, from HD97950b, at $t = 1.4$ Myr for $1.0M_\odot \leq m \leq 100.0M_\odot$. Here, σ_{1d} tends to increase for $R \gtrsim 40''(\approx 1.2$ pc) which can be attributed to the recent gas expulsion from the system causing its outer parts to still expand. Such a behaviour, which becomes more prominent the closer the epoch of observation is to the gas expulsion, can be tested by future, more accurate determinations of stellar proper motions in the outer regions of HD97950, e.g., by *Gaia*. Notably, the measured tangential velocities (from HST proper motions) of selected stars in Pang et al. (2013) indeed show an increasing trend with radial

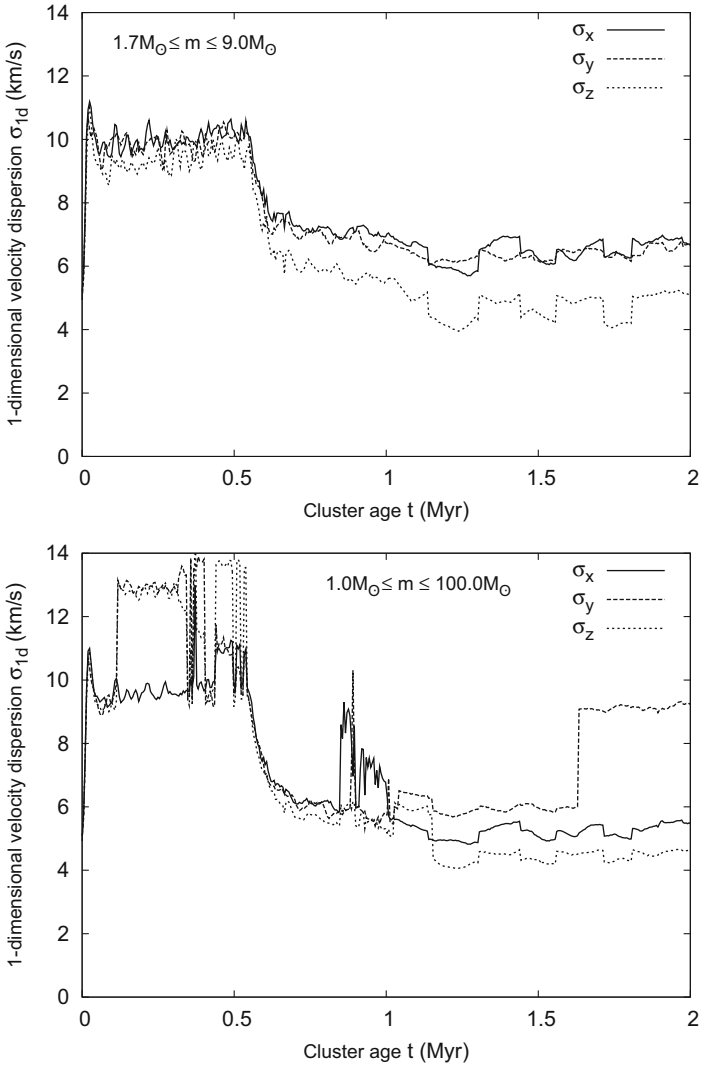

Fig. 6.12 The time evolution of the one-dimensional velocity dispersions, σ_{1d}s, for the model cluster HD97950b (see Table 6.1), the density profile of which is shown in Fig. 6.10. They are obtained for $R < 0.5$ pc ($\approx 15''$) and correspond to the stellar mass ranges $1.7M_\odot < m < 9.0M_\odot$ (as in Rochau et al. 2010; *top panel*) and $1.0M_\odot < m < 100.0M_\odot$ (as in Pang et al. 2013; *bottom panel*). The σ_{1d}s obtained here correspond to the COMs of the cluster single-stars and binaries. The computed values of σ_{1d} (*bottom panel*) differ in orthogonal directions as found in observations (Pang et al. 2013) and span the same range as observed (4.5–7.0 km s^{-1}) between 1.0 and 1.5 Myr cluster age, implying good agreement. These panels are reproduced from Banerjee and Kroupa (2014)

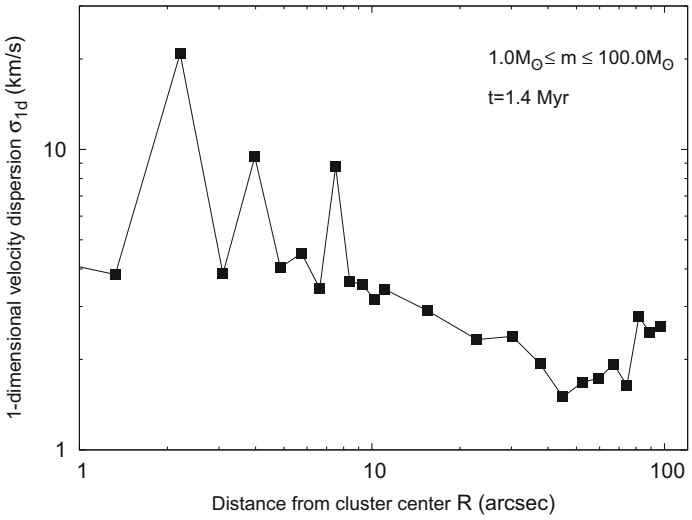

Fig. 6.13 Radial variation of one-dimensional velocity dispersion, σ_{1d}, for the computed HD97950b model (here in presence of a tidal field) at $t = 1.4$ Myr for stellar mass range $1.0M_{\odot} \leq m \leq 100.0M_{\odot}$. The overall increasing trend of σ_{1d} with R in the outer regions ($R \gtrsim 40''$ in this case) is due to the recent gas expulsion. The tangential velocities of selected stars in Pang et al. (2013) (for $R \lesssim 60''$) do show an increasing trend with R. This panel is reproduced from Banerjee and Kroupa (2014)

distance in the outer region (measured up to $R \approx 60''$) of HD97950. Note that the inner annuli of the above computed cluster are already virialized at $t = 1.4$ Myr but the outer region is still far from re-virialization (see Fig. 1 of Banerjee and Kroupa 2014). As demonstrated in Sect. 6.2.3.2, the overall re-virialization time for such a cluster is $\tau_{\rm vir} \approx 2$ Myr.

Hence, the HD97950 computed cluster well reproduces the structure and the internal kinetics of the observed HD97950 cluster. In other words, model HD97950b (also HD97950s to some extent) is a monolithic "solution" of the NGC 3603 cluster; it represents an initial stellar distribution that would evolve self-consistently to make the HD97950 cluster at its appropriate age.

Initial Plummer-profiled and highly compact ($r_h(0) \approx 0.2$–0.3 pc) monolithic embedded clusters, when subjected to residual gas expulsion, remarkably reproduce the hitherto known kinematic and structural properties of the well-observed young clusters the ONC, R136 and NGC 3603. The properties of the required gas expulsion are seemingly universal ($\epsilon \approx 0.3$, $\tau_d \approx 0.6$ Myr and $v_g \approx 10 \mathrm{km\,s^{-1}}$). Such computed model clusters are the only ones to date that directly reproduce these observed clusters.

6.3 Hierarchical Formation of Young Massive Clusters: The Case of NGC 3603 Young Cluster

Although an episodic and in situ formation scenario is well consistent with the detailed properties of several observed Galactic or local VYMCs (Sect. 6.2), it is still puzzling how such smooth initial condition can be connected with irregular, substructured and/or filamentary morphology of GMCs and embedded stellar distributions (see Sect. 6.1). Substructures are also found in several gas-free or near gas-free very young star clusters, even though they may have an overall core-halo profile (Kuhn et al. 2014). Computations of gravitational fragmentation in turbulent gas clouds also point to a highly substructured beginning of a star cluster (see Sect. 6.1).

One way to "add up" these two apparently conflicting pictures of VYMC formation is indicated by the timescale problem of hierarchical formation as discussed in Sect. 6.2.1. Essentially, the age, density and velocity dispersion profiles of observed VYMCs well constrain the admissible initial spatial scale of any subcluster system from which the VYMC may have formed. In particular, Fig. 6.3 implies that substructures can appear and migrate from sufficiently close separation to possibly form a VYMC within a few Myr. Such "prompt hierarchical merging" can connect a monolithic initial condition, which successfully explains observed VYMCs (Kroupa et al. 2001; Banerjee and Kroupa 2013, 2014) and general properties of young clusters (Pfalzner 2009; Pfalzner and Kaczmarek 2013), to the conditions in dense star-forming molecular regions. The detailed observed properties of the HD97950 cluster again provide a testbed for such a scenario as discussed below.

In Banerjee and Kroupa (2015), substructured initial conditions are generated by distributing compact Plummer spheres uniformly over a spherical volume of radius R_0. The total stellar mass distributed in this way is always the lower photometric mass estimate of $M_* \approx 10^4 M_\odot$ for HD97950, as motivated by Banerjee and Kroupa (2014); see Sect. 6.2.3.3. This fashion of initial subclustering is an idealization and extrapolation of what is found in the largest SPH calculations of cluster formation to date (Bate 2009, 2012; Girichidis et al. 2011) (see Sect. 6.1). As discussed in Sect. 6.2.2.1, the initial half-mass radii, $r_h(0)$, of these Plummer subclusters are taken typically between 0.1 and 0.3 pc, in accordance with the observed widths of these highly compact molecular-cloud filaments (André et al. 2011; Schneider et al. 2012). Such compactness of the subclusters is also consistent with those observed in stellar complexes, e.g., in the Taurus-Auriga (Palla and Stahler 2002). However, in some calculations, larger $r_h(0)$s are also used (see Table 6.4).

The number of subclusters, n, over which the $M_* \approx 10^4 M_\odot$ is subdivided has to be chosen somewhat arbitrarily. To keep a broad range of possibilities, two primary cases of the initial subdivision of the total stellar mass are considered. The "blobby" (type A) systems comprise 10 subclusters of $M_{\rm cl}(0) \approx 10^3 M_\odot$ each. Panels 1, 2, 4 and 6 of Fig. 6.14 are examples of such initial systems. Note that in this and all the subsequent figures, the panels are numbered left-to-right, top-to-bottom, unless stated otherwise. The "grainy" (type B) systems comprise $\approx$ 150 subclusters with

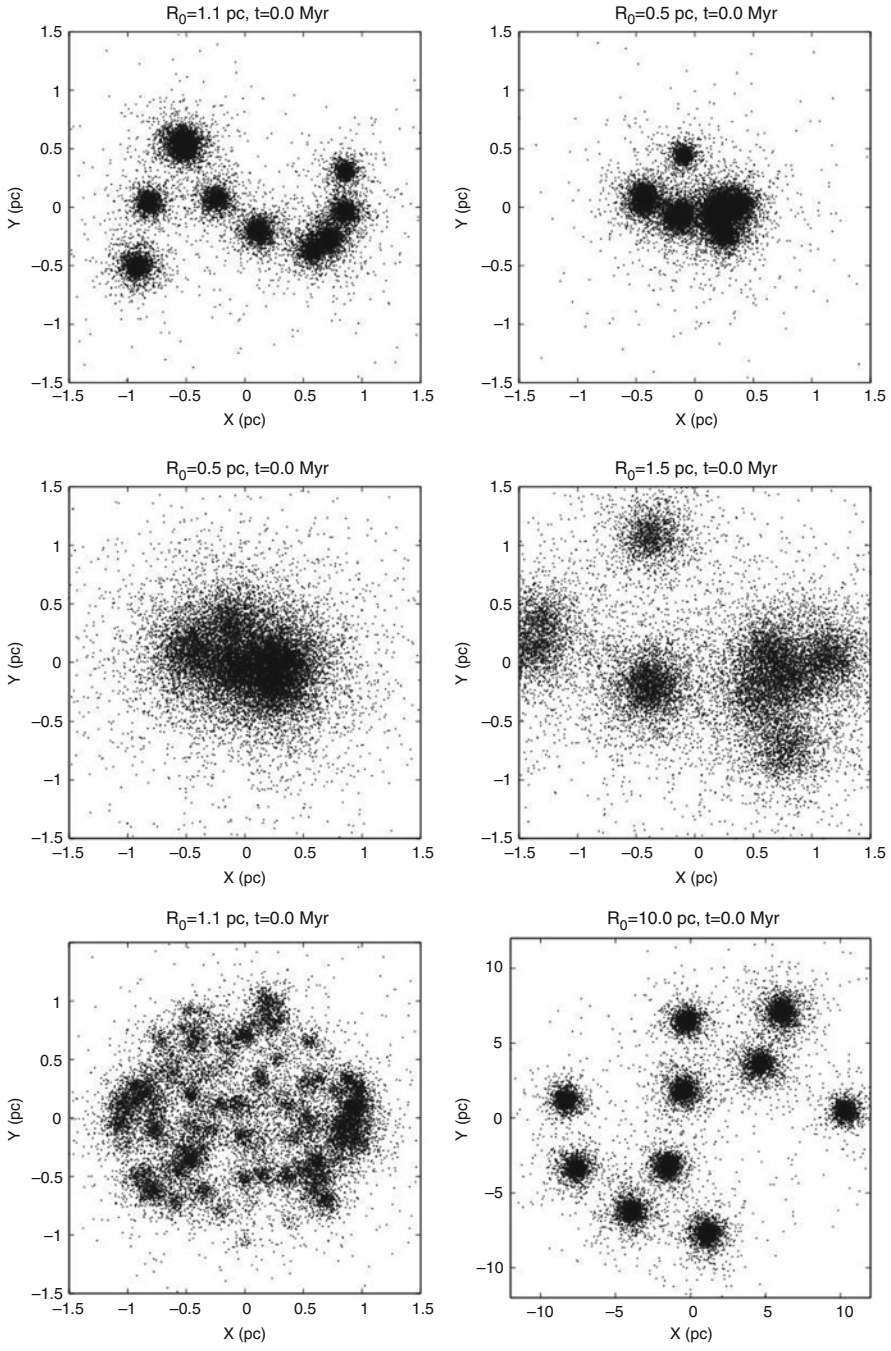

Fig. 6.14 The primary varieties of the *initial* configurations considered in Sect. 6.3, shown in projection. Here, the panels are numbered left-to-right, top-to-bottom. In each case, a set of Plummer spheres (subclusters) are uniformly distributed over a spherical volume of radius

mass range $10M_\odot \lesssim M_{\rm cl}(0) \lesssim 100M_\odot$ summing up to $M_* \approx 10^4 M_\odot$. The mode of initial subdivision does not influence the key inferences from these calculations.

The initial spanning radius, R_0, is taken over a wide range, viz., 0.5 pc $\lesssim R_0 \lesssim$ 10.0 pc, to explore the wide range of molecular cloud densities (see below) and spatial extents as observed in star-forming regions and stellar complexes. Table 6.4 provides a comprehensive list of the initial conditions for the computations in Banerjee and Kroupa (2015). The detailed nomenclature of the computed model, in its first column, is explained in Table 6.4 and the corresponding short names, in the second column, are self-explanatory.

As explained in Sect. 6.2.2.1, the proto-stellar mass function is taken to be canonical but without any upper bound. This would cause the IMF of the merged cluster, with stellar mass $M_*(\equiv M_{\rm cl})$, also to be canonical as often observed in VYMCs. Note that the gas accretion and the dynamical processes mostly determine the massive tail of the IMF and also set the maximum stellar mass, $m_{\rm max}$, of the *final* cluster, as seen in hydrodynamic calculations (e.g., Klessen et al. 1998; Girichidis et al. 2011). This gives rise to an $m_{\rm max}-M_{\rm cl}$ relation that is consistent with that found from observations (Weidner and Kroupa 2004; Weidner et al. 2013a). Note that if the $m_{\rm max} - M_{\rm cl}$ relation applies to the pre-merger subclusters, then the $m_{\rm max} - M_{\rm cl}$ relation for the final cluster will show features arising from the merging process (Weidner et al. 2010, 2013a).

All subclusters are initially at rest w.r.t. the centre of mass (COM) of the stellar system. While this condition is again an idealization, it is consistent with the results of detailed hydrodynamic computations in which the system(s) of subclusters formed is(are) typically sub-virial. Also, for the ease of computing, primordial binaries are excluded from these calculations. Test calculations show that primordial binaries do not influence the subcluster merging process significantly. The subclusters are generated using the `MCLUSTER` utility (Küpper et al. 2011) which is integrated in a special program that generates the overall subcluster system with the intended parameters.

The dense residual molecular cloud is represented by a background, external gravitational potential of a Plummer mass distribution which declines exponentially as discussed in Sect. 6.2.2. In this way the overall dynamical effect of the molecular cloud is included (as in the previous studies). In order to compare with the previous studies (Kroupa et al. 2001; Banerjee and Kroupa 2014), we adopt a local SFE of

Fig. 6.14 (continued) R_0, totalling a stellar mass of $M_* \approx 10000 M_\odot$. Panels 1, 2, 3, 4 and 6 are examples of type A or "blobby" systems containing ten subclusters of $m_{\rm cl}(0) \approx 10^3 M_\odot$ each. With smaller R_0, the subclusters overlap more with each other (c.f. , panels 1 and 2 with subcluster half-mass radius $r_h(0) \approx 0.1$ pc and panels 3 and 4 with $r_h(0) \approx 0.3$ pc). This is also true for increasing $r_h(0)$ (c.f. , panels 1 and 4). Panel 5 is an example of type B or "grainy" initial configuration containing ≈150 subclusters of mass range $10M_\odot \lesssim m_{\rm cl}(0) \lesssim 100M_\odot$. While panels 1–5 are examples of "compact" configurations, for which $R_0 \leq 2.5$ pc, panel 6, with $R_0 = 10$ pc, represents an "extended" configuration where the subclusters are much more distinct. See Sect. 6.3 for details of the initial setups. These panels are reproduced from Banerjee and Kroupa (2015)

$\epsilon \approx 33\%$ within the span of the subclusters, R_0. Such an SFE is as well consistent with those obtained from self-regulated hydrodynamic calculations and also with observations of embedded systems in the solar neighbourhood (see Sects. 6.1 and 6.2.2.1). Hence, the geometric/density centre of the Plummer gas sphere is coincident with the COM of the initial stellar system and its half-mass radius is equal to R_0 which contain $2M_*$ mass, giving $\epsilon = 1/3$ within R_0. For the entire Plummer cloud (of $4M_*$), $\epsilon = 1/5$. Inserting the adopted value $M_* = 10^4 M_\odot$ (see above), one gets $3 \times 10^4 M_\odot$ (gas + stars) within R_0. This gives an ONC-like $\rho_g \approx 6 \times 10^3 M_\odot$ pc^{-3} gas density for $R_0 = 1.06$ pc and $\approx 1/1000$th of this for $R_0 = 10$ pc which is appropriate for, e.g., the Taurus-Auriga complex.

6.3.1 General Evolutionary Properties of Subcluster Systems

As discussed in Sect. 6.2.1, the subclusters pass through each other for the first time at the system's potential minimum in a time t_{in} as given by Eq. (6.6). The final merger of the subclusters, however, is completed after an additional violent relaxation time, $t_{\rm vrx}$, which can be several subcluster orbital times. During this time, the orbital energy of the subclusters is dissipated, in multiple mutual passes, in the individual stellar orbits; this corresponds to the re-virialization process in initially monolithic systems (see Sect. 6.2). Both $t_{\rm in}$ and $t_{\rm vrx}$ increase with the initial span of the subclusters R_0 and hence the time for forming the final merged, (near) spherical cluster.

Table 6.4 summarizes the evolution (in Myr) of the subcluster systems of type A and B (see above) with increasing R_0 and in presence and absence of a gas potential (see above). Only the primary templates are included here which are computed using `NBODY6`. For description purposes, the evolving morphology of the stellar system is divided into four categories as in Table 6.3. All computed configurations initiate as SUB and evolve via the intermediate CHas phase to the final CH cluster in dynamical equilibrium. $R_0 \lesssim 1$ pc systems attain a CH structure in $t \lesssim 1$ Myr without a gas potential. On the other hand, initially wider configurations remain SUB at $t = 1$ Myr even with the gas potential and most of them do not attain the CH phase even in 2 Myr. In all such calculations, a negligible fraction of stars escape

Table 6.3 A basic classification of the different morphologies in the spatial distribution of stars that can occur in the process of subcluster merging

Morphology	Abbreviation
Substructured	SUB
Core + asymmetric and/or substructured halo	CHas
Core − halo with near spherical symmetry	CH
Core + halo containing satellite clusters	CHsat

These morphologies appear in the models computed here (Sect. 6.3). Note that the distinctions among these morphologies are only qualitative and are made for the ease of descriptions. This table is reproduced from Banerjee and Kroupa (2015)

Table 6.4 An overview of the evolutionary sequences of the primary systems as computed here (Sect. 6.3)

Config. name	Short name	Without gas potential			With gas potential ($\epsilon \approx 0.3$)		
m1000r0.1R1.1N10[a]	A-Ia	0.2,SUB	0.6,CHas	1.0,CH	0.2,SUB	0.6,CHas	1.0,CH
m1000r0.3R1.1N10	A-Ib	0.2,SUB	0.6,CHas	1.0,CHas	0.2,SUB	0.6,CHas	1.0,CHas
m1000r0.1R2.5N10	A-IIa	0.6,SUB	1.0,SUB	2.0,CH	0.6,SUB	1.0,CHsat	2.0,CHas
m1000r0.3R2.5N10	A-IIb	0.6,SUB	1.0,SUB	2.0,CHas	0.6,SUB	1.0,CHsat	2.0,CHas
m10-150r0.01-0.1R1.1N150[b]	B-Ic	0.2,SUB	0.6,CHas	1.0,CH	0.2,SUB	0.6,CHas	1.0,CHas
m10-150r0.1R1.1N150	B-Ia	0.2,SUB	0.6,CHas	1.0,CH	0.2,SUB	0.6,CHas	1.0,CHas
m10-150r0.1R2.5N150	B-IIa	0.6,SUB	1.0,SUB	2.0,CHas	0.6,SUB	1.0,CHas	2.0,CHas
m1000r0.5-1.0R5.0N10	A-IIId	1.0,SUB	2.0,SUB	3.0,CHas	1.0,CHsat	2.0,CHsat	3.0,CHsat
m1000r0.5-1.0R10.0N10	A-IVd	1.0,SUB	2.0,SUB	3.0,SUB	1.0,SUB	2.0,SUB	3.0,CHsat

A particular row indicates how the morphology (see Table 6.3) of the corresponding system evolves with evolutionary time (in Myr as indicated by the numerical values along the columns 3–5 and 6–8), for systems both without and with a background gas potential (see text). As expected, the systems, in general, evolve from substructured to a core-halo configuration with a timescale that increases with increasing initial extent R_0. See text for details. This table is reproduced from Banerjee and Kroupa (2015).

[a] mxryRzNn implies an initial system (at $t = 0$) comprising of N$= n$ Plummer clusters, each of mass m$= m_{\rm cl}(0) = xM_\odot$ and half-mass radius r$= r_h(0) = y$ pc, distributed uniformly over a spherical volume of radius R$= R_0 = z$ pc

[b] Further, when a range of values $x1 - x2$ is used instead of a single value, it implies that the corresponding quantity is uniformly distributed over $[x1, x2]$ at $t = 0$

the system during the infall and the merger process. In other words, the total bound stellar mass M_* remains nearly unaltered as the system evolves from SUB to CH configuration.

Figure 6.15 shows the snapshots at $t \approx 1$ Myr for a set of A-type configurations (Table 6.4) falling from increasing R_0 (without background gas potentials). With R_0, the morphology at 1 Myr changes from being CH, CHas to SUB. For $R_0 \gtrsim 2$ pc, the structure at 1 Myr substantially deviates from spherical symmetry (and dynamical equilibrium).

It is worth noting that due to energy conservation the size of the final cluster in dynamical equilibrium can be simply related to that of the initial subclusters (of equal or similar size and mass) as (Banerjee and Kroupa 2015),

$$\frac{1}{2R_*} \approx \frac{1}{2nR_{\rm cl}} + \frac{1}{R_0}. \tag{6.11}$$

Here, R_* is the half-mass radius of the final cluster and $R_{\rm cl}$ is that for the initial subclusters.

> The morphology of a gravitationally bound stellar population (of a given total mass) at a given age depends on the initial length scale over which the population is hatched (i.e., from the mutual separation from which they fall in the resultant potential well). The dynamical timescale of the stellar population is the key in determining the morphology and length scale of the stellar distribution at the epoch of observation. A sufficiently spread-out distribution can remain highly substructured for 10 s of Myr. On the other hand, a spherical massive star cluster in dynamical equilibrium can form out of a closely distributed (typically $\lesssim$2 pc) but highly substructured stellar population in $<$1 Myr.

6.3.2 *Comparison with NGC 3603 Young Cluster*

To assemble a HD97950-like star cluster by hierarchical merging of subclusters, the necessary but not sufficient condition is to arrive at a CH configuration in $t \lesssim 1$ Myr. The above calculations imply that to have a CH morphology at 1 Myr, one should have $R_0 \lesssim 2$ pc with or without a gas potential (c.f. Fig. 6.15). As discussed in Sect. 6.2.1, the gas potential would actually delay the approach to a CH configuration. How does this final cluster compare with the observed HD97950 cluster?

All the configurations, *without* the gas potential, that become CH in $t \lesssim 1$ Myr are found to form clusters that are much more dense and compact compared to the observed HD97950 profile (Harayama et al. 2008) at $t \approx 1$ Myr. This is found to be true irrespective of the mode of subdivision of the initial stellar mass M_*

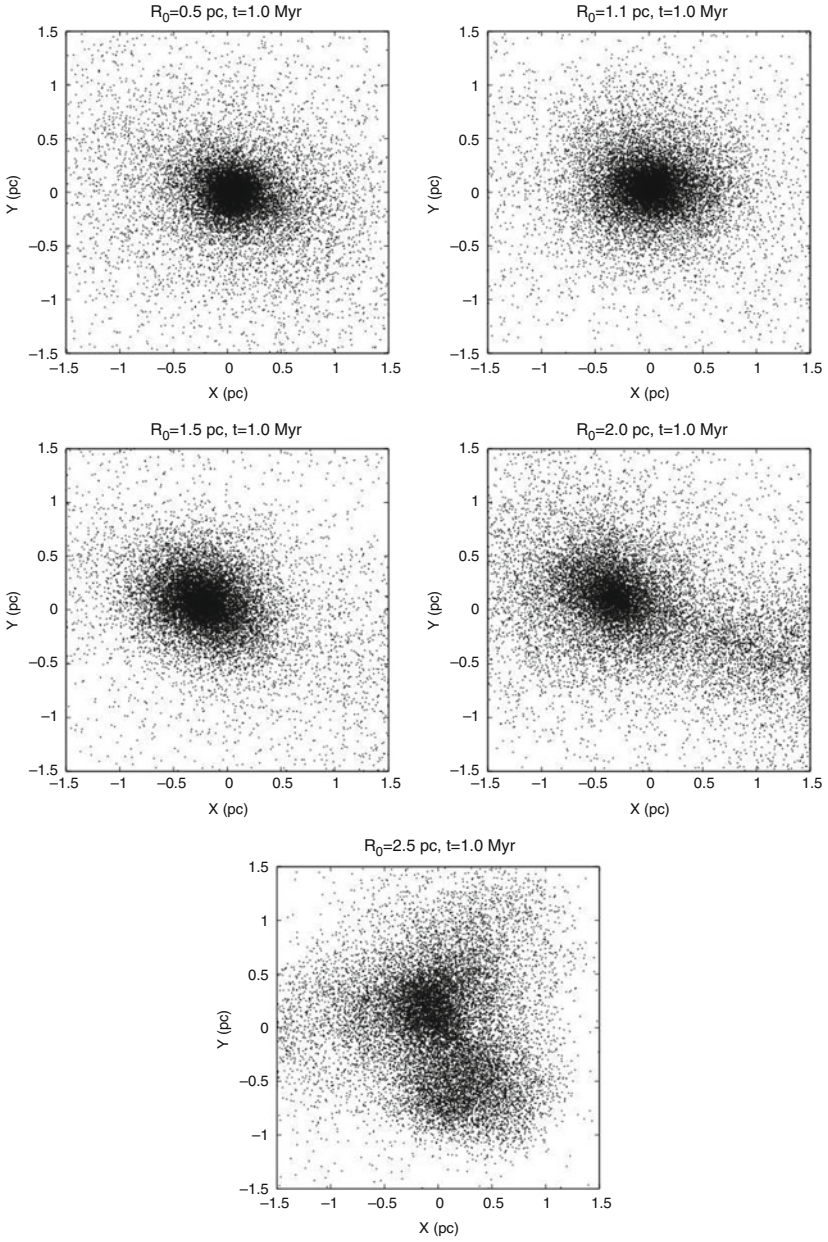

Fig. 6.15 Configurations obtained at $t \approx 1$ Myr with increasing initial span R_0 (without background gas potential). With increasing R_0, the system's morphology at $t \approx 1$ Myr changes from being near-spherical core-halo (CH; panels 1, 2; numbered left-to-right, top-to-bottom), asymmetric core-halo (CHas; panels 3, 4) to substructured (SUB; panel 5). For $R_0 \gtrsim 2$ pc (panels 4, 5), the stellar system is still well in the process of merging at $t \approx 1$ Myr after the subclusters' first pericentre crossings (i.e., it is in the violent relaxation phase $t_{\rm in} < t < t_{\rm in} + t_{vrx}$; see Sect. 6.3.1). These panels are reproduced from Banerjee and Kroupa (2015)

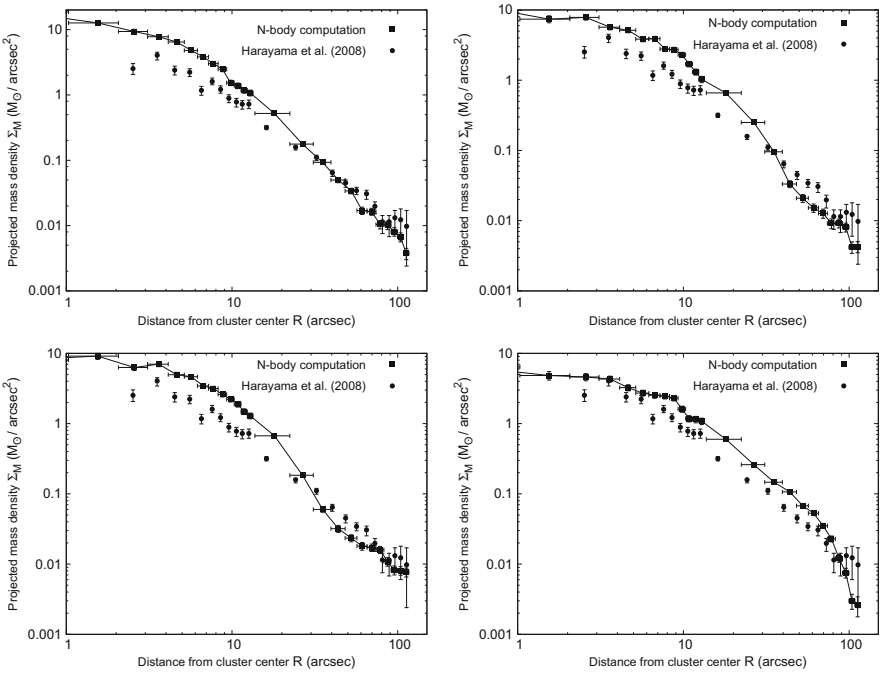

Fig. 6.16 Examples of surface mass-density profiles at $t \approx 1$ Myr for those computed configurations (*filled squares* connected with *solid line*) which evolve to form a star cluster with near-spherical core-halo structure (the CH-type morphology; see Table 6.3) within $t < 1$ Myr, in absence of a background gas potential. These computed profiles are significantly more compact and centrally overdense than that observed in HD97950 (Harayama et al. 2008; *filled circles*). For HD97950 $1'' \approx 0.03$ pc. These panels are reproduced from Banerjee and Kroupa (2015)

(c.f. Table 6.4). The latter fact can be expected from Eq. (6.11). This is demonstrated in Fig. 6.16. Note that all these calculations are for $M_* \approx 10000 M_\odot$ which is the lower mass limit of HD97950. For larger M_*, the assembled system will be even more overdense since the length scale of the final merged cluster, R_*, is nearly independent of the total stellar mass M_* (c.f. Eq. (6.11)). From test calculations, it is also found that the "heating effect" of primordial binaries and mass loss due to stellar winds do *not* expand and dilute the merged cluster's centre sufficiently.

One way to dramatically expand a star cluster, however, is to subject it to a substantial gas expulsion on a timescale of the order of its dynamical time, as discussed in the above sections. Figure 6.17 shows the computed stellar mass-density profiles at $t \approx 1$ Myr for similar calculations but including gas expulsion with parameters as discussed in Sect. 6.2.2.1. As in Sect. 6.2.3.3, they agree reasonably with the observed profile of HD97950 (Harayama et al. 2008), particularly in the inner regions. Note that in Fig. 6.17, the "natural" matchings with the observed profile are obtained *by simply overlaying it with the computed profiles at 1 Myr*

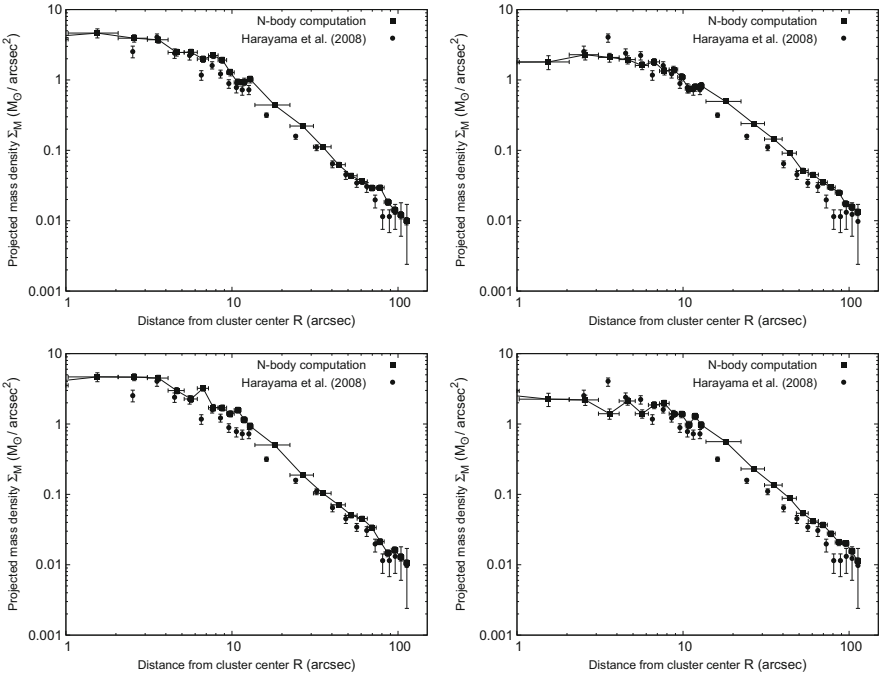

Fig. 6.17 Examples of surface mass-density profiles at $t \approx 1$ Myr for computed post-gas-expulsion configurations. Here, the systems evolve in a background residual gas potential (see Sect. 6.3) to form a star cluster with near-spherical core-halo structure (the CH-type morphology; see Table 6.3) within $t < 1$ Myr followed by residual gas dispersal at $\tau_d \approx 0.6$ Myr. The legends are the same as in Fig. 6.16. All these computed profiles agree well with the observed one for HD97950. These panels are reproduced from Banerjee and Kroupa (2015)

without any scaling or fitting, as in Banerjee and Kroupa (2014). The King-fit parameters to the observed and the computed profiles are also found to agree fairly.

We can now summarize the key inferences in the study discussed in this section, in logical sequence, as follows:

- A system of subclusters of total stellar mass $M_* \approx 10^4 M_\odot$ assemble into a (near) spherical core-halo star cluster by the age of HD97950 (i.e., in $t < 1$ Myr) provided these subclusters are largely born over a region of scale length more compact than $R_0 \lesssim 2$ pc. This can happen, e.g., in an intense starburst event at a dense "spot" in a molecular cloud.
- The initial sizes of the subclusters are constrained by the compact sections of molecular gas filaments or filament junctions which, in turn, determines the compactness of the final assembled cluster. Therefore, the mass density over the central region (within a virial radius) of the merged cluster is determined by the total stellar mass that is involved in its assembly.

- A "dry" merger of subclusters, i.e., infall in absence of any residual molecular gas (all gas consumed into stars) always leads to a star cluster that is centrally overdense w.r.t. HD97950, even for the observed lower mass limit $M_* \approx 10^4 M_\odot$. This holds irrespective of the initial mode of subclustering.
- A substantial residual gas expulsion ($\approx$70%) after the formation of the merged system expands the latter to obtain a cluster profile that is consistent with the observed HD97950. With the lower stellar mass limit $M_* \approx 10^4 M_\odot$ and an SFE of $\epsilon \approx$30%, the observed surface mass density profile of HD97950 can be fairly and optimally reproduced.

Notably, recent multi-wavelength observations of the Pismis 24 cluster of NGC 6357 (Massi et al. 2015) indicate that this cluster (age 1–3 Myr) contains distinct substructures which must have formed out of dense gas clumps packed within $\approx$1 pc radius. A similarly close-packed stellar substructures are found in the W3 complex (Román-Zúniga et al. 2015). Jaehnig et al. (2015) also find that the stellar distribution in young clusters (1–3 Myr) tend to smoothen out with age and local stellar density. This indicates an appearance of these systems as closely packed stellar overdensities which disappear on a dynamical timescale as seen above.

In the context of any scenario that involves infall and merger of subclusters in their parent gas cloud, it is important to keep in mind that the *effective* SFE at the location of the merger (deepest part of the potential well, see above) can be much higher than 30%, depending on the stellar concentration in the newly merged cluster. This is true for the calculations presented in this section also. Note that this enhanced SFE is essentially a "population effect" and does not reflect that with which the star formation has actually taken place (i.e., SFE within the gas clump(s)). The latter would be much smaller; $\lesssim$30% (see Sect. 6.2.2.1).

NGC 3603 young cluster (HD97950) has formed essentially monolithically followed by a substantial and violent gas dispersal. The initial monolithic stellar distribution has either formed in situ or has been assembled "promptly" (in $\lesssim$1 Myr) from closely packed (within $\lesssim$2 pc) less massive stellar clusters (subclusters). Both scenarios are consistent with the formation of HD97950's entire stellar population in a single starburst of very short ($\lesssim 10^5$ Myr) duration.

6.4 Globular Clusters and the Stellar IMF

The Milky Way (hereafter MW) contains approximately 160 globular clusters (hereafter GCs; see Harris 1996 for a compilation) most of which are nearly as old as the Universe. A major hot topic in astrophysics is to understand their birth and initial conditions. Here a discussion is provided which is consistent with and which is also based on the information gleaned from VYMCs as discussed in the previous sections.

Globular clusters appear to form a separate population of star clusters from those discussed above. However, Larsen (2002) has shown that star cluster formation extends from low stellar masses, $M_{\rm cl} \lesssim 10^3 M_\odot$, to the most massive very young clusters observed in the nearby universe in interacting galaxies ($M_{\rm cl} \gtrsim 10^5 M_\odot$) without a detectable change in their distribution with luminosity. It appears that star cluster formation is a continuous process in cluster mass, and that this mass distribution extends to high, GC-type masses in galaxies with high star formation rates (SFRs; Weidner et al. 2004; Randriamanakoto et al. 2013). However, three mass ranges are evident within each of which generically different physical processes play a role when clusters form (Kroupa and Boily 2002): low mass clusters ($<$ few $10^2 M_\odot$ in stars) do not have O-stars (Weidner et al. 2013a) such that they are more likely to loose their residual gas adiabatically. Intermediate-mass clusters (few $10^2 M_\odot$ to $\approx 10^5 M_\odot$) contain one to many O-stars (Weidner et al. 2013a) which photoionize the residual gas and expel it probably explosively with a disruptive effect on the stellar component, while very massive clusters ($M > 10^5 M_\odot$) have, with increasing mass, an increasingly deep potential such that even photo-ionized plasma may not be able to leave the cluster within many initial crossing times (Baumgardt et al. 2008). These three regimes lead to different reactions of the clusters to the blow-out of the residual gas, such that an initially power-law mass function of embedded clusters evolves to a form with a turnover or flattening near $10^5 M_\odot$. Globular cluster-mass young clusters survive with a larger fraction of their stars and do not dissolve within a Hubble time (Elmegreen and Efremov 1997; Kroupa and Boily 2002; Baumgardt et al. 2008).

Such GC-precursors would have formed with very high densities, as the study by (Marks and Kroupa 2010) suggests. This work is based on inferring the initial conditions of GCs subject to the constraint that their IMF for stars $\lesssim 1 M_\odot$ is canonical. Since GCs with a low concentration are observed to have a deficit of low-mass stars (De Marchi et al. 2007), and because neither a theoretical explanation through star formation is evident for this observation nor can it be explained with secular cluster evolution (fig.4 in Leigh et al. 2013), it is possible to infer that GCs may have formed mass segregated and increasingly compact with decreasing metallicity and that their initial radii are broadly consistent with Eq. (6.9).

Consistency is also found independently by the first-ever N-body computation of two low-concentration GCs by Zonoozi et al. (2011, 2014). This work confirms that such GCs must have formed mass segregated and must have lost a substantial part of their low-mass stellar population during emergence from their embedded state. This leads to an understanding of the star-formation events within $<$1 Gyr, as the first proto-Galactic gas cloud collapsed to form the MW population II halo and its associated present-day GCs at a time when the MW did not exist as the Galaxy (Marks and Kroupa 2010).

But the results also imply that in order for the young GCs to emerge with a "damaged" (low-mass depleted) stellar mass function and low concentration, the IMF may have been increasingly top heavy with increasing density and decreasing metallicity (Marks et al. 2012). The remarkable result here is that these dependencies are well-consistent with the entirely independent results on the

dependence of the IMF with density from the dynamical mass-to-light ratios and, independently, from the X-ray-source population of ultracompact dwarf galaxies (UCDs) by Dabringhausen et al. (2009, 2010, 2012). According to these results, the stellar IMF is canonical for SFR densities SFRD $< 0.1 M_\odot/(\mathrm{pc}^3\,\mathrm{yr})$ and becomes increasingly top-heavy for stellar mass $\gtrsim 1 M_\odot$ with increasing density and decreasing metallicity (see Eq. (4.65) in Kroupa et al. 2013). These constraints on the variation of the stellar IMF with the physical conditions of star-forming cloud cores on scales of a parsec and timescales of a Myr yield dependencies of M/L ratios of stellar populations which appear to be consistent with the observed values for the GCs of the Andromeda (Strader et al. 2011), as well as the high rate of type II supernovae in ULIRGs (Dabringhausen et al. 2012), as well as with the observed top-heavy galaxy-wide IMFs in star-forming galaxies within the IGIMF theory (Gunawardhana et al. 2011; Weidner et al. 2013b).[8] Leigh et al. (2015) have demonstrated that the initial population of binary stars in very young GCs must have been very similar to the presently occurring binary population in the Milky Way, and the currently available result that the stellar IMF below a few $M_\odot$ was also largely canonical (Marks et al. 2012) is consistent with this result and thus with the notion of an inherently largely universal process and outcome of star formation.

The generic formation of extremely massive, GC-like very young clusters is thus being understood increasingly better, but the detailed physical processes within these extremely dense (see Fig. 6.18) star-burst clusters remain a subject of intense study with major unsolved problems. In particular, the processes acting during the first few Myr in the highly dense plasma-star mixture, which may be pressurized from the ambient interstellar medium (ISM) in strongly star-bursting pre-galactic environments or in interacting galaxies, remain largely not understood (e.g., Krause et al. 2013). The fact that increasingly massive GCs show evidence for increasingly complex metal abundance anti-correlations and spreads are rather certainly due to these extreme physical conditions (Georgiev et al. 2009; Charbonnel et al. 2014; also see Jiang et al. 2014 and the references therein). But even the Hubble-time long dynamical evolution of GCs with a significant initial binary population may lead to hitherto not appreciated effects on the present-day chemical properties of GC stars (Jiang et al. 2014), while even intermediate-mass clusters and in particular very massive clusters may re-accrete ISM into their potential wells and this may occur repeatedly depending on the orbits of the clusters and of the ISM (Pflamm-Altenburg and Kroupa 2009).

[8] From purely dynamical considerations, Banerjee and Kroupa (2012) also infer that VYMCs, in particular R136, should have born with the massive end of their IMF top-heavy. Continued dynamical interactions, resulting in mergers among the most massive stellar members in a massive cluster like R136 ($\approx 10^5 M_\odot$), can make the stellar mass function top-heavy even at the present day (Banerjee et al. 2012b).

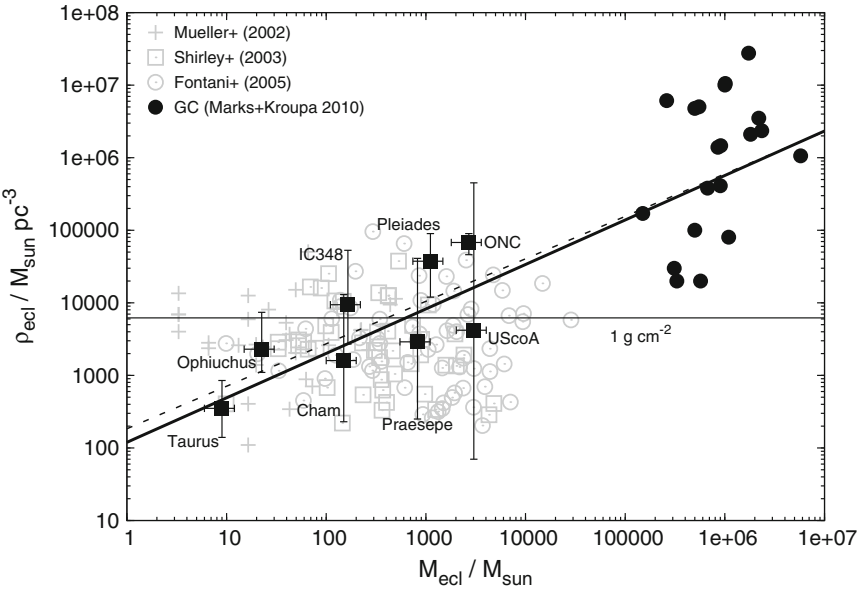

Fig. 6.18 Constraints on the initial volume-densities within the half-mass radius for the seven clusters (*filled squares*) versus the initial stellar mass as obtained by Marks and Kroupa (2012). The indicated errors in mass correspond to the observationally inferred present-day mass on the left end of a bar and two times the present-day mass on its right end, to be understood as an estimator of the possible range of initial mass. The *filled circles* are Galactic GCs. Underlaid as *grey symbols* are data of molecular cloud clumps as collated by Parmentier and Kroupa (2011). The clump masses are multiplied with an SFE of 1/3 to be comparable with the stellar masses and densities inferred in Marks and Kroupa (2012). The *thin solid line* is the threshold for massive star formation (Krumholz and McKee 2008). The *thick solid line* is a least-squares fit to both the young cluster and GC values, implying that there exists a mass-radius relation for star cluster-forming cloud clumps. The *dashed line* shows the same when the GCs are excluded from the fit. This figure is reproduced from Marks and Kroupa (2012)

6.5 Concluding Remarks: Embedded vs. Exposed Young Clusters

How VYMCs form is still an open question and even may not have a unique answer. As seen above, there are two primary directions of research that seek answer(s) to this question. The most physically detailed hydrodynamic calculations so far (including feedback; see Sect. 6.1), that led to star formation, currently range from a single proto-star to about $50 M_{\odot}$ gas spheres, i.e., less massive than the heaviest stellar member found in VYMCs (typically $> 100 M_{\odot}$). Scaling the inferences all the way to the VYMC mass ($> 10^4 M_{\odot}$) and size ($\approx$ pc) is grossly unreliable since the physical behaviour of the feedback processes (radiation, magnetic field) are scarcely understood.

On the other hand, dynamical modelling of monolithic stellar systems, using direct N-body calculations can reach up to several $10^5 M_\odot$, with the current technology. As seen in the above sections, the main drawback in such studies is the simplified treatment of the residual gas (see Sect. 6.2.2). It is impressive, though, that such an approach remarkably reproduces the detailed observed properties of several young star clusters (see Sect. 6.2.3). This is also true if VYMCs (and young clusters in general) can be considered as formed via "prompt merging" of smaller subclusters in a background gas potential (see Sect. 6.3). In other words, a 1–3 Myr old VYMC can as well form from a highly subclustered stellar distribution, far from having spherical symmetry, provided the dynamical time (infall + violent relaxation; see Sect. 6.2.1) for the initial stellar system is sufficiently small. Note that the studies mentioned in Sects. 6.2.3 and 6.3 are currently the only theoretical studies in the massive cluster scale that provide direct and detailed agreements with observed clusters.

These results imply that once "blasted off", the details of the gas hydrodynamics do not critically influence the dynamical evolution of the stellar system as long as cluster ages of the order of Myr are concerned. The key point is whether a rapid gas dispersal, with timescale of the order of stellar crossing times (c.f. Table 6.1), should always occur in reality. The issue arises since compact embedded systems of several Myr age appear to be found throughout our Galaxy. An interesting example, in this respect, is the embedded W3 Main (hereafter W3M) cluster (Bik et al. 2014; Feigelson and Townsley 2008). Located $\approx$2 kpc from the Sun, this is the most embedded region of the W3/W4/W5 star-forming complex in the outer Galaxy, containing hyper-compact to extended HII regions. From the age estimates of the most massive (O-)star (IRS2), it can be inferred that W3M is forming stars since 2–3 Myr at least (Bik et al. 2014). It is argued that triggering as well as dynamical effects might keep the star formation ongoing in this system (Feigelson and Townsley 2008). In particular, there are observational evidences that W3M is triggered externally by an expanding bubble from an OB association (Oey et al. 2005) and also internally by swept away material from OB stars (Wang et al. 2012). There are several similar-aged embedded clusters (e.g., W33 complex, Messineo et al. 2015), but W3M is among the most well-studied ones.

The existence of such systems appear to imply that not all forming stellar assemblies expel their residual gas promptly in an "explosive" (Kroupa 2005) manner. For those cases this does happen, a VYMC like NGC 3603 is born, otherwise one is left with a "VYMC-aged" embedded system like W3M. For the latter case, the SFE would keep increasing with time as an increasing amount of gas is converted into and/or accreted onto proto-stars. It is currently unclear which physical processes (or absence of them) would delay the prompt gas expulsion. It could be the inherent properties of the natal gas (e.g., its chemical abundances) and as well the surroundings that determines the fate of the star-forming clump. The presence or absence of ionizing O-stars could have been a plausible determining factor at a first glance, but several OB stars are found in W3M and other embedded clusters. The key question is as follows: *Despite the presence of ionizing OB stars in either case, why are some young star clusters (nearly) gas-free at an age of a*

few Myr and why are some others apparently deeply embedded in molecular gas at similar ages?

For an explosive gas expulsion, the (compact) HII regions should rapidly engulf the densest (most populous) parts of the molecular clouds within their lifetimes; typically < 1 Myr (see Sect. 6.2.2.1; Banerjee and Kroupa 2013). Hence, the embedded proto-stellar population (or a significant part of it) should form in one episode (i.e., with a small age spread) and within a compact enough region of the molecular cloud, typically < 1 pc (see Sect. 6.2.2.1; Banerjee and Kroupa 2013). The propagation of the (overlapped) HII region can be additionally powered by simultaneous presence of OB stars over a small region, further supporting compact and episodic star formation for VYMCs. An interesting example in this regard is the RCW 38 cluster (DeRose et al. 2009; Kuhn et al. 2014), which is as compact as ≈ 0.1 pc (Eric Feigelson: private communication) and where only the central region is gas free, indicating that the residual gas might have just begun being expelled from the cluster. Indeed, as seen in Sect. 6.2.3, N-body computations that reproduce present-day VYMCs begin from such initial conditions. The stellar distribution in W3M, on the other hand, is more extended, > 1 pc, and contains several compact HII zones (Bik et al. 2014). This may also indicate that this region has formed a number of compact embedded clusters containing O/B-stars (see, e.g., Testi et al. 1999). In future, more detailed observations will help to illuminate this possibility. Improved age estimates of the stellar population in W3M will be particularly important on this regard.

In other words, the fate of a newly hatched cluster might be governed by its scale length at birth. If the embedded stellar distribution is sufficiently compact (e.g., if formed at a molecular gas filament junction; see Sect. 6.2.2.1), the natal gas can be blown apart when the UCHII region(s) engulfs (and hence ionizes) the scale length (Churchwell 2002; Krumholz and Matzner 2009; Banerjee and Kroupa 2014). On the other hand, if the initial proto-stars are more widely distributed the gas may not be efficiently expelled and one is left with an embedded cluster. Of course, scale length may not be the only factor that determines if the gas expulsion "fails". The gas expulsion can fail if the propagation of the HII region from around OB stars is stalled for any reason so that the embedding gas is ionized at most locally. Of course, if the newborn assembly is not massive enough so that no OB stars are formed, the gas would not be expelled even if the assembly is highly compact. This could be the case with several compact, low-mass embedded clusters (see, e.g., Tapia et al. 2011). Note that a bimodal regime of cluster formation has been proposed earlier by Boily and Kroupa (2002) but in a somewhat different context.

If the fate of a newborn stellar assembly happens to depend on its length scale, a possibility as discussed above, the wider embedded systems can be expected to contain substructures. This is because, as seen in Sect. 6.3, the lifetime until which the substructures are erased to form a stellar cluster in dynamical equilibrium depends on the initial spatial span of the stellar distribution. This is consistent with the fact that substructures are found in many embedded clusters. If the embedded phase continues for a sufficiently long time the stellar system can virialize while remaining deeply embedded, as found recently (Foster et al. 2015). On the other

hand, for a sufficiently extended system, the substructure can remain even if the gas is largely dispersed, e.g., as seen in Cygnus OB2 (Wright et al. 2014).

Of course, it is important to re-consider the observationally inferred ages of the stellar members of the W3 Main and other embedded clusters *vis-á-vis* their distances, since age plays a crucial role in inferences such as above. This is true for gas-free VYMCs as well. For embedded clusters, the age estimates can be improved through even deeper and highly resolved observations, say, using *ALMA*. Such observations of dense molecular filaments and their junctions (or other sub-parsec scale dense structures) would reveal embedded clusters in them (or lack of them). For VYMCs, better parallax measurements with, e.g., *Gaia* would provide independent distance measurements that would improve their age estimates. It is as well important to better establish the depth of embedding of W3 Main and other embedded systems, in particular, whether the stellar system is actually embedded in gas or if it is a gas-free system inside or aside a molecular cloud, like, e.g., the ONC and NGC 3603. Increased detection of HII regions and as well mapping the gas velocities over and surrounding embedded clusters would help to resolve this. For lightly-embedded and exposed star clusters as well as for embedded clusters, ongoing surveys such as the *MYStIX* (Massive Young Star-Forming Complex Study in Infrared and X-ray; Feigelson et al. 2013) would improve their age estimates, where X-ray observations provide additional constraints on the individual stellar ages (Getman et al. 2014). More detailed observations of both embedded and exposed clusters is the key to answer the fundamental question raised above, without which no concrete conclusions regarding the differences between embedded and exposed young clusters can be drawn.

> The relation between exposed and embedded young clusters is currently unclear; the length scale over which the stellar population is hatched might play a role in determining whether the natal gas is expelled early (in < 1 Myr) or the stellar population remains embedded (slow gas dispersal and/or "gas consumption"). The detailed physical processes responsible for failing gas blow out in presence of the ionizing OB stars remain unclear. More detailed observations of embedded clusters like W3 Main is necessary to resolve this.

In summary, star formation is an intrinsically spatially and temporally correlated process which is evident to the astronomer as embedded clusters. The star formation process can be viewed as leading to a continuous distribution of embedded cluster masses where the most massive clusters, that can form, are constrained by the galaxy-wide SFR which, in turn, is controlled by the depth of the potential of the galaxy and thus the pressure in the turbulent interstellar medium (Elmegreen and Efremov 1997; Klessen 2001; Bonnell et al. 2011). VYMCs are a particularly shining part of this range of events, and GCs are the evolutionary fate of the most extreme VYMCs. The physics of the formation and of the emergence of VYMCs from their natal clouds carries through to the formation of GCs, but the extreme densities involved for them pose new and largely not-at-present-

understood challenges. It is therefore, broadly speaking, not surprising that GCs show complex properties which are not evident in VYMCs. Finally, it is thanks to the continued decade-long algorithmic and mathematical progress achieved by Sverre Aarseth and Seppo Mikkola that the astrophysical community has now access to realistic N-body codes which allow us to address the issues discussed here. With the continuously improving and universally adaptable software platform like the "AMUSE" (Portegies Zwart et al. 2008), such N-body calculations can be made even more realistic (e.g., introduce full hydrodynamical treatment) in foreseeable future.

References

Aarseth, S.J.: Gravitational N-Body Simulations. Cambridge University Press, Cambridge (2003)
Aarseth, S.J.: Mon. Not. R. Astron. Soc. **422**, 841 (2012)
Adams, F.C.: Astrophys. J. **542**, 964 (2000)
Adams, F.C., Fatuzzo, M.: Astrophys. J. **464**, 256 (1996)
Alves, J., Bouy, H.: Astron. Astrophys. **547**, A97 (2012)
Amaro-Seoane, P., Konstantinidis, S., Freitag, M.D., et al.: Astrophys. J. **782**, 97 (2014)
Andersen, M., Zinnecker, H., Moneti, A., et al.: Astrophys. J. **707**, 1347 (2009)
André, P., Meńshchikov, A., Koenyves, V., et al.: In: Alfaro Navarro, E.J., Gallego Calvente, A.T., Zapatero Osorio, M.R. (eds.) Stellar Clusters & Associations: A RIA Workshop on Gaia, vol. 321. IAA-CSIC, Granada (2011)
André, P., Di Francesco, J., Ward-Thompson, D., et al.: In: Beuther, H., Klessen, R., Dullemond, C., Henning, Th. (eds.) Protostars and Planets VI, p. 27. University of Arizona Press, Tucson (2014)
Banerjee, R.: Astron. Astrophys. (submitted, 2017). arXiv:1409.7584 (preprint)
Banerjee, S., Kroupa, P.: Astron. Astrophys. **547**, A23 (2012)
Banerjee, S., Kroupa, P.: Astrophys. J. **764**, 29 (2013)
Banerjee, S., Kroupa, P.: Astrophys. J. **787**, 158 (2014a)
Banerjee, S., Kroupa, P.: Mon. Not. R. Astron. Soc. **447**, 728 (2015)
Banerjee, S., Kroupa, P.: Astron. Astrophys. **597**, A28 (2017)
Banerjee, S., Baumgardt, H., Kroupa, P.: Mon. Not. R. Astron. Soc. **402**, 371 (2010)
Banerjee, S., Kroupa, P., Oh, S.: Astrophys. J. **746**, 15 (2012a)
Banerjee, S., Kroupa, P., Oh, S.: Mon. Not. R. Astron. Soc. **426**, 1416 (2012b)
Bastian, N., Silva-Villa, E.: Mon. Not. R. Astron. Soc. **431**, L122 (2013)
Bastian, N., Strader, J.: Mon. Not. R. Astron. Soc. **443**, 3594 (2014)
Bate, M.R.: Mon. Not. R. Astron. Soc. **392**, 590 (2009)
Bate, M.R.: Mon. Not. R. Astron. Soc. **419**, 3115 (2012)
Bate, M.R., Bonnell, I.A.: In: Lamers, H.J.G.L.M., Smith, L.J., Nota A. (eds.) The Formation and Evolution of Massive Young Star Clusters (ASP Conference Proceedings), vol. 322, p. 289. Astronomical Society of the Pacific, San Francisco (2004)
Bate, M.R., Tricco, T.S., Price, D.J.: Mon. Not. R. Astron. Soc. **437**, 77 (2014)
Baumgardt, H., Kroupa, P.: Mon. Not. R. Astron. Soc. **380**, 1589 (2007)
Baumgardt, H., Kroupa, P., Parmentier, G.: Mon. Not. R. Astron. Soc. **384**, 1231 (2008)
Bik, A., Stolte, A., Gennaro, M., et al.: Astron. Astrophys. **561**, A12 (2014)
Boily, C., Kroupa, P.: In: Grebel, E.K., Brandner, W. (eds.) Modes of Star Formation and the Origin of Field Populations (ASP Conference Proceedings), vol. 285, p. 141. Astronomical Society of the Pacific, San Francisco (2002)
Boily, C., Kroupa, P.: Mon. Not. R. Astron. Soc. **338**, 665 (2003a)

Boily, C., Kroupa, P.: Mon. Not. R. Astron. Soc. **338**, 673 (2003b)
Bonnell, I.A., Smith, R.J., Clark, P.C., Bate, M.R.: Mon. Not. R. Astron. Soc. **410**, 2339 (2011)
Brandner, W.: In: Beuther, H., et al. (eds.) Massive star formation: Observations confront Theory. ASP Conference Series (2008). arXiv:0803.1974 (preprint)
Brinkmann, N., Banerjee, S., Motwani, B., Kroupa, P.: Astron. Astrophys. **600**, A49 (2017)
Charbonnel, C., Chantereau, W., Krause, M., et al.: Astron. Astrophys. **569**, LL6 (2014)
Chini, R., Hoffmeister, V.H., Nasseri, A., et al.: Mon. Not. R. Astron. Soc. **424**, 1925 (2012)
Churchwell, E.: Annu. Rev. Astron. Astrophys. **40**, 27 (2002)
Crowther, P.A., Schnurr, O., Hirschi, R., et al.: Mon. Not. R. Astron. Soc. **408**, 731 (2010)
Dabringhausen, J., Kroupa, P., Baumgardt, H.: Mon. Not. R. Astron. Soc. **394**, 1529 (2009)
Dabringhausen, J., Fellhauer, M., Kroupa, P.: Mon. Not. R. Astron. Soc. **403**, 1054 (2010)
Dabringhausen, J., Kroupa, P., Pflamm-Altenburg, J., Mieske, S.: Astrophys. J. **747**, 72 (2012)
Dale, J.E., Ercolano, B., Bonnell, I.A.: Mon. Not. R. Astron. Soc. **451**, 5506 (2015)
De Marchi, G., Paresce, F., Pulone, L.: Astrophys. J. **656**, L65 (2007)
DeRose, K.L., Bourke, T.L., Gutermuth, R.A., et al.: Astron. J. **138**, 33 (2009)
Dib, S., Kim, J., Shadmehri, M.: Mon. Not. R. Astron. Soc. **381**, 40 (2007)
Duarte-Cabral, A., Dobbs, C.L., Peretto, N., et al.: Astron. Astrophys. **528**, A50 (2011)
Elmegreen, B.G., Efremov, Y.N.: Astrophys. J. **480**, 235 (1997)
Evans, C.J., Taylor, W.D., Hénault-Brunet, V., et al.: Astron. Astrophys. **530**, 108 (2011)
Feigelson, E.D., Townsley, L.K.: Astrophys. J. **673**, 354 (2008)
Feigelson, E.D., Townsley, L.K., Broos, P.S., et al.: Astrophys. J. Suppl. Ser. **209**, 26 (2013)
Fellhauer, M., Kroupa, P.: Astrophys. J. **630**, 879 (2005)
Foster, J.B., Cottaar, M., Covey, K.R., et al.: Astrophys. J. **799**, 136 (2015)
Fujii, M.S., Saitoh, T.R., Portegies Zwart, S.F.: Astrophys. J. **753**, 85 (2012)
Fukui, Y., Ohama, A., Hanaoka, N., et al.: Astrophys. J. **780**, 36 (2014)
Fukui, Y., Torii, K., Ohama, A., et al.: Astrophys. J. **820**, 26 (2016)
Furukawa, N., Dawson, J.R., Ohama, A., et al.: Astrophys. J. **696**, L11 (2009)
Gennaro, M., Goodwin, S.P., Parker, R.J., et al.: Mon. Not. R. Astron. Soc. (2017, accepted). arXiv:1708.04161 (Preprint)
Georgiev, I.Y., Hilker, M., Puzia, T.H., et al.: Mon. Not. R. Astron. Soc. **396**, 1075 (2009)
Getman, K.V., Feigelson, E.D., Kuhn M.A.: Astrophys. J. **787**, 109 (2014)
Geyer, M.P., Burkert, A.: Mon. Not. R. Astron. Soc. **323**, 988 (2001)
Girichidis, P., Federrath, C., Banerjee, R., Klessen, R.S.: Mon. Not. R. Astron. Soc. **413**, 2741 (2011)
Girichidis, P., Federrath, C., Allison, R., et al.: Mon. Not. R. Astron. Soc. **420**, 3264 (2012)
Gunawardhana, M.L.P., Hopkins, A.M., Sharp, R.G., et al.: Mon. Not. R. Astron. Soc. **415**, 1647 (2011)
Harayama, Y., Eisenhauer, F., Martins, F.: Astrophys. J. **675**, 1319 (2008)
Harris, W.E.: Astron. J. **112**, 1487 (1996)
Haworth, T.J., Tasker, E.J., Fukui, Y., et al.: Mon. Not. R. Astron. Soc. **450**, 10 (2015)
Heggie, D.C.: Mon. Not. R. Astron. Soc. **173**, 729 (1975)
Heggie, D.C., Hut, P.: The Gravitational Millon-Body Problem: A Multidisciplinary Approach to Star Cluster Dynamics. Cambridge University Press, Cambridge (2003)
Hénault-Brunet, V., Evans, C.J., Sana, H., et al.: Astron. Astrophys. **546**, A73 (2012)
Hennemann, M., Motte, F., Schneider, N., et al.: Astron. Astrophys. **543**, L3 (2012)
Hill, T., Motte, F., Didelon, P., et al.: Astron. Astrophys. **533**, A94 (2011)
Hillenbrand, L.A.: Astron. J. **113**, 1733 (1997)
Hillenbrand, L.A., Hartmann, L.W.: Astrophys. J. **492**, 540 (1998)
Hills, J.G.: Astron. J. **80**, 809 (1975)
Hills, J.G.: Astrophys. J. **235**, 986 (1980)
Hollyhead, K., Bastian, N., Adamo, A., et al.: Mon. Not. R. Astron. Soc. **449**, 1106 (2015)
Hurley, J.R., Pols, O.R., Tout, C.A.: Mon. Not. R. Astron. Soc. **315**, 543 (2000)
Jaehnig, K.O., Da Rio, N., Tan, J.C.: Astrophys. J. **798**, 126 (2015)
Jiang, D., Han, Z., Li, L.: Astrophys. J. **789**, 88 (2014)

Jones, B.F., Walker, M.F.: Astron. J. **95**, 1755 (1988)
Klessen, R.S.: Astrophys. J. **556**, 837 (2001)
Klessen, R.S., Burkert, A., Bate, M.R.: Astrophys. J. **501**, L205 (1998)
Krause, M., Charbonnel, C., Decressin, T., et al.: Astron. Astrophys. **552**, A121 (2013)
Kroupa, P.: Mon. Not. R. Astron. Soc. **277**, 1491 (1995a)
Kroupa, P.: Mon. Not. R. Astron. Soc. **277**, 1507 (1995b)
Kroupa, P.: Mon. Not. R. Astron. Soc. **300**, 200 (1998)
Kroupa, P.: Mon. Not. R. Astron. Soc. **322**, 231 (2001)
Kroupa, P.: In: Turon, C., OFlaherty, K.S., Perryman, M.A.C. (eds.) The Three-Dimensional Universe with Gaia (ESA SP-576), p. 629. ESA, Noordwijk (2005)
Kroupa, P., Boily, C.M.: Mon. Not. R. Astron. Soc. **336**, 1188 (2002)
Kroupa, P., Aarseth, S., Hurley, J.: Mon. Not. R. Astron. Soc. **321**, 699 (2001)
Kroupa, P., et al.: In: Oswalt, T.D., Gilmore, G. (eds.) Galactic Structure and Stellar Populations (Planets, Stars and Stellar Systems), vol. 5. Springer Science + Business Media, Dordrecht (2013)
Kruijssen, J.M.D.: Class. Quantum Grav. **31**, id. 244006 (2014)
Krumholz, M.R., Matzner C.D.: Astrophys. J. **703**, 1352 (2009)
Krumholz, M.R., McKee, C.F.: Nature **451**, 1082 (2008)
Krumholz, M.R., Bate, M.R., Arce, H.G., et al.: In: Beuther, H., Klessen, R., Dullemond, C., Henning, Th. (eds.) Protostars and Planets VI, p. 243. University of Arizona Press, Tucson (2014)
Kuhn, M.A., Feigelson, E.D., Getman K.V., et al.: Astrophys. J. **787**, 107 (2014)
Küpper, A.H.W., Maschberger, T., Baumgardt, H., Kroupa, P.: Mon. Not. R. Astron. Soc. **417**, 2300 (2011)
Lada, C.J., Lada, E.A.: Annu. Rev. Astron. Astrophys. **41**, 57 (2003)
Lada, C.J., Margulis, M., Dearborn, D.: Astrophys. J. **285**, 141 (1984)
Larsen, S.S.: Open, massive and globular clusters - part of the same family? In: Geisler, D., Grebel, E.K., Minniti, D. (eds.) Extragalactic Star Clusters. Proceedings of IAU Symposium 207, held in Pucon, 12-16 March 2001, p. 421. Astronomical Society of the Pacific, San Francisco (2002). http://esoads.eso.org/abs/2002IAUS..207..421L
Leigh, N., Giersz, M., Webb, J.J., et al.: Mon. Not. R. Astron. Soc. **436**, 3399 (2013)
Leigh, N.W.C., Giersz, M., Marks, M., et al.: Mon. Not. R. Astron. Soc. **446**, 226 (2015)
Longmore, S.N., Kruijssen, J.M.D., Bastian, N., et al.: In: Beuther, H., Klessen, R., Dullemond, C., Henning, Th. (eds.) Protostars and Planets VI, p. 291. University of Arizona Press, Tucson (2014)
Machida, M.N., Matsumoto, T.: Mon. Not. R. Astron. Soc. **421**, 588 (2012)
Malinen, J., Juvela, M., Rawlings, M.G., et al.: Astron. Astrophys. **544**, A50 (2012)
Marks, M., Kroupa, P.: Mon. Not. R. Astron. Soc. **406**, 2000 (2010)
Marks, M., Kroupa, P.: Astron. Astrophys. **543**, A8 (2012)
Marks, M., Kroupa, P., Dabringhausen, J., Pawlowski, M.S.: Mon. Not. R. Astron. Soc. **422**, 2246 (2012)
Marks, M., Leigh, N., Giersz, M., et al.: Mon. Not. R. Astron. Soc. **441**, 3503 (2014)
Massi, F., Giannetti, A., di Carlo, E.: Astron. Astrophys. **573**, id. A95 (2015)
Messineo, M., Clark, J.S., Figer, D.F., et al.: Astrophys. J. **805**, 110 (2015)
Oey, M.S., Watson, A.M., Kern, K., et al.: Astron. J. **129**, 393 (2005)
Oh, S., Kroupa, P.: Mon. Not. R. Astron. Soc. **424**, 65 (2012)
Oh, S., Kroupa, P., Banerjee, S.: Mon. Not. R. Astron. Soc. **437**, 4000 (2014)
Palla, F., Stahler, S.W.: Astrophys. J. **581**, 1194 (2002)
Pang, X., Grebel, E.K., Allison, R., et al.: Astrophys. J. **764**, 73 (2013)
Parmentier, G., Kroupa, P.: Mon. Not. R. Astron. Soc. **411**, 1258 (2011)
Patel, N.A., Curiel, S., Sridharan, T.K., et al.: Nature **437**, 109 (2005)
Pfalzner, S.: Astron. Astrophys. **498**, L37 (2009)
Pfalzner, S., Kaczmarek, T.: Astron. Astrophys. **559**, A38 (2013)
Pflamm-Altenburg, J., Kroupa, P.: Mon. Not. R. Astron. Soc. **397**, 488 (2009)

Portegies Zwart, S.F., McMillan, S.L.W., Nualláin, B.Ó., et al.: Lect. Notes Comput. Sci. **5102**, 207 (2008)
Portegies Zwart, S.F., McMillan, S.L.W., Gieles, M.: Annu. Rev. Astron. Astrophys. **48**, 431 (2010)
Price, D.J., Bate, M.R.: Plasmas in the laboratory and the Universe: Interactions, Patterns, and Turbulence (AIP Conference Proceedings), vol. 1242, p. 205 (2010)
Raboud D., Mermilliod J.-C.: Astron. Astrophys. **329**, 101 (1998)
Randriamanakoto, Z., Escala, A., Väisänen, P., et al.: Astrophys. J. **775**, L38 (2013)
Rathborne, J.M., Longmore, S.N., Jackson, J.M., et al.: Astrophys. J. **795**, L25 (2014)
Rochau, B., Brandner, W., Stolte, A., Gennaro, M., et al.: Astrophys. J. **716**, L90 (2010)
Román-Zúniga, C.G., Ybarra, J.E., Megias, G.D., et al.: Astron. J. **150**, 80 (2015)
Sana, H., Evans, C.J.: In: Neiner, C., Wade, G., Meynet, G., Peters, G. (eds.) Active OB Stars: Structure, Evolution, Mass Loss, and Critical Limits (IAU Symposium), vol. 272, p. 474. Cambridge University Press, Cambridge (2011)
Schneider, N., Csengeri, T., Bontemps, S., et al.: Astron. Astrophys. **520**, A49 (2010)
Schneider, N., Csengeri, T., Hennemann, M., et al.: Astron. Astrophys. **540**, L11 (2012)
Shin, J., Kim, S.S.: Mon. Not. R. Astron. Soc. **447**, 366 (2015)
Smith, R., Goodwin, S., Fellhauer, M., Assmann, P.: Mon. Not. R. Astron. Soc. **428**, 1303 (2013)
Spitzer, L. Jr.: Dynamical Evolution of Globular Clusters. Princeton University Press, Princeton (1987)
Stolte, A., Brandner, W., Brandl, B., et al.: Astron. J. **128**, 765 (2004)
Strader, J., Caldwell, N., Seth, A.C.: Astron. J. **142**, 8 (2011)
Tafalla, M., Hacar, A.: Astron. Astrophys. **574**, id. A104 (2015)
Takahira, K., Tasker, E.J., Habe, A.: Astrophys. J. **792**, 63 (2014)
Tapia, M., Roth, M., Bohigas, J., et al.: Mon. Not. R. Astron. Soc. **416**, 2163 (2011)
Tapia, M., Persi, P., Roth, M., et al.: Mon. Not. R. Astron. Soc. **437**, 606 (2014)
Testi, L., Palla, F., Natta, A.: Astron. Astrophys. **342**, 515 (1999)
Wang, Y., Beuther, H., Zhang, Q., et al.: Astrophys. J. **754**, 87 (2012)
Weidner, C., Kroupa, P.: Mon. Not. R. Astron. Soc. **348**, 187 (2004)
Weidner, C., Kroupa, P., Larsen, S.S.: Mon. Not. R. Astron. Soc. **350**, 1503 (2004)
Weidner, C., Kroupa, P., Bonnell, I.A.D.: Mon. Not. R. Astron. Soc. **401**, 275 (2010)
Weidner, C., Kroupa, P., Pflamm-Altenburg, J.: Mon. Not. R. Astron. Soc. **434**, 84 (2013a)
Weidner, C., Kroupa, P., Pflamm-Altenburg, J., Vazdekis, A.: Mon. Not. R. Astron. Soc. **436**, 3309 (2013b)
Wright, N,J., Parker, R.J., Goodwin, S.P., Drake, J.J.: Mon. Not. R. Astron. Soc. **438**, 639 (2014)
Wünsch, R., et al.: Astrophys. J. **740** 75 (2011)
Zeidler, P., Sabbi, E., Nota, A., et al.: Astron. J. **150**, 78 (2015)
Zonoozi, A.H., Küpper, A.H.W., Baumgardt, H., et al.: Mon. Not. R. Astron. Soc. **411**, 1989 (2011)
Zonoozi, A.H., Haghi, H., Küpper, A.H.W., et al.: Mon. Not. R. Astron. Soc. **440**, 3172 (2014)

Index

S. Stahler (ed.), *The Birth of Star Clusters*, Astrophysics and Space Science Library 424, DOI 10.1007/978-3-319-22801-3